

ON THE RESPONSE OF MARINE PHYTOPLANKTON TO
CHANGING NUTRIENT AND LIGHT CONDITIONS

A DISSERTATION

SUBMITTED TO THE DEPARTMENT OF CIVIL AND ENVIRONMENTAL
ENGINEERING AND THE COMMITTEE ON GRADUATE STUDIES

OF STANFORD UNIVERSITY

IN PARTIAL FULFILLMENT OF THE REQUIREMENTS

FOR THE DEGREE OF

DOCTOR OF PHILOSOPHY

Katherine Rose Marie Mackey

May 2010

ABSTRACT

Marine phytoplankton are photoautotrophic microorganisms that synthesize organic biomass from mineral nutrients and form the base of the marine food web. Marine phytoplankton are increasingly being recognized as important contributors to biogeochemical cycling of chemical elements, including carbon (C), and therefore play a role in controlling Earth's climate. A relatively recent estimate suggests that while the upper 100 meters of the ocean contains less than 1% of the total global photosynthetic biomass, this small fraction of the marine environment accounts for nearly 50% of global primary production, the process by which atmospheric carbon dioxide (CO₂) is incorporated into biomass through photosynthesis.

Nutrients and light affect phytoplankton growth, and their availability exerts considerable control on phytoplankton distributions in the ocean and their contribution to biogeochemical cycles. The global supply, distribution, and availability of nutrients in the ocean are driven by a range of physical and biological factors. However, light availability is determined primarily by attenuation within the water column. The ability of a phytoplankton group to respond to changes in nutrient and light availability ultimately determines whether that group will persist, or whether community succession will permit different, more ecologically competitive groups to prevail.

The overarching goal of this dissertation is to identify and understand how responses to changing resource availability influence the competitive success of phytoplankton, and to increase our understanding of how phytoplankton affect biogeochemical cycling of C and other important nutrients in the ocean. The

dissertation includes an Introduction (Chapter 1), and seven research chapters (Chapters 2-8) covering separate bodies of work, each focusing on a different topic as outlined below.

Chapter 1: Introduction

General background information is provided about nutrient and light regimes in the ocean, and about the basic biology and ecology of phytoplankton.

Chapter 2: The phosphorus cycle

This chapter provides an overview of the phosphorus (P) cycle including sources, sinks, and transport pathways of P in the environment, microbially-mediated processes and their genetic regulation, methods for assessing environmental P concentrations and microbial phosphate status, and a discussion of microbial responses to anthropogenic changes to the P cycle. This chapter was published in 2009 in *The Encyclopedia of Microbiology, 3rd Edition*, edited by Moselio Schaechter, Elsevier.

Chapter 3: Phosphorus availability, phytoplankton community dynamics, and taxon-specific phosphorus status in the Gulf of Aqaba, Red Sea

The study uses a novel cell stain to show that (1) coexisting groups of phytoplankton exposed to identical phosphate levels may have a different phosphate status, and (2) although increased alkaline phosphatase activity can serve as an indicator of phosphate limitation, it does not necessarily confer a competitive advantage to cells in oligotrophic waters, where smaller cell size may provide a more

important competitive edge. The affinity of individual groups of phytoplankton for P may help determine community composition and lead to seasonal community succession as P availability changes dramatically throughout the year. This chapter was published in 2007 in *Limnology and Oceanography* 52: 873-885.

Chapter 4: Nitrogen cycling in oligotrophic waters: the influence of light and substrate availability

This study demonstrates that two major processes contribute to formation of nitrite maxima in the Gulf of Aqaba: (i) spatially segregated microbial oxidation of ammonium and nitrite during nitrification; and (ii) incomplete nitrate reduction to ammonium by light-limited phytoplankton. Field data and ^{15}N tracer experiments show that physical and biological characteristics of the water column determine which of the two nitrite formation processes becomes dominant at a given season and depth. Rates are reported for major N transformation reactions occurring in the Gulf's N cycle. This chapter is currently in review with *Limnology and Oceanography*.

Chapter 5: Picophytoplankton responses to changing nutrient and light regimes during a bloom

In the Red Sea, the spring bloom is characterized by a rapid increase in photosynthetic biomass. Nutrient addition experiments and *in situ* monitoring show that picoeukaryotes and *Synechococcus* have a “bloomer” growth strategy, have higher P requirements relative to N, and are responsible for the majority of photosynthetic biomass in surface waters. In contrast, light limited populations show rapid

photoacclimation and community shifts following stratification. The traditional interpretation of “bloom” dynamics (i.e. increase in biomass) may therefore be confined to surface waters where light is not limiting, while other acclimation processes are more ecologically relevant at depth. This chapter was published in 2009 in *Marine Biology* 156: 1531-1546.

Chapter 6: A photosynthetic strategy for coping in a high light, low nutrient environment

This chapter reports field observations from the Atlantic and Pacific Oceans that show the reduction of oxygen (O_2) is important for preserving photosynthetic efficiency in oligotrophic waters where low Fe levels may limit PSI and cytochrome b_6f biogenesis. Despite midday photoinhibition (depression in the maximum photochemical yield, F_v/F_m), cells do not show a decreased capacity for CO_2 fixation. Instead, the fraction of oxidized functional PSII reaction centers increases at midday, counteracting the loss of functional centers stemming from photoinhibition. This process was not apparent in the coastal phytoplankton populations monitored in this study, and may be a strategy unique to open ocean phytoplankton. This chapter was published in 2008 in *Limnology and Oceanography* 53: 900-913.

Chapter 7: The influence of atmospheric nutrients on primary productivity in a coastal upwelling region

This chapter is the first study to quantify the role of atmospheric deposition in supporting productivity an upwelling-dominated system (coastal California). Soluble

nutrient measurements from locally-collected aerosols, oceanographic and atmospheric data from long-term monitoring programs and the MODIS satellite record, and laboratory culture experiments are used. The aerosol-Chlorophyll *a* relationship is significant in the summer, and is stronger at offshore locations than near the coast. Atmospheric nutrient sources are more important during El Niño periods when upwelling is suppressed, a phenomenon that may become more common due to climate warming. During high deposition non-upwelling periods aerosol N could support up to 20% of new production. Expanding our analysis to other regions, we find that atmospheric deposition may support up to 8% of production annually in other major coastal upwelling regions around the world. This chapter is currently in review with *Global Biogeochemical Cycles*.

Chapter 8: Toxicity of metals on marine *Synechococcus*

Atmospheric deposition of aerosols to the surface ocean is a source of nutrients for phytoplankton. However, this study demonstrates that atmospheric aerosols also contain components like copper (Cu), that are toxic to some phytoplankton above certain threshold levels. Incubations of natural phytoplankton assemblages with local aerosols show that metal toxicity can cause a major shift in phytoplankton community composition, suggesting that atmospheric aerosols may play a larger role in controlling phytoplankton species distributions than previously believed. Specific metal toxicity threshold concentrations were determined based on laboratory culture experiments with coastal and oceanic strains of *Synechococcus*, and oceanic strains are more susceptible to metal toxicity at lower concentrations and for a larger number of

metals. A portion of this chapter was published as part of a larger study that also included a global model for Cu deposition in aerosols that was published in 2009 in *The Proceedings of the National Academy of Science* 106: 4601-4605

Chapter 9 Future directions

A brief discussion of work to be done in the future as an extension of the work presented in this dissertation.

The dissertation provides valuable information about how phytoplankton respond to resource availability in a number of different marine environments. The physical environment is shown to play an important role in determining nutrient and light availability over short term periods (e.g. transient exposure to high light during mixing, episodic delivery of aerosol nutrients) as well as over predictable seasonal cycles (e.g. deep convective mixing and stratification). Physiological acclimation of individual phytoplankton to these perturbations allows each species to survive over a broader range of conditions, increasing their competitive advantage. Similarly, succession allows the phytoplankton community as a whole to thrive over the broadest possible range of environmental conditions. This dissertation also shows that phytoplankton play an important role in the P and N cycles by generating organic substrates from inorganic substrates. In doing so, phytoplankton contribute substantially to primary production in coastal and open ocean habitats, and form an important link between the biotic and abiotic environment.

ACKNOWLEDGEMENTS

It is a pleasure to thank those who made this dissertation possible. I would like to thank my committee members Kevin Arrigo, David Freyberg, Mark Jacobson, and Stephen Monismith for their help and support. Thanks to my co-authors and collaborators in the Altabet, Arrigo, Bruland, Doney, Genin, Grossman, Karl, Kudela, Lomas, Mahowald, Parks, Paytan, Post, Scanlan, Wollman, and Zehr lab groups, without whom this work would not have been possible. Special thanks to my colleagues at the Interuniversity Institute for Marine Science in Eilat, Israel for sharing lab space and helping collect field samples during numerous field excursions.

I would also like to thank my advisors, Arthur Grossman and Adina Paytan. Arthur has taught me many important lessons, perhaps the most important of which is to never settle for anything less than doing my very best work. Arthur always stresses the need for designing and conducting scientific work in the most careful, thoughtful way possible. He has challenged me and inspired me to become a better scientist, and for that I am grateful.

There are no words to adequately describe Adina, or to convey the respect and admiration I have for her. She is an exemplary scientist and role model from whom I have learned the importance of perseverance and patience, individual responsibility and teamwork, modesty and self confidence, and the balance between work and play. If I ever doubted my ability to persue the work I love, all I had to do was look to

Adina for guidance. And if I ever wondered how to excel at my research while also being an exceptional mother, all I had to do was look to Adina for inspiration. For all of these things, and for her continuing support and friendship, I am grateful.

Finally, I thank my friends and family for their support over the past seven years. They have encouraged me during tough times and celebrated with me during good times. In particular I thank my husband, Tim Culbertson, for his patience and support. Graduate school has been full of life changing experiences for both of us: we moved to California, got married, and now have Mark, the most beautiful, wonderful son anyone could hope for. From the start, Tim's emphatic certainty about my ability to succeed has been a source of strength from which I have drawn support. Without Tim's support this dissertation would not be a reality; the only reason I can do all the things I do is because Tim does all the things he does. I am grateful that he is so wonderful.

TABLE OF CONTENTS

ABSTRACT.....	iv
ACKNOWLEDGEMENTS.....	x
LIST OF TABLES.....	xv
LIST OF FIGURES.....	xvi
CHAPTER 1: INTRODUCTION.....	1
BACKGROUND.....	1
PHOTOSYNTHESIS AND PRODUCTION.....	4
LIGHT	7
NUTRIENT SUPPLY, DISTRIBUTION, AND AVAILABILITY.....	10
NUTRIENT UPTAKE, PHYTOPLANKTON GROWTH, AND COMPETITION.....	13
PHYTOPLANKTON DIVERSITY	18
REFERENCES	25
CHAPTER 2: THE PHOSPHORUS CYCLE.....	32
ABSTRACT	32
INTRODUCTION	33
MICROBially MEDIATED PROCESSES	44
GENETIC REGULATION OF MICROBially-MEDIATED PROCESSES.....	59
ANTHROPOGENIC ALTERATION OF THE P CYCLE:	
EUTROPHICATION IN AQUATIC ECOSYSTEMS	62
CONCLUSION	64
ACKNOWLEDGEMENTS	65
FURTHER READING	66
CHAPTER 3: PHOSPHORUS AVAILABILITY, PHYTOPLANKTON COMMUNITY DYNAMICS, AND TAXON-SPECIFIC PHOSPHORUS STATUS IN THE GULF OF AQABA, RED SEA.....	72
ABSTRACT	72
INTRODUCTION	74
MATERIALS AND METHODS	78
RESULTS	84
DISCUSSION	90
CONCLUSION.....	97
ACKNOWLEDGEMENTS.....	99
REFERENCES	101

CHAPTER 4: NITROGEN CYCLING IN OLIGOTROPHIC WATERS: THE IMPACT OF LIGHT AND SUBSTRATE AVAILABILITY.....	119
ABSTRACT	119
INTRODUCTION	121
MATERIALS AND METHODS	126
RESULTS	135
DISCUSSION	146
CONCLUSION.....	161
ACKNOWLEDGEMENTS	163
REFERENCES	165
 CHAPTER 5: PICOPHYTOPLANKTON RESPONSES TO CHANGING NUTRIENT AND LIGHT REGIMES DURING A BLOOM.....	192
ABSTRACT	192
INTRODUCTION	194
MATERIALS AND METHODS	197
RESULTS.....	204
DISCUSSION.....	213
ACKNOWLEDGEMENTS	225
REFERENCES	227
 CHAPTER 6: A PHOTOSYNTHETIC STRATEGY FOR COPING IN A HIGH LIGHT, LOW NUTRIENT ENVIRONMENT.....	245
ABSTRACT	245
INTRODUCTION.....	247
MATERIALS AND METHODS	251
RESULTS	259
DISCUSSION	265
ACKNOWLEDGEMENTS.....	277
REFERENCES	279
 CHAPTER 7 THE INFLUENCE OF ATMOSPHERIC NUTRIENTS ON PRIMARY PRODUCTIVITY IN A COASTAL UPWELLING REGION.....	301
ABSTRACT	301
INTRODUCTION	302
MATERIALS AND METHODS	304
RESULTS	318
DISCUSSION	322
CONCLUSION	333
ACKNOWLEDGEMENTS	334
REFERENCES	336

CHAPTER 8 TOXICITY OF METALS ON MARINE <i>SYNECHOCOCCUS</i>	370
ABSTRACT	370
INTRODUCTION	371
MATERIALS AND METHODS	373
RESULTS AND DISCUSSION	377
ACKNOWLEDGEMENTS	388
REFERENCES	389
CHAPTER 9 FUTURE DIRECTIONS.....	406

LIST OF TABLES

Chapter 2, Table 1: Phosphate minerals and their compositions	68
Chapter 4, Table 1: N assimilation rates	173
Chapter 4, Table 2: Nitrate reduction rates	174
Chapter 4, Table 3: Summary of N transformation rates.....	175
Chapter 5, Table 1: Nutrient data	234
Chapter 5, Table 2: Picophytoplankton cell concentrations during a nutrient addition experiment	235
Chapter 6, Table 1: Equations used in determining photosystem II fluorescence parameters	288
Chapter 6, Table 2: Photosynthesis-irradiance parameters	289
Chapter 7, Table 1: Aerosol soluble nutrient concentrations and fluxes	350
Chapter 7, Table 2: Depositional fluxes of nitrogen	351
Chapter 7, Table 3: Regression statistics for MODIS-derived chlorophyll concentration and aerosol optical thickness	352
Chapter 7, Table 4: Productivity supported by aerosol nitrogen	353
Chapter 7, Table 5: Production from aerosol nitrogen in California and six other major upwelling centers	354
Chapter 8, Table 1: Comparison of metal concentrations resulting from aerosol additions with metal toxicity thresholds	396
Chapter 8, Table 2: Toxicity of various metals on <i>Synechococcus</i> strains	397

LIST OF FIGURES

Chapter 1, Figure 1: Photosynthetic rates	28
Chapter 1, Figure 2: Ocean circulation patterns	29
Chapter 1, Figure 3: Nutrient uptake kinetics	30
Chapter 1, Figure 4: Resource ratio theory of competition.....	31
Chapter 2, Figure 1: The phosphorus cycle	69
Chapter 2, Figure 2: Alkaline phosphatase activity assays	70
Chapter 2, Figure 3: Enzyme labeled fluorescence assay for alkaline phosphatase activity	71
Chapter 3, Figure 1: Map of the Gulf of Aqaba, Red Sea	109
Chapter 3, Figure 2: ELF-97 micrographs of nanoplankton	110
Chapter 3, Figure 3: Density and nutrient profiles	111
Chapter 3, Figure 4: Surface nutrient concentrations	112
Chapter 3, Figure 5: Nutrient ratio profiles	113
Chapter 3, Figure 6: Phytoplankton relative abundance	114
Chapter 3, Figure 7: Phytoplankton relative abundance and ELF-97 labeling	115
Chapter 3, Figure 8: ELF-97 micrographs of picophytoplankton	117
Chapter 3, Figure 9: ELF-97 labeling phytoplankton following nutrient additions	118
Chapter 4, Figure 1: Schematic diagram of the nitrogen cycle	176
Chapter 4, Figure 2: Seasonal nitrate, nitrite, and chlorophyll <i>a</i> profiles	177
Chapter 4, Figure 3: Nutrient, chlorophyll <i>a</i> , and nitrogen inventory profiles during the spring bloom	179

Chapter 4, Figure 4: Density profiles during the spring bloom	180
Chapter 4, Figure 5: Cell density profiles	181
Chapter 4, Figure 6: Isotopic composition of nitrite plus nitrate	182
Chapter 4, Figure 7: Raleigh fractionation curves for nitrogen and oxygen	183
Chapter 4, Figure 8: Nitrogen and oxygen fractionation ratios	184
Chapter 4, Figure 9: Cell density and nitrite production and consumption during a nutrient addition experiment	185
Chapter 4, Figure 10: Microbial community composition in the ¹⁵ N tracer experiment	186
Chapter 4, Figure 11: Nitrogen assimilation into particulate biomass	187
Chapter 4, Figure 12: Change in nitrate, nitrite, and ammonium inventories during the spring bloom	188
Chapter 4, Figure 13: Light dependence of nitrate reduction rates	189
Chapter 4, Figure 14: Ammonium oxidation rates	190
Chapter 4, Figure 15: Schematic diagram of the principal regions of the primary nitrite maximum	191
Chapter 5, Figure 1: Nutrient, chlorophyll <i>a</i> , and cell density profiles	236
Chapter 5, Figure 2: Cellular fluorescence profiles	237
Chapter 5, Figure 3: Profiles of nutrient ratios and changes in nutrient inventories during the spring bloom	238
Chapter 5, Figure 4: Picophytoplankton cell densities during a simulated stratification experiment	239
Chapter 5, Figure 5: Photochemical efficiency of photosystem II	

in the simulated stratification experiment	240
Chapter 5, Figure 6: Chlorophyll <i>a</i> concentrations during	
a nutrient addition experiment	241
Chapter 5, Figure 7: Picophytoplankton cell densities during	
a nutrient addition experiment	242
Chapter 5, Figure 8: Picophytoplankton photosynthetic biomass	243
Chapter 5, Figure 9: Cellular fluorescence during a nutrient addition	
experiment under low light	244
Chapter 6, Figure 1: Principal components of the photosynthetic apparatus,	
and flow chart showing terminology used in the study	290
Chapter 6, Figure 2: Map of Hawai'i, USA and sampling sites	
in the Pacific Ocean, and Bermuda and sampling sites	
in the Atlantic Ocean	292
Chapter 6, Figure 3: Example photosystem II fluorescence trace	293
Chapter 6, Figure 4: Picophytoplankton cell densities	294
Chapter 6, Figure 5: Diel cycle of photosystem II fluorescence	295
Chapter 6, Figure 6: Photochemical quenching in waters from the	
surface and the deep chlorophyll maximum	296
Chapter 6, Figure 7: Photosynthesis-irradiance curves	297
Chapter 6, Figure 8: Photosynthetic electron flow	298
Chapter 6, Figure 9: Chlorophyll fluorescence traces under oxic	
and anoxic conditions, and with pgal treatment	299

Chapter 7, Figure 1: Map of sampling sites in Monterey Bay, California, USA	359
Chapter 7, Figure 2: Air mass back trajectories	360
Chapter 7, Figure 3: Aerosol concentration in air	361
Chapter 7, Figure 4: Nutrient ratios in aerosols	362
Chapter 7, Figure 5: Time series of MODIS-derived data, wind speed, and precipitation	363
Chapter 7, Figure 6: Annual correlations between chlorophyll and aerosol optical thickness	365
Chapter 7, Figure 7: Upwelling indices	366
Chapter 7, Figure 8: ENSO indices	367
Chapter 7, Figure 9: Growth of cultured phytoplankton with an aerosol nitrogen source	368
Chapter 7, Figure 10: Chlorophyll <i>a</i> concentrations during a nutrient addition experiment	369
Chapter 8, Figure 1: Chlorophyll <i>a</i> concentrations during a nutrient addition experiment	398
Chapter 8, Figure 2: Nutrient and metal contributions from aerosols	399
Chapter 8, Figure 3: Picophytoplankton cell densities during a nutrient addition experiment	400
Chapter 8, Figure 4: Example plots of culture optical density and photosynthetic efficiency in a metal toxicity assay	401
Chapter 8, Figure 5: Response of oceanic <i>Synechococcus</i> strain	

WH 8102 to metal additions	402
Chapter 8, Figure 6: Response of oceanic <i>Synechococcus</i> strain	
CCMP 841 to metal additions	403
Chapter 8, Figure 7: Response of coastal <i>Synechococcus</i> strain	
CCMP 838 to metal additions	404
Chapter 8, Figure 8: Response of coastal <i>Synechococcus</i> strain	
CCMP 2606 to metal additions	405

CHAPTER 1

INTRODUCTION: FACTORS AFFECTING THE GROWTH OF PHYTOPLANKTON IN THE OCEAN

BACKGROUND

Phytoplankton are single-celled, photoautotrophic, prokaryotic or eukaryotic microorganisms that inhabit the sunlit layers of the ocean. Using energy from sunlight, phytoplankton synthesize organic biomass from mineral nutrients and form the base of the marine food web. In generating this *primary production*, phytoplankton perform a vital ecological function that links all marine organisms to the abiotic ocean environment. Phytoplankton therefore play an integral role in supporting economically important commercial fisheries and contribute to the biogeochemical cycling of important chemical elements, including carbon (C).

The ability of phytoplankton to respond to environmental stimuli is an important determinant of the individual competitive success of specific taxonomic groups. This ability to respond to changes in the environment, which varies between different phytoplankton groups, often determines which groups will persist and how community succession will proceed; the more ecologically fit groups will prevail over both time and space. This dissertation explores factors and processes that influence growth and successional strategies of marine phytoplankton, and focuses on two main objectives:

1. How do phytoplankton perceive, acclimate, and adapt to changes in their environment, with particular emphasis on nutrients and light?
2. What interplay does this cause between and within natural populations of phytoplankton, and how does acclimation and adaptation influence their diversity, niche partitioning, and contributions to biogeochemical cycles?

This dissertation considers phytoplankton responses to changes in nutrient and light regimes that occur over different temporal scales. The marine environment is highly dynamic, and phytoplankton must constantly sense and adjust to changes in the external environment if they are to remain competitive. In the ocean, nutrient and light availability can change transiently due to short term perturbations, or gradually over predictable annual cycles. Phytoplankton, in turn, adjust to the environment over different time scales. *Adaptation* occurs through evolution over numerous generations as the environment selects for phenotypically advantageous traits from within a population (Falkowski and Raven 2007). These traits are heritable, and come about through chance genetic mutation or the lateral transfer (often virally-mediated) of useful genes. In contrast, *acclimation* refers to adjustments that phytoplankton make in response to their environment over short-term time scales relevant to a single cell or a particular phytoplankton assemblage. For each phytoplankton species, acclimation responses are adjustments that cells can make given the suite of genes they already possesses, such as induction of high-affinity nutrient transporters in response to low nutrients or restructuring of the photosynthetic apparatus in response to high light. Acclimation can also occur over several generations such as during certain types of

chromatic adaptation, where select photosynthetic pigments are passively diluted out of the cell lineage following successive cell divisions, rather than being actively degraded by the cell in one generation (although other pigments may be synthesized and integrated into the photosynthetic machinery within one generation (Kehoe and Grossman 1996)).

In addition to different temporal scales, phytoplankton responses to the environment occur over a range of hierarchical scales. These can include the responses of a single cell, a population of cells with some variability in their genetic compositions, or the overall mixed phytoplankton community. Understanding phytoplankton responses to nutrients and light regimes over these various scales provides different types of information. Cellular responses reveal physiological acclimation strategies, while populations persist or decline depending on the integrated effectiveness of those cellular acclimation strategies. In other words, population success provides information about how competitive a group of phytoplankton is under different environmental conditions. Cellular and population level responses are useful, for example, in understanding the roles that different species play in nutrient cycling. In contrast, the overall phytoplankton community acclimates by undergoing succession of different populations, and provides information on a broader scale. For example, understanding community responses to variable nutrient and light availability is useful for understanding the role of phytoplankton in contributing to marine primary production.

PHOTOSYNTHESIS AND PRODUCTION

The amount of biomass produced by phytoplankton (production) is dependent on photosynthesis, the process by which light energy is used to convert CO₂ and water into carbohydrates and oxygen, though it may be limited by nutrient availability. Photosynthesis has two principle stages: the light-dependent reactions and the light-independent reactions. The light reactions occur between proteins anchored within or associated with a photosynthetic membrane, where light energy is collected by photosynthetic pigments and passed to the reaction center chlorophyll of a protein complex called photosystem (PS)II. The light energy is used to generate a charge separation in the chlorophyll *a* molecule, freeing an electron that gets passed along a series of electron acceptors in an electron transport chain (ETC). As the electron is passed along the ETC, protons get pumped across the membrane, generating a pH gradient. A second charge separation occurs at PSI, allowing the molecule nicotinamide adenine dinucleotide phosphate (NADP⁺) to get reduced to NADPH. The reaction center chlorophyll of PSI receives a new electron from the ETC to replace the one it lost during the charge separation. However, the electron lost by the reaction center chlorophyll of PSII is replaced through the oxidation of water in a reaction that also produces O₂ as a byproduct and contributes to the pH gradient by generating protons. The electrochemical energy stored in the pH gradient is used to drive the synthesis of adenosine triphosphate (ATP), the energy currency of the cell. The photosynthetic reaction centers, electron transport chain, ATP synthase complex and light-harvesting pigment proteins complexes are depicted in Figure 1 of Chapter 6.

(For a detailed discussion of the light reactions of photosynthesis please refer to Chapter 6).

The light-independent reactions are not directly driven by light, although they are activated by and require the formation of products from the light reactions. These reactions include the steps of the Calvin-Benson-Bassham Cycle, in which the enzyme ribulose-1,5-bisphosphate carboxylase oxygenase (RuBisCO) catalyzes the incorporation of CO₂ into simple three carbon sugar phosphate molecules using the reducing energy stored in NADPH and ATP generated by the light reactions of photosynthesis (Bassham et al. 1950). This process is called carbon *fixation* because CO₂ becomes incorporated, or fixed, into organic molecules that can be used for generating energy through respiration or for the production of biomass (new cells, storage compounds).

The amount of global primary production, or fixed carbon, attributable to marine phytoplankton is often overlooked because they comprise a very small fraction of the total global photosynthetic biomass, which is dominated by terrestrial plants. Phytoplankton productivity rates range from <100 mg C m⁻² day⁻¹ in the open ocean gyres to > 1000 mg C m⁻² day⁻¹ in coastal upwelling regions, and have an average value of ~140 g C m⁻² year⁻¹ over an annual cycle (Field et al. 1998). Despite having lower than the average productivity rates compared to the terrestrial environment (426 g C m⁻² year⁻¹), the overall primary production of the ocean is 48.5 Gt C year⁻¹, or approximately half of total global primary production (105 Gt C yr⁻¹) (Field et al. 1998). This is due to the ubiquity of marine phytoplankton, which inhabit virtually all sun lit regions of the ocean. Therefore, even though the areal productivity rates are on

average lower in the ocean than on land, the larger overall area of the ocean compared to land makes its contribution more significant.

Nutrients and light are important environmental factors that control photosynthesis and the growth of phytoplankton, and both of these parameters are influenced by physical and biological processes in the ocean. Physical oceanic processes introduce constraints with respect to light and nutrient availability as a result of mixing and stratification processes. In the surface ocean where light intensity is relatively high, macronutrients are continuously stripped from the water as they are taken up by growing phytoplankton. These incorporated nutrients are retained in the grazing food web, regenerated through the microbial loop, or removed from the water column through sedimentation. This system, referred to as the “biological pump”, is responsible for the drawdown and sequestration of globally significant amounts of carbon in the ocean’s interior over geologic time scales. An estimate given by Sarmiento and Bender (1994) projects that if the biological pump were suddenly eliminated and the oceanic carbon cycle were driven entirely by physical and chemical processes, the amount of carbon released from the ocean as it equilibrated with the atmosphere would more than double the CO₂ concentration in the atmosphere. Therefore, in order to understand and predict the functioning of the biological pump, a thorough understanding of how light and nutrient availability affects the growth of the ocean’s producers is necessary.

LIGHT

Visible light (400-700 nm) comprises about half of the sunlight reaching the ocean's surface. This portion of the spectrum is also called *photosynthetically active radiation* (PAR) because the wavelengths can be used by photoautotrophs to drive the light reactions of photosynthesis. The remainder is composed mostly of infrared radiation >780 nm, with a small contribution from ultraviolet radiation <380 nm. Light becomes attenuated as it travels through water, and different wavelengths scatter and get absorbed at different rates. Infrared and ultraviolet radiation are rapidly attenuated in the surface ocean due to absorption and scattering. PAR penetrates deeper into the water column; however, it decreases exponentially with depth. The penetration depth of PAR varies depending on the wavelength of light and the amount and type of particulate material present in the water, which causes wavelength-specific scattering and absorption. In clear seawater with low particulate matter, red wavelengths are attenuated most rapidly, such that at 10 m only ~1% of red light remains compared to surface irradiance (Lalli and Parsons 1993). In contrast, blue light penetrates deepest and therefore plays a large role in determining the depth distributions of photosynthetic organisms within the water column.

Photosynthetic rates follow a predictable pattern in response to increasing irradiance. The relationship is shown graphically in a photosynthesis-irradiance curve described using a Michaelis-Menten type function (**Fig. 1**, adapted from Lalli and Parsons (1993)), in which photosynthetic rates can be measured based on carbon fixation, oxygen evolution, or fluorescence yield. In the first portion of the curve, photosynthesis increases linearly with increasing irradiance until a saturating

irradiance is reached. At this saturating irradiance the photosynthetic rate is maximal and is maintained at this value even as the irradiance increases. However, at very high irradiances photoinhibition can occur and cause a decline in the photosynthetic rate (photoinhibition is discussed in detail in Chapter 6). In general the slope of the linear portion of the curve is determined by the efficiency of the light-dependent reactions of photosynthesis, while the maximum photosynthetic rate reached in the saturated portion of the curve corresponds to the maximum rate of the light-independent reactions (Falkowski and Raven 2007). The maximum photosynthetic rate is therefore sensitive to environmental factors like nutrient availability that limit carbon fixation rates.

At any depth in the water column, photosynthetic rates are dependent on the amount of light that is available. In the upper portion of the water column, high light levels generally support high photosynthetic rates, although some photoinhibition occurs near the surface and non-photochemical quenching can redirect absorbed light energy into heat generation. The *euphotic zone* is the region of the water column in which photosynthesis exceeds respiration by phytoplankton. In the euphotic zone, excess organic carbon generated by photosynthesis that is not consumed by the phytoplankton goes into biomass that is made available to other trophic levels. This carbon is referred to as *net primary production*. The irradiance at which photosynthesis exactly balances phytoplankton respiration (and net primary production is zero) is called the *compensation irradiance*. The depth at which this occurs is called the *compensation depth*, and it defines the lower boundary of the euphotic zone. The compensation depth varies depending on how quickly light

becomes attenuated with depth, and can change over short time scales (e.g. over a period of days as phytoplankton bloom). In general, the compensation depth is greater when fewer phytoplankton are present in the water column; therefore, the compensation depth can vary substantially over seasons and in response to physical processes like mixing and stratification that determine light and nutrient availability.

Compensation depths in general are determined for a mixed phytoplankton community; however, each phytoplankton species has its own unique compensation irradiance, and the compensation depth for a natural water column represents an average value for the entire phytoplankton community on that day. Considerable difficulty exists in determining the compensation depth directly from rate measurements (Geider 1992). This is mainly because phytoplankton respiration is difficult to measure in natural samples that also contain respiring heterotrophs, and because phytoplankton respiration rates are rarely constant (Geider and Osborne 1989). The compensation depth is therefore generally taken to be the depth at which PAR is attenuated to 1% of surface irradiance. This convention provides a close approximation of the true compensation depth based on light attenuation, which is relatively straight forward to measure.

In a mixed water column, phytoplankton experience an average light environment that integrates high surface irradiance down to the irradiance at the depth of mixing (Falkowski and Raven 2007). To achieve net phytoplankton growth (e.g. a phytoplankton bloom), phytoplankton must generate enough photosynthetic production to support their own respiratory needs, but must also exceed the respiratory demands of higher trophic levels that they support. To determine the maximum

mixing depth that still permits net phytoplankton growth, it is helpful to identify the depth where net primary production exactly balances respiration by the entire community. Sverdrup (1953) defines this depth as the “critical depth,” and Platt et al (1991) note that all pathways by which carbon is lost from a water column can be treated as respiratory losses under this model. (For example, even organic carbon that sinks to the sediment would presumably undergo respiration by the benthic community of heterotrophic microbes, thus carbon export can be included as a respiratory loss.) The *critical depth* is the maximum depth to which phytoplankton can be mixed while still spending enough time above the compensation depth that they are able to satisfy integrated water column respiratory demands from their own photosynthetic production. Above the critical depth phytoplankton contribute net primary production that is available to other trophic levels; below the critical depth phytoplankton cannot support respiratory demands and will die.

NUTRIENT SUPPLY, DISTRIBUTION, AND AVAILABILITY

The global supply, distribution, and availability of nutrients in the ocean are driven by physical and biological factors. The source of nutrients supporting photosynthesis is of interest to oceanographers because only nutrients delivered from external sources will support net sequestration and export of C, which is referred to as *new production*. Nutrients may therefore be classified as either locally regenerated (i.e., recycled from organic material within the euphotic zone), or exogenous, originating from outside of the euphotic zone. Nutrients regenerated in deep water that enter the euphotic zone through mixing or upwelling are considered exogenous

because they support new production. Another major source of “new” nutrients to the ocean is from land via the weathering and transport of crustal material. Terrigenous nutrients are transported to the ocean by a number of physical processes, including fluvial discharge, runoff, precipitation, and atmospheric deposition. (For more detailed information on these processes please refer to Chapters 7 and 8). N fixation by diazotrophic bacteria and phytoplankton is a biological process that converts N_2 gas from the atmosphere into soluble, bioavailable forms of N and thus this N constitutes a new source of N to the ocean (see Chapter 4 for discussion of the N cycle). Nutrient inputs from terrigenous sources are generally greatest in coastal waters close to continental margins due to their proximity to land. In contrast, N fixation occurs in situ wherever diazotrophs are active.

Regeneration of particulate matter is an important source of “recycled” inorganic nutrients in the ocean that is moderated by biological processes. Regeneration is facilitated by the microbial loop, in which microbes use the reduced form of nutrients in organic matter as an energy source and generate oxidized “recycled” nutrients as a byproduct. Though regeneration occurs throughout the water column, inorganic nutrient levels tend to be higher in the deep ocean than in the euphotic zone. This is because assimilation rates in surface waters often exceed regeneration rates, and regenerated nutrients get consumed as soon as they are available. In contrast, assimilation rates are minimal at depth, and inorganic nutrients accumulate because they have time to undergo mineralization and subsequent regeneration steps. In addition to assimilation, the depth distribution of nutrients is also maintained because homogenization between deep water and the overlying

surface water (e.g. mixing) is physically prevented in many locations by a density gradient, or *pycnocline*, that helps maintain a stratified water column. Regeneration may occur rapidly (e.g. over days or seasons) for relatively labile compounds, but may be much slower (e.g. geological time scales) for refractory compounds that accumulate in the deep ocean and sediments.

Ocean circulation has a direct effect on the extent to which nutrients from deep water can enter the euphotic zone where they can be used by phytoplankton. Greater solar heating of water at the equator than at the poles causes thermal stratification at mid and low latitudes, and helps establish a thermohaline circulation pattern in which warm surface waters tend to flow pole-ward, while cold deep water tends to flow toward the equator (Stewart 2003). Together with the Coriolis Effect, the overall circulation pattern of surface waters throughout the world's oceans leads to the formation of large anticyclonic gyres in the open ocean (Stewart 2003). In the northern hemisphere the gyres flow in a clockwise orientation, while in the southern hemisphere their flow is counterclockwise (**Fig. 2**; Stewart 2003). These convergent, warm-core gyres draw warm, nutrient poor surface water toward their centers as they rotate. As the water accumulates in the center of the gyre, the pycnocline gets depressed and intrusion of cold, nutrient rich deep water is prevented. The gyres have very low productivity relative to other areas of the ocean due to this paucity of nutrients in the surface (Falkowski and Raven 2007).

In contrast to gyre circulation, wind driven divergent fronts increase the flux of deep water nutrients to the surface in regions where certain types of current systems come together or where currents flow along the western boundaries of continents. In

these regions, surface water is deflected due to the eastward rotation of the Earth (Stewart 2003), resulting in upwelling of nutrient rich deep water. In such divergent areas upwelling generally leads to high productivity (see Chapter 7 for more information about coastal upwelling regions).

Convective mixing is an important process over regional scales for introducing deep water nutrients to the surface. In waters that are seasonally stratified, such as in many subtropical latitudes, surface waters warm in the summer and therefore become less dense. This configuration sustains a stratified water column in which the denser, nutrient rich deep water remains trapped below the less dense, nutrient poor surface water. Cooling increases the density of surface waters in the winter and causes it to sink, leading to convective mixing. The degree of cooling determines the depth of mixing (Stewart 2003) and therefore the quantity of nutrients introduced from deep water into the mixed layer (for more information on the effects of seasonal convective mixing, see Chapters 3, 4, and 5). In permanently stratified waters, such as some low latitude regions, mixing is minimal and diffusion is the main process by which nutrients move from deep water into the euphotic zone.

NUTRIENT UPTAKE, PHYTOPLANKTON GROWTH, AND COMPETITION

Phytoplankton generate biomass by converting CO₂ into organic molecules during the light-independent reactions of photosynthesis. Along with C, phytoplankton require many other nutrients (e.g. N, P, Si, S, Fe, Mg) for proper cellular function. Redfield (1958) was the first to note that the elemental composition of living and dead marine organic matter is relatively constant throughout the world's

oceans regardless of location, and that the stoichiometric relationship of C:N:P is 106:16:1. This ratio is called the *Redfield ratio*, and has been used extensively in oceanography to understand and predict the growth of phytoplankton. However, while the chemistry of nutrient rich deep water conforms quite closely to the Redfield ratio, the elemental compositions of individual species of phytoplankton varies widely due to physiological flexibility (Klausmeier et al. 2004) and luxury uptake of nutrients by phytoplankton (Keenan and Auer 1974). In luxury uptake a cell takes up more nutrients than it needs while ambient nutrient concentrations are high and stores them for later use, which can alter cellular elemental composition significantly. The Redfield ratio therefore likely represents a global average for phytoplankton in surface waters (Arrigo 2005).

An important corollary to the concept that nutrients are required in certain ratios is Liebig's *Law of the Minimum*, which states that the scarcest nutrient with respect to the cell's requirements will ultimately limit growth (Falkowski and Raven 2007). This principle was originally developed to explain the limitation of agricultural crop monoculture yields, and indeed, it is more applicable to explaining nutrient limitation of a homogenous phytoplankton community than to a diverse assemblage with different nutrient requirements and uptake rates. For example, Liebig's Law applies well to populations of diatoms in the Southern Ocean, where fertilization with Fe induces large blooms and results in drawdown of other abundant essential nutrients. However, in many oligotrophic environments nutrient co-limitation is observed. This can occur as a result of either *multi-nutrient co-limitation* of one species, where the levels of two or more nutrients are depleted beyond the levels required for cellular

uptake (i.e., the critical threshold level, see section on Resource Ratio Theory below), or *community co-limitation*, where different species in the community are limited by different nutrients, and therefore addition of any one of these nutrients is sufficient to stimulate growth in part of the community, although all limiting nutrients must be added to yield the maximum amount of growth (Arrigo 2005). Within the ocean, photosynthetic biomass generally continues to be generated until the supply of one or more critical nutrients becomes limiting, assuming growth rates exceed grazing and other mortality rates. (For more information on nutrient limitation, please see Chapter 5).

Nutrient availability helps determine the growth rates and global distributions of phytoplankton taxa in the ocean. Just as photosynthetic rates increase with increasing irradiance, nutrient uptake rates increase with increasing nutrient concentration following a Michaelis-Menten type relationship (**Fig 3** adapted from Lalli and Parsons 1993). (Phytoplankton growth rates, which are roughly stoichiometrically related to nutrient uptake rates, have equivalent relationships with nutrient concentration, and the equation can be written to describe either parameter based on the units that are chosen. For simplicity, I discuss nutrient uptake rates here; however, the discussion is analogous for growth rate.) In the first portion of the curve, the nutrient uptake rate increases linearly with increasing nutrient concentration until a saturating concentration is reached. At this concentration the uptake rate reaches a maximal value that is maintained even as concentration increases.

The slope of the linear portion of the curve is determined by the affinity of the phytoplankton for the nutrient in question. A steep slope indicates high nutrient

affinity, where the maximal uptake rate is reached at very low concentrations. A shallow slope indicates that the maximal uptake rate is reached at higher concentrations. The nutrient affinity and maximum uptake rate play an important role in determining which species of phytoplankton thrive in certain environments (**Fig. 3**). For example, in waters with consistently or episodically high nutrient concentrations, organisms with higher maximal uptake rates dominate, whereas in oligotrophic (low nutrient) waters organisms with higher nutrient affinities tend to dominate. High maximal uptake rates often come with the cost of lower nutrient affinities, such that these organisms are unable to compete in waters where nutrients are very scarce. In contrast, organisms with slower maximal uptake rates may have better affinities for nutrients at very low concentrations and are quite competitive in nutrient poor waters. (For more information on the competitive strategies of phytoplankton, please refer to Chapter 5).

Many models exist for describing the competition and co-existence of microbial populations; however, the *Resource Ratio Theory* (MacArthur 1972; Tilman 1980) is one of the most useful because it draws directly from the principles of nutrient uptake kinetics and the Law of the Minimum. The theory is based on the observation that a myriad of growth limiting resources (e.g. nutrients, light, temperature) can co-occur in the environment, and that coexistence of different populations is only possible if each is limited by a different resource. The theory recognizes that there exists a *critical threshold value* for each essential resource below which a species can no longer survive. This could occur, for example, in a cell with low N affinity in a low N environment, because the cell would be physically unable to

acquire N using its enzymes that are adapted to work only under higher N concentrations. In this highly simplified example, the cell could only survive if N concentrations were above some critical threshold value. However, in the highly dynamic natural environment it is rare that a singular resource will ultimately determine the success of an organism. Rather the organism's ability to cope with an integrated set of conditions typically determines its success. This interplay is discussed below for a simple system in which 2 resources are limiting; however, the theory is analogous for systems with numerous resources.

In a system with two essential resources, Resource Ratio Theory predicts that there is a large range of resource ratios in which a single species will survive (**Fig. 4A** adapted from Tilman 1980) based on its critical threshold value for each nutrient. If a second species is added, the range of acceptable resource ratios for each species is limited by competition between the two species for the same resources. The theory predicts that the species able to survive at the lowest level of a limiting resource will be the best competitor for that resource, and that species dominance varies with the ratio of limiting resources. The possible outcomes of this competition scenarios can be represented graphically (**Fig. 4B**, adapted from Tilman 1980) and show that stable coexistence is only possible over a limited range of resource ratios. The exact ratios that bound each region are determined by the growth rate of each species under all of the various resource combinations. An important implication of this theory is that the number of coexisting species in an ecosystem is equal to or less than the number of limiting resources. This is an area of particular interest in the ocean where myriad types of phytoplankton co-exist. It suggests that each group has a specific niche

defined by a unique combination of requirements for numerous resources, many of which are still being identified. Moreover, it suggests that if any required resource falls below the critical threshold level for a given species, then that species will be succeeded by another more competitive species. Another layer of complexity may also arise if certain groups actively prevent other groups from growing, such as by producing extracellular exudates that inhibit growth of their competitors.

PHYTOPLANKTON DIVERSITY

The existence of diverse niches in the ocean allows for diverse assemblages of phytoplankton to exist and affects the distribution of various taxonomic groups. In contrast to land plants, phytoplankton comprise diverse taxonomic groups from all three domains of life, including eukaryotes, eubacteria, and archebacteria, and considerable diversity exists within each of these taxa. While a thorough review of phytoplankton taxonomy is outside the scope of this introduction, brief descriptions of the distributions and major resources used by the major phytoplankton groups discussed in the dissertation are included below.

Picophytoplankton

Picophytoplankton include cyanobacterial and eukaryotic phytoplankton cells $<2\ \mu\text{m}$ in diameter. Due to their small size and high surface area to volume ratios, picophytoplankton generally have lower nutrient requirements and higher nutrient affinities than larger cells. The low nutrient requirements of these organisms allow them to dominate large oligotrophic regions of the ocean where other phytoplankton

are unable to survive, such as the open ocean gyres. However, picophytoplankton are not confined exclusively to the open ocean, and some groups successfully colonize coastal waters. Picophytoplankton are therefore not only the most abundant organisms in the ocean, but are also globally ubiquitous.

The smallest and most abundant picophytoplankton are the cyanobacteria *Synechococcus* and *Prochlorococcus*, which account for nearly one-third of the total primary production on Earth (Partensky et al. 1999). Marine *Synechococcus* are a highly diverse species generally abundant in the upper 25 m of the water column where light is present in a broad range of wavelengths at relatively high intensities. The major light harvesting component of *Synechococcus* is the phycobilisome, a pigment protein complex that absorbs light over a broad range of wavelengths in the green and the red region of the spectrum. The *Synechococcus* lineage has diversified into four major clades with distinct light and nutrient requirements (Scanlan et al. 2009), allowing *Synechococcus* to inhabit a broad range of ocean environments from clear oligotrophic ocean waters to nutrient-rich coastal waters, which are enriched in green wavelengths. *Synechococcus* is found at nearly every latitude from the equator to the polar circle.

Prochlorococcus has photosynthetic antenna composed of divinyl chlorophyll a and b, and utilizes a more specific spectra of light at a broader range of intensities than *Synechococcus*. *Prochlorococcus* generally occupy depths from 25-200 m, and genetically distinct ecotypes have been identified based on their light requirements and nutrient preferences (Moore et al. 1998). Ecotypes abundant in the surface ocean are adapted to high light, low nutrient conditions, while ecotypes growing deeper in the

water column are adapted to lower light and utilize a broader range of nutritive substrates (Partensky, 1999). In contrast to *Synechococcus*, *Prochlorococcus* distributions tend to be limited to oligotrophic ocean environments in tropical and subtropical regions spanning from roughly 45°N to 40°S (Scanlan et al. 2009); however, a new lineage has recently been identified in the Antarctic polar waters of the Southern Ocean (A. Post, submitted).

Picophytoplankton also include diverse groups of eukaryotic cells, such as the Prasinophytes *Ostreococcus* and *Micromonas*. Photosynthetic picoeukaryotes have membrane bound chloroplasts and chlorophyll *a* based light harvesting apparatuses. These organisms are globally ubiquitous, and though their absolute cell numbers are generally lower than that of *Synechococcus* and *Prochlorococcus*, their slightly larger cell size makes them an important constituent of the particulate C biomass in the ocean. For example, in coastal areas photosynthetic picoeukaryotes can contribute up to 75% of coastal carbon fixation (Worden et al. 2004). However, they are also present in the oligotrophic oceans, where they have successfully colonized the deep euphotic zone. Assemblages within the same location often show high levels of diversity based on genetic analyses (Worden et al. 2004). Within the open ocean water column, the largest abundances of photosynthetic picoeukaryotes is typically near the deep chlorophyll maximum layer.

Diazotrophic cyanobacteria

Larger cyanobacteria cells also play important ecological roles in the marine environment. In this dissertation, two diazotrophic cyanobacteria are discussed. The

first is *Trichodesmium* spp., a genus of filamentous cells up to 2 mm in length that can exist as free floating filaments or as colonies. The second is *Cyanothece* spp., a coccoid single celled diazotroph 3-5 μm in diameter. These organisms are important because they contribute bioavailable N to oligotrophic waters. Interestingly, despite the fact that the nitrogenase enzyme responsible for the N_2 fixation reaction is poisoned by O_2 , PSII activity appears to be critically important for N_2 fixation in both genera. *Trichodesmium* spp. fix N_2 at maximal rates during daylight hours when photosynthetic activity, and hence O_2 production, are highest. These cells appear to have evolved a mechanism to consume O_2 from photosynthesis as soon as it is generated, thereby allowing their nitrogenase enzymes to remain functional (Kana 1993; Berman-Frank et al. 2001). In contrast, *Cyanothece* spp. utilizes a form of temporal regulation where photosynthesis and N_2 fixation each operate over 24 hour cycles that are 12 hours out of phase with each other (Sherman et al. 1998). *Trichodesmium* is a bloom forming organism that tends to be located in tropical and subtropical oligotrophic ocean environments. Less is known about the global distribution of *Cyanothece* spp., although limited metagenomic studies indicate it has similar distribution patterns to *Trichodesmium* spp. (OBIS 2010).

Diatoms

Diatoms are unicellular eukaryotic phytoplankton with an external frustule made of silicon (Si). Individual cells range in size from 2-1000 μm , and some are able to form chains. They can be classified as either centric (circular) or pennate (elongated), and approximately 100,000 diatom species exist in the modern ocean

(Hasle and Syvertsen 1997). Diatoms are important bloom forming organisms and can export significant amounts of C as they sink. Additionally, because the Si frustule accounts for up to half of the dry weight of a diatom cell, diatoms also play an important role in the biogeochemistry and sequestration of Si. Diatoms are commonly the dominant phytoplankton taxa in temperate and polar waters, and often bloom in response to Fe fertilization. Interestingly, diatom species inhabiting coastal and oceanic environments show remarkably different responses to Fe limitation. For example, oceanic species have lower amounts of Fe rich PSI than PSII (Strzepek and Harrison 2004), an adaptation that may have allowed them to colonize certain low Fe environments like the equatorial Pacific and the Southern Ocean.

Dinoflagellates

Dinoflagellates are large, motile flagellated protists (eukaryotes). About half of all dinoflagellate species are strictly heterotrophic and therefore cannot be classified as phytoplankton (Lalli and Parsons 1993). The other half are capable of autotrophy, but many adopt a mixotrophic strategy in which they graze on smaller phytoplankton and bacteria in addition to performing photosynthesis. Dinoflagellates generally inhabit coastal waters and, like diatoms, dinoflagellates are bloom forming organisms. A major issue of ecological and economic importance is the formation of red tides, in which dinoflagellates form intense blooms that visibly color the water, potentially forming neurotoxins that affect shellfish, marine mammals, and humans.

Dinoflagellates also play an important role in coral reefs, where they provide

fixed C for their cnidarian symbiotes in exchange for CO₂, nutrients, and protection from predation.

The overarching goal of this dissertation is to identify and understand how responses to changing resource availability influence the competitive success of phytoplankton, and to increase our understanding of how phytoplankton affect biogeochemical cycling of C and other important nutrients in the ocean. The following chapters each address a different aspect of the relationship between phytoplankton and the physical environment. The dissertation applies field, laboratory, and remote sensing approaches to answer key ecological questions, and draws on a wide range of biological and oceanographic techniques. The field research component includes measurements in the Gulf of Aqaba, Red Sea, the open ocean (Pacific and Atlantic), and coastal sites in California, Bermuda, and Hawai'i. The laboratory component has tested geographically-diverse strains of cyanobacteria to characterize physiological diversity. Methods include photosystem (PS) II fluorescence, ¹⁴C incorporation, bulk chlorophyll extraction, nutrient measurements (Lachat macronutrient analysis, ICP-MS trace metal analysis, bulk N and phosphorus, P), stable isotope techniques (¹⁸O and ¹⁵N in particulate and dissolved fractions), satellite image analysis (e.g. MODIS), phosphatase enzyme activity assays (enzyme labeled fluorescence ELF-97, PNP), flow cytometry, and microscopy. This dissertation shows that phytoplankton play an important role in the N, P, and C cycles by generating organic substrates from inorganic substrates. In doing so, phytoplankton contribute substantially to primary production in coastal and open

ocean habitats, and form an important link between the biotic and abiotic environment.

REFERENCES

- Arrigo, K. R. 2005. Marine micro-organisms and global nutrient cycles. *Nature* **437**: 349-355.
- Bassham J., A. Benson, M. Calvin. 1950. "The path of carbon in photosynthesis". *J Biol Chem* **185**: 781-7
- Berman-Frank I., P. Lundgren, Chen Yi-B, H. Küpper, Z. Kolber, B. Bergman, P. Falkowski. 2001. Segregation of nitrogen fixation and oxygenic photosynthesis in the marine cyanobacterium *Trichodesmium*. *Science* **294**: 1534-1537
- Falkowski, P. G. and J. A. Raven. 2007. *Aquatic Photosynthesis*, 2nd ed. Princeton University Press, Princeton, NJ.
- Field, C. B., M. J. Behrenfeld, J. T. Randerson, P. Falkowski. 1998. Primary production of the biosphere: Integrating terrestrial and oceanic components. *Science* **281**: 237 – 240
- Geider, R. J. 1992. Respiration: Taxation without representation? In: *Primary productivity and Biogeochemical Cycles in the Sea*. PG Falkowski and AD Woodhead, eds. New York, Plenum: 333-360
- Geider, R. J. and B. A. Osborne. 1989. Respiration and microalgal growth: a review of the quantitative relationship between dark respiration and growth. *New Phytol.* **112**: 327
- Hasle, G.R. E. E. Syvertsen. 1997. Marine Diatoms. In: *Tomas, C.R. Identifying marine diatoms and dinoflagellates*. Academic Press. pp. 5-385

- Kana T. M. 1993. Rapid oxygen cycling in *Trichodesmium thiebautii*. *Limnol. Oceanogr.* **38**: 18-24
- Keenan, J. D. and M. T. Auer. 1974. The influence of phosphorus luxury uptake on algal bioassays. *Water Pollution Control Federation* **46**: 532-542
- Kehoe, D. M. and A. R. Grossman. 1996. Similarity of a Chromatic Adaptation Sensor to Phytochrome and Ethylene Receptors. *Science* **273**: 1409 - 1412
- Klausmeier, C. A., E. Litchman, T. Daufresne, and S. A. Levin. 2004. Optimal nitrogen-to-phosphorus stoichiometry of phytoplankton. *Nature*. **429**: 171-174.
- Lalli, C. M. and T. R. Parsons. 1993. *Biological oceanography: an introduction*. Pergamon Press, New York, NY.
- MacArthur, R. H. 1972. *Geographical Ecology: patterns in the distribution of species*. Princeton University Press, Princeton, NJ.
- Moore L. R., G. Rocap, S. W. Chisholm. 1998. Physiology and molecular phylogeny of coexisting *Prochlorococcus* ecotypes. *Nature* **393**:464-468
- OBIS (Ocean Biogeographic Information System). [accessed March 2, 2010] www.iobis.org
- Partensky F. J., W. R. Hess, D. Vaultot. 1999. *Prochlorococcus*, a marine photosynthetic prokaryote of global significance. *Microbiology and Molecular Biology Reviews* **63**:106-127
- Platt, T., D. F. Bird, S. Sathyendranath. 1991. Critical depth and marine primary production. *Proceedings: Biological Sciences* **246**: 205-217
- Redfield, A. C. 1958. The biological control of chemical factors in the environment. *American Scientist*. **46**:221

- Sarmiento, J. and M. Bender. 1994. Carbon biogeochemistry and climate change. *Photosynthesis Research*. **39**:209-234
- Scanlan, D. J., M. Ostrowski, S. Mazard, A. Dufresne, L. Garczarek, W. R. Hess, A. F. Post, M. Hagemann, I. Paulsen, and F. Partensky. 2009. Ecological genomics of marine picocyanobacteria. *Microbiology and Molecular Biology Reviews* **73**: 249-299
- Sherman, L. A., P. Meunier, M. S. Colon-Lopez. 1998. Diurnal rhythms in metabolism: a day in the life of a unicellular, diazotrophic cyanobacterium. *Photosyn. Res.* **58**:25-42.
- Strzepek, R. F. and P. J. Harrison. 2004. Photosynthetic architecture differs in coastal and oceanic diatoms. *Nature* **431**:689-692.
- Stewart, R.H. 2003. Introduction to physical oceanography. Texas A&M University. Copyright by RH Stewart.
- Sverdrup, H. U. 1953. On conditions for the vernal blooming of phytoplankton. *J. Cons. Explor. Mer.* **18**:287-295
- Tilman, D. 1980. A graphical-mechanistic approach to competition and predation. *American Naturalist* **116**: 362-393
- Worden, A. Z., J.K. Nolan, B. Palenik. 2004. Assessing the dynamics and ecology of marine picophytoplankton: The importance of the eukaryotic component. *Limnol. Oceanogr.* **49**:168-174

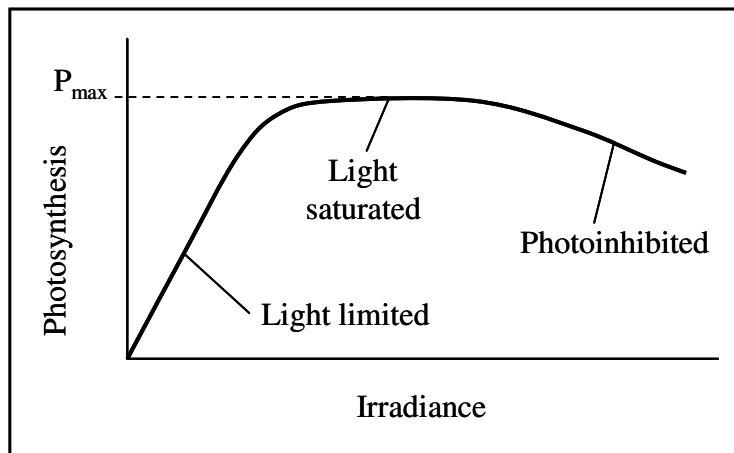


Figure 1: Photosynthetic rates are light dependent and follow a Michaelis-Menten type relationship. In the “light limited” portion of the curve, photosynthesis increases linearly with increasing irradiance. In the “light saturated” portion of the curve, a maximal photosynthetic rate is maintained even as irradiance increases. In the “photoinhibited” portion of the curve, photosynthetic rates decrease as irradiance increases. Figure is adapted from Lalli and Parsons (1993).

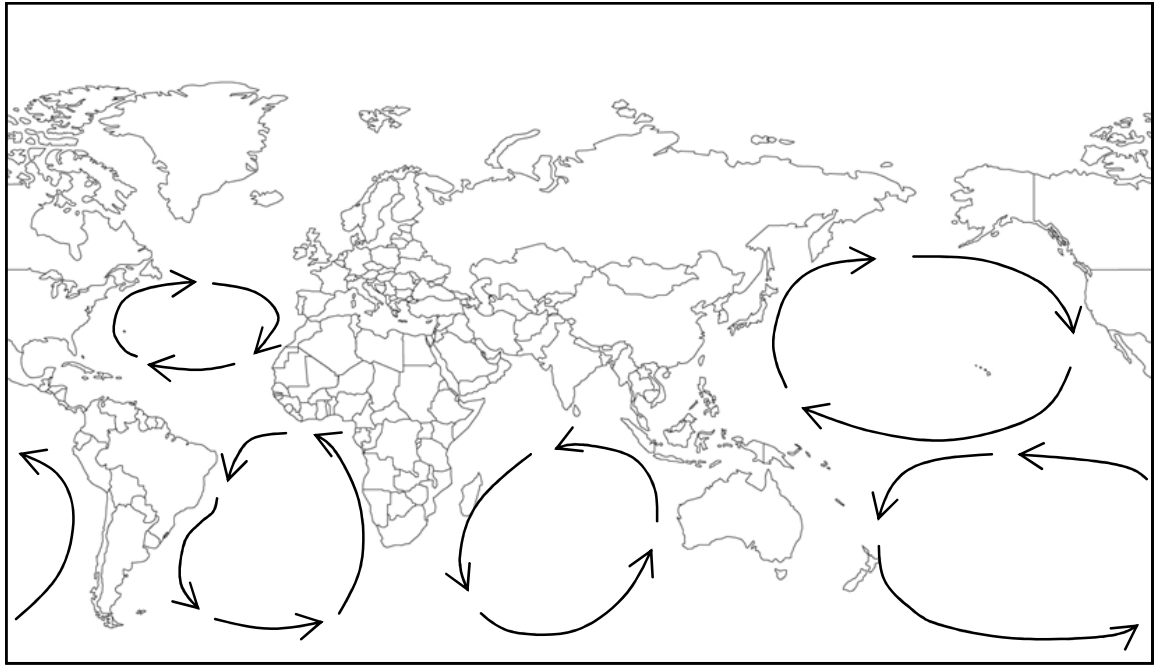


Figure 2: Schematic showing simplified surface circulation patterns of the central gyres in the ocean. Figure is adapted from Stewart (2003).

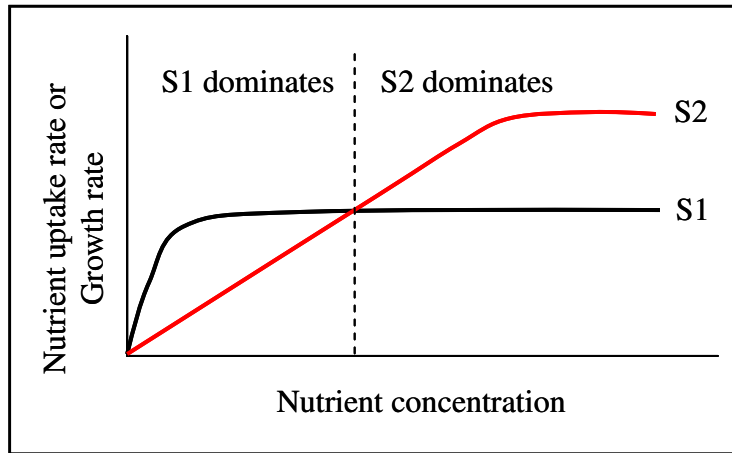


Figure 3: Nutrient uptake kinetics and phytoplankton growth rates are dependent on nutrient concentration and follow a Michaelis-Menten type relationship. In this hypothetical scenario, species 1 (S1, black curve) has a higher affinity for the nutrient and will dominate at low nutrient concentrations. In contrast, species 2 (S2, red curve) has a higher maximal uptake or growth rate and will dominate at higher nutrient concentrations. Figure is adapted from Lalli and Parsons (1993).

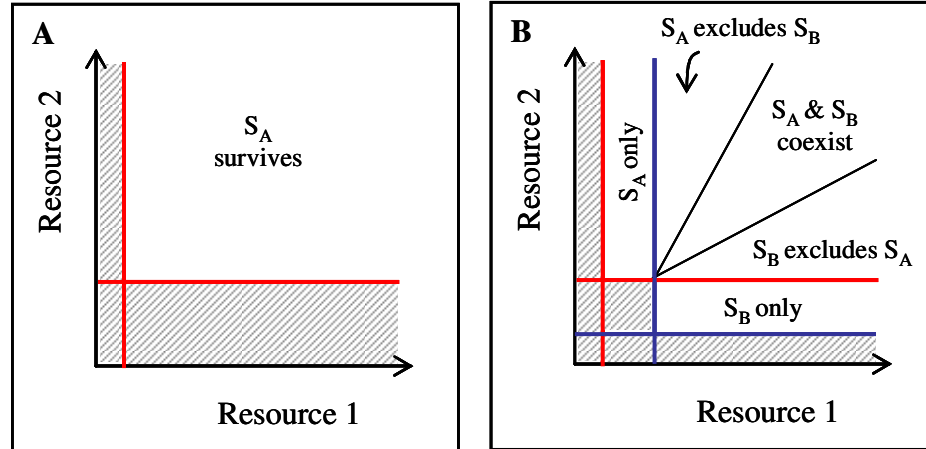


Figure 4: Graphical representations of the outcomes predicted by the resource ratio theory for two resources. (A) shows the range of conditions over which one species (S_A) can survive. When only S_A is present it can survive as long as both resources are available above the critical threshold levels for S_A (designated by red lines). Shaded regions indicate that one or both resources are below the critical threshold level, and S_A will not survive. (B) shows that when two species (S_A and S_B) compete for two resources, the theory predicts six possible outcomes based on the critical threshold levels of each resource for S_A (red lines) and S_B (blue lines): (1) both species die (shaded regions), (2) only S_A can survive, (3) only species S_B can survive, (4) both species can initially coexist but eventually S_A competitively excludes S_B , (5) both species can initially coexist but eventually S_B competitively excludes S_A , and (6) the two species coexist stably. Figure is adapted from Tilman (1980).

CHAPTER 2

THE PHOSPHORUS CYCLE

ABSTRACT

Microbially-mediated processes in the phosphorus cycle forge a critical link between the geosphere and biosphere by assimilating phosphorus within biological molecules and contributing to chemical transformations of phosphorus in the environment. In addition to acting as living reservoirs of phosphorus, microbes also contribute to the transformation of phosphorus within other non-living reservoirs, such as rock, soils, rivers, lakes, and oceans. Microbially-mediated phosphorus transformation includes processes that increase the bioavailability of phosphorus in the environment, such as weathering, solubilization, and mineralization, as well as those that decrease its bioavailability, such as assimilation and mineral formation. These large-scale environmental processes are the outcome of numerous biological pathways occurring in concert across diverse microbial communities. Genetic diversity and finely-tuned regulation of gene expression allow microbes to adapt and acclimate to harsh environments, and to contribute to the phosphorus cycle under numerous and diverse environmental conditions. Human alteration of the natural phosphorus cycle causes unintended consequences in microbial communities. Serious environmental, economic, esthetic, and human health problems can result from the proliferation of microbes in sensitive aquatic ecosystems as a consequence of anthropogenic introduction of excess phosphorus.

INTRODUCTION

Phosphorus is an essential nutrient for all living organisms, and the phosphorus cycle is an important link between Earth's living and non-living entities. The availability of phosphorus strongly influences primary production, the process by which photosynthetic organisms fix inorganic carbon into cellular biomass. Therefore, knowledge of the phosphorus cycle is critically important for understanding the global carbon budget and hence how biogeochemical cycles impact and are influenced by global climate.

The global significance of the phosphorus cycle

Natural assemblages of microbes have a critical role in the phosphorus cycle because they forge a link between phosphorus reservoirs in the living and non-living environment. Microbes facilitate the weathering, mineralization, and solubilization of non-bioavailable phosphorus sources, making orthophosphate available to microbial and plant communities and hence to higher trophic levels within the food web. However, microbes also contribute to immobilization of phosphorus, a process that diminishes bioavailable phosphorus by converting soluble reactive forms to insoluble forms. The mechanisms of microbial involvement in these processes vary from passive (e.g., resulting from microbial metabolic byproducts) to highly regulated active contributions (e.g., the regulation of gene expression in response to environmental cues).

Microbially-mediated processes also link the phosphorus cycle to the carbon cycle and hence to global climate. During photosynthesis, photoautotrophs incorporate

phosphorus and carbon at predictable ratios, with approximately 106 carbon atoms assimilated for every one phosphorus atom for marine photoautotrophs and terrestrial vegetation. The phosphorus cycle therefore plays an important role in regulating primary productivity, the process in which radiant energy is used by primary producers to form organic substances as food for consumers, as in photosynthesis.

Because phosphorus is required for the synthesis of numerous biological compounds, its availability in the environment can limit the productivity of producers when other nutrients are available in excess. This fact carries important implications for the global carbon budget because the rate of incorporation (fixation) of carbon dioxide into photosynthetic biomass can be directly controlled by the availability of phosphorus; if phosphorus is not available, carbon dioxide fixation is halted. The intersection of the phosphorus and carbon cycles is of particular significance for global climate, which is affected by atmospheric carbon dioxide levels. Hence, through the growth of producers the phosphorus cycle, along with other biogeochemical cycles, contributes to the regulation of global climate.

In aquatic environments photosynthetic microbes (i.e. phytoplankton) may comprise a substantial portion of the photosynthetic biomass and hence primary production. Marine and freshwater phytoplankton are characterized by extensive biodiversity and, as a group, inhabit an incredible number of different niches within aquatic environments. Phytoplankton, like other microbes, have strategies that enable them to acclimate to changes in the amounts and forms of phosphorus available within their environment. For example, the production of phosphatase enzymes, which hydrolyze organic P compound to generate inorganic phosphate, helps to mediate the

mineralization of organic phosphorus compounds in surface waters, and allows cells to acclimate when phosphate levels are low.

Recent estimates suggest that phytoplankton are responsible for as much as half of global carbon fixation, thereby contributing significantly to the regulation of Earth's climate. Phytoplankton productivity is strongly influenced by nutrient availability, and which nutrient ultimately limits production depends on (1) the relative abundance of nutrients and (2) the nutritional requirements of the phytoplankton. With some exceptions, production in most lakes is limited by the availability of phosphorus, whereas limitation of primary production in the ocean has traditionally been attributed to nitrogen, another nutrient required by cells in large quantities. However, phosphorus differs from nitrogen in that the major source of phosphorus to aquatic environments is the weathering of minerals on land that are subsequently introduced into water bodies by fluvial and aeolian sources. In contrast, microbially-mediated nitrogen fixation, in which bioavailable forms of nitrogen are generated from nitrogen gas in the atmosphere, is a major pathway by which phytoplankton gain access to nitrogen (in addition to continental weathering). Because there is no phosphorus input process analogous to nitrogen fixation, marine productivity over geological time scales is considered to be a function of the supply rate of phosphorus from continental weathering and the rate at which phosphorus is recycled in the ocean. Accordingly, the phosphorus cycle influences phytoplankton ecology, productivity, and carbon cycling in both marine and freshwater ecosystems.

Characterizing and measuring environmental phosphorus pools

Occurrence of elemental phosphorus in the environment is rare, given that it reacts readily with oxygen and combusts when exposed to oxygen, thus phosphorus is typically found in nature bound to oxygen. Phosphorus has the chemical ability to transfer a 3s or p orbital electron to a d orbital, permitting a relatively large number of potential configurations of electrons around the nucleus of the atom. This renders the structures of phosphorous-containing molecules to be quite variable and relatively reactive. These properties are likely responsible for the ubiquity and versatility of phosphorus-containing compounds in biological systems.

Because phosphorus exists in many different physical and chemical states in the environment, specific definitions are needed to clarify different parts of the phosphorus pool. Chemical names reflect the chemical composition of the phosphorus substance in question, whereas other classifications are based on methodological aspects of how the substance is measured. For example, “orthophosphate” is a chemical term that refers specifically to a phosphorus atom bound to four oxygen atoms – forming the orthophosphate molecule (PO_4^{3-} , also referred to as phosphate), whereas the term “soluble reactive phosphorus,” (SRP), is a methodological term referring to everything that gets measured when an orthophosphate assay is performed (such as the ascorbic acid method, described below). The majority of measured SRP comprises orthophosphate and other related derivatives (e.g. H_2PO_4^- , HPO_4^{2-} depending on pH) but other forms of P may be included as well due to experimental inaccuracy. Therefore, while SRP tends to closely reflect the amount of orthophosphate in a sample, the values may not be identical.

The most common assay for measuring SRP is the ascorbic acid method, which is approved by the US Environmental Protection Agency for monitoring phosphate in environmental samples. In this method, ascorbic acid and ammonium molybdate react with SRP in the sample forming a blue compound that can be observed visually or determined spectrophotometrically. Assays for measuring total phosphorus are also based on the ascorbic acid method, but begin with a step to transform all of the phosphorus in the sample to orthophosphate (typically through digestion by heating the sample in the presence of acid). Following digestion, the sample is analyzed by the ascorbic acid method. A filtration step is typically not included in either of these methods, and accordingly in such cases all size fractions are measured.

When phosphorus is measured in water samples, distinguishing forms that are part of particulate matter from those that are in solution is often useful. Phosphorus is therefore classified as “soluble” or “insoluble,” a distinction based on the method employed to measure the sample. Soluble phosphorus includes all forms of phosphorus that are distributed in solution and that pass through a filter with a given pore size (typically 0.45 μm), while the insoluble, or particulate fraction is the amount retained on the filter. Measurements of soluble phosphorus include both the “dissolved” and “colloidal” fractions. Dissolved phosphorus includes all forms that have entered a solute to form a homogenous solution. (For example, orthophosphate that is not bound to a cation is considered dissolved because it is associated with water molecules homogeneously in solution rather than being held within a salt crystal.) By contrast, colloidal forms include any tiny particles that are distributed evenly

throughout the solution but that are not dissolved in solution. Soluble phosphorus is commonly reported because colloidal phosphorus particles are very small, and differentiating between colloidal and dissolved phosphorus is methodologically difficult.

When living organisms assimilate phosphorus into their cells, the resulting phosphorus-containing compounds are collectively called “organic phosphorus.” It must be stressed that this definition of the biologically associated phosphorus as “organic phosphorus” is not identical to the chemical definition of organic compounds (e.g. containing carbon). For example some intracellular biologically synthesized compound such as polyphosphate may not contain C bonding. The term organic phosphorus encompasses molecules within living cells as well as molecules that are liberated into the environment following decay of an organism. The major source of terrestrial organic phosphorus is plant material, which is released as vegetation undergoes decay, but microbial and animal sources also contribute significantly. In the marine environment, organic phosphorus comes from a variety of sources (e.g. plankton, fish excrement, advection from land, etc), the relative contributions of which differ widely depending on location in the ocean. In contrast to organic forms, inorganic phosphorus compounds are not always directly of biogenic origin. Rather, they encompass also phosphorus derived from the weathering of phosphate containing minerals, including dissolved and particulate orthophosphate.

Phosphorus sources, sinks, and transport pathways

The phosphorus cycle encompasses numerous living and non-living environmental reservoirs and various transport pathways. In tracing the movement of phosphorus in the environment, the interplay between physical and biological processes becomes apparent. In addition to acting as reservoirs of phosphorus in the environment (as discussed in this section), microbes contribute to the transformation of phosphorus within other reservoirs such as in soil or aquatic environments (discussed below in section II, entitled “Microbially-mediated processes.”)

Within the earth’s crust, the abundance of phosphorus is 0.10-0.12% (on a weight basis), with the majority of phosphorus existing as inorganic phosphate minerals and phosphorus containing organic compounds. A phosphate mineral is any mineral in which phosphate anion groups form tetrahedral complexes in association with cations, although arsenate (AsO_4^{3-}) and vanadate (VO_4^{3-}) may also substitute into the crystalline structure. Apatite is the most abundant group of phosphate mineral, comprising hydroxyapatite, fluorapatite, and chlorapatite (**Table 1**). These three forms of apatite share nearly identical crystalline structures, but differ in their relative proportions of hydroxide, fluoride, and chloride, each being named for the anion that is most abundant in the mineral. Phosphate minerals generally form in the environment in magmatic processes or through precipitation from solution (which may be microbially-mediated), and the chemical composition of the minerals depends on the ion or ions present in solution at the time of precipitation. For this reason it is not uncommon for natural deposits of phosphate minerals to be heterogeneous, rather than composed of one homogenous type of phosphate mineral. These natural deposits of

phosphate minerals are collectively called “phosphorites” to reflect variations in their chemical compositions.

Soils and lake sediments are another terrestrial reservoir of phosphorus, comprising primarily inorganic phosphorus from weathered phosphate minerals, along with organic phosphorus from the decomposition, excretion, and lysis of biota (**Figure 1**). The behavior of phosphorus in soils is largely dependent on the particular characteristics of each soil and, in addition to microbial activity, factors such as temperature, pH, and the degree of oxygenation all influence phosphorus mobility. In soils, inorganic phosphorus is typically associated with Al, Ca, or Fe and each compound has unique solubility characteristics that determine the availability of phosphate to plants. The mobility and bioavailability of phosphate in soils is limited primarily by adsorption (the physical adherence or bonding of phosphate ions onto the surfaces of other molecules), and the rate of microbially-mediated mineralization of organic forms of phosphorus. Mineralization is discussed in detail below in section II, entitled “Microbially-mediated processes.”

Marine sediments also represent an important phosphorus reservoir, but because the physical and chemical factors affecting marine sediment differ considerably from those on land, processes controlling phosphorus dynamics in marine sediments are somewhat different than for soils. In marine sediment phosphate can be present in insoluble inorganic phosphates minerals (such as phosphorites) which are relatively immobile. Phosphate can also be sorbed onto iron or manganese oxyhydroxides. The sorbed phosphate can regain mobility in response to changes in the redox potential at the sediment-water interface and thus is considered more mobile.

As in terrestrial sediments, phosphorus in marine detrital organic matter can also become remobilized as decomposition progresses through microbially-mediated processes.

Biota (i.e. microbes, plants, and animals) serve as another reservoir of phosphorus in the environment, as they assimilate phosphorus within their cellular biomass. Biota can contribute significantly to environmental phosphorus levels; for example, microbial communities contribute 0.5-7.5% of total phosphorus in grassland and pasture topsoil, and up to 26% in indigenous forests. Microbes are also responsible for generating the myriad of organic phosphorus compounds found throughout the environment. In particular, microbes and primary producers play an important role in providing nutrition, including phosphorus, to higher trophic levels by making it biologically available (bioavailable). Phosphorus assimilation is a microbially-mediated process discussed in the “transitory immobilization” section below.

Phosphorus is transported within the environment through various mass transfer pathways. For example, rivers are important in the phosphorus cycle as both reservoirs and transport pathways. Phosphorus that has weathered from minerals and leached or eroded from soils enters rivers through a variety of vectors, including dissolved and particulate forms in water from overland flow and in groundwater, and particulates brought by wind. Approximately 95% of phosphorus in rivers is particulate, and approximately 40% of that is bound within organic compounds. Rivers influence the distribution of phosphorus in soils and lakes by contributing or

removing phosphorus, and riverine input is the single largest source of phosphorus to the oceans.

A number of outcomes are possible for phosphorus entering the ocean. Much of the riverine phosphorus flux is trapped in near shore areas of the ocean, such as continental margins and estuaries, through immediate sedimentation and biological assimilation. The remaining phosphorus enters the dynamic surface ocean, also called the euphotic zone, in which nearly all bioavailable phosphorus is sequestered within biota through primary production. Upon death of the organisms, a fraction of the biologically sequestered phosphorus sinks below the euphotic zone and most of it is regenerated into bioavailable forms like orthophosphate by heterotrophic organisms. This recycling is part of the so called “microbial loop.” Physical processes such as upwelling and deep convective mixing draw the deep water, which in most parts of the ocean is nutrient rich compared to the surface waters, back into the euphotic zone, where up to 95% of it is re-used in primary production. The remainder is removed from the ocean reservoir through particulate sedimentation, mineral formation (which may be microbially-mediated), and scavenging by iron and manganese oxyhydroxides, all of which deposit phosphorus as a component of ocean sediment.

The phosphorus cycle differs from the cycles of other biologically important elements, such as carbon, nitrogen, and sulfur, in that it lacks a significant gaseous component; nearly all phosphorus in the environment resides either in solid or aqueous forms. The one exception to this rule is the volatile compound phosphine (PH_3 , also called phosphane), a colorless, poisonous gas formed in the environment from the breakdown of alkali metal or alkali earth metal phosphides with water. This process is

poorly characterized and likely comprises various multistage chemical reactions. Microbially-mediated phosphine production can be a major source of the gas in engineered systems (e.g. sewage treatment facilities and constructed wastewater treatment wetlands) where organic phosphorus is abundant and reducing conditions are common, suggesting that microbes could also play a roll in phosphine formation in natural systems (although direct enzymatic production of phosphine has not yet been identified.) While phosphorus can exist as phosphine, the gas does not persist in the environment due to rapid autoxidation, precluding significant accumulation of phosphine in the atmosphere. Phosphine is therefore a minor component of the environmental phosphorus pool.

The absence of a significant gaseous phase does not eliminate the atmosphere as an important reservoir in the phosphorus cycle. When weathering and erosion of soils generates inorganic and organic particulate phosphorus, wind transports some of the particles from their source to a new location. These particles can include mineral dust, pollen and plant debris, insect fragments, and organic phosphorus bound to larger particles. This distribution of terrestrial particulate phosphorus, termed aeolian deposition, plays an important role in delivering nutrients to the oceans. In oligotrophic ocean waters where nutrient levels are naturally low, such as in the open ocean gyres where riverine inputs do not extend and significant upwelling does not occur, aeolian deposition may comprise a large portion of the nutrient flux that is available for primary production. The aeolian phosphorus flux to the oceans is approximately 1×10^{12} g yr⁻¹, of which approximately half is organic and half is inorganic. The solubility, and therefore bioavailability, of the phosphorus in aeolian

particulate matter differs significantly depending on its source; however, estimates suggest that approximately 15-50% is typically soluble.

MICROBially-MEDIATED PROCESSES

Weathering

Rock material exposed to the atmosphere breaks down, or weathers, as the result of numerous environmental processes. Weathering processes are classified into two categories. In mechanical weathering, physical processes (including thermal expansion, pressure release, hydraulic action, salt crystal formation, freeze-thaw, and frost wedge events) cause deterioration of rock material without changing the chemical composition of the parent material. In contrast, chemical weathering causes deterioration by altering the chemical structure of the minerals that the rock is made of. Chemical weathering processes include dissolution, hydrolysis, hydration, and oxidation-reduction (redox) reactions. Biological organisms can contribute to mechanical weathering by altering the microenvironments at the surface of the parent material (e.g., by increasing local humidity or forming bio-films on surfaces); however, most biological weathering processes are classified as chemical weathering because they chemically alter the composition of the parent rock material directly or indirectly. These biological weathering processes are also referred to as solubilization.

Solubilization

Inorganic phosphorus can occur in nature in soluble and insoluble forms. The solubility of the most abundant form of inorganic phosphorus, orthophosphate, is

determined by the ambient pH and the cation to which it is bound as a mineral (e.g. Ca^{2+} , Mg^{2+} , Fe^{2+} , Fe^{3+} , and Al^{3+}). Microbially-mediated phosphorus solubilization plays an important role in the conversion of insoluble phosphorus minerals to soluble forms of phosphorus. Solubilization directly benefits the microbes that perform it by providing bioavailable phosphorus needed for growth. Similarly, the process benefits other organisms (including other cells, fungi and higher plants) that can exploit the surplus of solubilized phosphorus.

Production of organic and inorganic acids is the primary mechanism of microbial phosphorus solubilization. In this process, biogenic acid interacts with phosphorus minerals to form mono and dibasic phosphates, thereby bringing phosphorus into solution. Chemoautotrophic bacteria (e.g. nitrifying bacteria and *Thiobacillus spp.*) generate nitric and sulfuric acids by oxidizing ammonium and sulfur respectively, and these acids are able to liberate soluble phosphorus from apatite, the most abundant phosphorus mineral. Production of organic acids occurs in numerous microbial taxa, and can also contribute to the solubilization of phosphorus minerals.

In addition to acid production, microbially-mediated redox reactions contribute to phosphorus solubilization through the reduction of iron oxyhydroxides and associated ferric phosphate (strengite). In this process, dissimilatory iron reduction of ferric phosphates liberates soluble ferrous iron as well as orthophosphate associated with it. This occurs under reducing conditions, such as in flooded, anoxic soils and in some benthic aquatic environments. In another redox process, hydrogen sulfide (H_2S) produced by sulfur reducing bacteria reduces the ferric iron in iron phosphate (FePO_4)

to ferrous iron. In this reaction iron sulfide and elemental sulfur are precipitated, and orthophosphate is generated.

Microbes also produce chelating compounds that contribute to phosphorus mineral solubilization. Chelation is the reversible binding (complexation) of a ligand to a metal ion. Chelators increase the solubility of insoluble phosphate mineral salts by complexing the metal cations, thereby making dissolution of the salt more energetically favorable. Examples of common chelators produced by microbes include citrate, oxalate, lactate and 2-ketogluconate.

Mineralization

Plant and animal detritus comprise a large reservoir of organic phosphorus in the soil environment. However, because organically bound phosphorus sources are generally unable to cross cell membranes, most of the organic phosphorus from the detrital pool is not directly available to many living organisms. In order to become bioavailable, phosphorus bound to organic material must first be mineralized to phosphate. Mineralization is the process in which organically bound phosphorus is converted to inorganic phosphate, which is accomplished through the activity of a suite of microbial enzymes. Because this process makes nutrients available that would otherwise be sequestered in non-reactive forms, mineralization provides a vital link between the detrital pool and living organisms. It is estimated that approximately 70-80% of soil microbes are able to participate in phosphorus mineralization.

In general, mineralization is optimal and more phosphorus is liberated in uncultivated soils than in soils undergoing extensive cultivation, and a higher

proportion of the organic phosphorus pool is mineralized in uncultivated soils. Further, mineralization rates tend to be higher in soils where inorganic phosphates are actively taken up and sequestered in plants and where microbial grazers are present, as would be expected in mature, uncultivated soils with fully developed, autochthonous (native) microbial communities and trophic structures. As in many enzyme catalyzed systems, mineralization is encouraged by higher levels of available substrate; however, high levels of inorganic phosphate (the product) do not impede the reaction, and mineralization will occur even if an abundance of phosphate is present. Other ambient conditions favoring phosphorus mineralization include warm soil temperatures and near-neutral pH values; conditions that also favor mineralization of other elements. Accordingly, phosphorus mineralization rates tend to reflect rates of ammonification and carbon mineralization in soils, and together these microbially-mediated mineralization processes yield a C:N:P ratio that is similar to the ratio of these elements in humus (i.e. the organic soil fraction consisting of decomposed vegetable or animal matter.)

Enzymes involved in mineralization comprise a diverse group of proteins, called phosphatases, with a broad range of substrates and substrate affinities, and varying conditions for optimal activity. In addition, phosphatases can either be constitutively expressed by an organism, or the expression can be up-regulated under conditions of low phosphate (and in some cases, low carbon). Enzyme synthesis allows microbial cells to access organic phosphorus during periods of phosphate limitation, thereby avoiding the growth limitation and physical stress associated with nutrient deprivation. Phosphatases can be classified on the basis of the type of carbon-

phosphorus bond they cleave, but any given phosphatase enzyme may catalyze reactions for numerous organic phosphorus compounds. In other words, a phosphatase enzyme has specific substrate requirements for a class of compounds, but lacks specificity in selecting substrates from within that class. The most common categories of microbial phosphatases contributing to phosphorus mineralization include phosphomonoesterases, phosphodiesterases, nucleases and nucleotidases, as well as phytases.

Phosphomonoesterases catalyze reactions with phosphomonoesters, which are compounds in which one phosphate group is covalently bound to one carbon atom. The reaction involves the hydrolysis of the phosphorus-carbon bond, generating a free phosphate molecule and an alcohol as products. One examples of a phosphomonoester is glycerol phosphate, a source of phosphate and carbon for some microbes. Phosphomonoesterases are further classified as “acid” or “alkaline” on the basis of their optimal pH ranges for maximum catalytic activity. Probably as a result of their ubiquity and importance in phosphorus mineralization, phosphomonoesterases tend to be referred to simply as phosphatases in the scientific literature, rather than by their full name, and context is often necessary to determine which group is being referenced. Therefore, a phosphomonoesterase with a pH optima near 8 might be referred to as an “alkaline phosphatase” rather than an “alkaline phosphomonoesterase” in the scientific literature.

A similar class of enzymes, phosphodiesterases, attack diester bonds in which a phosphate group is bonded to two separate carbon atoms, such as in phospholipids and nucleic acids. For example, the sugar-phosphate backbone in DNA comprises

phosphodiester bonds. Cleaving of a diester proceeds similarly to the monoester reaction, with water added across the phosphorus-carbon bond yielding phosphate and an alcohol. Once a diester has undergone hydrolysis, the resulting alcohol phosphomonoester must undergo another hydrolysis step, catalyzed by a phosphomonoesterase, in order for phosphorus mineralization to be complete.

Nucleic acids represent an important source of organic nutrients and are released from a cell upon lysis. Their rapid degradation and relatively low concentrations in the environment suggest an important role for nucleic acids as microbial nutrient sources. Many heterotrophic microbes are able to use nucleic acids as their only source of phosphorus, nitrogen and carbon, and numerous others can use nucleic acids to supplement their nutritional requirements. The mineralization of phosphorus from nucleic acids proceeds in a two-step process involving two different enzymes. In the first step, depolymerizing nuclease enzymes such as deoxyribonuclease (DNase) for DNA and ribonuclease (RNase) for RNA, cleave the nucleic acid molecules into their constituent monomer nucleotides. Complete phosphorus mineralization of the resulting fragments proceeds via the activity of nucleotidase enzymes, which yield a phosphate group and a nucleoside molecule following hydrolysis.

Phytins, which are complex organic molecules containing up to six phosphate groups, are mineralized by a class of enzymes called phytases. Phytases catalyze hydrolysis of the phosphate ester bonds that attach phosphate groups to the inositol ring, yielding reactive phosphate and a series of lower phosphoric esters. The location on the ring of the first hydrolysis reaction catalyzed by a phytase determines its

classification; 3-phytases initiate hydrolysis at the phosphate ester bond of the ring's third carbon atom, while 6-phytases initiate hydrolysis at the sixth carbon. Hydrolysis by 6-phytases always leads to complete dephosphorylation of the inositol ring, whereas the 3-phytases may lead to incomplete dephosphorylation. Phytases are produced broadly by microbes, plants, and animals. In general, plants produce 6-phytases and microbes produce 3-phytases; however, 6-phytase activity has been observed in *E. coli*. Microbial phytase activity is optimal over a broader range of pH values than plant phytases, with pH optima spanning from 2 to 6 (plant phytases are optimal near pH 5). In addition to being affected by ambient pH, hydrolysis by phytases is also influenced by the degree of complexation of the phytin substrate with metal cations

Because many phosphatase enzymes are synthesized in response to low environmental phosphate levels (i.e., when the cells experience phosphate limitation), phosphatase activity has been used extensively as a metric for determining the nutrient status of microbial communities. The activity of phosphatase enzymes has been measured in many terrestrial, limnic, and marine environments using a variety of methods, and numerous laboratory studies have also been conducted. In the environment, the bulk phosphatase activity of an entire microbial community is commonly measured by incubating soil, sediment, or water samples with a phosphate-bound substrate in which the hydrolytic product undergoes a color change that can be observed visually or spectrophotometrically, such as *para*-nitrophenyl phosphate (PNP) (**Figure 2A,B**), phenolphthalein phosphate (PPP), glycerophosphate, and 5-bromo-4-chloro-3-indolyl-phosphate (**Figure 2C**). In addition, measurements can be

made fluorometrically for the substrates 3-o-methylfluorescein phosphate (MFP) and 4-methylumbelliferyl phosphate (MUP). Radiometric analyses can similarly be made using ^{32}P labeled glycerol phosphate (or an equivalent molecule). Chemical analysis of the hydrolytic products of glycerol phosphate and other bioenergetically important molecules has also been used to estimate phosphatase activity in bulk populations.

A major drawback to measuring bulk phosphatase activity is that it provides limited information, if any, about which members of the microbial community experience phosphate limitation at the time of sampling. This can be addressed to some extent by size fractionating cells (as on a filter) prior to incubation with the substrate, thereby allowing phosphatase activity to be assigned to gross taxonomic classes of organisms. However, size fractionation introduces other obstacles for data interpretation, and results must be interpreted with care. For example, activity in different size fractions can be skewed by groups of bacteria that coalesce to form larger particles, although the individual cells are small and would otherwise be grouped with smaller size fractions. Studies with mixed populations of bacteria and green algae showed that 44% of the measured phosphatase activity was attributable to aggregated groups of cells. Moreover, in the marine environment substantial phosphatase activity has been shown to persist for 3-6 weeks at 50% of initial levels in water samples filtered to remove particles. These observations suggest that phosphatases free in solution or bound to soluble organic material can contribute a significant amount of phosphatase activity, potentially leading to overestimates of phosphatase activity in the small-cell size fraction. A difficulty common to both bulk and size fractionated samples is that phosphatases can persist for long periods of time

without being bound to a living cell. It is not uncommon for microbial cells to retain phosphatase activity for months or years after being dried or preserved, indicating that cell viability is not critical for maintaining phosphatase enzymes over these time periods, and dead cells may contribute to the overall phosphatase activity in a sample.

Several methods have been developed to overcome the limitations of bulk measurements by directly labeling cells when phosphatases are present. These methods allow phosphatase activity to be attributed to individual cells or taxa, allowing greater resolution of the phosphate status of organisms within a mixed community. Direct cell staining with azo-dyes or precipitation of lead phosphate at the site of enzyme-mediated phosphate release have been used together with light microscopy to visualize phosphatase activity on individual cells. Similarly, enzyme labeled fluorescence (ELF) labels individual cells with a fluorescent precipitate (ELF-97) following hydrolysis of the non-fluorescent substrate molecule ((2-(5'-chloro-2'-phosphoryloxyphenyl)-6-chloro-4-(3H)-quinazolinone) at the site of the enzyme (**Figure 2c**).

Immobilization

Immobilization refers to the process by which labile phosphorus is sequestered and removed from the environmental reservoir of reactive phosphorus for a period of time. Immobilization processes can generally be grouped into two categories. The first category, transitory immobilization or cellular assimilation, includes all processes that sequester phosphorus within living microbial cells and is rapidly reversible upon

cell death. The second category, mineral formation, encompasses processes that generate phosphorus-containing minerals.

Transitory immobilization

Transitory immobilization, or assimilation, is an important mechanism of phosphorus sequestration in soil and freshwater environments. Within cells, phosphorus is incorporated in numerous essential biological molecules and is required in larger quantities than many other elements. However, unlike other biologically important nutrients such as nitrogen and sulfur that must first undergo reduction prior to being incorporated into the cell, phosphorus remains oxidized before and after assimilation. Because mineralization of cellular material occurs rapidly following cell death, cellular assimilation of phosphorus into biological macromolecules leads to relatively short-term phosphorus retention in living cells where the duration is related to the characteristics of the microbial community in question. Within the cellular reservoir phosphorus is present as different compounds and serves various functions.

Phospholipids are triacylglycerides in which a phosphate group has replaced one of the fatty acid groups. Lipids are generally hydrophobic; however, phospholipids are amphipathic, meaning that each molecule has a hydrophilic portion and a hydrophobic portion. The phosphate group is responsible for giving phospholipids their partially hydrophilic character, hence imparting a wide range of biochemical properties. In the cell, phospholipids are important in the formation of biological membranes and in some signal transduction pathways.

Nucleotides are biological compounds consisting of a pentose sugar, a purine or pyrimidine base, and one or more phosphate groups. Nucleotides are the structural subunits (monomers) of RNA and DNA, and alternating bonds between the sugar and phosphate groups form the backbones of these nucleic acids. Specifically, the phosphate groups form phosphodiester bonds between the third and fifth carbon atoms of adjacent sugar rings, hence imparting directionality to the molecule. In addition, nucleotides are present as several major cofactors in the cell (e.g. flavin adenine dinucleotide (FAD), nicotinamide adenine dinucleotide phosphate (NADP), etc) that have important functions in cell signaling and metabolism.

Adenosine triphosphate (ATP) is a nucleotide that performs multiple functions of considerable importance to the cell. The primary function of ATP is to aid in intracellular energy transfer by storing chemical bond energy that is generated during photosynthesis and respiration so that it can be used in other cellular processes that require energy (e.g. cell division and biosynthetic reactions). In the cell, phosphate can be assimilated in ATP through substrate level phosphorylation, oxidative phosphorylation, photo-phosphorylation, and via the adenylate kinase reaction. ATP is also active in signal transduction pathways, where it can be used as a substrate for kinase enzymes in reactions that transfer phosphate groups to proteins and lipids, forming phosphoproteins and phospholipids respectively. Phosphorylation is an important and ubiquitous form of signal transduction in many organisms.

Phytic acid (also called inositol hexaphosphate, IP6, phytate, and myo-inositol 1,2,3,4,5,6-hexakis dihydrogen phosphate) is an organic, phosphorylated, cyclic, sugar alcohol produced by plants and found in high concentrations in seeds, but may also be

produced by microbes. In its fully phosphorylated form, six phosphate groups attach to the inositol ring; however, various isomers of the less-highly substituted inositol phosphate molecules also exist. Phytic acid is a highly reactive compound that forms stable complexes with a variety of mineral cations (e.g. Zn^{2+} , Fe^{2+} , Mn^{2+} , Fe^{3+} , Ca^{2+} , Mg^{2+}), as well as proteins and starches within mature seeds and when present in the environment. The complexed form of phytic acid, also known as phytin, can be a persistent phosphorus reservoir in the environment because it is less accessible to degradation by hydrolytic enzymes when complexed.

In addition to biological molecules like nucleic acids and phospholipids, which by weight consist primarily of carbon along with smaller portions of phosphorus, the intracellular accumulation of polyphosphate granules in microbial cells is an important type of transitory phosphorus immobilization. Polyphosphates are chains of 3-1000 phosphate residues connected by anhydride bonds that form through the activity of polyphosphate kinase enzymes, and therefore represent a highly concentrated reservoir of phosphorus in the cell. The energy stored in the anhydride bonds can be used by the microbial cell during periods of starvation. Polyphosphates are also involved in signaling within the cell. They serve as ligands for metal cations such as calcium, aluminum, and manganese in some microbes; however, the extent and elemental stoichiometry of intracellular polyphosphate cation complexation varies among organisms.

Phosphorus immobilized within cells is considered transitory because it is able to rapidly reenter the reactive phosphate pool following cell death through microbially-mediated mineralization processes. The immobilization of phosphorus via

cellular assimilation is therefore relatively brief (i.e., within the lifetime of a cell) compared to other processes within the phosphorus cycle, some of which occur over geological time scales.

Phosphate mineral formation

Phosphate mineral formation represents another phosphorus sink that is influenced by microbial activity; however, it encompasses processes other than cellular assimilation and short-term storage of phosphorus as biological molecules. In mineral formation (also called phosphogenesis), phosphate anions react with cations in the environment to form insoluble precipitates. Sediments that comprise significant amounts of phosphorus-containing minerals are called “phosphorites,” and may contain apatite, francolite, and a number of other phosphorus minerals. Mineral formation is generally an important mechanism of phosphorus sequestration in marine environments where the high seawater calcium levels facilitate microbially-mediated formation of insoluble phosphorites. The sequestration of phosphorus by this process retains (immobilizes) phosphorus for longer periods of time than does transitory immobilization.

In order for an insoluble mineral to form, the concentration of the ions forming the mineral should be high enough such that super saturation is reached and equilibrium of the precipitation reaction is shifted toward the product. In addition, the physical and chemical characteristics of the environment must be conducive to precipitation of that mineral based on its solubility characteristics, and factors such as pH, redox state, and concentrations of co-occurring ions all influence mineral

precipitation. The mineral should also be stable in the environment for mineral formation to constitute a long term sink for phosphorus.

Mineral formation occurs both authigenically and diagenetically in the environment. Authigenic mineral formation is the formation of insoluble precipitates (minerals) *in situ* rather than by having been transported or deposited in a location through secondary processes. In contrast, diagenetic mineral formation is the alteration of existing minerals by chemical changes occurring after the initial deposition of a mineral (i.e. during or after burial and lithification). The primary type of diagenetic phosphorus mineral formation in marine environments is the substitution of phosphate into calcium carbonate minerals such as calcite or aragonite. Microbes contribute to this process by mineralizing organic phosphorus to reactive phosphate, which then substitutes diagenetically into calcium carbonate.

In authigenic mineral formation, microbes may generate reactive phosphate from the mineralization of organic phosphorus sources, and the resulting localized high phosphate concentrations favor precipitation of phosphate minerals. In soils, microbes convert organic phosphorus to phosphate increasing its concentration in the soil and promoting formation of stable minerals such as apatite. In productive areas of the ocean, microbial mineralization of detrital matter at the sediment-water interface generates reactive phosphate, some of which reacts with seawater calcium to form phosphorite. (Reactive phosphate that does not contribute to mineral formation is available for biological assimilation by benthic microbes, or may be reintroduced to the euphotic zone by diffusion and upwelling for use by phytoplankton.)

The accumulation of phosphorus in microbial cells during transitory immobilization also contributes to mineral formation by increasing the pool of phosphate that could react with cations to form minerals. This is particularly important in anoxic areas of the ocean and soils where reactive phosphorus levels are low. Under oxic conditions where reactive phosphate is more abundant, luxury uptake and storage of phosphate as polyphosphate molecules occurs in some microbes (e.g. *Pseudomonas spp.*, *Actinobacter spp.*), as discussed above. Cells use the energy stored in polyphosphates to activate an alternative organic electron acceptor when conditions shift toward anoxia, freeing substantial levels of reactive orthophosphate in the process. The sequestration and release of phosphate by the cell under oxic and anoxic conditions respectively represents a mechanism by which microbes contribute to mineral formation because it generates locally-elevated reactive phosphate concentrations in the vicinity of the cells that are high enough to induce precipitation of minerals. Accumulation of phosphate within cells may also lead to phosphorus immobilization via mineral formation if phosphorus minerals are generated and stored within the cell. Intracellular formation of mineral apatite is an example of phosphorus immobilization that has been observed in some microbes (e.g. *Escherichia coli*, *Bacterionema matruchotii*) following incubation with calcium phosphate at a slightly basic pH. This process occurs in living and dead cells, suggesting that the locally-elevated reactive phosphate concentrations within the cell help initiate apatite formation. Similarly, the formation of carbonate fluorapatite following cell death has been observed in Gram-negative rods, possibly pseudomonads, in coastal marine

sediment, and is thought to be an important phosphorite formation process in locations where sedimentation rates are low.

GENETIC REGULATION OF MICROBIALLY-MEDIATED PROCESSES

Microbially-mediated processes, including those involved in the phosphorus cycle, are the outcome of numerous biological pathways occurring in concert across diverse microbial communities. Even cursory observations of natural microbial communities demonstrates that while microbially-mediated processes influence and change the environment, the environment likewise shapes the activity of microbes, in many cases by providing feedback that either inhibits or enhances the processes. (An example of this type of feedback is the synthesis of phosphomonoesterase enzymes, many of which are only present during periods of orthophosphate deprivation but not when orthophosphate is abundant in the environment.) Likewise, microbially-mediated processes can also be controlled indirectly by secondary factors (other than phosphorus) that influence growth and metabolism, such as the availability of oxidized nitrogen or sulfur in some chemoautotrophic microbes.

These processes, which are manifest in the environment as the combined outcome of activities from a diverse microbial community, are in fact a result of genetic mediation within single cells. The regulation of genes in response to environmental stimuli determines how a cell will respond to its environment, including if and how it will contribute to microbially-mediated processes in the phosphorus cycle. To understand gene regulation in greater detail, highly sensitive genetic and molecular methods have been developed. Under laboratory conditions,

these methods have elucidated pathways important in the immobilization (i.e. phosphorus assimilation into cell biomass) and mineralization (i.e. phosphatase production) of phosphorus, as well as countless other pathways and processes.

In *E. coli*, two major phosphate uptake pathways have been identified. The phosphate transport system (Pit), which comprises a proton-phosphate symport powered by proton motive force, is expressed constitutively and provides the cell with sufficient phosphorus for growth when phosphate concentrations in the media are not limiting. When media phosphate concentrations drop below a threshold concentration, the high affinity phosphate specific transport (Pst) system becomes engaged. This system has a 100 fold greater affinity for phosphate than Pit, enabling the cell to acquire phosphate from a limited reservoir. Uptake of phosphate through Pst is an ATP dependent process (e.g. requires energy input from the cell).

Pst is activated as part of the Pho regulon, a group of operons that is expressed when phosphate levels are low. Activation of the Pho regulon is initiated through phosphorylation of the PhoB cytoplasmic protein which, in its phosphorylated state, is a transcriptional activator of the operons within the Pho regulon. In addition to Pst, the Pho regulon also includes genes encoding alkaline phosphomonoesterase (PhoA), outer-membrane porin proteins that facilitate diffusion of phosphate into the periplasm (PhoE), and proteins for the uptake and processing of glycerol-3-phosphate (*ugp* operon) and phosphonates (*phn* operon).

Metabolism of glycerol-3-phosphate is an interesting strategy for heterotrophic microbes, such as *E. coli*, because it is a potential source of both phosphate and carbon for the cell. However, when grown under phosphate deplete conditions and

expressing *ugp* genes, cells are only able to use glycerol-3-phosphate as a phosphate source, not as a carbon source. In order for cells to grow with glycerol-3-phosphate as the only phosphate source, another carbon source must also be provided. The *ugp* system is less efficient when internal cell phosphate levels are high, and is no longer expressed if external phosphate levels increase above a threshold level. Another system that is not part of the Pho regulon, the *glp* transport system, is regulated by external and internal glycerol-3-phosphate levels rather than phosphate concentrations. Unlike in the Ugp system, glycerol-3-phosphate acquired by the Glp system is able to serve as the sole source of carbon and phosphate for the cell. Both Ugp and Glp systems facilitate direct cellular uptake of glycerol-3-phosphate; however, each is regulated by different internal and external cues (i.e. phosphate or glycerol-3-phosphate levels), and has a different nutritional strategy (i.e. supplying phosphate alone versus phosphate and carbon together).

These two systems are an example of how microbes, by developing multiple inter-related pathways, are able to contribute to microbially-mediated processes in the phosphorus cycle under a range of environmental and physiological conditions.

Experimental evidence shows that the phosphate assimilation pathways in other heterotrophic bacteria are similar to *E. coli*, and many microbes are known to have portions of the Pho regulon. In particular, the alkaline phosphomonoesterase gene (*phoA*) and homologues have been identified in numerous microbial taxa, and although the primary function of the protein remains the same, factors that influence its expression and activity vary from organism to organism. The diversity of organisms and environmental conditions in which this gene exist allow microbially-

mediated mineralization of phosphorus to occur in nearly every environment where microbes are found. For example, photosynthetic cyanobacteria in the genus *Synechococcus*, which populate freshwater environments, coastal waters, and vast areas of the open ocean, have the *phoA* gene along with many of the other genes encoded in the Pho regulon, highlighting the global ubiquity of microbially-mediated processes in the phosphorus cycle.

ANTHROPOGENIC ALTERATION OF THE P CYCLE: EUTROPHICATION IN AQUATIC ECOSYSTEMS

As discussed above, microbes have an important role in nearly every aspect of the phosphorus cycle, and their activities help control the relative rates at which phosphorus is mobilized and immobilized within the environment. However, humans also influence the phosphorus cycle and alter the structure of microbial communities, causing devastating ecological consequences.

Post-industrial human activities, including deforestation, phosphorus mining, and agricultural practices affect the phosphorus cycle by increasing the mobility of phosphorus in the environment and causing it to accumulate in soils and aquatic environments. Several factors contribute to the mobilization of phosphorus by these activities. Deforestation and mining expose phosphate (and other) minerals in rock and soil to the atmosphere, leading to increased rates of weathering and erosion. Agricultural soils are also highly susceptible to erosion, making the localized elevation of phosphorus levels from application of fertilizers a particularly large source of the anthropogenic phosphorus flux. As a result of these practices, recent estimates

suggest that the net storage of phosphorus in terrestrial and freshwater habitats has increased 75% over pre-industrial levels, and the total reactive phosphorus flux to the ocean is 2-fold higher than pre-human levels. Consequently, eutrophication (the excessive growth of phytoplankton in response to over-enrichment of a growth limiting nutrient) has become a widespread problem in lakes and estuaries throughout the world, carrying serious environmental, economic, esthetic, and human health consequences. Eutrophication has been observed in many ecosystems, including fresh water lakes like Lake Erie, large estuaries like the Chesapeake Bay, and coastal areas like the hypoxic “dead zone” of the Gulf of Mexico.

Organic fertilizers (e.g. poultry litter, manure) are typically applied to crops based on the rate of crop nitrogen uptake, resulting in over application of phosphorous and its rapid accumulation in soils. Elevated soil phosphorus levels increase the amount of phosphorus in runoff and ultimately lead to the accumulation of phosphorus in lakes and estuaries. When phosphorus from agriculture application is washed into water bodies where phosphorus limits production, substantial changes in the microbial community occur. Reversal of phosphorus limitation leads to the rapid growth of bloom-forming phytoplankton, some of which are toxic or nuisance species (like *Pfiesteria sp.*) that are harmful to aquatic organisms and humans. As the bloom exhausts the supply of phosphorus the phytoplankton senesce, sink to the bottom of the water body, and are decomposed by the heterotrophic microbial community. At depth, where light levels are low, photosynthetic phytoplankton are not able to balance the metabolic oxygen demands of the heterotrophs, and anoxia occurs in the bottom waters. Anoxia damages the benthic environment, leading to fish kills and harming

benthic invertebrate communities. Loss of submerged aquatic vegetation, coral reef death, human shellfish poisoning, and a reduction in biodiversity are among the possible outcomes caused by microbial responses to the anthropogenic introduction of excess phosphorus to sensitive aquatic ecosystems.

CONCLUSION

Microbially-mediated processes in the phosphorus cycle forge a critical link between the geosphere and biosphere by assimilating phosphorus within biological molecules and contributing to chemical transformations of phosphorus in the environment. In addition to acting as living reservoirs of phosphorus, microbes also contribute to the transformation of phosphorus within other non-living reservoirs, such as rock, soils, rivers, lakes, and oceans. Microbially-mediated phosphorus transformation includes processes that increase the bioavailability of phosphorus in the environment, such as weathering, solubilization, and mineralization, as well as those that decrease its bioavailability, such as assimilation and mineral formation. These large-scale environmental processes are the outcome of numerous biological pathways occurring in concert across diverse microbial communities. Genetic diversity and finely-tuned regulation of gene expression allow microbes to adapt to harsh environments, and to contribute to the phosphorus cycle under numerous and diverse environmental conditions. Human alteration of the natural phosphorus cycle causes unintended consequences in microbial communities, and serious environmental, economic, esthetic, and human health problems are caused by microbial responses to the anthropogenic introduction of excess phosphorus to sensitive aquatic ecosystems.

ACKNOWLEDGEMENTS

I acknowledge my co-author A. Paytan on this paper, which was published in 2009 in the *Encyclopedia of Microbiology*.

KRMM was supported through the National Science Foundation (NSF) Graduate Research Fellowship Program and the Department of Energy (DOE) Global Change Education Program.

Citation

Mackey, KRM and A Paytan. 2009. “Phosphorus Cycle”, in *The Encyclopedia of Microbiology*, 3rd Edition, Moselio Schaechter, ed., Elsevier.

Author contributions

KRMM– performed literature review; wrote the manuscript

AP- provided comments on the manuscript

FURTHER READING

- Alexander, M. 1967. Microbial transformations of phosphorus. *In* Introduction to soil microbiology, 2nd edition. John Wiley and Sons New York, NY.
- Compton, J., D. Mallinson, C. R. Glenn, G. Filippelli, K. Follmi, G. Shields, and Y. Zanin. 2000. Variations in the global phosphorus cycle: *in* Glenn, C.R., et al., eds., Marine authigenesis: From global to microbial: SEPM (Society for Sedimentary Geology) Special Publication 66.
- Dyhrman, S. T., J. W. Ammerman, and B. A. S. Van Mooy. 2007. Microbes and the marine phosphorus cycle. *Oceanography* **20**: 110-116.
- Ehrlich, H. L. 1999. Microbes as geologic agents: their role in mineral formation. *Geomicrobiology Journal* **16**: 135-153.
- Ehrlich, H. L. 2002. Geomicrobial interactions with phosphorus. *In* Geomicrobiology. 4th edition. CRC Press, Inc. New York, NY.
- Follmi, K. B. 1996. The phosphorus cycle, phosphogenesis and marine phosphate-rich deposits. *Earth-Science Reviews* **40**: 55-124.
- Heath, R. T. 2005. Microbial turnover of organic phosphorus in aquatic systems. *In* Organic Phosphorus in the Environment. B. L. Turner, E. Frossard and D. S. Baldwin, eds. CABI Publishing Cambridge, MA.
- Oberson, A., and E. J. Joner. 2005. Microbial turnover of phosphorus in soil. *In* Organic Phosphorus in the Environment. B. L. Turner, E. Frossard and D. S. Baldwin, eds. CABI Publishing Cambridge, MA.

- Paytan, A. and K. McLaughlin. 2007. The oceanic phosphorus cycle. *Chem. Rev.* **107**: 563-576.
- Ruttenberg, K. C. 2003. The global phosphorus cycle. *Treatise on Geochemistry*, Volume 8. Editor: William H. Schlesinger. Executive Editors: Heinrich D. Holland and Karl K. Turekian. pp. 682. ISBN 0-08-043751-6. Elsevier, 2003., p.585-643.
- Sharpley, A. N., T. Daniel, T. Sims et al. 2003. Agricultural phosphorus and eutrophication. 2nd edition. U.S. Department of Agriculture, Agricultural Research Service, ARS 149
- Stewart, J. W. B., and H. Tiessen. 1987. Dynamics of soil organic phosphorus. *Biogeochemistry* **4**: 41-60.
- Sundby, B., C. Gobeil, N. Silverberg et al. 1992. The phosphorus cycle in coastal marine sediments. *Limnology and Oceanography* **37**: 1129-1145.
- USEPA. 1983. Methods for chemical analysis of water and wastes. 2nd edition. Method 365.2. U.S. Environmental Protection Agency, Washington, DC.
- USEPA. 1996. Environmental indicators of water quality in the United States. Environmental Protection Agency, Washington, DC.
- Whitton, B. A., A. M. Al-Shehri, N. T. W. Ellwood et al. 2005. Ecological aspects of phosphatase activity in cyanobacteria, eukaryotic algae and bryophytes. *In* Organic Phosphorus in the Environment. B. L. Turner, E. Frossard and D. S. Baldwin, eds. CABI Publishing Cambridge, MA.

Table 1: Phosphate minerals and their chemical compositions. Apatite is the general term for the three minerals hydroxylapatite, fluorapatite, and chlorapatite.

Apatite	$\text{Ca}_5(\text{PO}_4)_3(\text{F}, \text{Cl}, \text{OH})$
Hydroxylapatite	$\text{Ca}_5(\text{PO}_4)_3\text{OH}$
Fluorapatite	$\text{Ca}_5(\text{PO}_4)_3\text{F}$
Chlorapatite	$\text{Ca}_5(\text{PO}_4)_3\text{Cl}$
Frankolite	Ca_{10-a-b}
	$\text{Na}_a\text{Mg}_b(\text{PO}_4)_{6-x}(\text{CO}_3)_{x-y-z}(\text{CO}_3\text{F})_y(\text{SO}_4)_z\text{F}_2$
Lazulite	$(\text{Mg}, \text{Fe})\text{Al}_2(\text{PO}_4)_2(\text{OH})_2$
Monazite	$(\text{Ce}, \text{La}, \text{Y}, \text{Th})\text{PO}_4$
Pyromorphite	$\text{Pb}_5(\text{PO}_4)_3\text{Cl}$
Strengite	$\text{FePO}_4 \cdot 2\text{H}_2\text{O}$
Triphylite	$\text{Li}(\text{Fe}, \text{Mn})\text{PO}_4$
Turquoise	$\text{CuAl}_6(\text{PO}_4)_4(\text{OH})_8 \cdot 5\text{H}_2\text{O}$
Variscite	$\text{AlPO}_4 \cdot 2\text{H}_2\text{O}$
Vauxite	$\text{FeAl}_2(\text{PO}_4)_2(\text{OH})_2 \cdot 6\text{H}_2\text{O}$
Vivianite	$\text{Fe}_3(\text{PO}_4)_2 \cdot 8\text{H}_2\text{O}$
Wavellite	$\text{Al}_3(\text{PO}_4)_2(\text{OH})_3 \cdot 5\text{H}_2\text{O}$

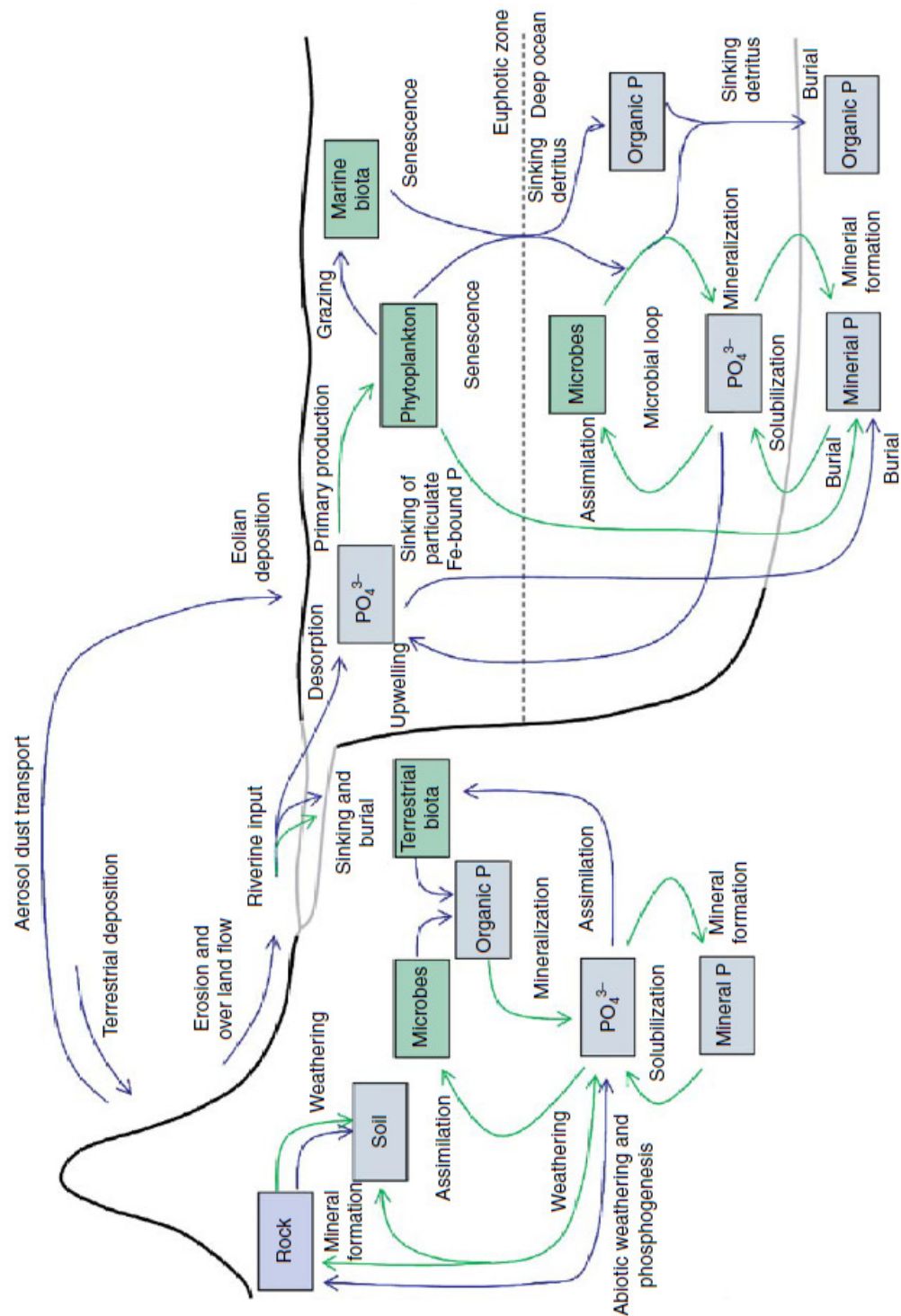


Figure 1: Schematic diagram of the phosphorus cycle showing phosphorus reservoirs (living in green boxes; non-living in blue boxes), physical transport pathways (blue arrows), and microbially-mediated transformations (green arrows).

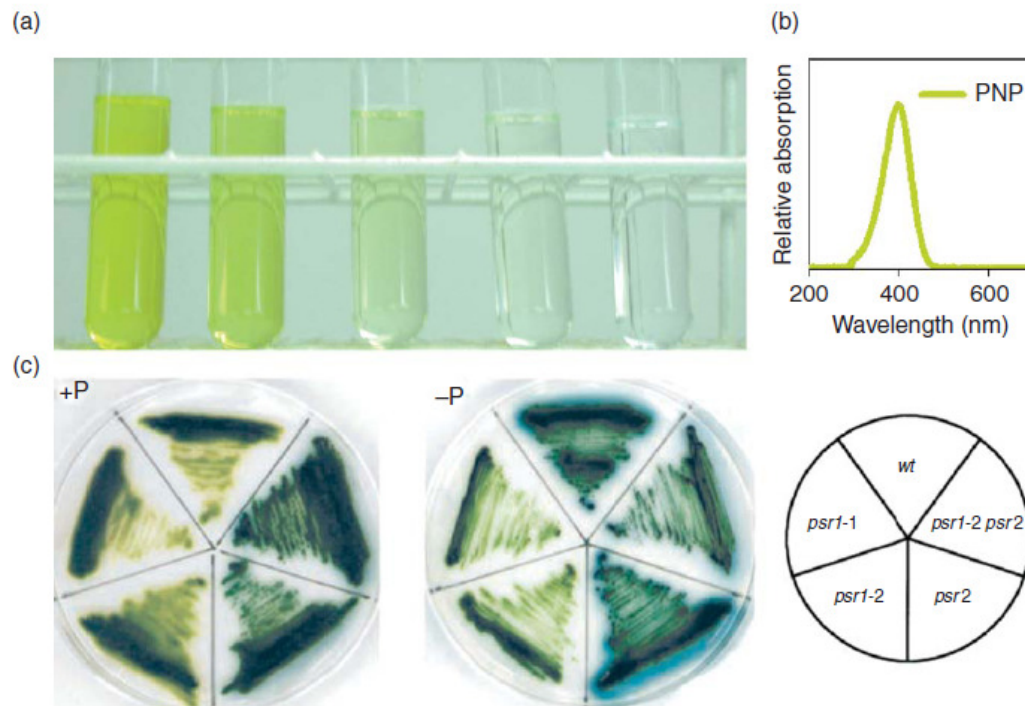


Figure 2: (A) The *para*-nitrophenyl phosphate (PNP) assay for alkaline phosphatase activity produces a yellow color in the presence of the enzyme. (B) The PNP assay quantifies alkaline phosphatase activity based on the absorption of light at 380nm. (C) The 5-bromo-4-chloro-3-indolyl-phosphate assay with *Chlamydomonas* algae under phosphate replete (left) and phosphate limited (middle) conditions shows phosphatase activity using the blue coloration formed around the cells when they express the enzyme. Key (right) identifies mutants used in the study (wt is wild type). The phosphatase of the wild type cells is induced in phosphate-free medium. Reproduced with permission from K. Shimogawara, D. D. Wykoff, H. Usuda, and A. R. Grossman. 1999. *Chlamydomonas reinhardtii* mutants abnormal in their responses to phosphorus deprivation. *Plant Physiology* 120: 685–693. Copyright 1999 by the American Society of Plant Biologists.

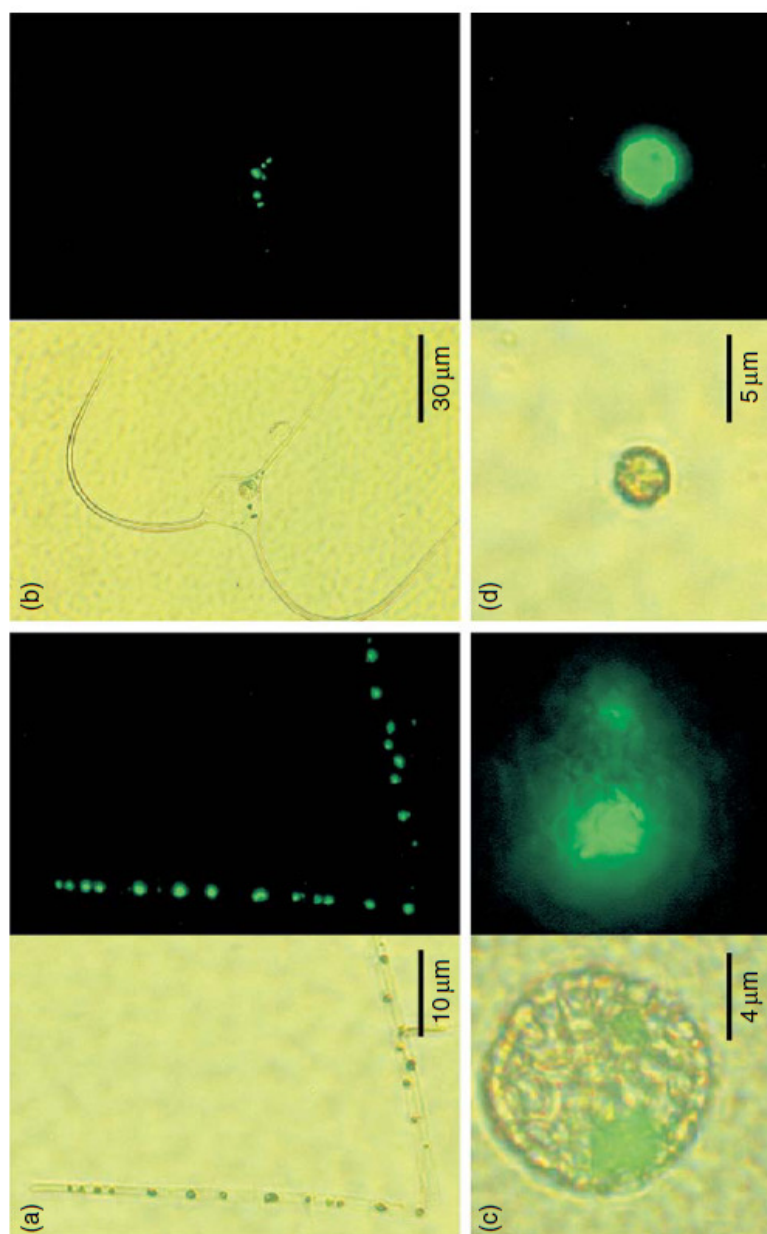


Figure 3: Micrographs of ELF-97 labeled phytoplankton from the euphotic zone in the Gulf of Aqaba (A) *Trichodesmium* sp., (B) *Ceratium* sp., (C) coccolithophore, and (D) *Cyanoshece* sp. For each pair, the left panel is a view under visible light and the right panel under UV illumination. ELF-97 labeled areas appear as bright areas under UV illumination and show the location of phosphatase enzymes on the cells. Reproduced with permission from K. R. M. Mackey, R. G. Labiosa, M. Calhoun, J. H. Street, A. F. Post , and A. Paytan. 2007. Phosphorus availability, phytoplankton community dynamics, and taxon-specific phosphorus status in the Gulf of Aqaba, Red Sea. *Limnology and Oceanography* 52: 873-885. Copyright 2007 by the American Society of Limnology and Oceanography, Inc.

CHAPTER 3

PHOSPHORUS AVAILABILITY, PHYTOPLANKTON COMMUNITY DYNAMICS, AND TAXON-SPECIFIC PHOSPHORUS STATUS IN THE GULF OF AQABA, RED SEA

ABSTRACT

The relationships among phytoplankton taxon-specific phosphorus-status, phytoplankton community composition, and nutrient levels were assessed over three seasons in the Gulf of Aqaba, Red Sea. During summer and fall, stratified surface waters were depleted of nutrients and picophytoplankton populations comprised the majority of cells (80% and 88% respectively). In winter, surface nutrient concentrations were higher and larger phytoplankton were more abundant (63%). Cell specific alkaline phosphatase activity (APA) derived from enzyme labeled fluorescence was consistently low (<5%) in the picophytoplankton population throughout the year, whereas larger cells expressed elevated APA (up to 68% labeling in some taxa) during the summer and fall but less in the winter. A nutrient addition bioassay during the fall showed that following addition of orthophosphate along with a nitrogen source, APA in larger cells was reduced by half relative to the control, whereas the APA of picophytoplankton groups remained low (<1%) across all treatments. These results indicate that the most abundant phytoplankton in the Gulf are not limited by orthophosphate and only some subpopulations (particularly of larger cells) exhibit orthophosphate-limitation throughout the year. Our results indicate that

orthophosphate availability influences phytoplankton ecology, correlating with shifts in phytoplankton community structure and the nutrient status of individual cells. The role of dissolved organic phosphorus as an important phosphorus source for marine phytoplankton in oligotrophic settings and the need for evaluating nutrient limitation at the taxa and/or single cell level (rather than inferring it from nutrient concentrations and ratios or bulk enzyme activity measurements) are highlighted.

INTRODUCTION

In oligotrophic oceans, phytoplankton growth, and community dynamics are strongly influenced by nutrient availability, and which nutrient ultimately limits production depends on the relative abundance of these nutrients with respect to the phytoplankton nutritional requirements (Redfield et al., 1963). Nutrient limitation of primary production in the ocean has traditionally been attributed to nitrogen (N) and, more recently, iron (Fe) availability; however, phosphorus (P) has been suggested as the ultimate limiting nutrient over geologic time scales (Redfield 1958, Follmi, 1996; Tyrrell 1999). The major source of P to the ocean is the weathering of minerals on land that are subsequently introduced into the ocean by fluvial and aeolian sources (Filippelli and Delaney, 1996; Benitez-Nelson, 2000). Because there is no P input process analogous to N fixation, marine productivity over geological time scales is considered to be a function of the supply rate of P from continental weathering and the rate at which P is recycled in the ocean (Scanlan and Wilson 1999). Accordingly, these factors and their effect on P input to the ocean are believed to be responsible for long term changes in marine ecology, phytoplankton productivity, carbon dioxide fixation, and carbon cycling via the biological pump (Follmi, 1996; Toggweiler 1999; Tyrrell 1999).

In recent years it has been recognized that P limitation in the ocean may be more prevalent than previously estimated, and that the efficiency of P uptake among individual groups of phytoplankton may in fact control the phytoplankton species composition observed in a given community. In the Sargasso Sea, orthophosphate (Pi) is suspected to play an important role in limiting production (Wu et al., 2000;

Ammerman et al., 2003). Research in the Pacific Ocean gyres indicates that biological Pi uptake rates far surpass the combined input from atmospheric and deepwater sources, suggesting that P is efficiently recycled within oligotrophic euphotic zones (Bjorkman and Karl, 1994). Further, it has been suggested that a transition from N limitation to P limitation has taken place over the last two decades in the North Pacific Subtropical Gyre, and that this favors the growth of prokaryotic picophytoplankton, such as *Prochlorococcus* and *Synechococcus*, which have a large surface area to volume ratio and take up nutrients more efficiently than larger phytoplankton (Karl et al., 2001). It is generally accepted that Pi is the limiting nutrient in parts of the Mediterranean sea based on findings of high N/P ratios (Krom et al., 1991), short turnover times for Pi (Thingstad and Rassoulzadegan, 1995) and high alkaline phosphatase activity (Thingstad and Mantoura, 2005). However, a recent study revealed that while the bacterial and copepod populations were P-limited, the phytoplankton populations in the Mediterranean Sea were limited by both N and P (Thingstad et al. 2005).

The N to P molar ratio (N:P) of dissolved inorganic N (DIN) to soluble reactive P (SRP) in surface seawater, when compared to the Redfield ratio of 16:1 (originally described by Redfield, Ketchum and Richards in 1963), traditionally forms the basis to evaluate which nutrient is limiting marine primary productivity (Redfield et al., 1963; Tyrrell, 1999). This approach, however, may be a poor measure of nutrient limitation for several reasons: (1) analytically determined DIN and SRP may deviate from “true” nutrient concentrations and do not necessarily reflect the bio-available fractions (Baldwin, 1998; Benitez-Nelson, 2000), (2) nutrient requirements

and uptake rates change with taxonomic affiliation and phytoplankton nutrient status and could differ from the Redfield ratio (Falkowski, 2000; Geider and LaRoche, 2002; Arrigo 2005), and (3) efficient nutrient uptake and recycling may satisfy the nutrition demands of the phytoplankton community despite low absolute nutrient concentrations. Accordingly, interpreting nutrient concentrations and their ratios in the water column as indicators of phytoplankton growth limitation must be done with caution (Cañellas et al., 2000; Hudson et al., 2000), and physiological (Scanlan et al., 1997) and molecular (Lindell et al., 2005) measures of nutrition status are better indicators of nutrient limitation of the growth of a particular phytoplankton taxon.

The activity of the enzyme alkaline phosphatase (AlkP) is induced by low Pi concentrations in many phytoplankton species (Dyhrman and Palenik, 1999; Lomas et al. 2004). Therefore, alkaline phosphatase activity (APA) is indicative of the P-status (specifically Pi limitation) of the phytoplankton groups in which it is measured. This enzyme hydrolyzes dissolved organic P (DOP) to Pi, which can then be taken up by the phytoplankton (Chrost, 1991; Karl and Yanagi, 1997). APA can be measured in environmental samples either through bulk (community) or cell-specific assays. Bulk APA has been used as a physiological indicator of Pi-stress in marine (1988; Li et al., 1998; Stihl et al., 2001) and other aquatic systems (Rose and Axler, 1998). However, bulk APA does not provide information about the specific groups of organisms expressing the enzyme activity. Moreover, it may include heterotrophic bacterial activity, which may overestimate the autotrophic component (Nicholson et al., 2006). To obtain information regarding the P-status of specific groups of marine phytoplankton, a cell-specific APA enzyme label fluorescence (ELF) assay, allowing

rapid qualitative assessment of the in situ physiological condition of phytoplankton with respect to Pi limitation, has been developed and used (Gonzalez-Gil et al., 1998; Dyhrman and Palenik, 1999).

In this study, we examined seasonal changes in the cell specific APA of phytoplankton populations collected at several locations and water depths in the Northern Gulf of Aqaba. The Gulf of Aqaba, Red Sea, is an oligotrophic region with a predictable seasonal cycle in macronutrient concentrations and phytoplankton community structure that is similar to other large oligotrophic areas of the world's oceans, such as the open ocean gyres. The Gulf's accessibility from land therefore provides a convenient opportunity to conduct investigations on the interplay between phytoplankton nutrient status, community dynamics, and water chemistry in an oligotrophic marine system. Changes in the dominance of phytoplankton groups occur as the deep mixing conditions in the winter relax and stratification intensifies, beginning in the early spring and continuing through the summer. Specifically, a bloom of eukaryotic nanophytoplankton characteristic of the winter-summer transition is replaced by a summer community dominated by picophytoplankton (cells <2 μm), of which *Prochlorococcus* and *Synechococcus* are the most numerous (Lindell and Post, 1995). Previous research (Lindell and Post, 1995; Labiosa et al., 2003) however, could only speculate about the driving forces behind this seasonal succession. Although Pi-limitation among the bulk community has been suggested based on bulk APA (Li et al. 1998), the authors were not able to comment on the limitation status of individual plankton taxa. The goal of the present study was to investigate how the Pi status varies among various phytoplankton groups in the Gulf during three major

seasons (winter, summer, and fall), and to determine how the nutrient dynamics of this system may influence natural phytoplankton assemblages from the individual to community level.

MATERIALS AND METHODS

Sampling

Water samples were collected from the Northern Gulf of Aqaba (Fig. 1) during three field excursions in the summer (August 2003), winter (March 2004), and fall (November 2004) seasons. Depth profiles were taken at stations A (29°28'N, 34°55'E) and B (29° 22'N, 34° 53'E), in Israeli and Jordanian waters, respectively, using a sampling CTD-Rosette (SeaBird) equipped with 12 L Niskin bottles, and water was transferred to large (8-20 L) low-density, flexible polyethylene cubitainers that had been previously rinsed with sample water. Stations A and B are located away from shore in open water. Both stations are located in deep (>700m) regions of the Northern Gulf away from coastline areas, thereby allowing for deep profiles to be taken and for the entire euphotic zone to be sampled. In addition, surface samples were collected from ~1 m depth at 15 sites located at various distances from shore and proximity to recreational and industrial areas along the coast. These samples were typically taken 1-2 days before or after the depth profile samples were taken, and thus represent different conditions both spatially and temporally. Surface temperature and salinity for the latter samples were measured with a digital probe (YSI). Water samples were pre-filtered over a 100 µm nylon mesh to remove zooplankton grazers and collected into cubitainers as described above. The cubitainers were shaded during

transport, and were delivered to the laboratory at the Inter University Institute (IUI) for Marine Science in Eilat, Israel within 2 hours of collection. Samples from all sites and depths were analyzed for dissolved nutrient concentrations, and samples from within the euphotic zone were also analyzed for chlorophyll *a* (Chl *a*) and cell-specific APA. Typical euphotic depths were approximately 60 m in the winter and 100 m in the summer and fall.

Nutrient analysis

Nitrate, nitrite, and SRP samples were analyzed using colorimetric methods described by Hansen and Koroleff (1999), and modified for a Flow Injection Autoanalyzer (FIA, Lachat Instruments Model QuickChem 8000). SRP was pre-concentrated by a factor of about 20 using the magnesium co-precipitation (MAGIC) method (Karl and Tien 1992), followed by measurement using the FIA. Total oxidized nitrogen and nitrite were measured using the FIA, and nitrate concentrations were calculated as the difference of total oxidized nitrogen and nitrite. The FIA was fully automated and peak areas were calibrated using standards prepared in low nutrient filtered seawater (summer surface water from the Gulf) over a range of 0-10 $\mu\text{mol L}^{-1}$. Using standard additions the recovery of inorganic P in this procedure was determined to be 100% and the blank was always below detection limits. The precision of the methods used in this work is 0.05 $\mu\text{mol L}^{-1}$ for NO_2 and NO_3 , and 0.02 $\mu\text{mol L}^{-1}$ for SRP. The detection limit was 0.02 $\mu\text{mol L}^{-1}$ for SRP, and 0.02 $\mu\text{mol L}^{-1}$ for nitrate and nitrite. At SRP levels near the limit of detection, dissolved arsenate has been shown to contribute to the analytically determined SRP in some systems

(Johnson, 1971; Karl and Tien 1992); however, a test for arsenate showed that it did not contribute significantly to the analytically determined SRP in our samples (T. Rivlin, personal communication). Ammonium levels were assessed with the fluorescence method employing ortho-phthalaldehyde as described by Holmes et al. (1999) with a precision of $0.01 \mu\text{mol L}^{-1}$ and a detection limit of $0.02 \mu\text{mol L}^{-1}$. We note that Pi is the biologically relevant form of P and low Pi levels stimulate APA; however, SRP is the form measured analytically. SRP concentrations tend to closely reflect the amount of Pi in the water although they are not necessarily identical (Benitez-Nelson, 2000). Therefore, to distinguish between these components in this study we use SRP when actual measurements are reported, whereas Pi is used when discussing APA and the physiological responses of cells.

Chl *a* measurement

Chl *a* measurements were made fluorometrically. Duplicate water samples (250 mL) were filtered through Whatman GFF filters. Surface samples were filtered upon arrival at the IUI laboratories, whereas samples from the deep casts were immediately filtered aboard the research vessel. Filters were placed in 10 mL vials and extracted using 90% acetone saturated with MgCO_3 (10 mL per filter) for 24 hours in the dark at 4°C . The extract was analyzed fluorometrically before and after acidification with 3.7% HCl on a Turner Fluorometer.

Enzyme labeled fluorescence (ELF) assay

Cell specific alkaline phosphatase activity (APA) was measured using the procedure for ELF-97 labeling as described in Dyhrman and Palenik (1999). In brief, approximately 5 L of seawater were filtered through Supor filters (Pall) (0.8 μm filters in August 2003 and 0.2 μm filters in March and November 2004) under a maximum pressure of 15 kPa, either in the laboratory at IUI (for surface water samples) or aboard ship (for the depth profiles). Cells were gently eluted from the filter with 1 mL of 70% ethanol, transferred into sterile microcentrifuge tubes, and allowed to incubate in the dark at 4° C for 30 minutes. The cells were then pelleted by centrifugation at 3,000 rpm for 5 minutes and the supernatant was discarded. The pellet was resuspended and incubated in 95 μL sterile seawater and 5 μL ELF-97 reagent (Molecular Probes) for 45 minutes in the dark, followed by centrifugation and removal of the supernatant. Cells were washed three times by alternating suspension and centrifugation in 100 μL sterile seawater, followed by a final suspension in 35 μL sterile seawater. Samples were stored in the dark at 4° C until microscopic analyses were done.

Microscopy

Samples were mounted on microscope slides using a small drop of mounting medium plus 5-8 μL of the seawater-cell suspension, and were viewed under a Nikon epifluorescent microscope with a DAPI filter set at 400X magnification. Digital photographs of the slides were captured for visible light and ultra violet irradiated conditions. Slides were visually scanned, and each cell was tallied as either positive or negative for ELF labeling based on the presence or absence of the fluorescent green

ELF-97 precipitate. For the purposes of this analysis, cells other than picophytoplankton (i.e., cells $> 2 \mu\text{m}$ in diameter) were binned into four groups on the basis of their taxonomy. The groups included two diazotrophic genera, *Trichodesmium* and *Cyanothece*, of the division Cyanophyta (cyanobacteria), members of the division Prymnesiophyta (coccolithophores), and a fourth group composed of all other cells $> 2 \mu\text{m}$ referred to as “nanoplankton” group (cells between 2-20 μm). This last group included all other families that are less abundant in the Gulf, such as Chlorophyta (green algae), Bacillariophyta (diatoms), and Dinophyta (dinoflagellates). While coccolithophores, *Trichodesmium*, and *Cyanothece* are classified on the basis of size as nanoplankton, they were grouped independently in this study; therefore, references to “nanoplankton” in this paper refer only to other groups of phytoplankton $>2 \mu\text{m}$ that were not coccolithophores, *Trichodesmium*, or *Cyanothece*. The term “non-picophytoplankton” is used when referring to the coccolithophore, *Cyanothece*, *Trichodesmium*, and nanoplankton groups collectively. The majority of phytoplankton cells in our samples were less than 20 μm in diameter. Figure 2 shows representative micrographs of ELF-97 labeled cells for the phytoplankton groups discussed herein.

The relative number of cells counted from each group provides a semi-quantitative estimate of phytoplankton group abundance for each sample and, because of the large volume filtered, offers the benefit of including groups of organisms that are relatively rare. The cell abundance data should be considered qualitative because the actual cell number per volume seawater was not determined on the same sample aliquots and it is possible that some cells were lost during the ELF sample preparation

procedure. It is also possible that due to their small size the picophytoplankton cell numbers were underestimated by this method (particularly in summer when filters with larger pore size were used). However, since the same procedure was applied the general differences in distribution of various taxa between seasons should be internally consistent across all samples compared herein. The average standard error for triplicate counts of 100 cells using the ELF-97 labeling technique was determined to be 3% by Dyhrman and Palenik (1999), and similar error is expected in the present study, where whenever possible greater than 100 cells in each group were counted for each sample (and in the case of picophytoplankton, the number of counts was often much higher). Counts from all 15 surface samples were combined into one analysis for each season (likely reducing the error to below 3% for these measurements), while depth profile measurements each reflect one sample per depth.

Nutrient addition bioassays

Nutrient addition bioassays were conducted to ascertain phytoplankton APA responses to the individual and combined effects of fertilization with inorganic nutrients and aerosol dust. Surface water was collected at 1 m depth from sampling station A in November, 2004. Eight liters of surface water per sample was pre-filtered over 100 μm nylon mesh to remove zooplankton grazers and collected into large (10 L) sample-rinsed, low-density, translucent polyethylene cubitainers. Water was shaded during transport, and arrived at the laboratory at the Inter University Institute (IUI) for Marine Science in Eilat, Israel within 2 hours of collection.

Samples were treated with various combinations of inorganic nutrients and aerosol dust. Samples given inorganic nitrogen received sodium nitrate (NaNO_3 , final concentration $20 \mu\text{mol L}^{-1}$) and ammonium chloride (NH_4Cl , final concentration $20 \mu\text{mol L}^{-1}$) together, samples treated with inorganic phosphorus received sodium phosphate monobasic (NaH_2PO_4 , final concentration $1 \mu\text{mol L}^{-1}$), and samples treated with inorganic iron received iron (II) sulfate (FeSO_4 , final concentration $0.016 \mu\text{mol L}^{-1}$). Samples receiving dust treatments were fertilized with approximately 6 mg aerosol dust collected previously on site at IUI, and dust additions were selected from a series of days with a common air mass back trajectory. Following nutrient additions, the samples were incubated for four days within a large flow-through outdoor tank through which water from the Gulf was circulated. A mesh tarp was used to attenuate the sunlight intensity reaching the samples. Following the four days of incubation, 5 L of each sample was assayed for APA using the ELF-97 assay as described above.

RESULTS

Density, Chl *a*, and nutrient concentrations of samples from depth transects and surface stations (Figs. 3 and 4) reveal a well-defined seasonal pattern that is driven by alternating periods of stratification and mixing in the Gulf of Aqaba. During the winter season the upper 300 m of the water column was well-mixed, and at the end of winter (March) surface nutrient concentrations were consistently higher than during the summer stratified season (August) (Fig. 4). November represents the beginning of fall, a time when short-term mixing episodes take place (adding nutrients to the

euphotic zone) followed by re-establishment of stratified conditions during warm days and rapid depletion of nutrients in the surface layer.

The nutrient depth profiles (Fig. 3) reveal nitrate concentrations that were 20 times higher in the winter ($1 \mu\text{mol L}^{-1}$) than in the summer and fall ($<0.05 \mu\text{mol L}^{-1}$) in the top 120 m of the water column. SRP concentrations remained low and close to the detection limit throughout the upper 120 m in the summer, increasing gradually with depth below 120 m, while winter concentrations were low but measurable ($0.04\text{--}0.08 \mu\text{mol L}^{-1}$). Mixing during the winter was also evident from the uniform distribution of Chl *a* with depth. The Chl *a* concentration was approximately $0.35 \mu\text{g L}^{-1}$ throughout the euphotic zone in the winter, whereas in the summer and fall Chl *a* was lower at the surface (0.1 and $0.2 \mu\text{g L}^{-1}$) and reached maximal concentrations (0.3 and $0.4 \mu\text{g L}^{-1}$) deeper within the euphotic zone (deep Chl *a* maxima).

The averaged nutrient concentration of the 15 surface water samples (Fig. 4) indicate that in winter SRP, nitrate, and ammonium concentrations were $0.04 \mu\text{mol L}^{-1}$, $0.37 \mu\text{mol L}^{-1}$, and $0.06 \mu\text{mol L}^{-1}$ respectively, whereas in the summer and fall these levels were near the limit of detection. It should be noted that nutrient concentrations for the combined surface samples (e.g. the average of 15 distinct stations sampled at 1 m depth) differ somewhat from the surface nutrient levels reported in the depth profiles for stations A and B. This is due to spatial and temporal variability, as discussed in the materials and methods section. Specifically, in winter the samples were collected during the transitional period at the end of winter/ beginning of spring, and the surface water samples were taken 1-2 days after the depth profiles. During this time the water column began to stratify, leading to relaxation of light limitation and

subsequent increases in phytoplankton growth, which drew down nutrient levels within the surface water.

The ratios of nitrate plus nitrite to SRP (Fig. 5) ranged from 14 to 22 throughout the water column during the winter, and was in that range below the euphotic zone during the summer and fall. However, during the summer and fall the ratios in the euphotic zone decreased dramatically reaching values as low as 3 in the surface and increasing with depth. The ratios in the euphotic zone in the summer and fall, however, are not reliable because the SRP concentrations were at or below the detection limit of the analysis.

Microscopic enumeration of cells from the ELF-97 assay provided a semi-quantitative measure of the relative abundance of dominant taxa comprising the phytoplankton communities during the winter, summer, and fall. The relative abundance of each phytoplankton group was estimated as the fraction of cells in a specified group divided by the total number of phytoplankton cells counted, and is reported as a percent. These relative abundances therefore include all cells within a given group regardless of ELF-97 labeling. Analysis of the combined surface water samples indicated that picophytoplankton (cells $<2\ \mu\text{m}$) represented a significant portion of the phytoplankton community throughout the year, particularly in the summer and fall when nutrient concentrations were very low (Fig. 6). This group represented about 37% of cells counted in the winter, whereas they represented 80-88% of cells in summer and fall, increasing in relative abundance as stratification progressed and nutrients became scarce. In the summer and fall when the water column was stratified, the relative abundance of the picophytoplankton remained high

throughout the euphotic zone (~100 m); all other groups show a sub surface maximum in the abundance (at ~10 m) during the summer (Fig. 7a).

Microscopic enumeration of the non-picophytoplankton taxa in the combined surface samples revealed seasonal shifts in their relative abundances. *Trichodesmium* was present in low numbers (~2% of cells) during the winter season; however, *Trichodesmium* filaments were even scarcer throughout the summer and fall, representing a negligible fraction of the phytoplankton community. By contrast, *Cyanothece* (a smaller N-fixing phytoplankter) represented a major portion (42%) of the phytoplankton community in the winter and was present (albeit in lower abundance) throughout the summer (7%) and fall (2%), following the observed decrease in surface nutrient levels (see Figs. 6 and 4). The coccolithophore population underwent a similar decline in relative abundance as the seasons progressed from winter through summer and into fall; however, the decline was not as gradual as observed in the *Cyanothece* group. Rather, the coccolithophores represented a constant proportion (~7% of cells) through winter and summer, but declined to <1% of the phytoplankton cells by the fall. The nanoplankton group, which comprised several different taxa of phytoplankton, was less abundant in the summer than in the winter, representing 6 and 9% of phytoplankton cells in the summer and fall respectively compared to 12% in the winter.

ELF-97 labeling was used to measure cell-specific APA within phytoplankton communities throughout the year, and cells were binned into groups as described above (Figs. 7 and 2). The overall ELF-97 labeling efficiency for all phytoplankton groups combined (e.g. number of cells labeled from total cells counted) did not change

much over the year, ranging from 11% in winter to 16% in the summer, and was only 6% in the fall, despite considerable changes in SRP concentrations. The ELF-97 labeling of the picophytoplankton was consistently low across all seasons (1.5-5% of cells). A small increase from 1.5% in winter to 5% in summer was observed as SRP concentration decreased, however, the percent labeling decreased from 5% in summer to 3.5% in early fall despite sustained low SRP concentrations, although these values are similar given the error estimate for this method. It is possible that the low ELF labeling observed in the picophytoplankton population in general (all seasons) is not a result of low APA but rather stems from lack of labeling of this group when using the ELF protocol (Rengefors et al. 2003). However, the few instances in which picophytoplankton were labeled in our field samples suggest that that this is not the case, as also shown by Lomas et al. (2004) where a stronger cell penetrating procedure was applied. In addition, when performed on pure cultures of *Prochlorococcus* sp. strain MED4 and *Synechococcus* sp. strain WH8102 grown in the laboratory, the procedure also showed that these cells could indeed exhibit ELF labeling (Fig. 8). Thus the lack of substantial ELF-97 labeling among picophytoplankton indicates that these populations are generally not Pi-limited and are able to satisfy their P requirements in the very low nutrient concentrations seen in the Gulf waters in the summer and fall months (see also Stihl et al. 2001; Fuller et al. 2005).

ELF-97 labeling was higher among the non-picophytoplankton, with a 3-fold increase from winter (when average labeling was 17%) to summer (58% labeling) followed by a decrease in fall, when 21% of cells exhibited ELF-97 labeling. The *Cyanothece* cells, which decreased in abundance from winter to summer and fall, were

characterized by a greater than 3-fold increase in ELF-97 labeling between winter (13% labeled) and summer (49% labeled), while in the fall they showed the lowest level of labeling (5%) (Fig. 7B). Similar trends were observed in the coccolithophore and nanoplankton groups. ELF-97 labeling within the coccolithophore group underwent a 2-fold increase between winter and summer (increasing from 33% labeling to 68% labeling), but decreased in the fall (43% labeling). Likewise, ELF-97 labeling in nanoplankton showed a 3-fold increase between winter (19% labeling) and summer (57% labeling), followed by a decrease in fall (23% labeling). When present (during the winter), 15% of *Trichodesmium* cells exhibited ELF-97 labeling (see Fig. 7B). *Trichodesmium* was not sufficiently abundant to accurately enumerate ELF-97 labeling during the summer; however, a general increasing trend in labeling was observed throughout the summer in the cells that were counted.

Analysis of samples from the nutrient addition bioassay demonstrated that samples receiving dust alone or together with N and/or P, as well as samples receiving inorganic N and P together showed 2-3 fold increases in Chlorophyll *a* (Chl *a*) relative to the control (no nutrient addition) sample (K. Mackey, J. Street, R. Labiosa, and A. Paytan, unpubl.) Of these samples, non-picophytoplankton represented approximately 10% of the population (data not shown), and the ELF-97 labeling of non-picophytoplankton decreased by half in treatments receiving phosphate (Fig. 9). By contrast, treatments receiving dust alone or in combination with N (but not phosphate) showed labeling similar to the control (~40%) despite having increased levels of Chl *a*. At the beginning of the incubation ELF-97 labeling indicated that 32% of the non-picophytoplankton cells were labeled. In these samples, approximately 90% of cells

comprised the picophytoplankton group, which showed very low (<1%) ELF-97 labeling across all treatments (data not shown). Samples receiving single nutrient amendments of N or P alone or with Fe had Chl *a* levels similar to the control, and had no clear change in APA.

DISCUSSION

Density and nutrient measurements in this study (Figs. 3 and 4) are consistent with previous reports for the Gulf of Aqaba (Lindell and Post, 1995; Fuller et al. 2005; Badran et al. 2005) and show the seasonal patterns typical of this and other oligotrophic oceans (Venrick, 1993). The phytoplankton community dynamics in the Gulf appear to be heavily influenced by the seasonal changes in physical and chemical characteristics of the water column, as found in other studies (Lindell and Post, 1995; Li et al, 1998; Labiosa et al. 2003). Seasonal shifts in the relative abundances of various phytoplankton groups correspond to pronounced seasonal changes in the trophic state of the Gulf, switching from mesotrophic conditions in the winter to oligotrophic conditions in the summer and fall (Lindell and Post, 1995).

The increase in the relative abundance of picophytoplankton as stratification progresses and nutrient concentrations in the surface decrease indicates that there is an advantage for small cells in the low nutrient waters of the Gulf. This may be due to the greater cellular surface area to volume ratios, higher nutrient uptake efficiencies (Bertilsson et al. 2003; Heldal et al. 2003), and/or lower nutrient requirements of these organisms (Van Mooy et al. 2005). Further, flow cytometry and cell count data show that the relative abundances of the phytoplankton groups comprising the

picophytoplankton population (i.e., *Prochlorococcus*, *Synechococcus*, and picoeukaryotes) also varied seasonally as nutrient levels changed (R. Labiosa, unpubl.) By contrast, the relative abundances of all non-picophytoplankton groups decrease from winter to summer, and with the exception of the group composed of mixed nanoplankton cells, continue to decrease from summer to fall as oligotrophic conditions progress.

In general, picophytoplankton showed low levels of labeling throughout the year (Fig. 7A and 7B). Depth profiles show very little labeling for picophytoplankton throughout the water column in the winter, while in the summer and fall labeling was particularly low at greater depths where nutrients are recycled (potentially yielding higher Pi availability) (Fig. 3). Further, while the ELF-97 labeling of picophytoplankton in the combined surface samples was consistently low across all seasons, winter labeling (1.5%) was lower than summer (5.0%) and fall (3.5%) labeling (although when comparing the fall and winter values the error associated with these measurements should be kept in mind). These trends are consistent with decreased APA with higher Pi concentrations, but they also indicate that picophytoplankton in the Gulf were, for the most part, not Pi-limited during all seasons.

In contrast to the picophytoplankton, ELF-97 labeling trends in all other phytoplankton groups reveal seasonal variability, indicative of various degrees of Pi limitation. Cells other than picophytoplankton are therefore responsible for the majority of the autotroph APA in our samples, despite representing only a fraction (and sometimes a very small fraction) of the entire phytoplankton community.

Overall, ELF-97 labeling among the non-picophytoplankton was lowest in winter, highest in summer (2-3 fold greater than winter), and moderately low in fall (~2 fold less than summer). The trend of increased labeling between winter and summer is expected, as APA would increase with decreasing SRP concentrations in each of these groups. The observed decreases in APA between summer and fall despite SRP concentrations below the detection limit during both sampling periods is less intuitive, and could be related to a transient increase in Pi within the euphotic zone preceding our sampling in the fall. In the fall, air temperatures begin to decrease, and when they are below the surface water temperature transient mixing (brought about by the initial degradation of stratified layers) occurs. This can be followed by re-stratification of the upper water column if warm days re-occur. Field observations and modeling indicate that this process begins in the Gulf around the month of November (R. Labiosa, unpubl.) We suspect that such a transient mixing and re-stratification event may have introduced Pi from depth prior to our sampling and led to a corresponding decrease in APA in our fall samples. The low nutrient concentration we measured resulted from rapid uptake following re-stratification. Lower levels of APA within this time frame (compared to summer) is feasible given that there is a lag between AlkP expression and Pi concentration due, on the one hand, to the time required for enzyme synthesis and depletion of internal P stores and, on the other hand, the time required for enzymes to be broken down when they are no longer needed by the cell (Dyhrman and Palenik, 1999; Lomas et al. 2004). If Pi were transiently available from a brief mixing event before our sampling date, as might be expected for this season, the resulting decrease in APA could have been sustained at the time of our sampling in

spite of the low ambient Pi concentrations because of the lag time to synthesize new AlkP, and may have led to the reduced labeling (relative to summer) of the coccolithophore, *Cyanothece*, and nanoplankton populations in surface waters in the fall (Fig. 7B). Interestingly, *Cyanothece* labeling in the fall is even lower than in the winter. Although a pre-sampling mixing event could explain lower APA activity in the fall than that expected based on SRP concentrations, the activity is not likely to be lower than the winter values. It may be possible that a different strain of *Cyanothece* with different constitutive levels of APA is present in winter than in fall, however; our data cannot resolve this and more work should be done to address this possibility.

When considering the bulk ELF labeling of the entire phytoplankton community (expressed as percent of all cells labeled from total cells counted) our study indicates that the observed seasonal changes are relatively small throughout the year (6-16%). Similarly, in both surface samples and along depth profiles the total fraction of ELF-97 labeled cells does not seem to decrease in a consistent manner as SRP concentrations increase. At first glance, this would seem to imply little or no affect of the seasonal SRP concentration changes (from less than $0.01 \mu\text{mol L}^{-1}$ in summer to a maximum of $0.08 \mu\text{mol L}^{-1}$ in winter) on the Pi status of the phytoplankton. However, when shifts in phytoplankton relative abundances are taken into account along with labeling, the effects of Pi deficiency are better resolved. Our data show that during seasons when Pi and other nutrient levels are low, the phytoplankton population is dominated by picophytoplankton that are generally not Pi limited, whereas higher levels of Pi and other nutrients support a greater diversity of phytoplankton taxa (some of which may still be limited by Pi despite the detectable

SRP concentrations). Therefore, while variation in Pi availability is not the only factor controlling seasonal phytoplankton succession, it does affect the nutrient status of some phytoplankton groups and parallels changes in community composition.

It has been suggested that in warm ($>25^{\circ}\text{C}$), highly stratified, calm water where nitrogen sources are impoverished and Fe is available, the diazotroph *Trichodesmium* may be abundant (Carpenter and Romans, 1991; Mulholland et al. 2002). It is interesting that *Trichodesmium* in the Gulf of Aqaba was not abundant in the summer months during the time of our sampling despite these favorable conditions. We suggest that *Trichodesmium* populations were limited by Pi availability, and due to the low Pi concentrations in the euphotic zone could not flourish during the summer months despite their ability to utilize DOP (Mulholland et al. 2002, Dhyrman et al. 2006). In contrast, during the winter when Pi was more abundant, *Trichodesmium* cells were observed and a substantial portion of them exhibited APA, indicative of their higher P requirements and ability to utilize organic P to satisfy the P nutrition needs. This confirms work of Stihl et al. (2001), which determined the bulk APA of *Trichodesmium* colonies (when these were found) in the Gulf and suggested that they were Pi-stressed.

Interestingly, the diazotroph *Cyanothece* is more abundant than *Trichodesmium* in all seasons, comprising about 42% of cells in the winter. As with *Trichodesmium*, there is a measurable decline in *Cyanothece* abundance as stratification progresses and Pi becomes scarce. However, compared to *Trichodesmium*, *Cyanothece* is present in higher numbers throughout the summer, indicating that it may be better adapted than *Trichodesmium* to survival under low Pi

conditions. Because both *Trichodesmium* and *Cyanothece* are able to utilize DOP, the ability to synthesize AlkP is probably not the source of *Cyanothece*'s competitive advantage. Rather, *Cyanothece* likely dominates because of its smaller size, which may enable it to grow more efficiently than *Trichodesmium* when acquiring Pi from the limited pool. The dominance of *Cyanothece* over *Trichodesmium* under extremely low Pi conditions underscores the fact that a growth-limiting nutrient, in this case Pi, likely influences competition among the phytoplankton here. Although the majority of phytoplankton (i.e., the picophytoplankton) in the Gulf are not Pi limited, some subgroups within the population exhibit Pi-deficiency, and the ability of these phytoplankton groups to use organic P sources may enable them to survive extreme oligotrophic conditions. Further, these data demonstrate that while elevated APA can be used as an indicator of Pi limitation, it does not necessarily confer a competitive advantage to cells; cell size may in fact provide a more important competitive edge in oligotrophic waters.

These results highlight the variability in Pi status of different taxa within the same community. Traditional Pi limitation assays that measure the bulk APA of the community are therefore somewhat limited because they cannot attribute enzyme activity to specific individuals and groups. Fortunately, ELF-97 labeling allows APA to be assessed in a way that is taxonomically meaningful and ecologically relevant. When we compare each group across the seasons, we generally observe lower ELF-97 labeling during the winter, indicating less APA when Pi (and other nutrients) is more abundant. Thus, despite an apparently small seasonal change in APA for the population as a whole, change in APA within each non-picophytoplankton group is

evident. These conclusions are also supported by the nutrient addition bioassay, which demonstrated that the numerous picophytoplankton were not limited by Pi alone, and only some of the larger cells (representing a small fraction of the overall phytoplankton community) were Pi limited.

In addition to highlighting the importance of interpreting community dynamics and nutrient status together, our results also underscore two potential difficulties associated with inferring nutrient limitation from nutrient concentration and ratio data, particularly in oligotrophic waters where the nutrient concentrations are close to the limits of detection. First, dissolved nutrient ratios neglect organic nutrient sources and can fail to account for nutrient preferences (i.e., the range in N:P ratio demands among species) and nutrient source preferences among different taxonomic groups. Specifically, these ratios may not be a good measure of nutrient status in waters where *Prochlorococcus* dominates because recycled sources of N (e.g., ammonium, urea, dissolved organic N), which are not considered in the N:P ratio calculation, are the primary N sources for these cells (Dufresne et al. 2003). The second difficulty is that as nutrient levels approach their respective detection limits, the ratios of these values become more prone to error. To illustrate this point, our data show that in the winter surface N:P ratios range from 15 to 20 (in the range of the Redfield ratio, see Fig. 5), and non-picophytoplankton cells are abundant. By contrast, in the summer when picophytoplankton are dominant, surface ratios fall to 3, a ratio that would typically be interpreted as indicative of N limitation. However, the large error associated with this ratio and its inability to account for some biologically relevant nutrient sources for picophytoplankton suggest that the ratio may not be a good indicator of nutrient

limitation during this oligotrophic season. Indeed, trends in seasonal succession and ELF-97 labeling indicate that Pi may limit some phytoplankton groups in the summer despite the low calculated N:P ratios. Therefore, while N:P ratios can still provide information about nutrient levels in many marine systems and may have validity at the community level they should not be applied indiscriminately or exclusively when assessing nutrient limitation; rather, the approach is strengthened by including measures that account for taxonomic variability.

The relation between Pi concentrations and the degree of response of individual phytoplankton taxa to Pi availability is reflected in the APA status of the cells and, to an extent, in the relative abundances of phytoplankton groups. Our data show that while Pi availability may limit some phytoplankton taxa in this system, the majority of cells (i.e., the picophytoplankton) are not Pi limited throughout the year. Indeed, Pi is likely not the sole nutrient affecting phytoplankton distribution patterns; SRP and oxidized nitrogen concentrations in the water column are highly coupled (i.e., both have higher concentrations in the winter and lower concentrations in the summer), and co-control of phytoplankton production and abundance patterns is very likely. Similar investigation of the physiological responses of various phytoplankton groups to N and light limitation should be carried out.

CONCLUSION

Our data have shown that although co-existing groups of phytoplankton may encounter identical environmental conditions, physiological differences among them, such as variability in cellular nutrient quotas and acquisition mechanisms, ultimately

cause each group to have a different nutrient status. The importance of collecting accurate nutrient status information over a broad range of ecological scales becomes apparent as more complex and robust biogeochemical models require such information. In many regions, changes in phytoplankton community structure resulting from changing nutrient availability and species-specific adaptations to variable nutrient levels may directly affect the amount of export production from these systems because cell size, density, and aggregation potential affect sinking rate (Karl et al. 1997; Arrigo et al. 1999; Boyd and Newton, 1999). Accordingly, as phytoplankton are major contributors to global primary production (Behrenfeld and Falkowski, 1997; Partensky et al. 1999), understanding nutrient controls and stress responses of natural phytoplankton populations is necessary for understanding the interplay between nutrient cycling, phytoplankton community composition, primary production, and the global carbon cycle at present and in the future.

ACKNOWLEDGMENTS

I acknowledge my co-authors Rochelle G Labiosa , Mike Calhoun , Joseph H Street, Anton F Post , and Adina Paytan for help on this manuscript, which was published in 2007 in *Limnology and Oceanography*. As a group, we thank our colleagues at the Interuniversity Institute for Marine Science in Eilat, Israel for assisting in data collection and providing laboratory space and equipment during the study. T. Rivlin conducted the nutrient analyses for this study. L. Sherman and E. Carpenter helped in identifying *Cyanothece* sp. cells. Y. Chen, A. Genin, S. Monismith, and A. Rivlin provided valuable insight about the Gulf. M. Mills and two anonymous reviewers provided valuable comments on the early drafts of this manuscript. This research was supported under the NASA New Investigator Program NAG5-12663 to AP. KRMM was supported through the NSF Graduate Research Fellowship Program. RGL was supported through the NASA ESS Fellowship 01-000-0234.

Citation

Mackey, KRM, RG Labiosa, M Calhoun, J Street, AF Post, and A Paytan. 2007. Phosphorus availability, phytoplankton community dynamics, and taxon-specific phosphorus status in the Gulf of Aqaba, Red Sea. *Limnol. Oceanogr.* 52: 873-885.

Author contributions

KRMM - helped plan experimental design; processed field and culture samples for microscopy from March and November 2004; analyzed and interpreted data; wrote the manuscript

RGL– processed chlorophyll *a* samples for Fig. 3C; gave comments on the manuscript

MC– processed microscopy samples from August 2003

JS– helped conduct field work

AFP– provided funding; provided comments on the manuscript

AP- provided funding; helped plan experimental design; helped conduct field work;
provided comments on the manuscript

REFERENCES

- Ammerman, J. W., R. R. Hood, D. A. Case, and J. B. Cotner. 2003. Phosphorus deficiency in the Atlantic: An emerging paradigm in oceanography. *EOS Trans. AGU* **84**: 165.
- Arrigo, K. R. 2005. Marine microorganisms and global nutrient cycles. *Nature* **437**: 349-355.
- Arrigo, K. R., D. H. Robinson, D. L. Worthen, R. B. Dunbar, G. R. DiTullio, M. VanWoert, and M. P. Lizotte. 1999. Phytoplankton community structure and the drawdown of nutrients and CO₂ in the Southern Ocean. *Science* **283**: 365-367.
- Badran, M. I., M. Rasheed, R. Manasrah, and T. Al-Najjar. 2005. Nutrient flux fuels the summer primary productivity in the oligotrophic waters of the Gulf of Aqaba, Red Sea. *Oceanologia* **47**: 47-60.
- Baldwin, D. S. 1998. Reactive “organic” phosphorus revisited. *Wat. Res.* **32**: 2265-2270.
- Behrenfeld, M. J. and P. G. Falkowski. 1997. Photosynthetic rates derived from satellite-based chlorophyll concentration. *Limnol. Oceanogr.* **42**: 1-20.
- Benitez-Nelson, C. 2000. The biogeochemical cycling of phosphorus in marine systems. *Earth Sci. Rev.* **51**: 109-135.
- Bertilsson, S., O. Berglund, D. M. Karl, and S. W. Chisholm. 2003. Elemental composition of marine *Prochlorococcus* and *Synechococcus*: Implications for the ecological stoichiometry of the sea. *Limnol. Oceanogr.* **48**: 1721-1731.
- Bjorkman, K., and D. M. Karl. 1994. Bioavailability of inorganic and organic

- phosphorus compounds to natural assemblages of microorganisms in Hawaiian coastal waters. *Mar. Ecol. Prog. Ser.* **111**: 265–273.
- Boyd, P. W., and P. P. Newton. 1999. Does planktonic community structure determine downward particulate organic carbon flux in different oceanic provinces? *Deep-Sea Research I* **46**: 63-91.
- Cañellas, M., S. Sgusti, and C. M. Duarte. 2000. Latitudinal variability in phosphate uptake in the Central Atlantic. *Mar. Ecol. Prog. Ser.* **194**: 283-294.
- Carpenter, E. J., and K. Romans. 1991. Major role of the cyanobacteria *Trichodesmium* in nutrient cycling in the North Atlantic Ocean. *Science* **254**: 1356-1358.
- Chrost, R. J. 1991. Microbial enzymes in aquatic environments. Springer-Verlag.
- Dufresne A., M. Salanoubat, F. Partensky, F. Artiguenave I. M. Axmann, V. Barbe, S. Duprat, M. Y. Galperin, E. V. Koonin, F. Le Gall, K. S. Makarova, M. Ostrowski, S. Oztas, C. Robert, I. B. Rogozin, D. J. Scanlan, N. Tandeau de Marsac, J. Weissenbach, P. Wincker, Y. I. Wolf, and W. R. Hess.. 2003. Genome sequence of the cyanobacterium *Prochlorococcus marinus* SS120, a nearly minimal oxyphototrophic genome. *Proc Natl Acad Sci USA* **100**: 10020–10025.
- Dyhrman, S., and B. Palenik. 1999. Phosphate stress in cultures and field populations of the dinoflagellate *Prorocentrum minimum* detected by a single-cell alkaline phosphatase assay. *Appl. Environ. Microbiol.* **65**: 3205-3212.
- Falkowski, P. G. 2000. Rationalizing elemental ratios in unicellular algae. *J. Phycol.* **36**: 3-6.

- Filippelli, G. M., and M. L. Delaney. 1996. Phosphorus geochemistry of equatorial Pacific sediments. *Geochimica et Cosmochimica Acta*. **60**: 1479-1495.
- Follmi, K. B. 1996. The phosphorus cycle, phosphogenesis and marine phosphate-rich deposits. *Earth-Science Reviews* **40**: 55-124.
- Fuller, N. J., D. Marie, M. Yallop, T. Rivlin, N. J. West, A. F. Post, and D. J. Scanlan. 2005. Dynamics of community structure and phosphate status of picocyanobacterial populations in the Gulf of Aqaba, Red Sea. *Limnol. Oceanogr.* **50**: 363-375.
- Geider, R. J., and J. La Roche. 2002. Redfield revisited: variability of C:N:P in marine microalgae. *Eur. J. Phycol.* **37**: 1-17.
- Gonzalez-Gil, S., B. A. Keafer, R. V. M. Jovine, A. Aguilera, S. Lu, and D. M. Anderson. 1998. Detection and quantification of alkaline phosphatase in single cells of phosphorus-limited marine phytoplankton. *Mar. Ecol. Prog. Ser.* **164**: 21-35.
- Heldal, M., D. J. Scanlan, S. Norland, F. Thingstad, and N. H. Mann. 2003. Elemental composition of single cells of various strains of marine *Prochlorococcus* and *Synechococcus* using X-ray microanalysis. *Limnol. Oceanogr.* **48**: 1732-1743.
- Holmes, R. M., A. Aminot, R. Kerouel, B. A. Hooker, and B. J. Peterson. 1999. A simple and precise method for measuring ammonium in marine and freshwater ecosystems. *Canadian Journal of Fisheries and Aquatic Sciences* **56**: 1801-1808.
- Hudson, J. J., W. D. Taylor, and D. W. Schindler. 2000. Phosphate concentrations in lakes. *Nature* **406**: 54-56.

- Jansson, M., H. Olsson, and K. Pettersson. 1988. Phosphatases: origin, characteristics and function in lakes, *Hydrobiol.* **170**: 157-175.
- Johnson, D. L. 1971. Simultaneous determination of arsenate and phosphate in natural waters. *Environmental Science and Technology* **5**: 411-414.
- Karl, D. M., and K. Yanagi. 1997. Partial characterization of the dissolved organic phosphorus pool in the oligotrophic North Pacific Ocean. *Limnol. Oceanogr.* **42**: 1398-1405.
- Karl, D. M., and G. Tien. 1992. MAGIC: A sensitive and precise method for measuring dissolved phosphorus in aquatic environments. *Limnol. Oceanogr.* **37**: 105-116.
- Karl, D. M., K. M. Bjorkman, J. E. Dore, L. Fujieki, D. V. Hebel, T. Houlihan, R. M. Letelier, and L. M. Tupas. 2001. Ecological nitrogen to- phosphorus stoichiometry at station Aloha. *Deep-sea Res. II* **48**: 1529-1566.
- Karl, D., R. Letelier, L. Tupas, J. Christanss, and D. Hebel. 1997. The role of nitrogen fixation in biogeochemical cycling in the subtropical North Pacific Ocean. *Nature*. **388**: 533-538.
- Krom, M. D., N. Kress, S. Brenner, and L. I. Gordon. 1991. Phosphorus limitation of primary productivity in the eastern Mediterranean Sea. *Limnol. Oceanogr.* **36**: 424-432.
- Labiosa, R.G., K. R. Arrigo, A. Genin, S. G. Monismith, and G. van Dijken. 2003. The interplay between upwelling and deep convective mixing in determining the seasonal phytoplankton dynamics in the Gulf of Aqaba: Evidence from SeaWiFS and MODIS. *Limnol. Oceanogr.* **48**: 2355-2368.

- Li, H., M. J. W. Veldhuis, and A. F. Post. 1998. Alkaline phosphatase activities among planktonic communities in the northern Red Sea. *Mar. Ecol. Prog. Ser.* **173**: 107-115.
- Lindell, D., S. Penno, M. Al-Qutob, E. David, T. Rivlin, B. Lazar, and A. F. Post. 2005. Expression of the N-stress response gene *ntcA* reveals N-sufficient *Synechococcus* populations in the oligotrophic northern Red Sea. *Limnology and Oceanography* **50**: 1932-1944.
- Lindell, D., and A. F. Post. 1995. Ultraphytoplankton succession is triggered by deep winter mixing in the Gulf of Aqaba (Eilat), Red Sea. *Limnol. Oceanogr.* **40**: 1130-1141.
- Lomas, M. W., A. Swain, R. Shelton, and J. W. Ammerman. 2004. Taxonomic variability of phosphorus stress in Sargasso Sea phytoplankton. *Limnol. Oceanogr.* **49**: 2303-2310.
- Mackey, K. R. M., R. G. Labiosa, J. H. Street, and A. Paytan. 2006. Nitrogen and phosphorus co-limit growth and control community composition and taxon specific nutrient status in the Gulf of Aqaba, Red Sea. *EOS. Trans. AGU.* **86**: 52.
- Mulholland, M. R., S. Floge, E. J. Carpenter, and D. G. Capone. 2002. Phosphorus dynamics in cultures and natural populations of *Trichodesmium* spp. *Mar. Ecol. Prog. Ser.* **239**: 45-55.
- Nicholson, D., S. Dyhrman, F. Chavez, and A. Paytan. 2006. Phosphorus status of marine phytoplankton communities in Monterey Bay and San Francisco Bay. *Limnology and Oceanography* **51**: 874-883.

- Partensky, F., W. R. Hess, and D. Vaultot. 1999. *Prochlorococcus*, a Marine Photosynthetic Prokaryote of Global Significance. *Microbiology and Molecular Biology Reviews*. **63**: 106-127.
- Redfield, A., B. H. Ketchum, and F. A. Richards. 1963. The influence of organisms on the composition of seawater, pages 26-77 in M. N. Hill [ed.], *The sea*. V. 2. Wiley Interscience.
- Rengefors, K., K. C. Ruttenberg, C. L. Hauptert, C. Taylor, B. L. Howes, and D. M. Anderson. 2003. Experimental investigation of taxon-specific response of alkaline phosphatase activity in natural freshwater phytoplankton. *Limnol. Oceanogr.* **48**: 1167-1175.
- Rose, C., and R. P. Axler. Use of alkaline phosphatase activity in evaluating phytoplankton community phosphorus deficiency. *Hydrobiol.* **361**: 145-156.
- Scanlan, D. J., and N. J. West. 2002. Molecular ecology of the marine cyanobacterial genera *Prochlorococcus* and *Synechococcus*. *FEMS Microbiol. Ecol.* **40**: 1-12.
- Scanlan, D. J., and W. H. Wilson. 1999. Application of molecular techniques to addressing the role of P as a key effector in marine ecosystems. *Hydrobiol.* **401**: 149–175.
- Scanlan, D. J., N. J. Silman, K. M. Donald, W. H. Wilson, N. G. Carr, I. Joint, and N. H. Mann. 1997. An immunological approach to detect phosphate stress in populations and single cells of photosynthetic picoplankton. *Appl. Environ. Microbiol.* **63**: 2411-2420.
- Stihl, A., U. Sommer, and A. F. Post. 2001. Alkaline phosphatase activities among populations of the colony-forming diazotrophic cyanobacterium

- Trichodesmium* spp. (cyanobacteria) in the Red Sea. J. Phycol. **37**: 310-317.
- Thingstad, T. F., M. D. Krom, R. F. C. Mantoura, G. A. F. Flaten, S. Groom, B. Herut, N. Kress, C. S. Law, A. Pasternak, P. Pitta, S. Psarra, F. Rassoulzadegan, T. Tanaka, A. Tselepidis, P. Wassmann, E. M. S. Woodward, C. Wexels Riser, G. Zodiatis, and T. Zohary. 2005. Nature of Phosphorus Limitation in the Ultraoligotrophic Eastern Mediterranean. Science. **309**: 1068-1071.
- Thingstad, T.F. and R.F.C. Mantoura. 2005. Titrating excess-N content of P-deficient Eastern Mediterranean surface water using alkaline phosphatase activity as a bio-indicator. Limnology and Oceanography **49**: 1582–1592.
- Thingstad, T. F., and F. Rassoulzadegan. 1995. Nutrient limitations, microbial food webs, and biological carbon pumps- suggested interactions in a P-limited Mediterranean. Mar. Ecol. Prog. Ser. **117**: 299-306.
- Toggweiler, J. R. 1999. Variation of atmospheric CO₂ by ventilation of the ocean's deepest water. Paleoceanography **14**: 571-588.
- Tyrrell, T. 1999. The relative influences of nitrogen and phosphorus on oceanic primary production. Nature **400**: 525-531.
- Van Mooy, B. A. S., G. Rocap, H. Sturt, C. T. Evans, and A. H. Devol. 2005. Glycolipid membranes relieve marine *Prochlorococcus* of a major requirement for phosphate. Abstract, ASLO meeting, Spain.
- Venrick, E. L. 1993. Phytoplankton seasonality in the central North Pacific: The endless summer reconsidered. Limnol. Oceanogr. **38**: 1135-1149.
- Wu, J., W. Sunda, E. A. Boyle, and D. M. Karl. 2000. Phosphate depletion in the

western North Atlantic Ocean. *Science* **289**: 759-762.

Zohary, T., and R. D. Robarts. 1998. Experimental study of microbial P-limitation in the eastern Mediterranean. *Limnol. Oceanogr.* **43**: 387-395.

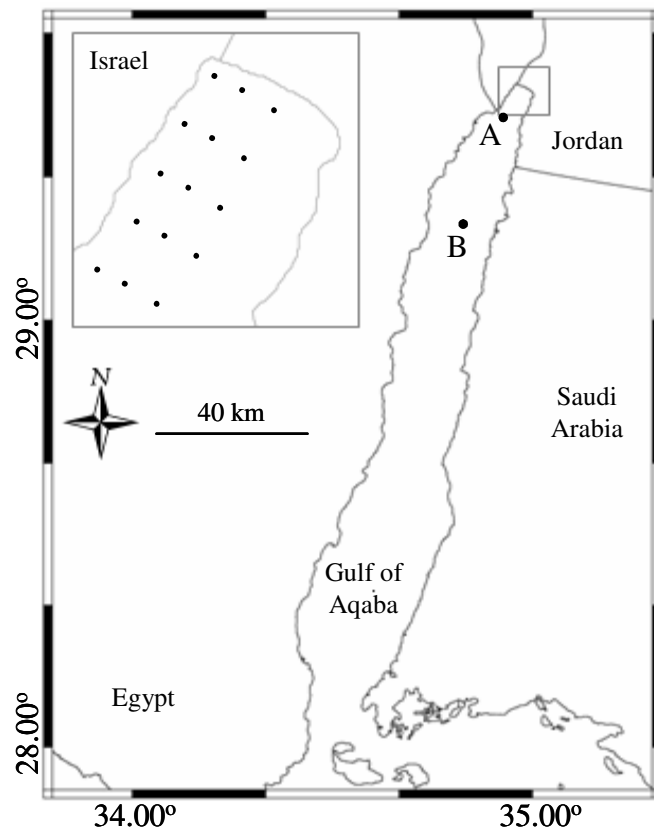


Figure 1: Map of the Gulf of Aqaba, Red Sea and surrounding lands. Inset shows the northern tip of the Gulf of Aqaba and the location of Stations A and B. Shaded portion represents the area over which surface samples were collected.

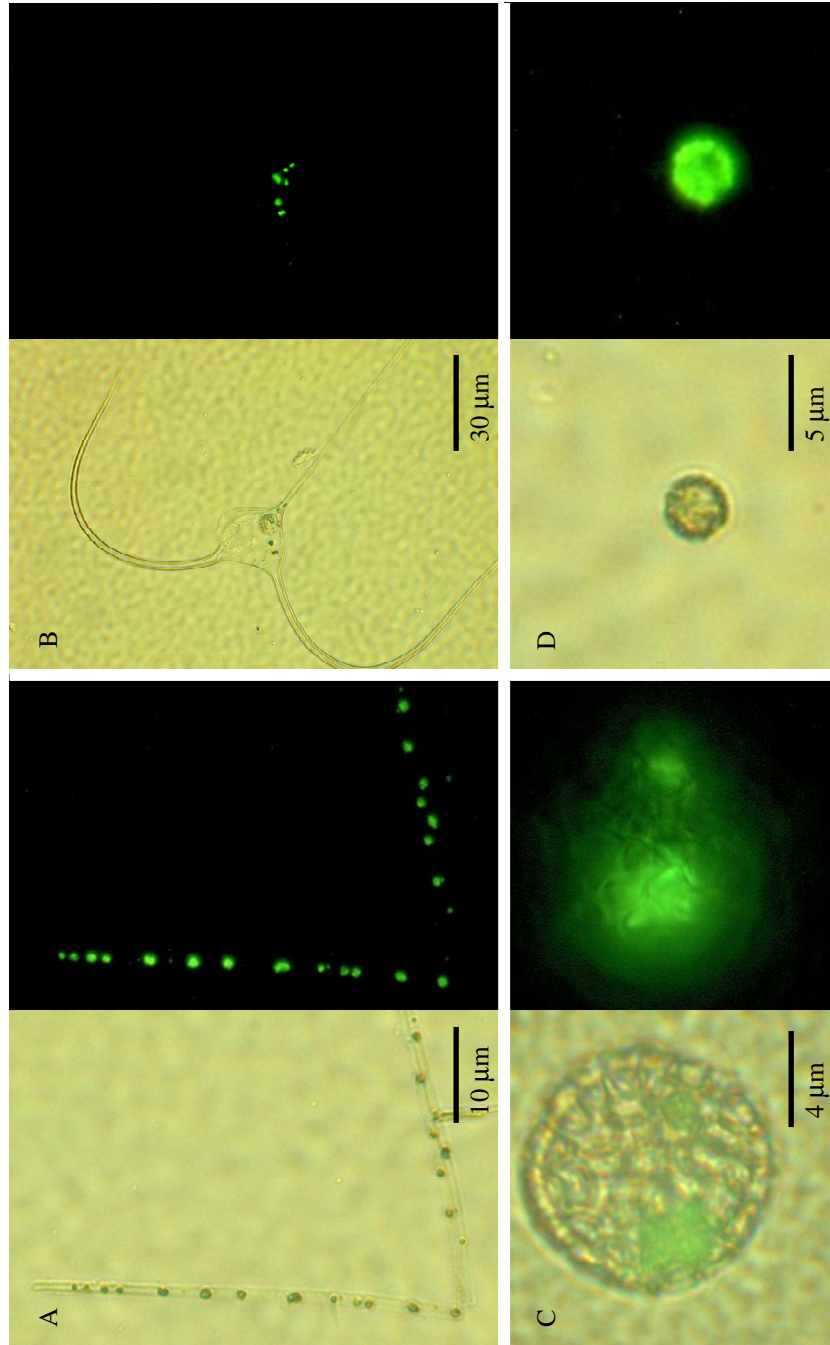


Figure 2: Micrographs of ELF-97 labeled phytoplankton from the euphotic zone in the Gulf of Aqaba (A) *Trichodesmium* sp., (B) nanoplankton (*Ceratium* sp.), (C) coccolithophore, and (D) *Cyanothece* sp. For each pair, the left panel is a view under visible light and the right panel under UV illumination. ELF-97 labeled areas appear as bright areas under UV illumination.

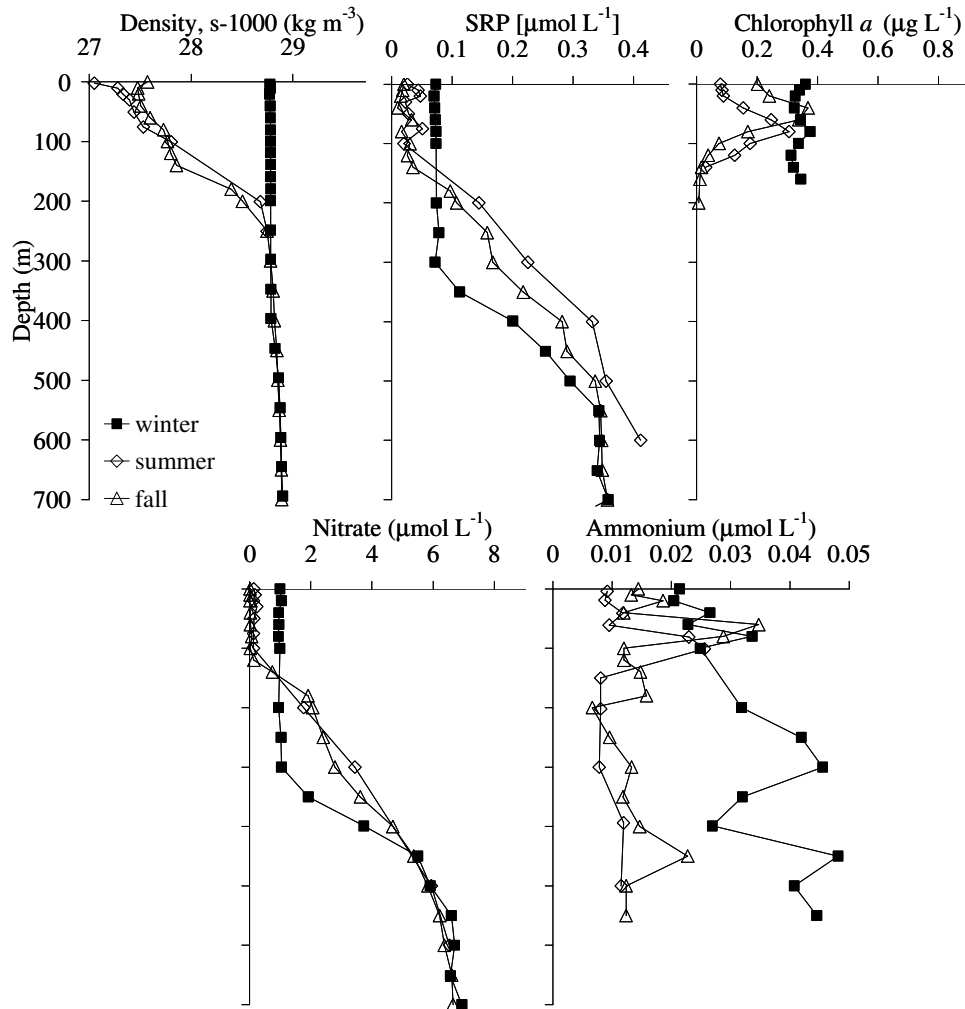


Figure 3: Typical depth profiles of (A) density, (B) SRP concentration, (C) Chl *a* concentration, (D) nitrate concentration, and (E) ammonium concentration for winter, summer, and fall. Profiles for stations A and B were similar; for simplicity only the station A profile is shown.

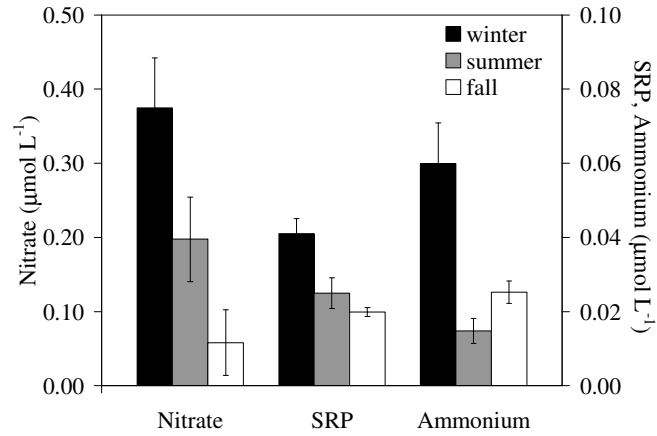


Figure 4: Surface nutrient concentrations in winter ($n=12$), summer ($n=28$) and fall ($n=15$) for nitrate, SRP, and ammonium. Error bars represent standard error of the mean.

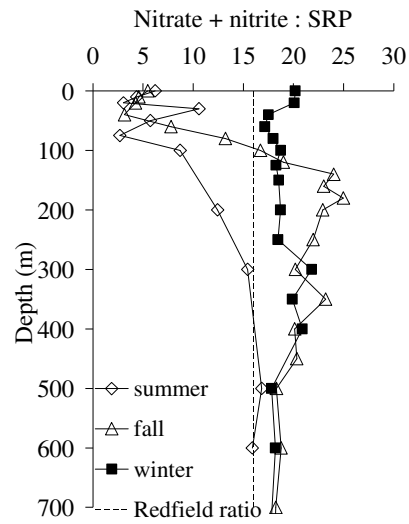


Figure 5: Depth profiles of the ratio between nitrate plus nitrite and SRP during winter, summer, and fall. Dashed line indicates the canonical Redfield ratio value of 16. Please note that the summer and fall ratios in samples shallower than 150 m are unreliable as they are calculated from concentrations of N+N and SRP below detection limits.

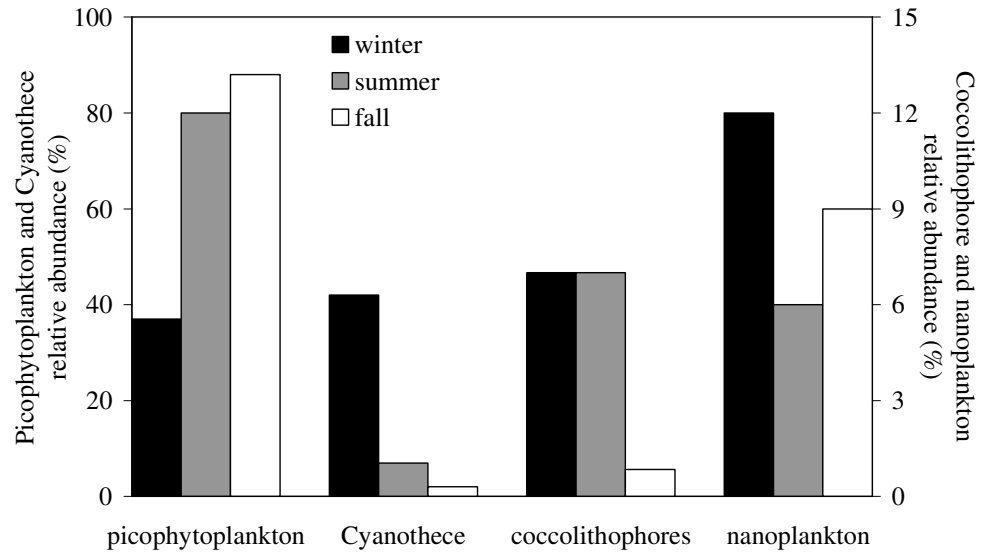


Figure 6: Relative abundances of phytoplankton groups in surface water for the winter, summer, and fall. Note the different scales for the various species.

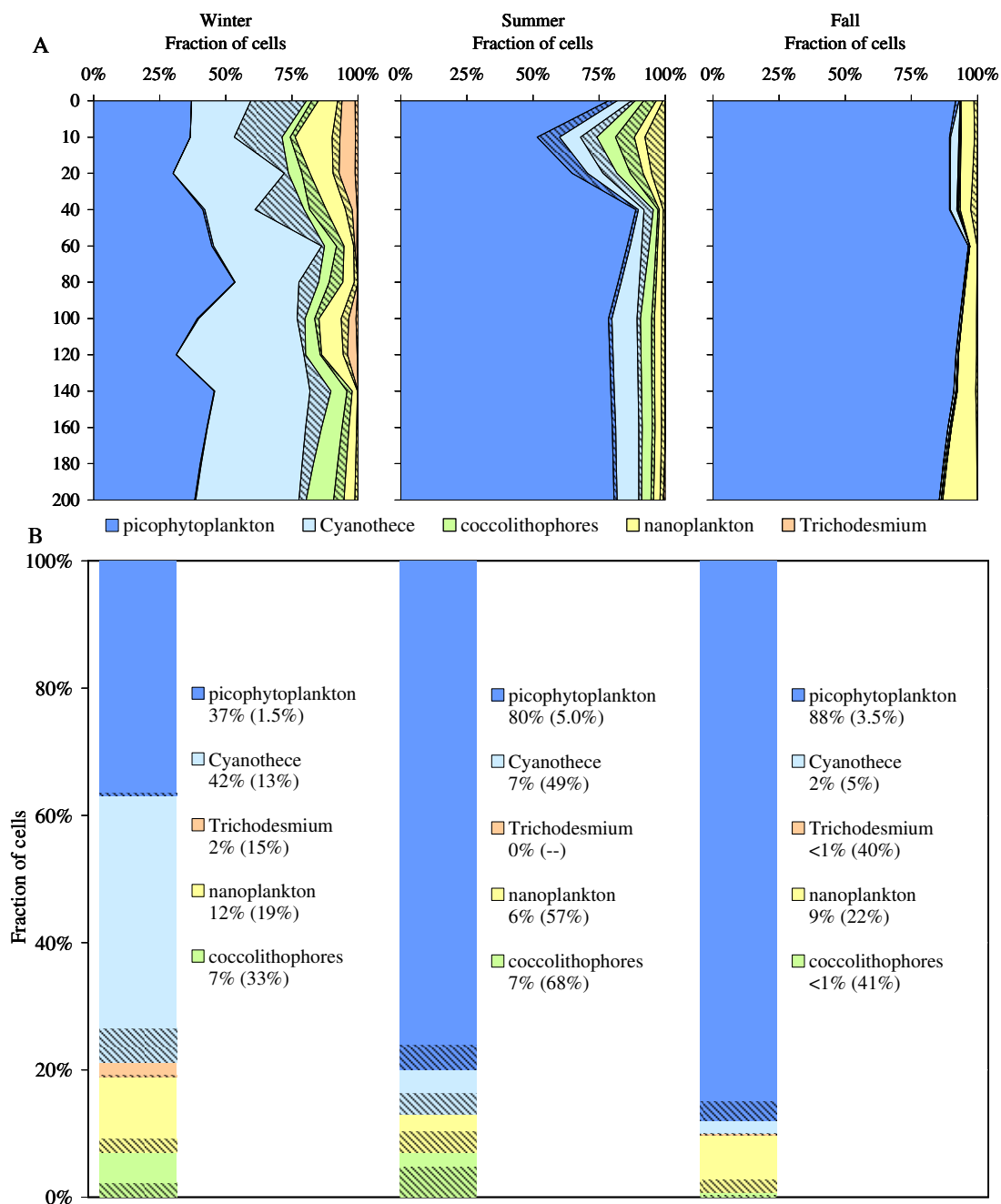


Figure 7: (A) Depth profiles of the relative abundances of phytoplankton groups throughout the euphotic zone for (from left to right) the winter, summer, and fall. Hatched areas represent the percent ELF labeled cells from each group (e.g. % picophytoplankton labeled from total picophytoplankton counted etc.). (B) Community alkaline phosphatase activity showing relative abundance (solid colors) and ELF-97 labeled fractions (hatched colors) for each phytoplankton group in the combined surface samples for (from left to right) the winter, summer, and fall. The

percent values are the percent of each group of phytoplankton from the total counted population. Hatched areas represent the percent ELF labeled cells from each group (i.e., Percent of picophytoplankton labeled from total picophytoplankton counted etc.)

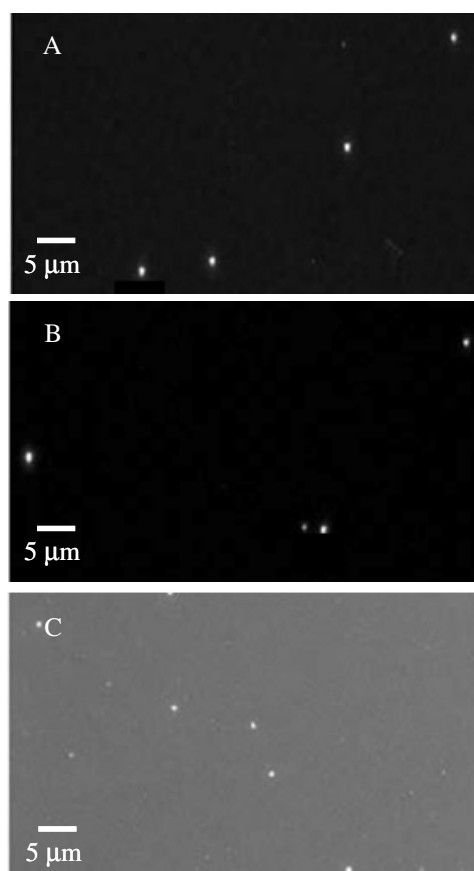


Figure 8: Micrographs of ELF-97 labeled picophytoplankton (A) *Prochlorococcus* sp. strain MED4 grown in culture (B) *Synechococcus* sp. strain WH8102 grown in culture, (C) picophytoplankton from the euphotic zone in the Gulf of Aqaba. Pictures taken under UV illumination, bright spots indicate ELF-97 labeled cells.

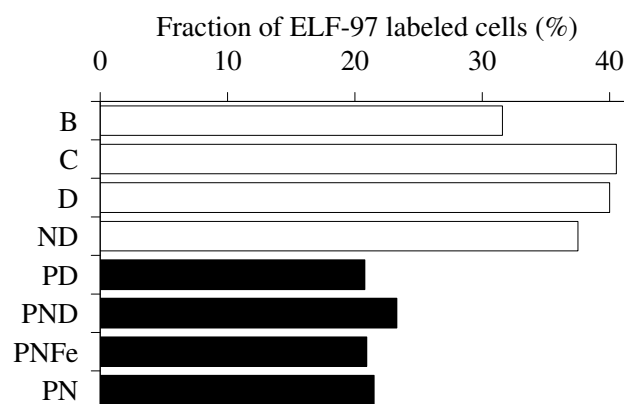


Figure 9: ELF-97 labeling of non-picophytoplankton cells ($>2\ \mu\text{m}$) in samples that showed Chl *a* increases greater than the control in enrichment experiments. Values are expressed in percents as the fraction of ELF-97 labeled cells out of the total number of cells counted. Shaded bars represent samples receiving phosphate. (Key to data labels/ nutrient additions: B= baseline, C= control (no nutrient addition), D= dust, N= nitrate + ammonium, P= phosphate, Fe= iron.)

CHAPTER 4

NITROGEN CYCLING IN OLIGOTROPHIC WATERS:

THE IMPACT OF LIGHT AND SUBSTRATE AVAILABILITY

ABSTRACT

To determine the influence of light and substrate availability on nitrogen (N) cycling in the oligotrophic Red Sea, nutrient additions, ^{15}N tracer experiments, and *in situ* monitoring were used to determine N transformation rates, with a focus on processes contributing to the formation of the primary nitrite (NO_2^-) maximum (PNM). *In situ* generation of NO_2^- following spring stratification was strongly correlated with decreasing irradiance and chlorophyll *a* (chl *a*), suggesting that incomplete nitrate (NO_3^-) reduction by light limited phytoplankton generated a substantial portion of the NO_2^- during the days immediately following stratification. However, as stratification progressed, NO_2^- continued to be generated around 1% light levels where ammonium (NH_4^+) oxidation rates exceeded NO_2^- oxidation rates, possibly due to differential photoinhibition of nitrifying populations. *In situ* NH_4^+ oxidation rates were correlated with NH_4^+ concentration (ranging from 10-320 $\text{nmol L}^{-1} \text{ day}^{-1}$). The ratios of $\delta^{18}\text{O}$ to $\delta^{15}\text{N}$ in $\text{NO}_3^- + \text{NO}_2^-$ increased from ~2:1 to 5:1 as the bloom progressed, suggesting efficient assimilation of recycled N. In ^{15}N tracer experiments, assimilation rates for NO_3^- , NO_2^- , and urea by bulk plankton samples were all higher in the light than in the dark, while NH_4^+ assimilation rates were not light dependent. High urea uptake rates (up to 1285 $\text{nmol L}^{-1} \text{ day}^{-1}$) and rates of coupled urea mineralization with subsequent

nitrification ($14.4 \text{ nmol L}^{-1} \text{ day}^{-1}$) suggest that dissolved organic N is an important source of N for assimilation and nitrification. Our results demonstrate that the N transformation rates throughout the water column are controlled by light over diel and seasonal cycles. Changing light regimes during the spring transition from mixing to stratification affect the plankton community, allowing phytoplankton and nitrifying microbes to contribute jointly to PNM formation.

INTRODUCTION

Nitrogen (N) is a limiting nutrient for primary producers in many oceanic settings, and nitrogen compounds are an important energy source for marine microbes. In this study we seek to improve our understanding of how key physical and biological processes affect the N cycle in the oligotrophic, seasonally stratified Gulf of Aqaba, Red Sea. Specifically, our approach uses ^{15}N tracer experiments together with natural abundance stable isotope measurements to quantify N transformation rates and determine the extent and importance of N regeneration from organic matter. This combined approach has the benefit of characterizing different pathways in the N cycle over different temporal scales under both manipulated (experimental) and in situ conditions.

In the traditional model for N cycling in the surface ocean, the most important source of new N is the supply of nitrate (NO_3^-) from deep water by mixing, advection, or diffusion over the nitracline. In many regions of the ocean N fixation also provides substantial new N (Sañudo-Wilhelmy et al. 2001; Gruber and Sarmiento 1997; Montoya et al. 2004). Phytoplankton assimilate NH_4^+ , NO_3^- , and NO_2^- , collectively referred to as dissolved inorganic N (DIN), into their biomass during autotrophic growth, forming particulate and dissolved organic N (PON and DON) compounds. Organic N is released directly into the environment during cell lysis or excretion, or is remineralized back to NH_4^+ by heterotrophic microbes during ammonification. To complete the cycle, NH_4^+ is converted first to NO_2^- and then NO_3^- in successive oxidation reactions by marine nitrifiers during nitrification.

Recent findings have demonstrated that the marine N cycle is more complex than previously understood, and more overlap exists in the roles phytoplankton and non-photosynthetic microbes play in N uptake than previously believed. For example, certain non-photosynthetic microbes possess genes for NO_3^- , NO_2^- , and NH_4^+ uptake similar to phytoplankton, and are a potentially important “sink” for DIN that is independent of light (Allen et al. 2001; Allen et al. 2005; Cai and Jiao 2008; Starkenburg et al. 2006; Tupas et al, 1994). Likewise, certain phytoplankton utilize DON to satisfy their N demands, similar to heterotrophs (Palenik and Morel 1990; Moore et al. 2002; Zubkov et al. 2003). Our understanding of the conditions and setting in which the various processes of the N cycle occur has also been refined. For example, some marine nitrifier populations are inhibited by light and thus nitrification was thought to be confined to deeper waters. However, high nitrification rates within surface waters were observed directly using ^{15}N tracers (Ward et al. 1989) or calculated using natural abundance ^{15}N and ^{18}O data (Wankel et al. 2007).

Despite the complexity of the N cycle, several important characteristics remain apparent. The N cycle comprises numerous N reservoirs, and their concentrations and vertical distributions are affected by physical and biological factors. Each reservoir may have numerous sources and sinks, some of which have yet to be characterized. Importantly, the dynamic nature of the N cycle, with multiple reactions taking place simultaneously, may result in large fluxes into and out of each reservoir. Yet these fluxes are difficult to quantify by measuring concentration changes alone because the turnover can be very rapid and shuttle N back and forth between reservoirs. Therefore, the reservoir of any nitrogen compound in the water column can be

constant or below detection even though turnover (production and consumption) may be rapid.

Nitrite is an important intermediate in numerous N cycle redox pathways. NO_2^- may be a negligible component of the dissolved N pool when consumption exceeds production. However, it becomes a major component when production exceeds assimilation, such as in stratified waters where accumulation of NO_2^- leads to formation of a primary NO_2^- maximum (PNM, Lomas & Lipschultz 2006). Two mechanisms have been proposed to describe how NO_2^- maxima form: (1) spatially segregated microbial oxidation of NH_4^+ and NO_2^- during nitrification (Olsen 1981; Guerra and Jones 1996); and (2) incomplete NO_3^- reduction to NH_4^+ by phytoplankton, particularly when light limited (Collos 1998; Lomas and Lipschultz 2006). Nitrite maxima throughout the world's oceans are generally attributed to one of these two processes (Lipschultz & Lomas 2006 and references therein). However, whether these processes co-occur in a single location and, if so, how physical forcing in the water column influences which process dominates is not clear. The relative importance of nitrifying organisms and phytoplankton in generating NO_2^- is difficult to quantify primarily because both groups of organisms consume and produce nitrogen from shared pools.

Isotopic analysis of coupled nitrogen ($\delta^{15}\text{N}$) and oxygen ($\delta^{18}\text{O}$) is an attractive method for discriminating between biologically mediated N transformation processes, such as those that contribute to formation of the PNM, since each process imparts a unique isotopic signature to both the N and O composition of the sample (Casciotti et al. 2002; Wankel 2006). In processes where NO_3^- and NO_2^- (N+N) are consumed,

such as assimilation (and denitrification under anaerobic conditions), the $\delta^{18}\text{O}_{\text{N+N}}$ and $\delta^{15}\text{N}_{\text{N+N}}$ in the water both become heavier because the light isotopes of O and N are preferentially consumed. The fractionation of N and O during assimilation are of similar magnitude, which causes the $\delta^{18}\text{O}_{\text{N+N}}$ and $\delta^{15}\text{N}_{\text{N+N}}$ of the residual NO_3^- to increase proportionately at a 1:1 ratio (Granger et al. 2004). Samples from depths where assimilation is minimal typically are characterized by $\delta^{18}\text{O}_{\text{N+N}} : \delta^{15}\text{N}_{\text{N+N}}$ values similar to deep water, whereas in waters where assimilation is the dominant consumption process, the $\delta^{18}\text{O}_{\text{N+N}}$ and $\delta^{15}\text{N}_{\text{N+N}}$ shift from the source signature towards heavier values following a line with a slope of 1:1 (Casciotti et al. 2002).

Whereas N and O fractionation during phytoplankton assimilation is coupled, fractionation is uncoupled in processes like nitrification, which cause the $\delta^{18}\text{O}_{\text{N+N}} : \delta^{15}\text{N}_{\text{N+N}}$ ratio to deviate from the 1:1 ratio (Wankel 2007). During nitrification, NO_3^- is formed by NH_4^+ oxidation in a series of reactions. The source of NH_4^+ is remineralization of DON, which comprises an array of N compounds resulting from cell lysis and as metabolic byproducts. Because the NH_4^+ from DON remineralization derives from biological processes that generally accumulate the lighter ^{14}N isotope, it is a source of isotopically light N to the NO_3^- pool during nitrification. NH_4^+ also undergoes very strong fractionation (up to 38 ‰) during oxidation to NO_2^- , resulting in isotopically light N+N. The source of O during nitrification in seawater is predominantly from ambient water and the $\delta^{18}\text{O}$ of NO_3^- generated from nitrification generally approaches that of ambient water or ~3 ‰ above the seawater value (Casciotti et al., 2002; Sigman et al., 2005). Accordingly, if assimilation occurs in the

absence of nitrification we expect $\delta^{18}\text{O}_{\text{N+N}}$ and $\delta^{15}\text{N}_{\text{N+N}}$ measurements to deviate from the nitrate source signature and increase equally along a slope of 1 (Wankel et al. 2007). If nitrification also occurs, we expect $\delta^{15}\text{N}_{\text{N+N}}$ values to be lighter (e.g. originating from NH_4^+ derived from DON), and the $\delta^{18}\text{O}_{\text{N+N}} : \delta^{15}\text{N}_{\text{N+N}}$ ratios will plot along a line with a slope greater than 1 (Wankel et al. 2007). The relative rates of NO_3^- formation by nitrification and NO_3^- consumption by assimilation (or denitrification) determine the exact slope.

The goal of this work is to improve our understanding of the N cycle in the Gulf of Aqaba, Red Sea; a system with nutrient cycles that are similar to many other seasonally stratified subtropical seas. Specifically, the work seeks to identify temporal and spatial trends in N transformation processes and rates, and relate them to the concurrent physical and biological water column characteristics. We quantitatively measure N transformation rates in natural seawater samples using concentration data and dual $\delta^{15}\text{N}$ and $\delta^{18}\text{O}$ analyses in conjunction with ^{15}N tracer experiments. Particular attention is given to processes influencing NO_2^- maxima. This study identifies important environmental factors that control nitrogen cycling throughout the year in the Gulf, where seasonal variability in mixing depth and stratification influence the contributions of phytoplankton and non-photosynthetic microbes to the N cycle.

MATERIALS AND METHODS

Field site

The Gulf of Aqaba is a seasonally stratified, subtropical sea extending from the northern Red Sea. During the summer, thermal stratification leads to oligotrophic conditions and picocyanobacteria dominate the phytoplankton community (Lindell and Post 1995; Mackey et al. 2007). During the mixed winter season, mesotrophic conditions prevail, favoring eukaryotic phytoplankton (Lindell and Post 1995). A spring bloom generally occurs in March or April at the onset of stratification in which eukaryotic phytoplankton typically dominate and are later succeeded by a secondary bloom of *Synechococcus* (Lindell and Post 1995; Mackey et al. 2009). Throughout the year the entire water column is highly oxygenated.

In situ sampling

Monthly samples were collected from Station A (29°28'N, 34°55'E) in the Northern Gulf of Aqaba as part of a monitoring program (<http://www.iui-eilat.ac.il/NMP>). Depth profiles were taken using a sampling CTD-Rosette (SeaBird) equipped with 12 L Niskin bottles. Depth profiles were also collected at station A before (March 18) and during (March 24 and 25) the spring bloom in 2008.

Nutrient addition experiment

A nutrient addition experiment was conducted to characterize the effect of labile organic nutrient enrichment on seawater N concentrations and speciation and phytoplankton community structure over a period of 4 days. Surface water was

collected at 1 m depth from an offshore site in the Northern Gulf of Aqaba during the end of the stratified, oligotrophic summer season. Surface water was pre-filtered with 20 μm nylon mesh to remove zooplankton grazers and kept in the dark during transport (<2 hours) to the Interuniversity Institute for Marine Science (IUI) in Eilat, Israel. In the lab water was distributed into sample bottles (three replicates per treatment) and incubated in an outdoor tank through which water from the Gulf circulated to ensure in situ temperature conditions were maintained. Screening material was used to attenuate the sunlight intensity by 50% yielding a maximum midday irradiance of $\sim 1000 \mu\text{mol m}^{-2} \text{s}^{-1}$, which is equivalent to the upper 10 m of the euphotic zone of the Gulf during summer months.

Nutrients were added singly or in combination to the incubation bottles. Phosphorus final concentration was $0.4 \mu\text{mol L}^{-1}$, and N final concentration was $7 \mu\text{mol L}^{-1}$ which are representative of concentrations in the Gulf deep water (Mackey et al. 2007). P was provided as sodium phosphate monobasic (hereafter PO_4^{3-}). N was provided as ammonium chloride (hereafter NH_4^+), sodium nitrate (hereafter NO_3^-), sodium nitrite (hereafter NO_2^-), glycine (hereafter Gln), or urea. The following 10 treatments were included: control (no nutrient addition), NO_3^- alone, NO_2^- alone, Gln alone, urea alone, PO_4^{3-} alone, NO_3^- and PO_4^{3-} , NO_2^- and PO_4^{3-} , Gln and PO_4^{3-} , urea and PO_4^{3-} . Dissolved nutrient and flow cytometry analyses were performed as described below on samples taken on days 0, 2, 3, and 4.

^{15}N tracer experiments

To determine N transformation rates, two 1-day ^{15}N tracer experiments were conducted on back-to-back days. Surface water (1 m depth) was collected in March (during the start of the spring bloom) at ~02:00 hr on each day from an offshore station and transported back to IUI within 1 hr. Water was dispensed into acid-washed, sample-rinsed transparent polyethylene bottles (2 L per bottle, 15 bottles per treatment). Isotopically enriched nitrogen additions were made from ^{15}N 99 atom % salts (Icon Isotopes) at the following concentrations: $0.1\ \mu\text{mol L}^{-1}\ \text{NO}_3^-$, $0.1\ \mu\text{mol L}^{-1}$ urea, $0.07\ \mu\text{mol L}^{-1}\ \text{NO}_2^-$, or $0.005\ \mu\text{mol L}^{-1}\ \text{NH}_4^+$. Because surface phytoplankton communities in the stratified Gulf of Aqaba are typically co-limited for N and P (Mackey et al. 2009), no fertilization effects were expected or observed from these low-level nitrogen additions. NO_3^- and urea treatments were done during the 1st day of the experiment and NO_2^- and NH_4^+ treatments were done in the 2nd day of the experiment. The NO_3^- treatment was repeated on the 2nd day, though only t_0 and t_2 time points were taken (see below for sample timing schedule). Control (no addition) bottles were included in both experiments.

Ten baseline samples were collected at ~04:00 hr prior to adding the nitrogen spikes. Spikes were administered before dawn at approximately 05:00 hr, and three bottles from each treatment were immediately sampled at 06:00 hr within 1 hr of adding the spike. All remaining bottles (12 per treatment) were incubated in a flow-through tank that maintained ambient surface seawater temperature (~21°C). For each treatment, 6 bottles were incubated in the light under screening material as described above (50% light attenuation), and 6 were incubated in the dark under a black cloth that yielded 100% light attenuation. Three light and three dark bottles were collected

for each treatment at two time points. The first time point was at 12:00 hr, 7 hours after the tracer was added and the second time point was at 18:00 hr, 13 hours after the tracer was added. Each time point took approximately 1 hr to process. Samples were collected for flow cytometry, dissolved nutrient, and dissolved and particulate ^{15}N analyses as described below. In processing samples, separate dedicated sets of equipment (e.g. filter funnels, filtration manifolds, forceps, etc) were always used for isotopically enriched and control samples. All equipment was acid washed and thoroughly rinsed with seawater prior to use.

Dissolved nutrients, chl *a* and irradiance

NO_3^- and NO_2^- concentrations were collected during all in situ monitoring, as well as during the nutrient addition experiment and ^{15}N tracer experiment. Concentrations of NO_3^- and NO_2^- were determined using colorimetric methods described by Hansen and Koroleff (1999) modified for a Flow Injection Autoanalyzer (FIA, Lachat Instruments Model QuickChem 8000) as described previously (Mackey et al. 2007). The precision of the methods is $0.05 \mu\text{mol L}^{-1}$ for NO_2^- and NO_3^- . The detection limit for these nutrients was $0.02 \mu\text{mol L}^{-1}$. Ammonium samples from in situ field samples collected during the spring bloom progression were measured using the ortho-phthaldehyde method described by Holmes et al. (1999) with a precision of $0.02 \mu\text{mol L}^{-1}$ and a detection limit of $0.01 \mu\text{mol L}^{-1}$. Photosynthetically available radiation (PAR, 400-700 nm) was measured using a standard high-resolution profiling reflectance radiometer (Biospherical PRR-800), and provided courtesy D. Iluz. Chl *a* was measured fluorometrically using a Turner Fluorometer (Turner Designs 10-AU-

005-CE) following 90% acetone extraction at 4°C for 24 hr as described previously (Mackey et al. 2009).

Flow cytometry

Flow cytometry was used to determine concentrations of phytoplankton and non-photosynthetic microbes in the *in situ* sampling and nutrient addition and ^{15}N tracer experiments. Samples were preserved with 0.1% glutaraldehyde, flash frozen in liquid nitrogen, and stored at -80°C until analysis. Cell densities in samples from the *in situ* bloom monitoring and the ^{15}N tracer experiment were measured using a LSRII cell analyzer (Becton Dickinson Immunocytometry Systems, San Jose, CA). Before analysis SYTO 42 blue fluorescent nucleic acid stain (Invitrogen, Molecular Probes) was added at a final concentration of 8 $\mu\text{mol L}^{-1}$ and samples were incubated at room temperature for 5 minutes. The SYTO 42 stain has excitation and emission peaks at 433 nm and 460 nm respectively, and offers strong fluorescence enhancement upon binding nucleic acids such that the fluorescence signal from stained cells is maximized relative to background. Cell populations were identified using 90° light scatter autofluorescence of photopigments and SYTO 42 fluorescence. Chlorophyll positive (phytoplankton) cells were identified as *Synechococcus* based on positive phycoerythrin content. *Prochlorococcus*, picoeukaryotes (eukaryotic phytoplankton <2 μm in diameter) and nanophytoplankton (phytoplankton >2 μm in diameter) were identified based on their relative scatter and chlorophyll fluorescence levels. Non-photosynthetic cells were identified based on lack of chlorophyll fluorescence and positive SYTO 42 staining. Cell numbers were determined by spiking each sample

with a known volume and concentration of 1µm fluorescent yellow green calibration beads (Polysciences). Cell densities in the nutrient addition experiment were measured on a FACSAria cell sorter (Becton Dickinson) as described above, except that no nucleic acid stain was used and non-photosynthetic cells were not enumerated.

Particulate nitrogen ^{15}N analysis

Samples for particulate N concentration and isotopic composition were collected for the in situ bloom monitoring and for the ^{15}N tracer experiment. Samples were obtained by filtering 1 L aliquots of sample water through pre-combusted (500°C, 5 hr) 25 mm glass fiber filters (GF/F, Whatman). Sample filters were analyzed at the Stable Isotope Facility at University of California, Davis using a PDZ Europa ANCA-GSL elemental analyzer interfaced to a PDZ Europa 20-20 isotope ratio mass spectrometer (IRMS, Sercon Ltd., Cheshire, UK). Sample $\delta^{15}\text{N}$ values were calculated by adjusting the measured values using an empirical calibration scale based on correct values for laboratory standards. Two laboratory standards (NIST 1547 and acetanilide) were analyzed every 12 samples. Laboratory standards were calibrated against NIST Standard Reference Materials (IAEA-N1, IAEA-N2, IAEA-N3, IAEA-CH7, and NBS-22). The standard deviation of repeated measurements for the method is 2‰.

N uptake kinetics was determined from particulate N samples collected at the beginning and end of the ^{15}N tracer experiment. Uptake rates were measured for NO_3^- , NO_2^- , NH_4^+ and Urea using two equations based on a constant uptake model (Dugdale and Wilkerson 1986).

$$\rho_t = \frac{c_t}{t} \times \frac{{}^{15}N_s - \langle F \rangle}{{}^{15}N_{enr} - \langle F \rangle} \quad (1)$$

$$\rho_0 = \frac{c_0}{t} \times \frac{{}^{15}N_s - \langle F \rangle}{{}^{15}N_{enr} - {}^{15}N_s} \quad (2)$$

Where ${}^{15}N_s$ is the atom% ${}^{15}N$ in the sample measured by mass spectrometer as described above; ${}^{15}N_{enr}$ is the atom% ${}^{15}N$ in the initially labeled pool of NO_3^- , NO_2^- , NH_4^+ or Urea; $\langle F \rangle$ is the natural abundance of ${}^{15}N$ (in atom%); and t is the incubation time. The quantities c_t and c_0 denote the particulate N concentration ($\mu\text{mol L}^{-1}$) at time t and time zero respectively, and allow the specific uptake rate to be expressed in units of concentration. Equation 1 tends to underestimate and equation 2 tends to overestimate the uptake rate if there is a significant change in the amount of particulate matter over the course of the experiment. This effect is small for low uptake rates but can have a greater impact as uptake rates increase. We found that estimates from these equations agreed well for all but our two highest uptake rates. We therefore report an average of ρ_t and ρ_0 as suggested by Dugdale and Wilkerson (1986).

$\delta^{15}N$ of dissolved inorganic nitrogen

Water samples for dissolved NO_3^- and NO_2^- (N+N) isotopic composition were collected during the in situ bloom monitoring and during the ${}^{15}N$ tracer experiment. Samples were filtered through pre-combusted (500°C , 5h) glass fiber filters (GF/F,

Whatman) by hand under low pressure using a syringe and Swinnex filter holder. Filtrate was immediately acidified to $\text{pH} < 3$ with trace metal grade hydrochloric acid. The $\delta^{15}\text{N}$ and $\delta^{18}\text{O}$ were determined using the method of McIlvern and Altabet (2005). Briefly, the samples were rendered alkaline by addition of excess MgO , and NO_3^- was reduced to NO_2^- by shaking overnight with activated Cd . NO_2^- was then reduced to nitrous oxide with sodium azide in an acetic acid buffer for one hour, followed by analysis on a continuous flow isotope ratio mass spectrometry (IRMS). Data obtained by this method include contribution from NO_3^- and NO_2^- , which we refer to in the text as N+N for simplicity. The isotopic composition of NO_2^- alone was determined in the ^{15}N tracer experiment samples by omitting the NO_3^- reduction step.

All samples were calibrated and blank corrected using the international isotopic standards USGS 32 and USGS 35 for NO_3^- and three in house standards for NO_2^- . The reference scale for N and O isotopic composition were atmospheric N_2 and SMOW (standard mean ocean water), respectively. NO_2^- standards were run before, after, and at 12-15 sample intervals during the run. Analytical precision measured from multiple determinations on standards was 0.2% for $\delta^{15}\text{N}$ and 0.7% for $\delta^{18}\text{O}$. The detection limit for successful isotopic determination was ~ 2 nmol of N (corresponding to ~ 130 nmol N L^{-1} based on the volumes of sample we used). For samples falling below this concentration threshold in the ^{15}N tracer experiment, it was possible to increase the N concentration by addition of a known quantity of standard NO_2^- material because even a small fraction of tracer in the NO_2^- pool would measurably affect the isotopic composition of the mixture. The isotopic composition of the sample was then calculated from the measured composition of the mixture and the

known composition of the standard based on conservation of mass. This was not possible for natural abundance samples collected during the spring bloom, and only the isotopic composition of the combined N+N was determined.

All natural abundance N+N isotope data was pooled for all samples collected in situ during the bloom monitoring such that field based fractionation factors could be determined for N and O. The fractionation factor provides information about the degree of isotopic discrimination that occurs in an equilibrium process. Curves were fitted using the following equations:

$$\delta^{15}N_t = \delta^{15}N_i - \epsilon \ln \frac{[N + N]_t}{[N + N]_i} \quad (3)$$

$$\delta^{18}O_t = \delta^{18}O_i - \epsilon \ln \frac{[N + N]_t}{[N + N]_i} \quad (4)$$

Where $\delta^{15}N$ and $\delta^{18}O$ are the isotopic compositions of N and O respectively (‰), [N+N] is the concentration of N+N, subscript t denotes measurement taken at time t, subscript i denotes initial value (i.e. during mixing), and ϵ is the fractionation factor (‰).

NH_4^+ and urea oxidation rates were determined from the isotopic composition of NO_2^- measured at the 1 hr time point in the ^{15}N tracer experiment using the following equation:

$$r = \frac{1}{t} \times \frac{{}^{15}N_t c_t - \langle F_{NO_2} \rangle c_0}{{}^{15}N_{enr} - \langle F_{NO_2} \rangle} \quad (5)$$

Where r is the net reaction rate, ${}^{15}N_t$ is the atom% ^{15}N in the sample NO_2^- measured by mass spectrometer as described above for the first time point; ${}^{15}N_{enr}$ is the atom% ^{15}N

in the initially labeled pool of NH_4^+ or Urea; $\langle F \text{ NO}_2^- \rangle$ is the natural abundance of ^{15}N of NO_2^- in the baseline sample water (in atom%); and t is the incubation time. The quantities c_t and c_0 denote the NO_2^- concentration ($\mu\text{mol L}^{-1}$) at time t and time zero (before additions were made), respectively.

Because the turnover rates were more rapid than we expected and isotope dilution of the labeled pool occurred we were unable to quantify dissolved N transformations based on the 7 and 13 hour time points, thus we use the 1 hour point only. Additionally, in some cases the amount of ^{15}N spike added was too small and got consumed before these time points were reached (see discussion below).

RESULTS

Field sampling: Monthly monitoring

Time series analyses of NO_3^- and NO_2^- over a multi-year period showed a clear relationship with seasonal mixing and stratification (**Fig. 2**). In February 2008 the water column was mixed down to the seafloor before stratification occurred in March (**Fig 2A**). In the winter (e.g. January-March), NO_3^- and NO_2^- levels were inversely correlated, with higher NO_2^- levels in the upper mixed layer than at depth. In the summer (e.g. May-September), when the typical euphotic depth is approximately 100 m, primary NO_2^- maxima (PNM) emerged in the stratified water column between 50-200 m. NO_3^- concentrations remained below detection limit ($0.05 \mu\text{mol L}^{-1}$) throughout the euphotic zone, and increased gradually with depth below 100 m. This trend is typical of other years, although the actual NO_3^- and NO_2^- concentrations within and below the mixed layer vary with mixing depth. For example in 2003, when

the mixing depth was only down to ~400 m, NO_3^- and NO_2^- concentrations and inventories differed starkly from those in 2008, but still retained their inverse correlation in the winter and PNM formation occurred in summer months (**Fig. 2B**).

Monthly monitoring of chl *a* also showed seasonal changes (**Fig. 2**), with homogeneously mixed profiles in the winter months and the formation of deep chlorophyll maxima (DCM) between 50-100 m in the stratified summer months. The PNM was located at or below the depth of the DCM in 2008 and 2003.

Field sampling: Spring bloom monitoring

To determine the roles microbial communities play in controlling NO_2^- levels throughout the water column, we compared 3 profiles during early stages of stratification in 2008. The first profile was taken when the water column retained many of its characteristics from previous deep mixing. The other profiles were taken on two consecutive days after stratification was firmly established. During the spring bloom in 2008, mixing depths extending to greater than 600 m as judged from nutrient (**Fig. 3A**) and density profiles (**Fig. 4**). Field sampling conducted on March 18 at the very onset of stratification (**Fig. 3A**) showed nearly homogenous NO_3^- levels (~3 $\mu\text{mol L}^{-1}$) throughout the water column, with a tendency to lower concentrations in surface waters (~2 $\mu\text{mol L}^{-1}$). In these surface waters, NO_2^- was slightly higher (0.23 $\mu\text{mol L}^{-1}$) than throughout the rest of the euphotic zone (~0.18 $\mu\text{mol L}^{-1}$), whereas NH_4^+ levels peaked at 100 m (0.42 $\mu\text{mol L}^{-1}$). Sampling conducted on the 24 and 25 March 2008 (**Fig. 3A**) following stratification and during the spring bloom showed continued drawdown of NO_3^- in surface waters, as well as the formation of a PNM

peak between 200-250 m (reaching $0.59 \mu\text{mol L}^{-1}$ at 200 m on 25 March). NH_4^+ levels were variable throughout the euphotic zone, with maximum levels occurring between 160-200 m above the NO_2^- maxima, and reaching $0.59 \mu\text{mol L}^{-1}$ at 200 m on 25 March. Particulate N levels increased in surface waters from ~ 5 to $\sim 35 \mu\text{g N L}^{-1}$ between March 18-24, and decreased slightly to $\sim 20 \mu\text{g N L}^{-1}$ by March 25 (**Fig. 3C**).

Chl *a* profiles from 18, 24, and 25 March 2008 (**Fig. 3B**) showed the progression of the phytoplankton bloom following stratification. On 18 March, the chl *a* profile was homogenous throughout the euphotic zone ($\sim 0.2 \text{ mg m}^{-3}$), except in the upper 20 m where it increased to $\sim 0.5 \text{ mg m}^{-3}$ (**Fig. 3B**). Chl *a* maxima were apparent in both the 24 and 25 March profiles, reaching maximum concentrations of $0.8\text{-}0.9 \text{ mg m}^{-3}$ between 40-60 m.

Flow cytometry measurements show that by March 24 and 25, phytoplankton populations were highest in the upper water column and were dominated by *Synechococcus* and nanophytoplankton (**Fig. 5**). Picoeukaryotes were present in smaller numbers (**Fig. 5**), and no substantial populations of *Prochlorococcus* were identified (data not shown). In the surface, *Synechococcus* reached $\sim 80,000 \text{ cells mL}^{-1}$ and nanophytoplankton reached $\sim 20,000 \text{ cells mL}^{-1}$. Both populations increased more than two-fold between March 24 and 25 between depths of 60-120 m despite being below the euphotic depth (60 m). The picoeukaryote population decreased from ~ 3000 to $\sim 800 \text{ cells mL}^{-1}$ between March 24-25 in surface waters, whereas a small increase in cell density was observed between 100-140 m. Non-photosynthetic cells were more evenly distributed throughout the water column, ranging from 5×10^5 - $2 \times 10^6 \text{ cells mL}^{-1}$ (**Fig. 5**).

Isotopes of dissolved nitrate

On March 18th the $\delta^{15}\text{N}_{\text{N+N}}$ and $\delta^{18}\text{O}_{\text{N+N}}$ profiled were homogenous averaging $1.0 \pm 0.08 \text{ ‰}$ and $6.7 \pm 0.17 \text{ ‰}$, respectively. As stratification progressed and the bloom developed, $\delta^{15}\text{N}_{\text{N+N}}$ and $\delta^{18}\text{O}_{\text{N+N}}$ values both increased in surface waters. $\delta^{15}\text{N}_{\text{N+N}}$ reached peak values of $\sim 10 \text{ ‰}$ at 60 and 20 m on March 24 and 25 respectively (**Fig. 6A**), whereas maximum $\delta^{18}\text{O}_{\text{N+N}}$ values of 53 and 40 ‰ were seen at the surface (**Fig. 6B**). The $\delta^{15}\text{N}$ also showed a subsurface peak of $\sim 11 \text{ ‰}$ at 160 m. N and O both roughly followed Raleigh fractionation patterns during the bloom (**Fig. 7**), and had field based fractionation factors (ϵ) of 1.9 ‰ and 10.3 ‰ respectively.

On March 18 the $\delta^{18}\text{O}_{\text{N+N}} : \delta^{15}\text{N}_{\text{N+N}}$ ratios plotted along a straight line with a slope of 2:1 (**Fig. 8**). Because the water column was well mixed, all of the $\delta^{18}\text{O}_{\text{N+N}} : \delta^{15}\text{N}_{\text{N+N}}$ data clustered near the values for deep water. By March 24 increased assimilation and nitrification were apparent. The $\delta^{18}\text{O}_{\text{N+N}} : \delta^{15}\text{N}_{\text{N+N}}$ values plotted along a line with slope 3:1 (**Fig. 8B**), indicating the impact of nitrification. Recycling of N continued to increase as the DIN inventory was further depleted during the bloom, and by March 25 the $\delta^{18}\text{O}_{\text{N+N}} : \delta^{15}\text{N}_{\text{N+N}}$ values plotted along a line with slope 5:1 (**Fig. 8C**). As in the March 24 profiles, both isotopes were generally heavier in the surface where assimilation of NO_3^- was highest, and decreased with depth.

Nutrient addition experiment

Natural phytoplankton assemblages in the Gulf at the time of the nutrient addition experiment included predominantly picophytoplankton (phytoplankton < 2

μm in diameter), and the initial population comprised picoeukaryotes ($300 \text{ cells mL}^{-1}$), *Synechococcus* ($900 \text{ cells mL}^{-1}$), and *Prochlorococcus* ($19,700 \text{ cells mL}^{-1}$). Control populations decreased slightly by the fourth day of the incubation (**Fig. 9A**). By day 4, the picoeukaryote population increased over an order of magnitude in all treatments receiving N and P together (**Fig. 9A**), except for the treatment receiving $\text{NO}_2^- + \text{PO}_4^{3-}$. This treatment, along with all treatments receiving N without P, clustered near control levels. *Synechococcus* populations increased in all treatments receiving N and P together (**Fig. 9A**). With the exception of NO_3^- alone, all treatments receiving N without P increased approximately 1-2 orders of magnitude over control levels. *Synechococcus* populations in bottles treated with NO_3^- alone crashed completely within 1-2 days of incubation (note this treatment is not included in **Fig. 9A** because the values are off scale). The *Prochlorococcus* population remained similar to time zero levels across all treatments receiving N alone or together with P (**Fig. 9A**).

In the majority of treatments the NO_2^- levels increased (NO_2^- was generated) between the first and last days of the experiment relative to the control (**Fig. 9B**); however, NO_2^- decreased (was consumed) in treatments receiving PO_4^{3-} alone, NO_2^- alone, or NO_2^- together with PO_4^{3-} . All treatments differed significantly from the control ($p < 0.05$), with the exception of treatments receiving Gln alone, urea alone, or urea together with PO_4^{3-} .

^{15}N tracer experiment

During the ^{15}N tracer experiment the phytoplankton population was dominated by *Synechococcus*, followed by nanophytoplankton and picoeukaryotes (**Fig. 10**).

Non-photosynthetic cells were approximately an order of magnitude more abundant than phytoplankton (**Fig. 10**). There were no substantial differences in the community composition of the baseline water used on the 1st and 2nd day of the experiment (**Fig. 10**).

Background N concentrations during the ¹⁵N tracer experiment were 0.2 $\mu\text{mol L}^{-1}$ NO_3^- , 0.03 $\mu\text{mol L}^{-1}$ NO_2^- , and 0.025 $\mu\text{mol L}^{-1}$ NH_4^+ . Urea concentrations were $\sim 1 \mu\text{mol L}^{-1}$ (A. Post and E. Meeder unpublished data).

Calculation of N transformation rates

In order to estimate fluxes of N between different N pools, we used isotope data from the ¹⁵N tracer experiment where possible. Because the turnover rates were very rapid and isotope dilution of the labeled pool increased with time, we based these calculations on the 1 hour time point where these error sources would be minimal. Where calculations based on tracer data were not feasible due to limitations in the experimental design, we used changes observed in concentration data from *in situ* monitoring (March 18-25) and inventory mass balance. For the mass balance calculations we selected depth intervals over which a specific process is likely to dominate the pool and contribution from other processes is minimal. (For example, we assume assimilation by phytoplankton to be negligible in deep water where light is very low). When both data sets allowed estimation calculations using both approaches were compared. We sought to quantify rates for the following N transformations: (1) biological assimilation for NO_3^- , NO_2^- , NH_4^+ , and urea; (2) incomplete NO_3^- reduction to NO_2^- by phytoplankton; (3) oxidation of NO_2^- to NO_3^- during nitrification; and (4)

oxidation of NH_4^+ and urea (via NH_4^+ intermediate) to NO_2^- during nitrification.

Biological N assimilation

N uptake and assimilation rates were estimated in the ^{15}N tracer experiment based on direct measurements of enrichment in the particulate fraction after 7 and 13 hr of incubation for both light and dark treatments. Urea uptake ($\sim 1200 \text{ nmol N L}^{-1} \text{ day}$) was approximately three-fold faster than NO_3^- uptake ($\sim 430 \text{ nmol N L}^{-1} \text{ day}$) in the light (**Table 1, Fig. 11A,B**). For both urea and NO_3^- uptake rates were higher in light bottles than in dark bottles and the uptake rates were constant over the course of the experiment (**Table A, Fig. 11A,B**).

Our calculations assume an excess pool of ^{15}N was available for uptake during the experiment, and this may not have been the case for NO_2^- and NH_4^+ . Because of the small ^{15}N enrichment in the NO_2^- and NH_4^+ treatments, the uptake calculations for these species could underestimate their actual uptake rates if all of the ^{15}N was assimilated before the measurement was taken. Based on the uptake curves from the particulate N data (**Fig. 11D**) and comparison to the maximum rates that could theoretically be measured based on the size of the spike added and the time resolution of the experiment, it appears that all of the $^{15}\text{NH}_4^+$ was assimilated prior to the 7 hr sampling in both light and dark bottles, so the values we report for NH_4^+ ($\sim 160\text{-}170 \text{ nmol N L}^{-1} \text{ day}$) largely underestimate the real uptake rates. For NO_2^- , all of the $^{15}\text{NO}_2^-$ was assimilated before the 13 hr sampling; however, we can still base our estimates for NO_2^- on the 7 hr sampling when ^{15}N was still available (**Fig. 11C**). NO_2^-

uptake was three-fold higher in the light ($\sim 90 \text{ nmol N L}^{-1} \text{ day}$) than in the dark ($\sim 30 \text{ nmol N L}^{-1} \text{ day}$).

Reduction of NO_3^- to NO_2^-

The rate of NO_3^- reduction to NO_2^- by phytoplankton is dependent on light and on phytoplankton community structure. Because the process is driven by light, we were unable to measure this process in the ^{15}N tracer experiment, as phytoplankton in our pre-dawn samples received no light to initiate this process. Therefore, the rate of NO_3^- reduction based on the 1 hr time point in the ^{15}N tracer experiment was essentially zero, as expected. To determine NO_3^- reduction rates at specific light levels and chl *a* concentrations, we calculated a range of NO_3^- reduction rates based on changes in the *in situ* NO_2^- concentrations determined during the spring bloom. Because NO_2^- has various sources and sinks, we calculated rates for 60-200 m where NO_3^- reduction by phytoplankton was likely the dominant process. We based our calculations on these depths because they have low but consistent light levels where phytoplankton exist (**Fig. 5**) but photosynthetic N assimilation is light limited. At these depths phytoplankton biomass still far exceeds biomass from nitrifying microbes. Moreover, phytoplankton doubling times (and hence their N utilization activities) are considerably faster than for nitrifying microbes, occurring on the scale of 1-3 days versus ~ 2 weeks, so they are likely to be the dominant source of NO_2^- at these depths. We do not calculate values for depths below 200 m because (1) nitrification at these permanently dark depths where phytoplankton are scarce could substantially impact the NO_2^- pool (**Fig. 12A**), and (2) light would likely be too low to

support the de novo uptake and reduction of NO_3^- by the small residual phytoplankton population that did persist at these depths following stratification. Similarly, we do not calculate NO_3^- reduction rates based on depths within the euphotic zone (0-60 m) because we expect photosynthetic assimilation to consume a substantial portion of the NO_2^- pool, thus estimates from this region would underestimate the rate of NO_2^- generated from NO_3^- . Rather, we base our NO_3^- reduction rates on concentration data from depths of 60-200 m, and we used the period between March 18-24 (**Fig. 12A**) because phytoplankton were replete with NO_3^- on the 18th, so NO_3^- concentrations would not have limited the measured rates.

Although we expect NO_3^- reduction to be the dominant process at depths of 60-200 during the first part of the bloom (**Fig. 12A**), nitrification likely occurred at these depths and introduces a certain degree of error to our estimates. NO_3^- reduction rates were strongly correlated with light ($R^2=0.99$, **Fig. 13B, Table 2**) and ranged from 2.2-58 $\text{nmol L}^{-1} \text{ day}^{-1}$ (0.092-2.4 $\text{nmol L}^{-1} \text{ hr}^{-1}$). Chl *a* concentration was also correlated with NO_3^- reduction rates; however, this relationship was primarily because chl *a* abundance is controlled by light (**Fig 12C**). To parse the independent effect of chl *a* concentration on NO_3^- reduction rate we compared the residual chl *a* and NO_3^- reduction rate data after subtracting out the influence of light on each according to the following procedure. The influence of light on each parameter was calculated based on the equations best fit as shown in **Fig. 13B** and **C**. The calculated value was subtracted from the actual measured value to obtain the residual value. The residual values are the portions of the actual chl *a* and NO_3^- reduction rate measurements that are not accounted for by light. The residual values of chl *a* and NO_3^- reduction rate

were then plotted (**Fig. 13D**) to determine the relationship between chl *a* and NO_3^- reduction rate. With the exception of one outlier point (showing a lower NO_3^- reduction rate than expected), a strong linear relationship existed between residual chl *a* levels and residual NO_3^- reduction rates (**Fig. 13D**). Interestingly, the outlier point coincided with an NH_4^+ peak at 120 m that got consumed between March 18 and 24 (**Fig. 3A**). The NO_3^- reduction rate at this depth did not correspond to chl *a* because a portion of the NO_2^- at that depth was formed by NH_4^+ oxidation. If all of the NH_4^+ drawn down at this depth between March 18-24 was oxidized to NO_2^- it would have contributed $\sim 115 \text{ nmol NO}_2^- \text{ L}^{-1}$, or approximately 80% of the NO_2^- inventory at that depth. While the NO_3^- reduction rate we calculated for 120 m contains a non-quantified, low input from NH_4^+ oxidation, the strong correlations between NO_3^- reduction and light and chl *a* at the other depths are consistent with our assumption that NO_3^- reduction was the dominant NO_2^- forming process at these depths.

Oxidation of NO_2^- to NO_3^-

The rate of NO_2^- oxidation was estimated from changes in the NO_3^- concentrations at depths where we expected the NO_2^- oxidation to be the dominant process. NO_2^- oxidation is the only process likely to generate NO_3^- (assuming lateral advection and vertical diffusion or shoaling were minimal), so we selected depths of 250-275 m between March 24-25 (**Fig. 12B**), where a substantial amount of NO_3^- was generated and, to prevent falsely low NO_2^- oxidation rates, where assimilation of NO_3^- by phytoplankton was likely very low due to lack of light. We compared concentration profiles taken on March 24 and 25 because enough NO_2^- had

accumulated at these depths between March 18-24 (**Fig. 12A**) that NO_2^- concentrations would not limit the NO_2^- oxidation rates as may have been the case deeper in the water column. (For example, over March 18-24 NO_2^- oxidation reached a maximum rate of $\sim 30 \text{ nmol L}^{-1} \text{ day}$ for depths greater than 300 m, but may have been limited by substrate availability.) Based on NO_3^- concentration increases from March 24 and 25, the rates of NO_2^- oxidation at 250 and 275 m were 350 and 490 $\text{nmol N L}^{-1} \text{ day}$, respectively.

Oxidation of NH_4^+ and urea to NO_2^-

NH_4^+ and urea oxidation rates were determined based on measurements of NO_2^- isotopic composition 1 hour after ^{15}N enriched spikes of NH_4^+ or urea were added in the ^{15}N tracer experiment. We were unable to quantify rates for these reactions from the 7 and 13 hr time points because the ^{15}N enrichments were too small and the turnover of the N pools was too rapid for accurate estimates to be made over these longer time scale (isotope dilution impacted the results). Oxidation of NH_4^+ to NO_2^- occurred at a rate of $16.4 \pm 8.1 \text{ nmol N L}^{-1} \text{ d}^{-1}$ (or $0.68 \pm 0.34 \text{ nmol N L}^{-1} \text{ hr}^{-1}$; **Table 3**). However, if the organisms performing these reactions are light-sensitive, these reactions could be limited to night within the upper water column, so the daily rates would need to be scaled accordingly.

The calculated rate for NH_4^+ oxidation agrees remarkably well with NH_4^+ consumption data from March 24-25 below 200 m and March 18-24 below 450 m where net NH_4^+ consumption occurred (**Fig. 12A,B; Fig. 14**). At these depths where photosynthetic assimilation of NH_4^+ is small due to lack of light, the main process

consuming NH_4^+ is nitrification (NH_4^+ oxidation). The highest rate we observed was $320 \text{ nmol L}^{-1} \text{ day}^{-1}$ at 200 m where a large reservoir of NH_4^+ existed (reaching up to 600 nmol L^{-1}) on March 24 (**Fig. 14**). The rates were lower at depths with lower NH_4^+ concentrations, suggesting that NH_4^+ oxidation rates were concentration dependent (Ward 1985). **Fig. 14** shows that NH_4^+ oxidation was significantly linearly correlated with NH_4^+ concentration ($R^2=0.95$), and had not become saturated at NH_4^+ concentrations up to 600 nmol L^{-1} . Oxidation of urea to NO_2^- (likely via NH_4^+ as an intermediate) occurred at a rate of $14.1 \pm 7.6 \text{ nmol N L}^{-1} \text{ d}^{-1}$ ($0.59 \pm 0.32 \text{ nmol N L}^{-1} \text{ hr}^{-1}$).

DISCUSSION

NO_2^- dynamics during the transition from mixing to stratification

The persistence of NO_2^- in the ocean results from an imbalance in the processes that produce and consume nitrite. In the aerobic water column, NO_2^- is produced by ammonium oxidizing organisms during the first step of nitrification, and by phytoplankton during incomplete NO_3^- assimilation. It is consumed by NO_2^- oxidizers during the second step of nitrification, and by phytoplankton during assimilation. Nitrite accumulates when production exceeds consumption as long as dispersion rates are sufficiently low. In the Gulf of Aqaba in winter, NO_2^- accumulates throughout the mixed layer, whereas in the summer NO_2^- accumulates below the euphotic zone, forming a PNM (**Fig. 2**; Al-Qutob et al. 2002; Meeder et al. submitted).

Phytoplankton are likely the major source of NO_2^- during convective winter

mixing. We base this conclusion on three main observations. First, *substantial* NO_2^- accumulation is observed throughout the mixed layer, which is the depth of the water column occupied by phytoplankton, regardless of the exact mixing depth (**Fig 2**). NO_2^- does not accumulate below the mixing depth where phytoplankton do not survive. If the major source of the NO_2^- were NH_4^+ oxidizers, which can occupy the entire water column including deep waters below the mixing depth, then the accumulation of NO_2^- would not be confined exclusively to the mixed layer. Phytoplankton, on the other hand, can only inhabit the mixed layer and would not survive in the permanent darkness of the deep water. Second, *the strong inverse correlation between* NO_3^- *and* NO_2^- *in winter profiles is maintained regardless of shoaling or deepening of the mixing depth throughout the winter* (**Fig. 2**). This correlation suggests that NO_3^- is the source of NO_2^- generated within the mixed layer because as NO_3^- decreases, NO_2^- increases. Third, *the* NO_2^- *and* NO_3^- *inventories in the winter mixed layer agree well with measured ratios of* NO_2^- *excretion following* NO_3^- *uptake by light limited phytoplankton*. During 2003 NO_3^- in the winter mixed layer was drawn down by 4-6 $\mu\text{mol L}^{-1}$ compared to deep water, and NO_2^- in the mixed layer increased to $\sim 0.4 \mu\text{mol L}^{-1}$. Similarly in 2008 when mixing was deeper, NO_3^- was drawn down by $\sim 2 \mu\text{mol L}^{-1}$ and NO_2^- increased $\sim 0.3 \mu\text{mol L}^{-1}$. These NO_2^- release-to- NO_3^- uptake ratio of ~ 10 -15% are consistent with the range of ratios for light limited phytoplankton cultures measured in other studies (Collos 1998 and references therein), and is supported by incubation studies in the Gulf in which NO_2^- was produced by phytoplankton (Al-Qutob et al. 2002).

In a mixed water column, biological N transformation rates reflect the

“average” light conditions because their products get distributed over the entire mixed layer as mixing occurs throughout the day. The homogeneity of NO_2^- in the mixed layer suggests that the mixing rate (e.g. the time required for a parcel of water to complete one cycle of mixing from surface to depth and back to surface) exceeds the rates of NO_2^- production and consumption such that no localized accumulation or drawdown of NO_2^- is observed in the mixed layer.

In contrast, organisms at any given depth in a stratified water column are subject to relatively predictable light regimes. This allows different groups of organisms to populate depths they are best adapted to occupy. The PNM forms when stratification imposes a range of physical and chemical gradients on organisms, allowing different steady states to be reached between NO_2^- production and consumption at different depths in the water column. This is evident from summer profiles of NO_2^- from 2003 and 2008, where NO_2^- accumulates at ~100 m, but not in surface or deep waters. These monthly “snapshots” provide information on steady state nutrient levels; they reveal the net result of all processes that produce and consume NO_2^- at a given depth. To parse the individual contributions of different N transformation rates, better time resolution is needed. Our data of nutrient concentrations and isotope values from in situ monitoring during the transition from mixing to stratification, in conjunction with ^{15}N uptake and transformation rates obtained during the tracer experiment can be used to shed light on N transformation rates at different depth in the water column of the Gulf of Aqaba during summer.

We define four principal regions of the water column based on their different combinations of N cycle processes and rates (**Fig. 15**). The “euphotic zone” (0-60 m

during our study), which extends from the surface to the compensation depth (i.e., the depth at which light is attenuated to 1% of surface irradiance and photosynthesis balances respiration, **Fig. 13A**). The “sub-euphotic zone” (60-160 m during our study) extends to the depth at which light is attenuated to 0.001% of surface irradiance (**Fig. 13A**). The upper PNM (180-225 m during our study), which encompasses depths with substantial accumulation of NO_2^- . The “disphotic zone” extends from the depth where the NO_2^- concentrations of the PNM starts decreasing and extends to the sea floor (> 225 m during our study). We note that the absolute depths given above for our study are not universal for all water columns because they would change depending on the depth of the mixed layer prior to stratification, latitude, amount of chl *a* present, and other factors influencing light penetration. Below we describe how the N cycling processes that produce and consume NO_2^- generate conditions that give rise to the PNM.

The euphotic zone

The euphotic zone is the layer in which sufficient light is available for photosynthesis to exceed community respiration, and where the majority of photosynthetic biomass is generated. Between March 18 and 25, most of the available NO_3^- and NO_2^- in the euphotic zone was assimilated and converted into biomass (e.g. photosynthesis) (**Fig. 3A,C**). In this process the lighter isotopes of N and O are preferentially assimilated causing the residual pool of NO_3^- to become enriched in ^{15}N and ^{18}O . $\delta^{15}\text{N}_{\text{N+N}}$ values within the euphotic zone below 0 m show elevated values (up to 11.75 ‰ at 20 m on March 25) compared to deep water $\delta^{15}\text{N}_{\text{N+N}}$ (~2 ‰) indicative

of substantial uptake (**Fig. 6A**).

Nitrification played an important role in regenerating N from organic matter in the euphotic zone, where DIN concentrations are vanishingly low due to efficient phytoplankton uptake. On March 18, $\delta^{18}\text{O}_{\text{N+N}} : \delta^{15}\text{N}_{\text{N+N}}$ ratios in the mixed water column fell along a slope of ~2:1. The $\delta^{18}\text{O}_{\text{N+N}} : \delta^{15}\text{N}_{\text{N+N}}$ ratios increased as the spring bloom progressed, and by March 25 the ratios were close to 5:1 (**Fig. 8C**), suggesting that nitrification was a substantial source of NO_3^- to phytoplankton throughout the bloom. Indeed, particulate N concentration increased by $\sim 30 \mu\text{g L}^{-1}$ between March 18-24 (**Fig 3C**), yet the DIN inventory was only depleted by $\sim 20 \mu\text{g L}^{-1}$ (**Fig. 3C; Fig 11A**). Therefore, at least 33% ($\sim 10 \mu\text{g L}^{-1}$) of the N assimilated by phytoplankton in the surface was derived from recycled sources, but could be more since a molecule could be assimilated and regenerated more than once. This efficient recycling is also evident from the light $\delta^{15}\text{N}_{\text{N+N}}$ values at 0 m relative to values slightly deeper in the euphotic zone (**Fig. 8B,C**). Assimilation generally serves to make the $\delta^{15}\text{N}_{\text{N+N}}$ pool heavier; however, if all the NO_3^- was consumed at 0 m by assimilation in the first part of the bloom, then no fractionation would be apparent. The low DIN concentrations and light $\delta^{15}\text{N}_{\text{N+N}}$ values in the surface suggest that assimilation and nitrification were closely coupled.

Another potential source of light N in surface waters is biological fixation of N_2 . Indeed the diazotrophs *Trichodesmium* sp. (Post et al. 2002; Mackey et al. 2007; Foster et al. 2009), *Cyanothece* sp. (Mackey et al 2007), and γ proteobacteria (Foster et al. 2009) have all been identified in the Gulf of Aqaba. DIN originating from N_2

fixation reflects the $\delta^{15}\text{N}$ of atmospheric N gas, which is by definition zero. Two studies have investigated N_2 fixation rates in the Gulf of Aqaba at different times throughout the year. Hadas and Erez (2004) found that fixation was below detection in the mid to late summer under stratified oligotrophic conditions, as well as in the winter under mixed mesotrophic conditions. However, Foster and coworkers (2009) found that N fixation occurred at low but measurable rates ($1\text{-}2\text{ nmol L}^{-1}\text{ day}^{-1}$) in both the late summer and spring, and suggested that these rates represent background fixation rates for the Gulf under conditions where diazotrophs are not blooming. These rates are very small compared to our calculated nitrification rates ($\sim 450\text{ nM day}^{-1}$) thus the $\delta^{15}\text{N}_{\text{N+N}}$ of our samples would not be affected significantly by N fixation. However, if fixation rates were closer to those observed in other oligotrophic regions (e.g. $\sim 0.2\text{-}3\text{ }\mu\text{mol L}^{-1}\text{ day}^{-1}$; Montoya et al. 2004) then the isotopic composition of N in our samples could have been affected by fixation. We did not observe a *Trichodesmium* bloom during our sampling; however, we did not measure N_2 fixation directly, and the possibility that the low $\delta^{15}\text{N}_{\text{N+N}}$ observed in our surface samples is partially due to N^2 fixation cannot be confirmed or ruled out.

The sub-euphotic zone

In this zone light is attenuated below the compensation threshold, and respiration by the entire microbial community exceeds photosynthesis by phytoplankton. Regression analysis for depths in the sub-euphotic zone and down to 200 m showed that NO_2^- production rates correlated very strongly with decreasing irradiance (**Fig. 13B**), which is expected since phytoplankton NO_2^- release and

nitrification are both expected to increase with decreasing irradiance. However, regression analysis of residual chl *a* and residual NO₂⁻ production data (i.e. with the influence of irradiance removed) also showed a remarkably strong correlation (**Fig. 13D**), and suggested that NO₃⁻ uptake and released as NO₂⁻ by light limited phytoplankton was the dominant N transformation process in the sub-euphotic zone (**Fig 11A**) during the beginning of the bloom (March 18-24). An exception occurred at 120 m, where a significant portion of NO₂⁻ was generated from NH₄⁺ oxidation rather than NO₃⁻ reduction based on regression statistics (**Fig. 14**). The contribution of NH₄⁺ oxidation to the NO₂⁻ pool highlights the substrate limitation of NH₄⁺ oxidation rates at other depths (Fig. 13D), because it suggests that NH₄⁺ oxidation can match or exceed NO₃⁻ reduction within the sub-euphotic zone when ample NH₄⁺ is available.

Further evidence for phytoplankton mediated NO₃⁻ reduction is that the ratio of NO₂⁻ excretion to NO₃⁻ uptake ranged from 0% above 60 m to 26% at 160 m (**Fig 11A**), which is similar to observations from the Atlantic and Pacific Oceans (Collos 1998 and references therein). By March 24, a broad region of accumulated NO₂⁻ had formed between 60-300 m as a result of this phytoplankton NO₂⁻ release (**Fig. 3A**). However, between March 24 and 25th there was a net decrease in the NO₂⁻ inventory (**Fig. 3A; Fig 11A**), indicating that consumption of NO₂⁻ by assimilation and/or microbial oxidation had surpassed NO₂⁻ production.

While the sub-euphotic zone is below the compensation point and net respiration occurs on a community scale, it is important to note that phytoplankton continue to perform photosynthesis and uptake nutrients in this dimly illuminated layer (these rates are simply exceeded by community respiration rates). The $\delta^{15}\text{N}_{\text{N+N}}$

was slightly elevated in the sub-euphotic zone (**Fig. 6A**), indicating that assimilation of N by phytoplankton or other microbes was occurring. While it may at first seem counterintuitive that phytoplankton could be both a source and a sink for NO_2^- in the sub-euphotic zone over the course of a bloom, this observation simply underscores that the phytoplankton community is a diverse assemblage of different sub-populations, each with its own light requirements and N assimilation strategies. During the bloom succession occurs within the phytoplankton community, and different sub-populations coexist, compete, and eventually either survive or get out competed. Therefore, while one sub-population may take up NO_3^- and release NO_2^- due to light limitation, another may be able to complete the assimilation of NO_3^- into biomass. Heterotrophic assimilation of NO_3^- and NO_2^- , which is not light-dependent, could also have caused the high $\delta^{15}\text{N}_{\text{N+N}}$ values at these depths.

Between March 24-25 cell concentrations of *Synechococcus* and non-photosynthetic microbes approximately doubled within the sub-euphotic zone, and nanophytoplankton also increased slightly (**Fig. 5**). Nanophytoplankton include phytoplankton taxa such as diatoms, dinoflagellates, and cyanobacteria $>2\ \mu\text{m}$, and monitoring conducted after our sampling period showed that the spring bloom became dominated by diatoms by the beginning of April (Iluz et al. 2009). NO_3^- and NO_2^- uptake is not light dependent in some diatoms, and uptake (though not necessarily assimilation if the N is stored within a vacuole) by these comparatively large cells may have played a role in the drawdown of NO_2^- .

The upper PNM

The upper PNM (180-225 m) is a dynamic region where NO_2^- accumulates. Within this layer light is attenuated to virtually non-existent levels too low for phytoplankton populations to grow (**Fig 12**). During the first part of the bloom NO_2^- dynamics in the upper PNM were similar to the sub-euphotic zone in that NO_2^- production was strongly correlated with chl *a* levels, implicating phytoplankton as the main source of NO_2^- (**Fig. 13**). However, over the next day, NO_2^- continued to be produced within the upper region of the PNM and was no longer correlated to chl *a* (**Fig. 12B**). The NO_2^- produced by phytoplankton during the first part of the bloom was derived from NO_3^- taken up during the mixed period (e.g. March 18) when, due to mixing, light was episodically high enough to support NO_3^- uptake. Following stratification phytoplankton trapped below the euphotic depth would have dispelled that N as NO_2^- due to a lack of light energy needed to complete the reduction and assimilation process. However, by March 24 phytoplankton trapped within the upper PNM would have been without significant light for approximately one week. It is unlikely that these cells could initiate de novo uptake of fresh NO_3^- and be the source of NO_2^- generated at this depth between March 24 and 25. NH_4^+ oxidizers, on the other hand, would thrive under the low light conditions and would have access to an increasingly large pool of DON from which to access their NH_4^+ substrate.

NO_2^- can only accumulate if production exceeds consumption (and dispersion is sufficiently low). The NO_2^- accumulation in the upper PNM (180-225 m) during the second part of the bloom indicates that NO_2^- production and consumption were decoupled, with production (primarily by NH_4^+ oxidizers) exceeding consumption.

The main NO_2^- consumption process at these depths would have to be NO_2^- oxidation because photosynthetic NO_2^- assimilation would not be possible at these dark depths. Based on increases in the NO_3^- concentration at these depths, NO_2^- oxidation indeed occurred between 180-225 m; however, the rate was not sufficient to consume all of the NO_2^- that was generated. This balance was only reached below 225 m, where NO_3^- was generated while both NH_4^+ and NO_2^- were consumed (Fig L-B), strongly implicating coupled NH_4^+ and NO_2^- oxidizing communities in the lower PNM. Olsen (1981) postulated that the greater sensitivity of NO_2^- oxidizers than NH_4^+ oxidizers to light could be a mechanism by which PNM form. Guerrero and Jones (1996) added to this model, noting that NH_4^+ oxidizers recover more rapidly from photoinhibition than do NO_2^- oxidizers. Based on these observations, NH_4^+ oxidizers are postulated to be more active in shallower regions of the water column than NO_2^- oxidizers, and this spatial segregation of the populations leads to accumulation of NO_2^- . In our profiles, NO_3^- concentration data suggests that NO_2^- oxidation was closely coupled to NH_4^+ oxidation beginning at ~225 m, below which production of NO_3^- was observed concurrently with NH_4^+ and NO_2^- consumption (**Fig. L-B**). However, above this depth NO_2^- accumulation was noted between March 24-25, indicating that NO_2^- oxidation rates were too low to match the rate at which NO_2^- was generated in the upper PNM.

The disphotic zone

The disphotic zone contains the lower portion of the PNM (e.g. 225-300 m; Fig. F-A) as well as deep water. (This region differs from the “aphotic zone,” which includes depths below about 1000 m where light no longer penetrates.) Within the

disphotic zone, sunlight is attenuated to less than 0.001% of surface irradiance and phytoplankton are unable to perform photosynthesis. Therefore, non-photosynthetic microbial processes dominate the N cycle at these depths, and indeed, several observations are indicative of a nitrification-dominated system. First, as noted above, NH_4^+ and NO_2^- were consumed while NO_3^- was produced below 225 m (**Fig. 12B**), consistent with microbially mediated oxidation of NH_4^+ and NO_2^- into NO_3^- . Second, the $\delta^{15}\text{N}_{\text{N+N}}$ in this layer was relatively light ($\sim 3\text{‰}$), suggesting that its source was organic matter regenerated by nitrifiers. Third, particulate N concentrations decreased in this layer between March 24-25 by $0.2\text{--}0.3\text{ }\mu\text{mol N L}^{-1}$ (**Fig. 3C**), and NO_2^- levels decreased $0.1\text{--}0.3\text{ }\mu\text{mol NO}_2^- \text{ L}^{-1}$ (**Fig. 12B**). These changes agree well with the amount of NO_3^- generated in this layer over the same time period (up to $\sim 0.3\text{--}0.5\text{ }\mu\text{mol NO}_3^- \text{ L}^{-1}$; **Fig. 12B**), and suggest that the abundant supply of dead phytoplankton cells trapped in this layer during stratification were remineralized by the microbial loop. Microbial nitrification therefore refined the shape of the lower PNM by consuming a portion of the broad band of NO_2^- that was generated during the beginning of stratification. The effect can be seen on March 25, where the falling limb of the PNM was much steeper than on March 24 (**Fig. 3A**).

Interesting features of N cycling in the Gulf of Aqaba

Two interesting observations were apparent from the isotopic composition of O and N as the bloom developed. First, the background $\delta^{18}\text{O}_{\text{N+N}}$ measured in the mixed water column and in deep water samples from the stratified water column was $\sim 6.5\text{‰}$, much heavier than in other marine waters (Leichter et al. 2007).

One possible explanation for the heavier $\delta^{18}\text{O}_{\text{N+N}}$ could be the composition of exogenous NO_3^- sources to the Gulf. Because of its arid location, the Gulf receives very little NO_3^- input from precipitation or rivers; however, NO_3^- input from atmospheric dry deposition is significant. Wankel and coworkers (2009) measured the NO_3^- content, isotopic composition, and deposition rates of atmospheric dry deposition for the Gulf, and found that the $\delta^{18}\text{O}_{\text{N+N}}$ in dust ranged from 65.1-84.9 ‰. High deposition rates of this ^{18}O enriched NO_3^- source could skew the overall $^{18}\text{O}_{\text{N+N}}$ toward higher values. To check the validity of this assumption, we calculated what the background $\delta^{18}\text{O}_{\text{N+N}}$ would be if the signal from dry deposition were removed using a simple mass balance/ box model approach. We based our estimates on the portion of the Gulf of Aqaba north of Station A, which has a surface area of 44.1508 km^2 , and a volume of 9.1931 km^3 (Cohen and Ottolenghi 2004). Assuming an average flux of NO_3^- from dry deposition ($35 \mu\text{mol m}^{-2} \text{d}^{-1}$; Wankel et al. 2009) we calculated the total load of NO_3^- from dry deposition to over a 2 year period, which is the residence time for water in the Gulf. The total NO_3^- inventory in the seawater was calculated from the volume of the northern Gulf and NO_3^- concentration data from the 2008 mixing period when NO_3^- was homogeneously distributed from the Gulf's surface to the seafloor. Based on these estimates, the total NO_3^- inventory for the northern Gulf is 27,579,300 moles NO_3^- , of which 1,128,052 moles NO_3^- derives from dry deposition over a 2 year period. We then assumed an average $\delta^{18}\text{O}_{\text{N+N}}$ of 79 ‰ for NO_3^- in dry deposition (Wankel et al. 2009) and the background $\delta^{18}\text{O}_{\text{N+N}}$ of 6.5 ‰ for the mixture measured in this study. Based on conservation of mass, the background

$\delta^{18}\text{O}_{\text{N+N}}$ in the Gulf would be $\sim 3.4\text{‰}$ without the contribution from atmospheric deposition, which is within the range of values reported for other marine waters.

In addition to a source contribution from dry deposition, other processes may also contribute to the Gulf's anomalously high $\delta^{18}\text{O}_{\text{N+N}}$ values. Casciotti and coworkers (2002) observed that the $\delta^{18}\text{O}_{\text{N+N}}$ on the North Pacific was very close to 0‰, and argued that most or all of the O in deep water NO_3^- derived from seawater rather than dissolved O_2 , which generally ranges from 23.8-35.5‰. However, in the highly oxygenated waters of the Gulf O_2 saturation is near 100%, and it is possible that nitrifiers utilize this O source in addition of H_2O to oxidize NH_4^+ and NO_2^- . Because molecular O_2 is isotopically heavy relative to VSMOW, its incorporation would be a pathway for generating NO_3^- with high $\delta^{18}\text{O}_{\text{N+N}}$. The $\delta^{18}\text{O}$ of H_2O in the Gulf is also elevated relative to VSMOW (1.5-2.5‰, B. Lazar personal communication), which would also serve to elevate the $\delta^{18}\text{O}_{\text{N+N}}$ above levels observed in marine waters with $\delta^{18}\text{O}$ values closer to 0‰.

The second interesting observation from the isotope data is the importance of regenerated N in the Gulf of Aqaba. The importance of nitrification is underscored by the net isotope effects for O and N derived from Raleigh fractionation curves. The O curve clearly shows the effects of assimilation on this system, and the measured $^{18}\epsilon$ value of 10.3‰ agrees well with the range of isotope effects measured for NO_3^- uptake by phytoplankton in other studies (Granger et al. 2004; Needoba and Harrison 2004; Granger et al. 2009). In contrast, the $^{15}\epsilon$ differed from $^{18}\epsilon$ and has a value of 1.3‰, suggesting another process, likely nitrification, was causing the isotopic signature

of $\delta^{15}\text{N}_{\text{N+N}}$ to be lighter than it would be if assimilation alone were the dominant process. Moreover, the very high ratio of $\delta^{18}\text{O}_{\text{N+N}} : \delta^{15}\text{N}_{\text{N+N}}$ (from 2-5; **Fig. 8**) indicates that regenerated organic matter is a major source of N for primary producers in the Gulf of Aqaba. This observation is consistent with other studies that have found high rates of primary productivity despite relatively low standing stocks of phytoplankton in the Gulf (Hase et al. 2006). Together these findings suggest that primary productivity is tightly coupled to grazing food webs and the microbial loop such that N is efficiently sequestered within biomass as soon as it becomes bioavailable, and does not accumulate as DIN or DON.

During our monitoring of the spring bloom the concentration of N in particulate matter (PON) and DIN together decreased by $\sim 15 \mu\text{g L}^{-1}$ (**Fig. 3C**). Because processes that remove N from the system (e.g. denitrification, anammox) are not expected to have a significant role in this oxygenated water column, the most likely reservoir for the missing N is the DON pool. DON clearly plays an important role in the Gulf's biogeochemical N cycling, representing an important nutrient resource for marine autotrophs and heterotrophs. Indeed in the nutrient addition experiment, urea and glycine (representing organic N) were utilized by phytoplankton and stimulated growth (**Fig. 9A**). These and similar compounds likely constituted a source of N to nitrifiers based on accumulation of NO_2^- (**Fig. 9B**). The role of DON could be particularly important in ultra-oligotrophic marine environments where DIN concentrations are very low and the reservoir of DON can be an order of magnitude larger than DIN.

The DON concentration in the system can also impact NH_4^+ oxidation rates

derived from ^{15}N labeling experiments or changes in NH_4^+ inventory. Rate estimates based on the ^{15}N tracer technique require knowledge of the ambient NH_4^+ concentration as well as the amount of $^{15}\text{NH}_4^+$ spike added. The actual flux of N from NH_4^+ to NO_2^- is calculated based on the ratio of $^{15}\text{NH}_4^+ : ^{14}\text{NH}_4^+$ in the water at time zero when the spike is added. If N is shunted directly from the DON pool to the NO_2^- pool by nitrifiers without the intermediate NH_4^+ first being expelled by the cells, then this latent pool of NH_4^+ cannot be accounted for and an accurate rate for NH_4^+ oxidation will not be captured experimentally. Rates based purely on NH_4^+ concentration changes are similarly vulnerable to this uncertainty. Thus, in waters where labile DON is a substantial portion of the total N pool, NH_4^+ oxidation kinetics may be underestimated using these methods.

Ward (1985) noted that it is unclear if NH_4^+ oxidation follows Monodian kinetics due to the apparently very high NH_4^+ affinity of nitrifiers in oligotrophic waters. However, application of the Monod model to our limited data set suggests that the maximum NH_4^+ oxidation rate would be on the order of $4 \mu\text{mol L}^{-1} \text{ day}$, approximately an order of magnitude higher than the maximum rate observed in our samples (**Fig. 14**). Substrate limitation was likely the main constraint on our estimated NH_4^+ oxidation rates based on water column inventories in the dark. However, it is also possible that our *in situ* estimates, which are based on changes in NH_4^+ concentration, may underestimate actual rates if rapid mineralization of organic N was adding NH_4^+ back into the reservoir. This input of NH_4^+ would have yielded apparent NH_4^+ consumption rates lower than the actual rate (though the rate determined from the ^{15}N tracer experiment independently suggests that NH_4^+ oxidation was not

occurring at maximal rates.)

To obtain a better estimate of the overall rate for NH_4^+ oxidation, NH_4^+ generated during mineralization of DON would also need to be accounted for. In this study the rate of coupled urea mineralization and NH_4^+ oxidation were measured in the ^{15}N tracer experiment. Urea hydrolysis to NH_4^+ and carbon dioxide is catalyzed by the urea amidohydrolase (urease) enzyme, which is ubiquitous among marine phytoplankton (Fan et al. 2003; Collier et al. 1999) and heterotrophs (Klotz et al. 2006; Koper et al. 2004). The overall rate of urea mineralization and NH_4^+ oxidation obtained was remarkably close to that of NH_4^+ oxidation alone, suggesting that mineralization is not a rate limiting step for nitrification, at least when the DON pool is relatively large and labile. However, the composition of DON is difficult to characterize, and the portion that is refractory would change substantially based on community composition, grazing rates, mixing, and numerous other factors, making mineralization rates difficult to quantify meaningfully. More work is needed to characterize the DON pools in different waters and determine their influence on marine nitrification rates.

CONCLUSION

Several major processes and many diverse microbial groups contribute to the formation of PNM in the Gulf of Aqaba during the transition from mixing to stratification. Within the euphotic zone, phytoplankton assimilate N during growth drawing down NO_2^- levels sharply in surface waters. Below the euphotic depth during the initial stages of stratification, a large inventory of NO_2^- is generated from

incomplete NO_3^- reduction by trapped light limited phytoplankton. NO_2^- from this process is distributed over a range of depths, creating a broad swath of NO_2^- with a subsurface peak. Later, once stratification is firmly established, net NO_2^- is generated by NH_4^+ oxidizers over a narrower range of depths coinciding with the upper part of the PNM. Deeper in the water column, NO_2^- oxidation rates increase to match NH_4^+ oxidation, and NO_2^- gets drawn down, defining the lower portion of the PNM.

Regenerated organic material is an important source of N for primary producers in the Gulf of Aqaba, where assimilation rates for urea were similar to those of NO_3^- , and regeneration of NO_3^- from NH_4^+ and urea likewise occurred at similar rates. The rate and type of N transformation processes operating throughout the water column are strongly influenced by light, which determines the maximum depths for net photosynthesis, but substrate concentrations may also limit nitrification rates. Because the effects of light are strongly influenced by physical process such as stratification and mixing, the relative contribution of the major N transformation processes to the overall N budget varies in space (e.g. depth within the water column) and time (e.g. over diel and seasonal cycles).

ACKNOWLEDGEMENTS

I acknowledge my co-authors Laura Bristow, David R Parks, Mark A Altabet, Anton F Post, and Adina Paytan for help on this manuscript, which is submitted to Limnology and Oceanography. As a group we thank our colleagues at the Interuniversity Institute for Marine Science in Eilat, Israel for assisting in data collection and providing laboratory space and equipment during the study. C. Danford and R. Foster assisted with sampling, D. Iluz provided PAR data, and T. Rivlin and M. Chernichovsky assisted with sampling and nutrient analyses. This research was supported under the National Aeronautics and Space Administration (NASA) New Investigator Program NAG5-12663 to AP, the North Atlantic Treaty Organization (NATO) Science for Peace Grant SfP 982161 to AP and AFP, a grant from the Koret Foundation to AP, and Israel Science Foundation grant 135/05 to AFP. KRMM was supported through the National Science Foundation (NSF) Graduate Research Fellowship Program and the Department of Energy (DOE) Global Change Education Program.

Author contributions

KRM Mackey - planned experimental design; conducted field work; developed analytical methods; processed samples; analyzed and interpreted data; wrote the manuscript

L Bristow – helped process isotope samples for Figures 6, 7, 8; provided comments on the manuscript

DR Parks – helped develop analytical method for flow cytometry cell staining

MA Altabet – provided funding; provided comments on the manuscript

AF Post - provided funding; provided comments on the manuscript

A Paytan - provided funding; helped plan experimental design; helped conduct field work; provided comments on the manuscript

REFERENCES

- Allen, A. E., M. G. Booth, M. E. Frischer, P. G. Verity, J. P. Zehr, and S. Zani. 2001. Diversity and detection of nitrate assimilation genes in marine bacteria. *Appl. Environ. Microbiol.* **67**:5343-5348
- Allen, A. E., M. G. Booth, P. G. Verity, M. E. Frischer. 2005. Influence of nitrate availability on the distribution and abundance of heterotrophic bacterial nitrate assimilation genes in the Barents Sea during summer. *Aquatic Microbial Ecology* **39**: 247–255
- Al-Qutob, M, C Hase, MM Tilzer, B Lazar. 2002. Phytoplankton drives nitrite dynamics in the Gulf of Aqaba, Red Sea. *Marine Ecology Progress Series*. 239: 233-239.
- Cai, H. and N. Jiao. 2008. Diversity and Abundance of Nitrate Assimilation Genes in the Northern South China Sea. *Microb Ecol* 56:751–764 DOI 10.1007/s00248-008-9394-7
- Casciotti, KL. 2009. Inverse kinetic isotope fractionation during bacterial nitrite oxidation. *Geochimica et Cosmochimica Acta*.
- Casciotti, K. L., D. M. Sigman, M. Galanter-Hastings, J. K. Boehlke, and A. Hilkert. 2002. Measurement of the Oxygen Isotopic Composition of Nitrate in Seawater and Freshwater Using the Denitrifier Method. *Anal. Chem.*, **74**: 4905–4912.

- Casciotti, K. L. and B. B. Ward. 2006. Phylogenetic analysis of nitric oxide reductase gene homologues from aerobic ammonia-oxidizing bacteria. *FEMS Microbiology Ecology* **52**: 197-205
- Casciotti, K. L., and B. B. Ward. 2001. Dissimilatory Nitrite Reductase Genes from Autotrophic Ammonia-Oxidizing Bacteria *Applied and Environmental Microbiology*, **67**: 2213-2221
- Cohen Y. and M. Ottolenghi. 2004. Gulf of Eilat Monitoring and Research Program - IET Recommendations - Final Report. http://sviva.gov.il/Environment/Static/Binaries/Articals/final_report04_1.pdf
- Collier, J. L., B. Brahamsha and B. Palenik. 1999. The marine cyanobacterium *Synechococcus* sp. WH7805 requires urease (urea amidohydrolase, EC 3.5.1.5) to utilize urea as a nitrogen source: molecular-genetic and biochemical analysis of the enzyme. *Microbiology* **145**: 447-459
- Collos, Y. 1998. Nitrate, nitrite release and uptake, and new production estimates. *Marine Ecology Progress Series* **171**: 293-301
- Cornell, S., A. Randell, and T. Jickells. 1995. Atmospheric inputs of dissolved organic nitrogen to the oceans. *Nature* **376**: 243 – 246.
- D'Elia, C.F., P.A. Steudler, and N. Corwin. 1977. Determination of total nitrogen in aqueous samples using persulfate digestion. *Limnol. Oceanogr.* **22**: 760-764.
- Dugdale, R. C. and F. P. Wilkerson. 1986. The Use of ^{15}N to Measure Nitrogen Uptake in Eutrophic Oceans; Experimental Considerations. *Limnol. Oceanogr.* **31**: 673-689

- Falkowski, P. G. 1997. Evolution of the nitrogen cycle and its influence on the biological sequestration of CO₂ in the ocean. *Nature* **387**: 272 – 275.
- Fan, C., P. M. Glibert, J. Alexander, M. W. Lomas. 2003. Characterization of urease activity in three marine phytoplankton species, *Aureococcus anophagefferens*, *Prorocentrum minimum*, and *Thalassiosira weissflogii*, *Mar. Biol.* **142**: 949–958.
- Foster, R. A., A. Paytan, and J. P. Zehr. 2009. Seasonality of N₂ fixation and *nifH* gene diversity in the Gulf of Aqaba (Red Sea). *Limnol. Oceanogr.* **54**: 219–233
- Francis, C. A., J. M. Beman and M. M. M. Kuypers. 2007. New processes and players in the nitrogen cycle: the microbial ecology of anaerobic and archaeal ammonia oxidation. *The ISME Journal* **1**:19-27.
- Granger, J., D. M. Sigman, J. A. Needoba and P. J. Harrison. 2004. Coupled Nitrogen and Oxygen Isotope Fractionation of Nitrate during Assimilation by Cultures of Marine phytoplankton. *Limnology and Oceanography* **49**: 1763-1773
- Granger, J., D. M. Sigman, M. M. Rohde, et al. 2009. N and O isotope effects during nitrate assimilation by unicellular prokaryotic and heterotrophic phytoplankton. *Geochimica et Cosmochimica Acta*.
- Gruber, N., and J. L. Sarmiento (1997), Global Patterns of Marine Nitrogen Fixation and Denitrification, *Global Biogeochem. Cycles*, **11**: 235–266.
- Guerrero, M. A., and R. D. Jones. 1996. Photoinhibition of marine nitrifying bacteria. I. Wavelength-dependent response. *Marine Ecology Progress Series* **141**: 183-192.

- Hadas, O. and J. Erez. 2004. IET Project No. C Nitrogen Fixation in the Gulf of Eilat
In M. J. Atkinson, Y. Birk and H. Rosenthal [eds.], Evaluation of Fish Cages
in the Gulf of Eilat, a technical report for the Israeli Ministries of Infrastructure
Environment and Agriculture.
- Hase, C., M. Al-Qutob, Z. Dubinsky, E. A. Ibrahim, B. Lazar, N. Stambler, M. M.
Tilzer. 2006. A system in balance? Implications of deep vertical mixing for the
nitrogen budget in the northern Red Sea, including the Gulf of Aqaba (Eilat).
Biogeosciences Discussions **3**:383-408.
- Karl, D., R. Letelier, L. Tupas, J. Dore¹, J. Christian, and D. Hebel. 1997. The role of
nitrogen fixation in biogeochemical cycling in the subtropical North Pacific
Ocean. *Nature* **388**: 533-538.
- Klotz M. G., et al. 2006. Complete Genome Sequence of the Marine,
Chemolithoautotrophic, Ammonia-Oxidizing Bacterium *Nitrosococcus oceani*
ATCC 19707. *Applied and Environmental Microbiology* **72**: 6299-6315
- Koper, T., A. F. El-Sheikh, J. M. Norton, and M. G. Klotz. 2004. Urease-encoding
genes in ammonia-oxidizing bacteria. *Applied and Environmental
Microbiology* **70**: 2342-2348
- Leichter, J. J., A. Paytan, S. Wankel, K. Hanson, S. Miller and M.A. Altabet. 2007.
Nitrogen and oxygen isotopic signatures of subsurface nitrate: evidence of
deep water nutrient sources to the Florida Keys reef tract. *Limnology and
Oceanography* **52**: 1258-1267.

- Lindell, D., and A. F. Post. 1995. Ultraphytoplankton succession is triggered by deep winter mixing in the Gulf of Aqaba (Eilat), Red Sea. *Limnol. Oceanogr.* **40**: 1130-1141.
- Lomas, M. W. and F. Lipschultz. 2006. Forming the primary nitrite maximum: Nitrifiers or phytoplankton? *Limnol. Oceanogr.*, **51**: 2453–2467.
- Mackey, K. R. M, R. G. Labiosa, M. Calhoun, J. Street, A. F. Post, A. Paytan. 2007. Phosphorus availability, phytoplankton community dynamics, and taxon-specific phosphorus status in the Gulf of Aqaba, Red Sea. *Limnol. Oceanogr.*, **52**: 873–885.
- Mackey, KRM, T Rivlin, A. Grossman, A Post, and A Paytan. 2009. Picophytoplankton responses to changing nutrient and light regimes during a bloom. *Marine Biology* **156**: 1531-1546
- McIlvin, M. R., and M. A. Altabet. 2005. Chemical conversion of nitrate and nitrite to nitrous oxide for nitrogen and oxygen isotopic analysis in freshwater and seawater. *Anal. Chem.* **77**: 5589 -5595.
- Montoya, J. P., C. M. Holl, J. P. Zehr, A. Hansen, T. A. Villareal & D. G. Capone. 2004. High rates of N₂ fixation by unicellular diazotrophs in the oligotrophic Pacific Ocean. *Nature* **430**:1027-1032
- Moore, L. R., A. F. Post, G. Rocap and S. W. Chisholm. 2002. Utilization of Different Nitrogen Sources by the Marine Cyanobacteria *Prochlorococcus* and *Synechococcus*. *Limnology and Oceanography* **47**: 989-996

- Needoba, J. A. and P. J. Harrison. 2004. Influence of low light and a light: dark cycle on nitrate uptake, intracellular nitrate, and nitrogen isotope fractionation by marine phytoplankton. *Journal of Phycology* **40**: 505-516
- Olson, R. 1981. Differential photoinhibition of marine nitrifying bacteria: A possible mechanism for the formation of the primary nitrite maximum. *J. Mar. Res.* **39**: 227–238.
- Opsahl, S. and R. Benner. 1997. Distribution and cycling of terrigenous dissolved organic matter in the ocean. *Nature* **386**: 480–482.
- Palenik, B., and F. M. Morel. 1990. Amino acid utilization by marine phytoplankton—a novel mechanism. *Limnol. Oceanogr.* **35**:260-269
- Post, A. F., Z. Dedej, R. Gottlieb, H. Li, D. N. Thomas, M. Elabsawi, A. El-Naggar, M. El-Gharabawi, and U. Sommer. 2002. Spatial and temporal distribution of *Trichodesmium* spp. in the stratified Gulf of Aqaba, Red Sea. *Mar. Ecol. Prog. Ser.* **239**: 241–250.
- Robertson, L. A., T. Dalsgaard, N.-P. Revsbeck, and J. G. Kuenen. 1995. Confirmation of aerobic denitrification in batch cultures, using gas chromatography and ^{15}N mass spectrometry. *FEMS Microbiology Ecology* **18**:113-120
- Sanudo-Wilhelmy, S. A. et al. 2001. Phosphorus limitation of nitrogen fixation by *Trichodesmium* in the central Atlantic Ocean. *Nature* **411**: 66–69
- Schreiber, F., B. Loeffler, L. Polerecky, M. M. Kuypers, and D. de Beer. 2009. Mechanisms of transient nitric oxide and nitrous oxide production in a complex biofilm. *The ISME Journal* **3**: 1301–1313

- Sigman, D. M., J. Granger, P. J. DiFiore, M. M. Lehmann, R. Ho, G. Cane, and A. van Geen. 2005. Coupled nitrogen and oxygen isotope measurements of nitrate along the eastern North Pacific margin, *Global Biogeochem. Cycles*, **19**, GB4022, doi:10.1029/2005GB002458.
- Starkenburg S. R. 2006. Complete Genome Sequence of *Nitrobacter hamburgensis* X14 and Comparative Genomic Analysis of Species within the Genus *Nitrobacter*. *Applied and Environmental Microbiology* **74**: 2852-2863
- Su, J.-J., B.-Y. Liu, and D.-Y. Liu. 2001. Comparison of aerobic denitrification under high oxygen atmosphere by *Thiosphaera pantotropha* ATCC 35512 and *Pseudomonas stutzeri* SU2 newly isolated from the activated sludge of a piggery wastewater treatment system. *J. Appl. Microbiol.* **90**:457-462
- Tupas, L. M., I. Koike, D. M. Karl, and O. Holmhausen. 1994. Nitrogen metabolism by heterotrophic bacterial assemblages in Antarctic coastal waters. *Polar Biol.* **14**:195-204
- Wankel, S. D., C. Kendall, J. T. Pennington, F. P. Chavez, and A. Paytan. 2007. Nitrification in the euphotic zone as evidenced by nitrate dual isotopic composition: Observations from Monterey Bay, California, *Global Biogeochem. Cycles*, **21**, GB2009, doi:10.1029/2006GB002723
- Wankel, S. D., C. Kendall, and A. Paytan. 2009. Using nitrate dual isotopic composition ($\delta^{15}\text{N}$ and $\delta^{18}\text{O}$) as a tool for exploring sources and cycling of nitrate in an estuarine system: Elkhorn Slough, California
- Ward, B. B. 1985. Light and substrate concentration relationships with marine ammonium assimilation and oxidation rates. *Marine Chemistry* **16**: 301-316

- Ward, B. B., K. A. Kilpatrick, E. Renger, and R. W. Eppley. 1989. Biological nitrogen cycling in the nitracline. *Limnol. Oceanogr.* **34**: 493-513
- Zehr, J. P. and B. B. Ward. 2002. Nitrogen cycling in the ocean: new perspectives on processes and paradigms. *Applied and Environmental Microbiology* **68**: 1015-1024
- Zubkov, M. V., B. M. Fuchs, G. A. Tarran, P. H. Burkill, & R. Amann. 2003. High rate of uptake of organic nitrogen compounds by *Prochlorococcus* Cyanobacteria as a key to their dominance in oligotrophic oceanic waters. *Appl. Environ. Microbiol.* **69**: 1299–1304

Table 1: N assimilation rates into particulate biomass for NO_3^- , NO_2^- , urea, and NH_4^+ determined during the ^{15}N tracer experiment. “N addition” indicates the form of ^{15}N enriched spike added. “Light” uptake rates indicate bottles incubated at 50% surface sunlight irradiance, and “dark” uptake rates indicate bottles incubated in full darkness.

N addition	Experiment number	Time (hr)	Light uptake rate ($\text{nmol N L}^{-1} \text{ hr}^{-1}$)*	Dark uptake rate ($\text{nmol N L}^{-1} \text{ hr}^{-1}$)*
NO_3^-	1	7	434±24	58±14
NO_3^-	1	13	415±103	65±19
NO_3^-	2	13	420±82	137±79
NO_2^-	2	7	94±17	29±14
NO_2^-	2	13	ND	ND
Urea	1	7	1194±48	476±31
Urea	1	13	1285±32	308±10
NH_4^+	2	7	163±5	173±5
NH_4^+	2	13	ND	ND

*Values reported are the mean \pm standard error of triplicate measurements from independent bottles (i.e., three independent bottles per treatment per time point). ND indicates that the rate was not determined for the second time interval of 13 hrs because all of the ^{15}N spike had been exhausted (taken up) within the first 7 hrs of incubation.

Table 2: NO_3^- reduction rates by light limited phytoplankton. Rates were calculated from the change in concentration of NO_2^- between March 18-24 at depths where NO_2^- uptake was most likely to be minimal and where NO_3^- reduction by phytoplankton was most likely to be the dominant process generating NO_2^- . Rates are given on a per volume basis as well as on a per unit chl *a* basis. No values were calculated for 180 m because this depth was not sampled on March 18, so no change in NO_2^- concentration could be calculated.

Depth (m)	Light attenuation (% surface PAR)	$\Delta [\text{NO}_2^-]$ (nmol L ⁻¹)	chl <i>a</i> (μg L ⁻¹)	NO_3^- reduction rate (nmol L ⁻¹ day ⁻¹)	NO_3^- reduction rate (nmol μg chl <i>a</i> ⁻¹ day ⁻¹)
60	1	13	0.44	2.2	5.0
80	0.2	58	0.39	9.7	25
120	0.01	143	0.26	24	93
160	0.0004	275	0.17	46	270
200	0.00002	345	0.19	58	290

Table 3: Summary table of rates for various processes in the N cycle calculated in this study.

Substrate	Product	Process	Light condition	Rate (nmol N L ⁻¹ day ⁻¹)	Method of calculation
NO ₃ ⁻	Biomass	Assimilation	50% surface PAR	415-434	¹⁵ N tracer experiment
NO ₃ ⁻	Biomass	Assimilation	Dark	58-137	¹⁵ N tracer experiment
NO ₃ ⁻	NO ₂ ⁻	Reduction by phytoplankton	0.00002-1% surface PAR	2.2-58	Change in water column NO ₂ ⁻ inventory over time
NO ₂ ⁻	Biomass	Assimilation	50% surface PAR	94	¹⁵ N tracer experiment
NO ₂ ⁻	Biomass	Assimilation	Dark	29	¹⁵ N tracer experiment
NO ₂ ⁻	NO ₃ ⁻	Nitrification (NO ₂ ⁻ oxidation)	Dark	30-490	Change in water column NO ₃ ⁻ inventory over time
Urea	Biomass	Assimilation	50% surface PAR	1194-1285	¹⁵ N tracer experiment
Urea	Biomass	Assimilation	Dark	308-476	¹⁵ N tracer experiment
Urea	NO ₂ ⁻	Oxidation (via NH ₄ ⁺ intermediate)	Dark	14.1	¹⁵ N tracer experiment
NH ₄ ⁺	Biomass	Assimilation	50% surface PAR	163	¹⁵ N tracer experiment
NH ₄ ⁺	Biomass	Assimilation	Dark	173	¹⁵ N tracer experiment
NH ₄ ⁺	NO ₂ ⁻	Nitrification (NH ₄ ⁺ oxidation)	Dark	16.4	¹⁵ N tracer experiment
NH ₄ ⁺	NO ₂ ⁻	Nitrification (NH ₄ ⁺ oxidation)	Dark, concentration dependent	10-320	Change in water column NH ₄ ⁺ inventory over time

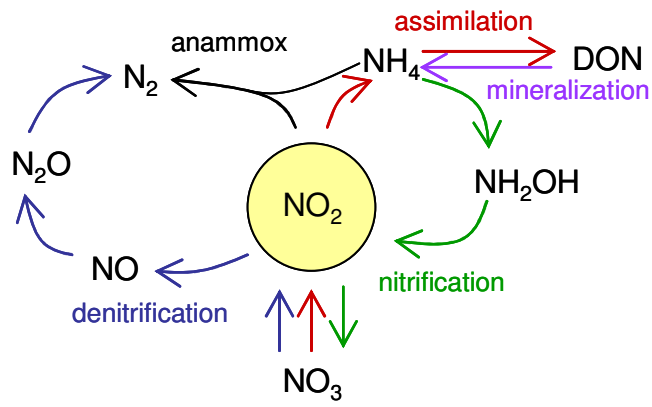


Figure 1: The N cycle, showing an overview of the major N transformation pathways

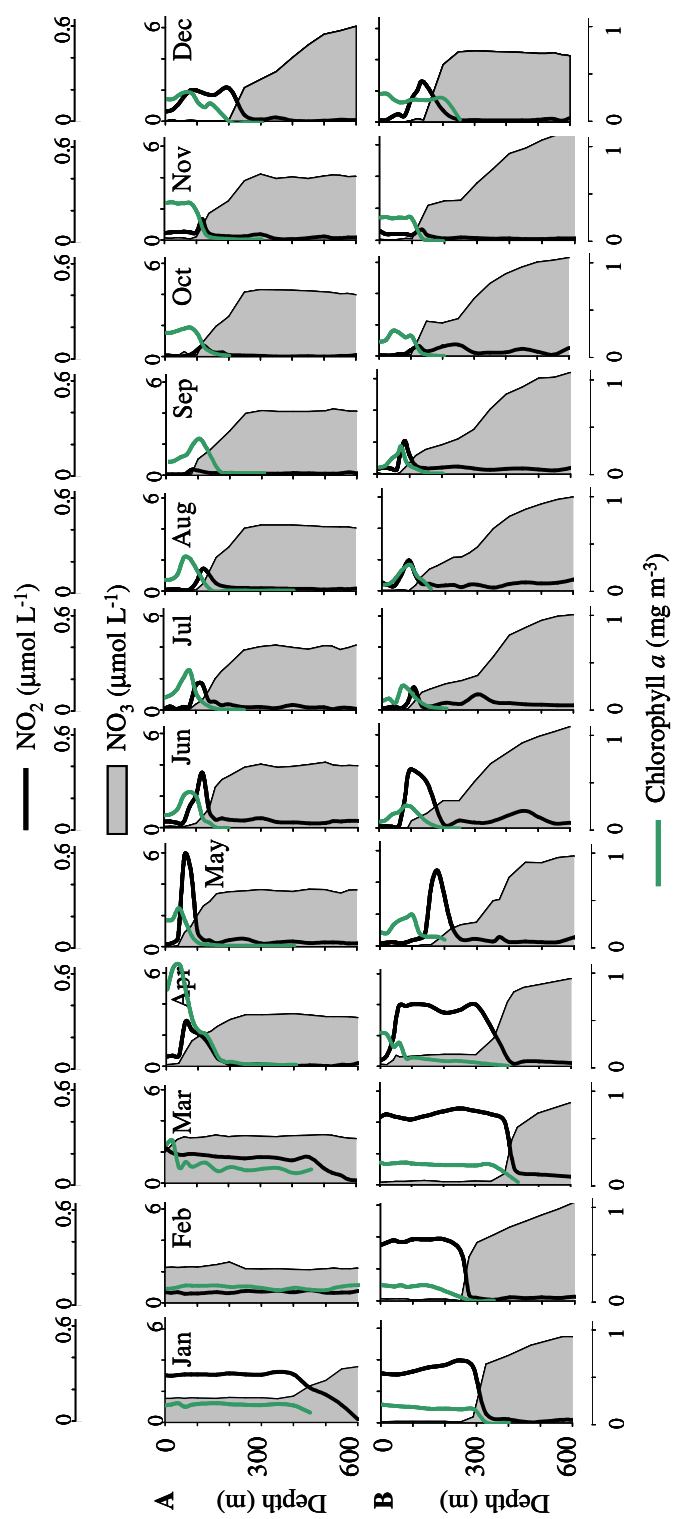


Figure 2: Depth profiles of NO_3^- (shaded area), NO_2^- (black line), and chl *a* (green line) for January - December in (A) 2008 when the water column mixed down to the seafloor, and (B) 2003 when the mixing depth was ~400 m. During winter mixing NO_2^- accumulates and chl *a* is homogenously distributed in the mixed layer. During summer stratification a PNM forms at or below the DCM.

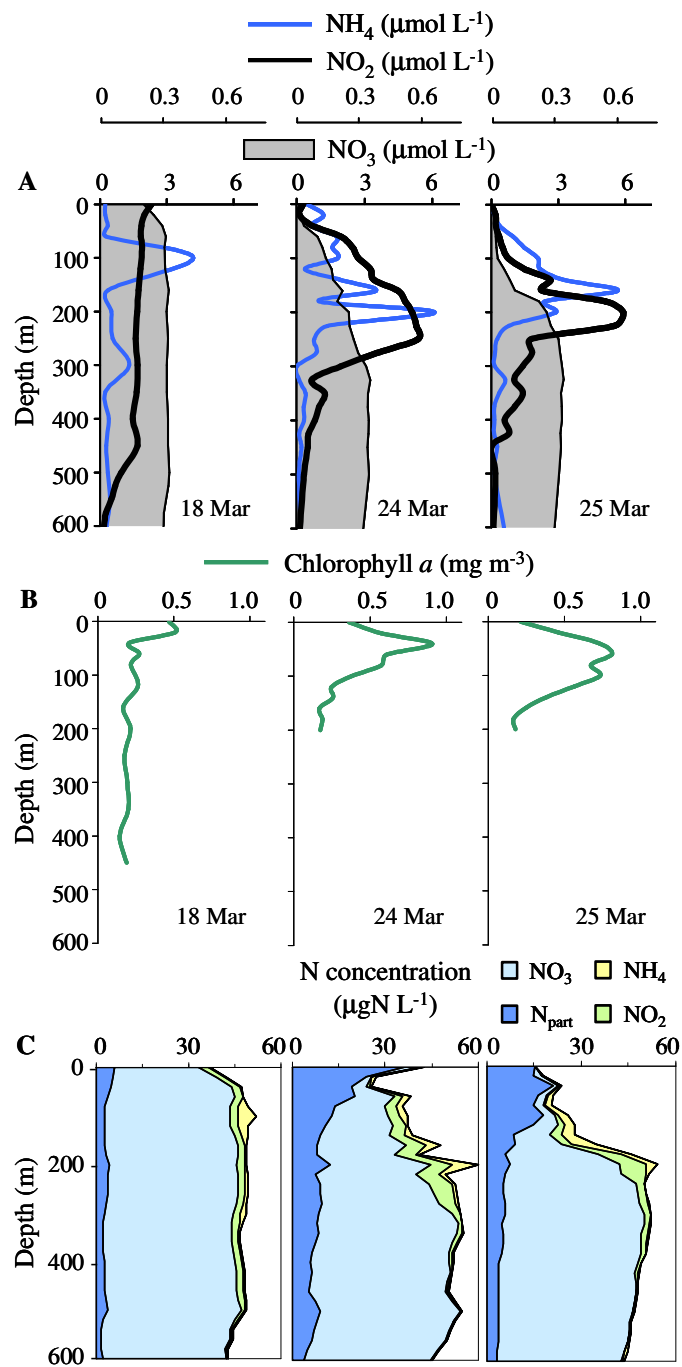


Figure 3: Depth transects collected at station A before (March 18) and during (March 24 and 25) the spring stratification event in 2008 showing (A) NO_3^- , NO_2^- , and NH_4^+ concentrations, and (B) chl *a* concentration. (C) Cumulative N inventories for depth transects collected at station A before (March 18) and during (March 24 and 25) the spring stratification event in 2008.

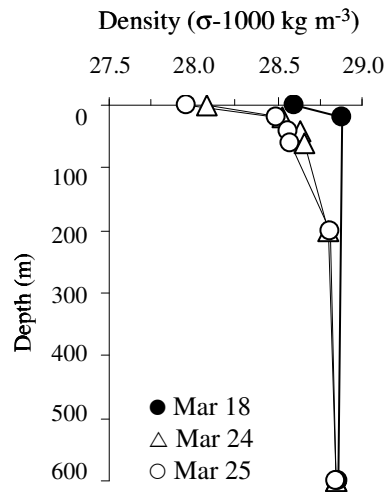


Figure 4: Seawater density profiles for March 18 (black circles), 24 (white triangles), and 25 (white circles) showing the progression of stratification.

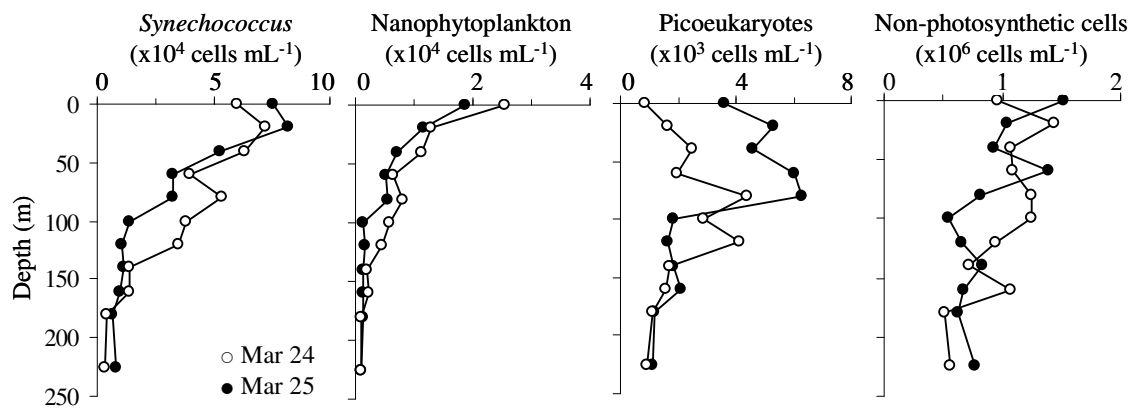


Figure 5: Cell concentrations of *Synechococcus*, nanophytoplankton, picoeukaryotes, and non-photosynthetic microbes on March 24 (closed circles) and 25 (open circles). Note that different scales are used for each transect.

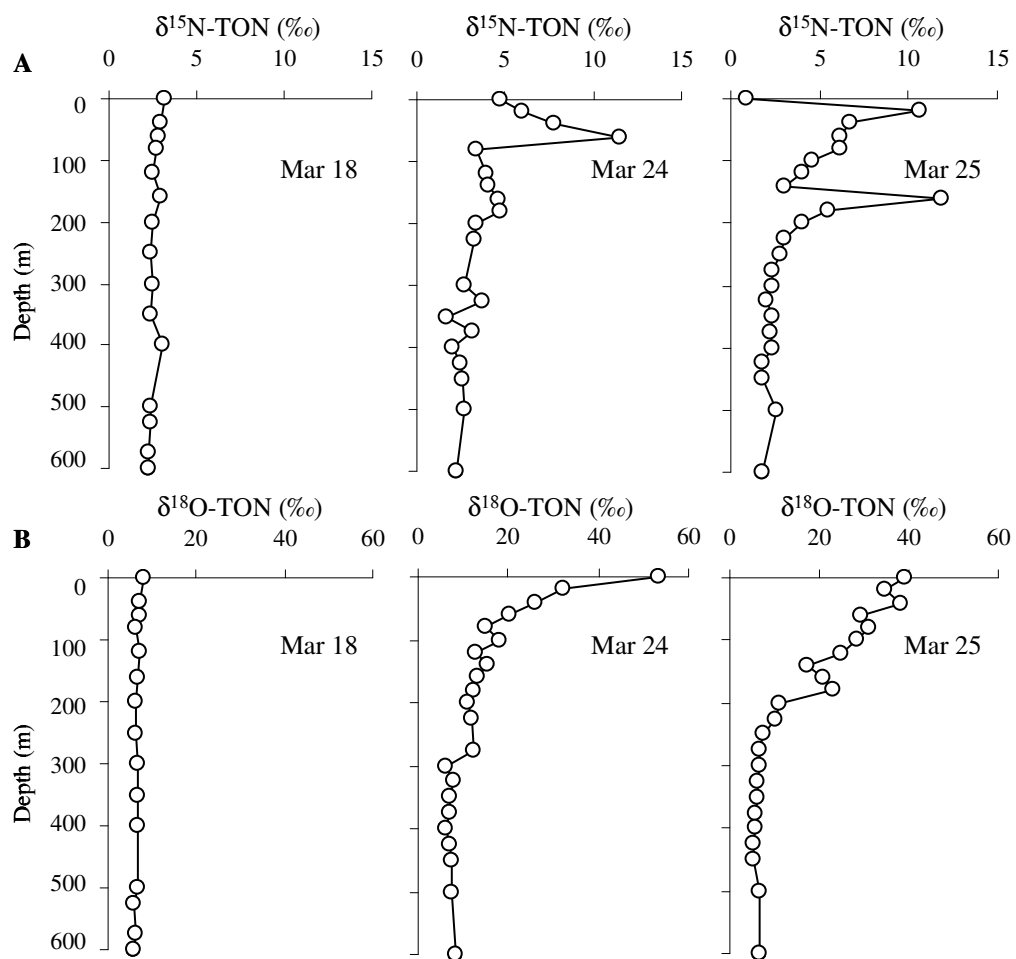


Figure 6: Isotopic composition of N+N on March 18, 24, and 25, showing (A) $\delta^{15}\text{N}_{\text{N+N}}$, and (B) $\delta^{18}\text{O}_{\text{N+N}}$.

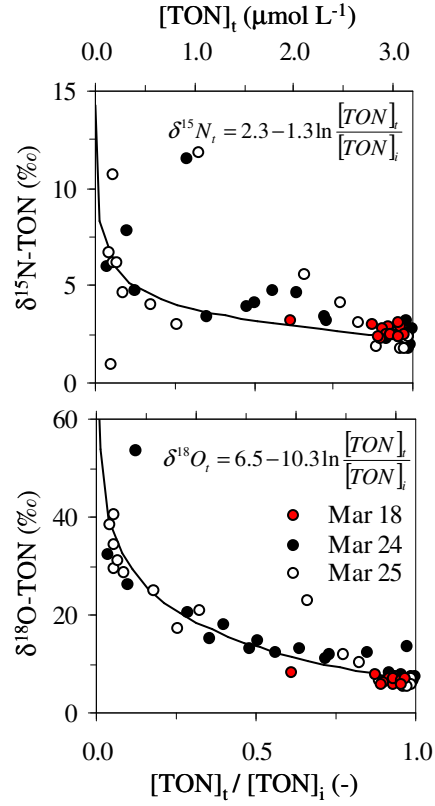


Figure 7: Raleigh fractionation curves for $\delta^{15}\text{N}_{\text{N+N}}$ and $\delta^{18}\text{O}_{\text{N+N}}$ for March 18 (red circles), March 24 (black circles), and March 25 (white circles). While $\delta^{18}\text{O}_{\text{N+N}}$ followed a traditional Raleigh fractionation pattern throughout the stratification event, many of the $\delta^{15}\text{N}_{\text{N+N}}$ values deviated from Raleigh fractionation, indicating that the data cannot be explained by simple two end member mixing.

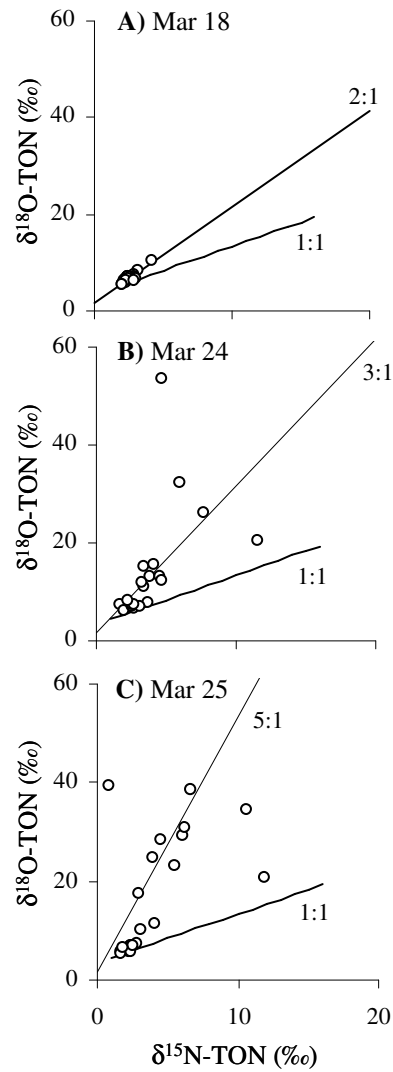


Figure 8: Relationships between $\delta^{18}\text{O}_{\text{N+N}}$ and $\delta^{15}\text{N}_{\text{N+N}}$ for (A) March 18, (B) March 24, and (C) March 25. In (B) and (C) points are connected to show relative depths in the water column.

A line with slope 1:1 is shown on each plot and represents how the data would plot if only assimilation affected the TON pool. Actual data plot along lines with slopes 2:1, 3:1, and 5:1 for March 18, 24, and 25 respectively, indicating that nitrification played an increasingly large role in supplying the N+N pool as stratification progressed.

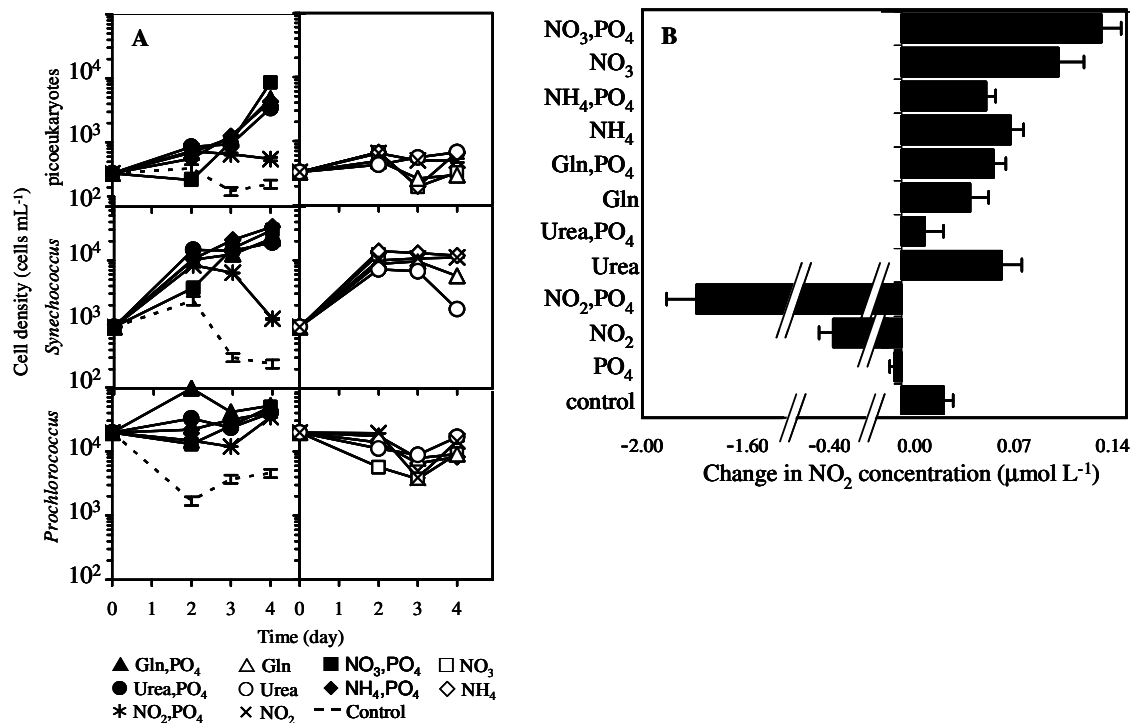


Figure 9: (A) Cell concentration time series for picoeukaryotes, *Synechococcus*, and *Prochlorococcus* during the organic N enrichment experiment. Error bars show standard error and are smaller than the symbols when not visible. (B) Production (positive values) and consumption (negative values) of NO₂⁻ between the first and last day of the organic N enrichment experiment. NO₂⁻ concentration increased in all treatments except when PO₄³⁻ was added alone and or when NO₂⁻ was added alone or together with PO₄³⁻. Error bars show standard error.

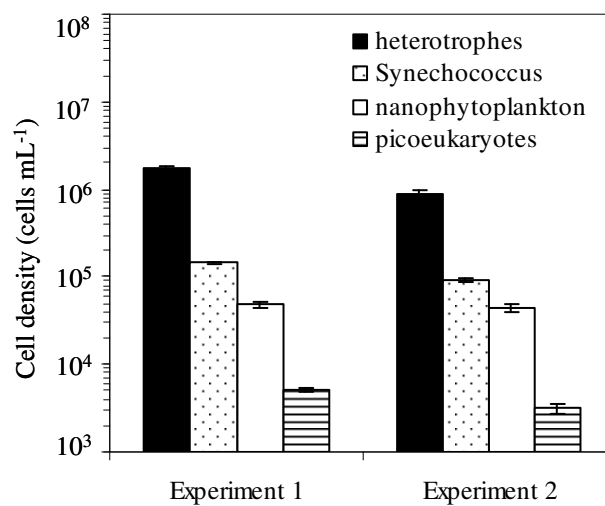


Figure 10: Composition of the microbial community during the ^{15}N tracer experiments.

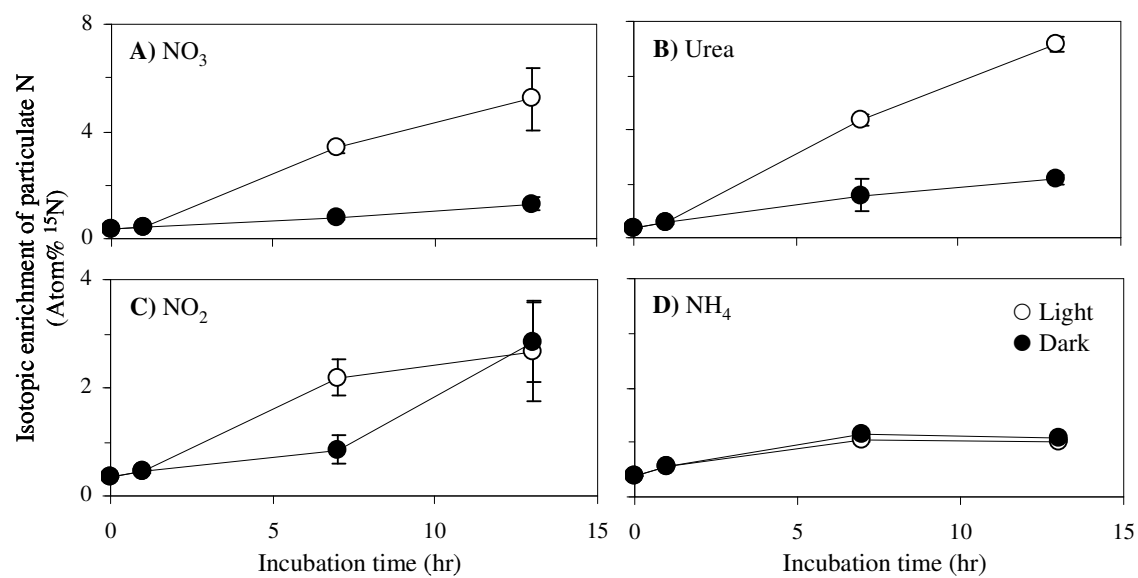


Figure 11: N assimilation into particulate biomass in the ^{15}N tracer experiment for treatments spiked with A) NO_3^- , B) urea, C) NO_2^- , and D) NH_4^+ . Error bars show standard error and are smaller than the symbols when not visible.

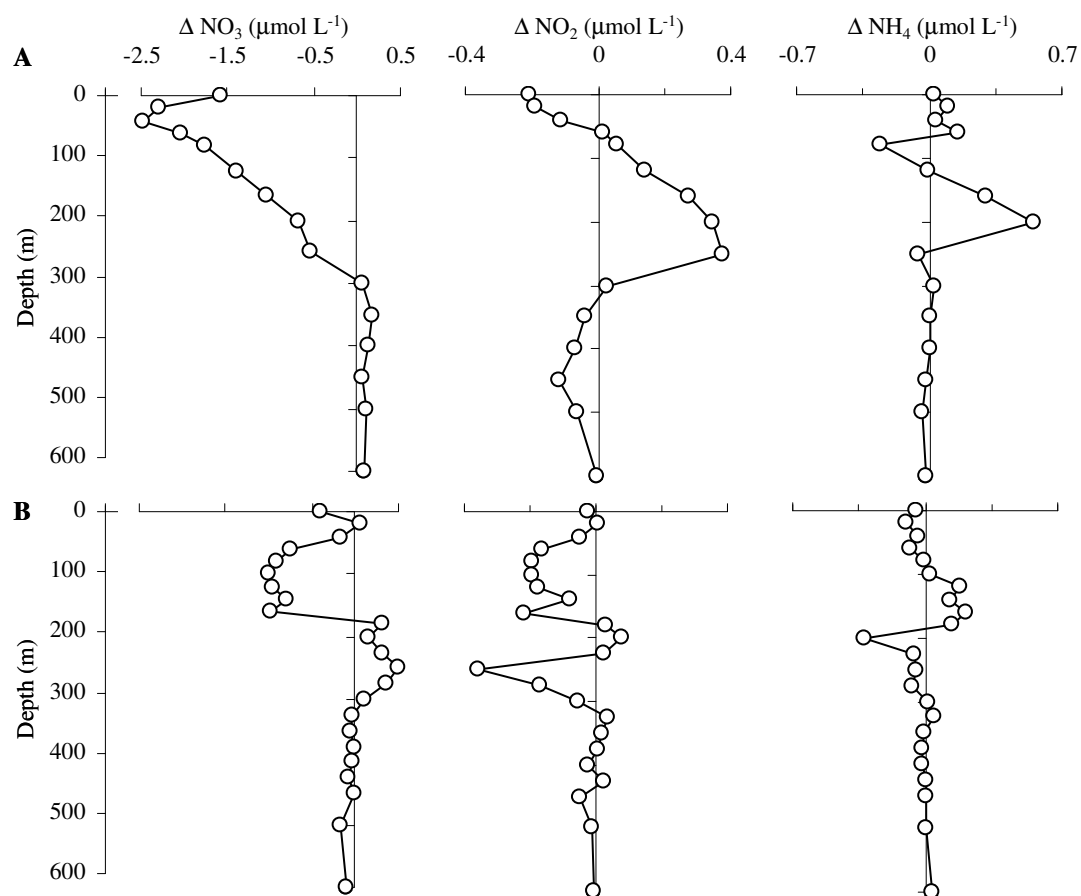


Figure 12: Change in N inventories for NO_3^- , NO_2^- , and NH_4^+ between (A) March 18 to 24, and (B) March 24 to 25.

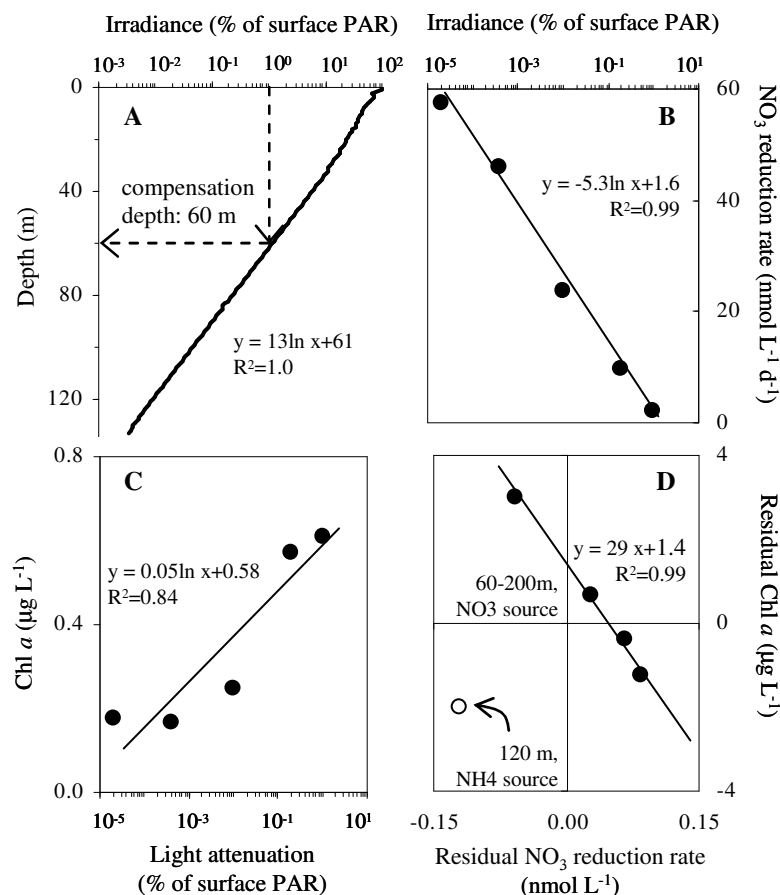


Figure 13: NO_3^- reduction to NO_2^- by phytoplankton is dependent on light and phytoplankton abundance (measured as chl a). (A) Light attenuation of photosynthetically active radiation (PAR) with depth on March 25 showing the compensation depth (i.e., base of the euphotic zone determined by 1% surface PAR; designated by dotted arrows); (B) dependence of NO_3^- reduction rate on irradiance; (C) dependence of chl a on irradiance; (D) dependence of NO_3^- reduction on chl a with the effects of light removed for both parameters (ie residuals are plotted). Analysis of residuals revealed that nitrification contributed substantially to NO_2^- formation at 120 m (open circle), where the data deviates from the best fit line (the best fit is based only on the closed circles).

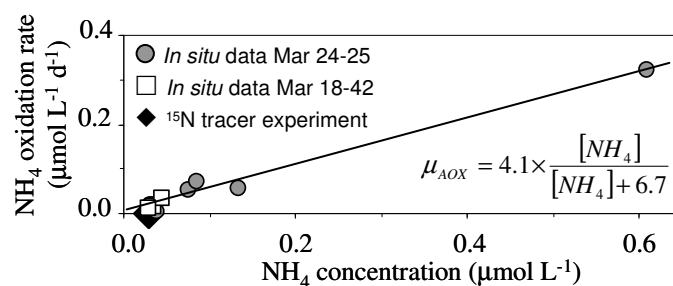


Figure 14: NH_4^+ oxidation rates based on NH_4^+ consumption from March 24-25 below 200m (shaded circles) and March 18-24 below 450 m (open squares) where net NH_4^+ consumption occurred in the water column. Closed diamond shows the rate of NH_4^+ oxidation to NO_2^- measured in the ^{15}N tracer experiment (standard error is smaller than the symbol).

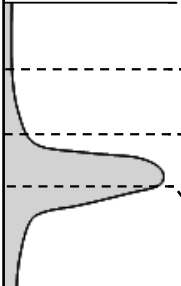
NO₂⁻ inventory	Water column region	PAR (%)	Photosynthetic assimilation	NO₃⁻ reduction	Nitrification
	Euphotic zone	>1	maximal	minimal	active; limited to darkness (e.g. at night)
	Sub-euphotic zone	0.001 – 1	minimal	maximal	active; limited to darkness (depth dependent)
	Upper PNM	<0.001	NA	maximal at onset, minimal de novo activity in ongoing stratification	uncoupled; NH ₄ ⁺ oxidation exceeds NO ₂ ⁻ oxidation
	Disphotic zone	<<0.001	NA	NA	coupled; NH ₄ ⁺ oxidation balances NO ₂ ⁻ oxidation

Figure 15: Schematic diagram showing the principal regions of the NO₂⁻ profile as defined in this study.

CHAPTER 5

PICOPHYTOPLANKTON RESPONSES TO CHANGING NUTRIENT AND LIGHT REGIMES DURING A BLOOM

ABSTRACT

The spring bloom in seasonally stratified seas is often characterized by a rapid increase in photosynthetic biomass. To clarify how the combined effects of nutrient and light availability influence phytoplankton composition in the oligotrophic Gulf of Aqaba, Red Sea, phytoplankton growth and acclimation responses to various nutrient and light regimes were recorded in three independent bioassays and during a naturally-occurring bloom. We show that picoeukaryotes and *Synechococcus* maintain a “bloomer” growth strategy, which allows them to grow quickly when nutrient and light limitation are reversed. Picoeukaryotes and *Synechococcus* appear to have higher P requirements relative to N, and are responsible for the majority of photosynthetic biomass accumulation during a bloom. Following stratification events, populations limited by light show rapid photoacclimation (based on analysis of cellular fluorescence levels and photosystem II photosynthetic efficiency) and community composition shifts without substantial changes in photosynthetic biomass. The traditional interpretation of “bloom” dynamics (i.e. as an increase in photosynthetic biomass) may therefore be confined to the upper euphotic zone where light is not limiting, while other acclimation processes are more ecologically relevant at depth. Characterizing acclimation processes and growth strategies is important if

we are to clarify mechanisms that underlie productivity in oligotrophic regions, which account for approximately half of the global primary production in the ocean. This information is also important for predicting how phytoplankton may respond to global warming-induced oligotrophic ocean expansion.

INTRODUCTION

Phytoplankton blooms occur when the rates of cell growth and division significantly exceed the rates of cell loss, resulting in rapid biomass accumulation. Sufficient nutrients and light, as well as an absence of grazers, are conditions that stimulate phytoplankton growth. A transient occurrence of any of these favorable growth factors can be the causal event in bloom initiation. For example, mixing periods in permanently and seasonally stratified oligotrophic seas can result in episodic inputs of growth-limiting nutrients that trigger rapid, transient increases in photosynthetic biomass (i.e. blooms). Blooms are also initiated following delivery of exogenous nutrients via processes such as nitrogen fixation and atmospheric deposition. The nature and magnitude of a bloom is linked to composition of the phytoplankton community, which determines growth rates, acclimation strategies, and competitive interactions that ensue during the bloom. However, understanding how nutrient levels and physiological factors contribute to bloom dynamics is confounded by the ambient physical characteristics of the water column, where light may supersede nutrient availability as the growth limiting variable.

The Gulf of Aqaba, an oligotrophic water body fed by nutrient-depleted surface waters from the Red Sea, has seasonal cycles of stratification and mixing similar to other subtropical oligotrophic seas. Its water column is stratified during summer, and surface water nutrient levels are near the limits of detection (Levanon-Spanier et al. 1979; Reiss & Hottinger 1984; Mackey et al. 2007). During the summer months atmospheric dry deposition is a significant source of nutrients to the euphotic zone, supporting transient phytoplankton blooms (Chen et al. 2007; Paytan et al. in

review). Beginning in the fall, cooling of surface waters initiates convective mixing, and a deeply mixed (> 300 m or more) water body is observed by winter (Wolf-Vetch et al. 1992). Nutrients entrained from depth as a consequence of this mixing result in mesotrophic conditions (Lindell & Post 1995), with productivity likely limited by light (Labiosa et al. 2003). The water column begins to re-stratify in the spring as surface waters warm, trapping nutrients and phytoplankton in the euphotic zone along a steep light gradient. Phytoplankton take advantage of the favorable nutrient and light conditions within the newly stratified euphotic zone forming a surface bloom over a period of days (Labiosa 2007), while the growth of phytoplankton trapped at depth is limited by low light. Picophytoplankton (cells <2 μm) are the dominant cell type in the Gulf of Aqaba; however, ultraplankton (cells <8 μm) and some larger diatoms and dinoflagellates (cells 5-100 μm) also occur in phytoplankton assemblages, particularly during the mesotrophic winter season (Lindell and Post 1995; Sommer 2000; Mackey et al. 2007).

Permanently and seasonally stratified waters similar to that of the Gulf of Aqaba account for a significant portion (> 50%) of the surface area of the ocean and therefore represent a significant fraction of the area available for carbon sequestration. Identifying the major factors that control phytoplankton growth, species abundance, and acclimation processes in these habitats is an important step in understanding their role in the global carbon cycle. Indeed, many studies have sought to address these issues, and recent findings suggest that the factors controlling Chl *a* levels and primary production may be different from those controlling cell division rate (Davey et al. 2008). Ecotypic variation among phytoplankton genera adds another level of

complexity by helping to shape local and global phytoplankton distributions (Moore 1998; Partensky et al. 1999; Rocap et al. 2003; Fuller et al. 2005; Johnson et al. 2006; Litchman and Klausmeier, 2008). Lindell and coworkers (2005) suggest that the dominance of certain phytoplankton taxonomic groups may be due to the ability of different ecotypes within those groups to thrive under specific environmental conditions, thereby allowing the entire population to acclimate to environmental stimuli. Clearly the factors influencing phytoplankton abundance in oligotrophic waters, and as a consequence the marine carbon cycle, are complex and more work is needed to fully elucidate phytoplankton growth dynamics in these regions. Moreover, observations of prolonged stratification (Karl et al. 2001) and projections of oligotrophic ocean expansion in response to global warming (Sarmiento et al. 1998; Matear & Hirst 1999; Sarmiento et al. 2004) highlight the importance of characterizing phytoplankton dynamics in these regions.

This study investigates survival strategies of naturally occurring phytoplankton communities in the oligotrophic, stratified Gulf of Aqaba in response to nutrient availability under various light regimes. We use field measurements from the euphotic zone of the Gulf of Aqaba, Red Sea before and during stratification at the onset of a spring bloom, as well as nutrient addition incubation experiments (at different light regimes) performed during the ultra-oligotrophic summer season to: (1) assess shifts in phytoplankton community composition and photophysiology in response to the combined effects of nutrient and light availability; (2) identify key competition, acclimation, and nutrient uptake strategies of picoeukaryotes, *Synechococcus*, and *Prochlorococcus* during a bloom; and (3) estimate the

contribution of picoeukaryotes, *Synechococcus*, and *Prochlorococcus* to total photosynthetic biomass during blooms as well as periods of sustained oligotrophy.

MATERIALS AND METHODS

Spring bloom monitoring

Water samples were collected from Station A (29°28'N, 34°55'E) in the Northern Gulf of Aqaba during the spring season when the water column transitions from mixed to stratified. Station A is located off shore in a deep (>700 m) open water region where the water column extends well below the euphotic zone; this permits analysis of an entirely pelagic euphotic zone. Depth profiles were taken on 12 March 2007 and 16 March 2007 using a sampling CTD-Rosette (SeaBird). Dissolved nutrient concentrations, Chl *a*, and flow cytometry measurements were taken as described below with the following modifications. For Chl *a* samples, filters were transferred immediately to 10 mL 90% acetone aboard the ship, and the pigment was extracted for 24 hrs at 4 °C. Flow cytometry measurements were taken with a Becton Dickinson FACScan flow cytometer. On the basis of autofluorescence characteristics, cells were classified as picoeukaryotes or *Synechococcus*. Due to their relatively low autofluorescence compared to other phytoplankton, *Prochlorococcus* cannot be reproducibly differentiated from other non-photosynthetic bacteria using the FACScan flow cytometer. Therefore, *Prochlorococcus* concentrations are not available from the field data set due to the fluorescence detection limit of the machine.

Simulated stratification experiment

A simulated stratification experiment was conducted to measure photoacclimation with higher time resolution than was possible for the field measurements described above. The experiment was designed to simulate the reversal of light limitation experienced by cells during the natural transition from mixing to stratification that occurs during the spring bloom. Surface water (1 m) was collected from a pier 20 m offshore on 12 March 2007 (prior to the spring bloom), and placed into 10 L sample-rinsed translucent polyethylene bottles (3 replicate bottles per treatment) one hour before sunrise at the InterUniversity Institute for Marine Science (IUI) in Eilat, Israel. Water was pre-filtered through 20 μm mesh to remove grazers. Because nutrients were naturally abundant in sample waters as a consequence of deep mixing that preceded the experiment, it was not necessary to amend the sample water with additional nutrients to elicit a bloom response.

Sample bottles were incubated under light conditions designed to simulate either “shallow” (high light, HL) or “deep” (low light, LL) locations in the stratified water column. Bottles were incubated in an outdoor tank through which water from the Gulf circulated, and screening material was used to attenuate the sunlight intensity to which the bottles were exposed. In HL treatment, 50% light attenuation yielded maximum midday irradiance of $\sim 1000 \mu\text{mol quanta m}^{-2} \text{ s}^{-1}$ and was equivalent to the upper 10 m of the euphotic zone of the Gulf during summer months. In the LL treatment, $\sim 95\%$ light attenuation yielded maximum midday irradiance of $\sim 100 \mu\text{mol quanta m}^{-2} \text{ s}^{-1}$ and was equivalent to the light intensity at approximately 80 m in the summer months (similar to the upper boundary of the deep chlorophyll maximum (D. Iluz, personal communication)). No alteration of the natural light spectrum was done

in the HL treatment. The light spectrum in the LL treatment was enriched in blue-green wavelengths using a tinted shade cloth to more closely resemble the natural light spectrum at 70-80 m depth. Comparison of spectra for unattenuated sunlight and light transmitted through the tinted cloth (each normalized to irradiance at 694 nm) showed that the cloth enriched the proportions of blue wavelengths at 443 and 490 nm by 280% and 210%, respectively, and green wavelengths at 510 and 555 nm by 190% and 150%, respectively, relative to the unfiltered visible spectrum.

The bottles were incubated for 2 days and aliquots were removed approximately every 3-4 hours during the day for sampling. Flow cytometry samples were removed and processed as described below at each time point. Photosystem II (PSII) chlorophyll fluorescence measurements were taken by concentrating cells in the dark onto GF/F filters (Whatman) using a low pressure peristaltic pump. One liter of seawater was collected onto each sample filter. Chlorophyll fluorescence measurements were made with a WATER-PAM fluorometer and WinControl software (Heinz Walz GmbH). An automated program was run to determine the photochemical efficiency of PSII under dark-adapted (F_v/F_m) and light-adapted (Φ_{PSII}) states. (For detailed discussion of fluorescence parameter calculations and measurement techniques used in this study see Mackey et al. 2008). The program delivered the following light treatments and measuring pulses: 10 min dark adaptation and delivery of a saturating pulse to determine F_v/F_m , followed by 3 min exposure to actinic light at $100 \mu\text{mol quanta m}^{-2} \text{s}^{-1}$ and delivery of a saturating pulse to determine Φ_{PSII} at this light intensity (hereafter $\Phi_{PSII-100}$), followed by 3 min exposure to actinic light at $1000 \mu\text{mol quanta m}^{-2} \text{s}^{-1}$ and delivery of a saturating pulse to determine Φ_{PSII} at this light

intensity (hereafter Φ_{PSII} -1000). These actinic light exposure durations were determined empirically as sufficient for the cells to reach steady state.

Nutrient enrichment experiments

Nutrient enrichment experiments were conducted to ascertain phytoplankton responses to fertilization with exogenous inorganic nutrients (N and P) under incubation with HL and LL intensities simulating “shallow” and “deep” depths, respectively, within the water column. These experiments were designed to simulate bloom conditions resulting from delivery of new nutrients (e.g. via nitrogen fixation or atmospheric deposition) to a stratified, oligotrophic water column. Surface water was collected at 1 m depth from an offshore site in the Northern Gulf of Aqaba during two field excursions in September 2005 and October 2006 (note that community structure during these months is quite consistent from year to year (Lindell & Post 1996; Mackey et al. 2007)). Surface water was pre-filtered with 20 μm nylon mesh to remove grazers larger than 20 μm , collected into sample-rinsed translucent polyethylene bottles, and kept in the dark during transport (less than two hours) to the IUI facility. All incubations were performed with three replicate bottles per treatment.

The LL nutrient enrichment experiment was conducted in September 2005 and the HL nutrient enrichment experiment in October 2006. Light attenuation and incubation setup were performed exactly as described above for the simulated stratification experiment, using the same screening materials and incubation conditions. Phosphorus was added as 0.4 $\mu\text{mol L}^{-1}$ sodium phosphate monobasic (hereafter PO_4), and N was added as 7 $\mu\text{mol L}^{-1}$ sodium nitrate (hereafter NO_3) or

ammonium chloride (hereafter NH_4). Sample bottles contained 6 L water and were incubated for 4 days. The nutrient concentrations used in the enrichments were based on typical PO_4 and NO_3 concentrations for deep water from the Gulf (Mackey et al. 2007) because phytoplankton are naturally exposed to N and P at these levels following deep mixing and upwelling events. Nutrients were therefore added at an N:P ratio of 17.5:1, rather than the canonical Redfield ratio of 16:1, to better simulate natural bloom forming conditions.

Nutrient analyses

Total oxidized nitrogen (nitrate and nitrite, N+N) and soluble reactive phosphorus (SRP) concentrations were determined using colorimetric methods described by Hansen & Koroleff (1999), modified for a Flow Injection Autoanalyzer (FIA, Lachat Instruments Model QuickChem 8000). In all treatments not receiving sodium phosphate, SRP was pre-concentrated before analysis by a factor of about 20 using the magnesium co-precipitation (MAGIC) method (Karl and Tien 1992). Using standard additions, the recovery of inorganic P in this procedure was determined to be 100% and the blank was always below detection limits. The FIA was calibrated using standards prepared in low nutrient filtered seawater (summer surface water from the Gulf) over a range of 0-10 $\mu\text{mol L}^{-1}$. The precision of the methods used in this work is 0.05 $\mu\text{mol L}^{-1}$ for N+N, and 0.02 $\mu\text{mol L}^{-1}$ for SRP. The detection limit for these nutrients was 0.02 $\mu\text{mol L}^{-1}$.

Chlorophyll *a*

Daily samples for chlorophyll *a* (Chl *a*) determination were taken during both nutrient addition bioassays by filtering 200 mL aliquots onto Whatman GF/F glass fiber filters. In the HL nutrient enrichment experiment, samples were analyzed daily following extraction at 4°C in 90% acetone for 24 hrs in the dark. In the LL nutrient enrichment experiment, aliquots were removed from each bottle beginning at 3 pm each day, refrigerated overnight in the dark and filtered beginning at 10 am the following morning. These filters were placed within sterile 2 mL cryovials, stored at -80°C, and extracted for 24 hrs in 90% acetone (7 mL per sample) within 1 week. No significant effect of storage was observed based on comparisons between sample sets analyzed with and without storage; Chl *a* concentrations determined by the two methods were statistically indistinguishable. Fluorescence was measured with a Turner Fluorometer (Turner Designs 10-AU-005-CE) before and after acidification with 3.7% HCl and was converted to a Chl *a* concentration using a standard conversion method (JGOFS 1994). The standard error determined from triplicate samples was below 0.03 and 0.06 mg m⁻³ in the HL and LL nutrient enrichment experiments, respectively.

Flow cytometry

Aliquots were removed daily during the nutrient addition bioassays for flow cytometry, fixed with glutaraldehyde (final concentrations 0.1%) and stored at -80°C until analyzed on a FACS Aria flow cytometer. Data analysis was performed using FlowJo software (TreeStar, Inc.). Picophytoplankton (photosynthetic cells <2 µm diameter) were classified as picoeukaryotes, *Prochlorococcus*, or *Synechococcus* on

the basis of autofluorescence characteristics as described in Mackey et al. (2007). Growth curves generated from the cell concentration data represent net growth for each group, i.e. growth minus mortality. Cell concentrations were determined by spiking samples with a known volume and concentration of 1 μm fluorescent yellow-green beads (Polysciences). The coefficient of variation for cell concentrations determined from triplicate samples was below 0.15 in both experiments. Mean and median cellular red fluorescence levels for picoeukaryotes, *Synechococcus*, and *Prochlorococcus* populations were estimated from the logarithmic signals collected on the Cy55-PE channel (488 nm excitation, 665 nm emission) of the flow cytometer.

Estimation of photosynthetic biomass

The contribution of each cell type to the overall picophytoplankton photosynthetic carbon biomass was estimated using the equation of Verity and coworkers (1992), which relates cell volume to carbon (C) biomass. Estimates of cell dimensions for *Prochlorococcus* ($\sim 0.7 \mu\text{m}$) and picoeukaryotes ($\sim 1.5 \mu\text{m}$) were based on light microscopy with a Nikon epifluorescent microscope at 400X magnification and from side-scatter measurements (a proxy for cell size) taken during flow cytometry of fixed cells collected in the field. Measurements fell within the typical range observed in other studies (Campbell et al. 1994). Both *Prochlorococcus* and picoeukaryotes were spherical, giving conversion factors of 98 fg C cell⁻¹ and 708 fg C cell⁻¹, respectively. The conversion factor for *Prochlorococcus* is within the range of calculated estimates (29 and 124 fg C cell⁻¹) reported in other field studies (Partensky et al. 1999 and references therein; Zubkov et al. 2000; Grob et al. 2007), but is higher

than an estimate of 49 fg C cell⁻¹ measured from laboratory cultures (Cailliau et al. 1996). Conversion factors for picoeukaryotes vary substantially due to the broader range of possible cell diameters; however, our estimate is within the range of calculated estimates (530-863 fg C cell⁻¹) for picoeukaryotes from the Pacific Ocean (Worden et al. 2004) with diameters similar to those determined for this study. Microscopy revealed rod-shaped *Synechococcus* cells (dimensions ~0.8- ~1.2 μ m), with a composition of 279 fg C cell⁻¹, which is similar to previous estimates of ~250 fg C cell⁻¹ (Kana & Gilbert 1987; Campbell et al. 1994). Conversion factors were multiplied by cell concentration (determined from flow cytometry) to estimate photosynthetic biomass. While natural variability of phytoplankton cell size within the population introduces some error into our estimates, approximations of cellular C content from cell biovolume can inform productivity models if the potential for error is adequately considered when interpreting the results (Campbell et al. 1994; Worden et al. 2004).

RESULTS

Spring bloom monitoring

To investigate phytoplankton responses to nutrient and light availability during the spring bloom, *in situ* monitoring of Chl *a*, flow cytometry, and nutrient draw down were carried out before and during the 2007 spring bloom. **Fig. 1** shows depth profile measurements of SRP, NO₃, Chl *a*, and *Synechococcus* and picoeukaryotes cell concentrations from the euphotic zone before (12 March 2007) and after (16 March 2007) stratification had begun to occur. Prior to stratification, 60 m is the typical depth

at which light is attenuated to 1% of surface intensity ($\sim 20 \mu\text{mol quanta m}^{-2} \text{ s}^{-1}$) in the mixed Gulf water column (D. Iluz, personal communication). Because the water column was homogeneously mixed down to $>600 \text{ m}$ on March 12 and the salinity profiles did not change over the course of the sampling (data not shown), we conclude that the observed changes in the water column during this period are due to stratification rather than introduction of different water masses to the euphotic zone via other physical processes in the water column. This interpretation is consistent with the current understanding of the circulation in the Gulf (Wolf-Vetch et al. 1992). NO_3 and SRP levels were relatively homogenous ($1.7 \mu\text{mol L}^{-1}$ and $0.11 \mu\text{mol L}^{-1}$, respectively) throughout the mixed water column (on March 12) (**Fig. 1a,b**), whereas drawdown was evident in the upper 50 m of the stratified water column (March 16). Based on temperature profiles, the surface mixed layer was approximately 25 m on March 16 during stratification. In these profiles, NO_3 levels were $0.8 \mu\text{mol L}^{-1}$ at the surface and increased to $1.8 \mu\text{mol L}^{-1}$ at depth, and SRP levels were $0.05 \mu\text{mol L}^{-1}$ at the surface and increased to $0.08 \mu\text{mol L}^{-1}$ at depth (**Fig. 1a,b**).

A Chl *a* maximum (1.26 mg m^{-3}) was observed in the stratified water column at 20 m depth, whereas the Chl *a* distribution was homogenous throughout the mixed water column on March 12th (0.2 mg m^{-3} ; **Fig. 1c**). In the mixed profile, picoeukaryotes were present at approximately 3000-4000 cells mL^{-1} , and *Synechococcus* were present at approximately 2000-3000 cells mL^{-1} throughout the euphotic zone (**Fig. 1d,e**). The maximum picoeukaryote cell concentration in the stratified profile on March 16 occurred at 60 m ($17,000 \text{ cells mL}^{-1}$), and another smaller peak was apparent near 120 m ($11,000 \text{ cells mL}^{-1}$). In contrast,

Synechococcus cell concentration profiles showed two small peaks at 20 m (7,000 cells mL⁻¹) and 100 m (8,000 cells mL⁻¹) that were offset from the picoeukaryote peaks (**Fig. 1d,e**). Cell abundances of *Prochlorococcus* and larger phytoplankton were not available for these casts, so it is not possible to know their vertical distributions. However, in typical years in the Gulf, *Prochlorococcus* numbers remain relatively constant throughout the spring bloom (Lindell and Post 1995; A. Paytan unpublished data). The profiles of Chl *a* would include input from both *Prochlorococcus* and larger cells. In particular, inputs from larger cells in surface waters (Mackey et al. 2007) may explain the Chl *a* peak at 20 m that is offset from *Synechococcus* and picoeukaryote peaks.

On March 16, picoeukaryote cellular fluorescence showed no systematic trends with depth (**Fig. 2a**), whereas *Synechococcus* cellular fluorescence was higher for cells at 100 m, the depth of the deep cell maximum, than at 20 m, the depth of the surface maximum (**Fig. 2b**).

Fig. 3a shows the ratio of NO₃ to PO₄ (NO₃:PO₄) calculated from NO₃ and SRP measurements at each depth for the mixed and stratified casts. A dashed line at 16 indicates the value of the Redfield ratio (Redfield et al. 1963). In the mixed profile the NO₃:PO₄ ratio was approximately 16 throughout the water column except at the surface where it was approximately 14. In the stratified cast the NO₃:PO₄ ratio was also near 14 in surface waters, but increased to approximately 20 at greater depths. The drawdown of NO₃ and SRP determined from changes in water nutrient concentrations over the period of sampling are shown in **Fig. 3b and c**, respectively, and show that larger decreases in the concentrations of both nutrients (i.e., greater

drawdown) occurred in the upper 50 m of the euphotic zone. The ratios of NO_3 and PO_4 drawdown (**Fig. 3d**) are close to the Redfield ratio of 16 in the surface, but decrease drastically at 60 m ($\text{NO}_3:\text{PO}_4$ of approximately 1) before increasing again with depth but still remaining below Redfield ratios ($\text{NO}_3:\text{PO}_4$ between 5-10). These uptake ratios are indicative of the ratios at which these nutrients are removed from the water during the sampling period, e.g. through biological immobilization or export (Eppeley & Patterson 1979) assuming (1) the inventory of nutrients (i.e. dissolved plus particulate) in the euphotic zone was constant over the time of our sampling, and (2) that there was no vertical or horizontal flux of nutrients due to lateral diffusion or isopycnal mixing. These assumptions are reasonable for the northern Gulf, given that the north-south gradient in surface waters nutrients is low throughout the year (Klinker et al. 1977; A. Paytan, unpublished data), the short time scale of our calculation (four days), and given that a one dimensional mixed layer model accurately describes the convective/advective water balance at the northern end of the Gulf where our sampling was conducted (Wolf-Vetch et al. 1992).

Simulated stratification experiment

The picophytoplankton community responded similarly to incubation under HL and LL conditions in the simulated stratification experiment. The initial population was composed of picoeukaryotes (14,500 cells mL^{-1}), *Synechococcus* (19,600 cells mL^{-1}), and *Prochlorococcus* (12,900 cells mL^{-1}). Picoeukaryotes and *Synechococcus* increased in abundance, and *Prochlorococcus* decreased in abundance, over 2 days in both the HL (**Fig. 4a**) and LL (**Fig. 4b**) treatments.

Midday (noon) PSII fluorescence measurements for the simulated stratification experiment are shown in **Fig. 5**. F_v/F_m and Φ_{PSII} measurements increased slightly compared to initial midday levels within one day of incubation in the HL treatment (**Fig. 5a**). In contrast, F_v/F_m measurements remained relatively stable in the LL treatment (**Fig. 5b**), while both Φ_{PSII}^{-100} and Φ_{PSII}^{-1000} decreased by over 75% by midday on the second day of the experiment (i.e. hour 36) compared to initial midday levels (hour 12).

Nutrients uptake in nutrient enrichment experiments

Ambient seawater nutrient concentrations measured prior to the addition of experimental amendments in the HL and LL nutrient enrichment experiments are shown in **Table 1**, and reflect the oligotrophic character of surface waters in the Gulf during the stratified season in which the experiments were conducted in both years. The nutrient data from the HL and LL nutrient enrichment experiments are discussed semi-quantitatively because nutrient levels in several of the treatments were close to detection limits and differences between treatments were, in some cases, close to the analytical precision. However, while statistical statements are not made, the conclusions herein are nevertheless based on comparison of averages and standard deviations of triplicate samples. In the HL nutrient enrichment experiment, SRP decreased in treatments receiving PO_4 together with added sources of N (i.e., NO_3 or NH_4 , **Table 1**). The changes in SRP concentration for all other treatments were not substantially different from the control. Decreases in inorganic N (N_i) were observed in treatments with NO_3 and PO_4 together, and NO_3 alone. In the LL nutrient

enrichment experiment, SRP concentrations similarly decreased only in treatments with PO₄ when NH₄ or NO₃ were also added. All other treatments showed slight decreases in SRP concentration but were not substantially different from the control. N_i decreased following treatment with NO₃ and PO₄ together but not with NO₃ alone, while all other changes were similar to the control (**Table 1**).

Chlorophyll *a* in nutrient enrichment experiments

Chl *a* levels were monitored daily throughout the HL and LL nutrient enrichment experiments using Chl *a* extraction. **Fig. 6a** shows the Chl *a* time series in the HL nutrient enrichment experiment. The initial Chl *a* level was 0.15 mg m⁻³. The Chl *a* concentration in the control decreased to 0.02 mg m⁻³ by the final day of the experiment. The largest increase in Chl *a* was observed in the treatment receiving NH₄ and PO₄ together (0.41 mg m⁻³), which showed a greater than 3-fold increase over the initial level and a 17-fold increase relative to the control on the final day (**Fig. 6a**). Treatment with PO₄ and NO₃ together yielded a smaller but measurable increase (0.18 mg m⁻³). By the final day of the experiment, treatments of PO₄, NO₃, or NH₄ alone (i.e. single nutrient amendments) showed decreased Chl *a* levels relative to the initial level (0.06, 0.05, and 0.05 mg m⁻³ respectively) that were similar or slightly higher than that of the control (**Fig. 6a**). The standard error determined from triplicate samples in the HL nutrient enrichment experiment was below 0.03 mg m⁻³ for all treatments.

In the LL nutrient enrichment experiment all treatments (including the control) resulted in elevated Chl *a* levels relative to the initial level (0.08 mg m⁻³); however,

none of the nutrient addition treatments resulted in Chl *a* levels that were significantly higher than the control (0.24 mg m⁻³) by day 4 of the experiment (**Fig. 6b**). Treatment with PO₄, NH₄, or NO₃ alone resulted in 2- fold increases in Chl *a* compared to the initial values (0.17 mg m⁻³, 0.13 mg m⁻³, and 0.21 mg m⁻³, respectively). Treatments of PO₄ given together with either NH₄ or NO₃ showed Chl *a* levels above initial levels but similar to the control (0.27 mg m⁻³ and 0.19 mg m⁻³, respectively). The standard error determined from triplicate samples in the LL nutrient enrichment experiment was below 0.06 mg m⁻³ for all treatments.

Flow cytometry cell counts in nutrient enrichment experiments

To determine how picophytoplankton community composition changes in response to nutrients and light availability, we measured the changes in cell densities of picoeukaryotes, *Synechococcus*, and *Prochlorococcus* in the HL and LL nutrient enrichment experiments using flow cytometry. **Fig. 7** shows picoeukaryotes, *Synechococcus*, and *Prochlorococcus* cell concentrations throughout the course of the HL and LL nutrient enrichment experiments, and **Table 2** shows the final concentrations and the relative increases for each treatment compared to the control on the last day of the experiment. (The coefficient of variation for cell concentrations determined from triplicate samples was below 0.15 for both the HL and LL nutrient enrichment experiments.) *Prochlorococcus* (**Table 2, Fig. 7a.3**) was the dominant cell type at the start of the HL experiment, followed by *Synechococcus* (**Table 2, Fig. 7a.2**) and picoeukaryotes (**Table 2, Fig. 7a.1**), whereas *Synechococcus* (**Fig. 7b.2**) was the dominant cell type at the start of the LL nutrient enrichment experiment,

followed by *Prochlorococcus* (**Fig. 7b.3**) and picoeukaryotes (**Fig. 7b.1**). In the HL nutrient enrichment experiment, the greatest increases in picoeukaryote and *Synechococcus* cell numbers (1-2 orders of magnitude increase compared to control) occurred in treatments receiving N and P together. *Prochlorococcus* cell concentrations also increased relative to the control for treatments receiving PO₄ together with either NO₃ or NH₄, but were less than an order of magnitude greater than the control and remained similar to initial levels (**Table 2, Fig. 7a**). In contrast, cell concentration measurements for all three organisms were typically less than or comparable to that of the control for treatments in the LL nutrient enrichment experiment (**Table 2, Fig. 7b**).

Photosynthetic biomass in nutrient enrichment experiments

To estimate the relative contributions of picoeukaryotes, *Synechococcus*, and *Prochlorococcus* to primary production during a bloom, we estimated changes in the photosynthetic biomass of each of these groups during the HL and LL nutrient enrichment experiments. **Fig. 8** shows the change from initial picophytoplankton photosynthetic biomass levels to those on day 4 of each experiment for picoeukaryotes, *Synechococcus*, and *Prochlorococcus*. There were no substantial net changes in picophytoplankton photosynthetic biomass for any treatments relative to initial levels in the LL nutrient enrichment experiment, where the photosynthetic biomasses for all treatments were similar to initial levels (6.8 mg C m⁻³). In these low light samples, the contribution from *Prochlorococcus* and *Synechococcus* decreased in all treatments except for the control, while the contribution of picoeukaryotes

increased for all treatments (**Fig. 8b**). The HL nutrient enrichment experiment (**Fig. 8a**), in contrast, showed net increases in picophytoplankton photosynthetic biomass relative to initial levels (2.4 mg C m^{-3}) when N and P were added together (16.3 and 19.3 mg C m^{-3} for treatments NH_4+PO_4 and NO_3+PO_4 respectively), similar levels following additions of PO_4 (4.2 mg C m^{-3}) or NH_4 (4.6 mg C m^{-3}), and decreased levels for the control and only NO_3 treatments (1.1 mg C m^{-3}).

Flow cytometry cellular fluorescence in nutrient enrichment experiments

To assess photoacclimation in the picoeukaryote, *Synechococcus*, and *Prochlorococcus* populations HL and LL nutrient enrichment experiments we estimated cellular fluorescence, a proxy for cellular pigment content (Sosik et al. 1989; Li et al. 1993), from flow cytometry. **Figure 9** shows the mean and median red fluorescence of cells on day 0 and 4 of the LL nutrient enrichment experiment. By day 4 of the experiment, red fluorescence increased 2- fold in the picoeukaryote population (**Figure 9a**) and 5-fold in the *Synechococcus* population (**Figure 9b**) regardless of nutrient treatment. Red fluorescence in the *Prochlorococcus* population was similar on day 4 and day 0 in all nutrient treatments (**Figure 9c**). Red fluorescence levels in cell populations on day 4 of the HL nutrient enrichment experiment did not show any systematic trends relative to day 0 levels (data not shown).

DISCUSSION

Nutrient limitation refers to the slowing or cessation of photosynthetic biomass production in response to low availability of an essential nutrient. Together, the Redfield ratio and Liebig's law of the minimum have been used in oceanography to identify nutrient limitation at the phytoplankton community level (von Liebig 1840; Redfield et al. 1963). These interpretations are based on the assumption that phytoplankton communities assimilate macronutrients at a constant ratio, and therefore deviations from such ratios indicate limitation by one nutrient over another. However, nutrient co-limitation can occur in oligotrophic waters (Seppala et al. 1999; Mills et al. 2004) where addition of one nutrient may rapidly induce limitation for another nutrient as soon as limitation by the former is relieved. In these cases phytoplankton communities are effectively co-limited because addition of both nutrients is required to elicit substantial increases in biomass. Therefore, while only one nutrient can be physiologically limiting at a given point in time, more than one nutrient may effectively co-limit phytoplankton on ecologically relevant time scales. In this study, the term "co-limitation" refers to inhibition of photosynthetic biomass production, rather than to the physiological nutrient status of a cell or group of cells per se.

In the stratified Gulf of Aqaba, N and P co-limit the phytoplankton community. Under irradiances similar to levels that would be seen in the upper euphotic zone (HL nutrient enrichment experiment), additions of inorganic N and P together resulted in elevated Chl *a* levels, while addition of N or P independently did not (**Fig. 6a**) (Fe, Si, and other trace metal concentrations are elevated in the waters of

the Gulf (Longhurst 1998; Chase et al. 2004; Chen et al. 2007), thus limitation by these elements was not considered here). Indeed, estimates of picophytoplankton photosynthetic biomass for the HL nutrient enrichment experiment showed that the largest increases occurred when N and P were added simultaneously (**Fig. 8a**). We therefore conclude that during the time of our experiments, oligotrophic conditions in surface waters (**Table 1**) caused co-limitation of the phytoplankton community by N and P when light was not limiting (**Fig. 6a and 8a**) (see also Labiosa 2007). This type of limitation is referred to as “multi-nutrient co-limitation,” and results when the levels of two or more nutrients are depleted beyond the levels required for cellular uptake (Arrigo 2005 and references therein).

The HL nutrient enrichment experiment showed that the phytoplankton community did not respond homogeneously to nutrient additions under sufficient irradiances. Cell concentration measurements indicated that picoeukaryotes and *Synechococcus* responded to nutrient additions during the 4-day incubation period, whereas *Prochlorococcus* (the dominant organism at the start of our sampling) did not (**Fig. 7a**). Therefore, the majority of the photosynthetic biomass produced following addition of N and P was attributable to picoeukaryotes and *Synechococcus* (**Fig. 8a**). Similar results were observed in the simulated stratification experiment, where picoeukaryote and *Synechococcus* populations bloomed over a 2 day period when light limitation was reversed (**Fig. 4**). In this study we focused on picophytoplankton bloom dynamics; larger cells are also bloom components in the Gulf of Aqaba (Lindell and Post 1995; Mackey et al. 2007), contributing additional photosynthetic biomass. Our results indicate that when growth limiting nutrients become available and light is

not limiting, blooms of specific subpopulations within the overall phytoplankton community can yield substantial increases in photosynthetic biomass as a result of their rapid growth responses.

The relatively rapid increase in the cell densities of picoeukaryotes and *Synechococcus* when N and P were provided together in the HL nutrient enrichment (**Fig. 7a.1 and 7a.2**), and the simulated stratification (**Fig 4a and b**) experiments suggested that these phytoplankton have a “bloomer” growth strategy (Margalef 1978; Smayda and Reynolds, 2001; Klausmeier et al. 2004; Labiosa 2007; see Arrigo 2005 for discussion of terminology). This growth response is similar to the *in situ* changes that occurred as the water column started to stratify and nutrient and light limitation are reversed, which show that the cell concentrations of picoeukaryotes (and to a lesser extent *Synechococcus*) increase 2- to 3- fold in the upper euphotic zone over a period of days (**Fig. 1d,e**). Moreover, picoeukaryotes were not numerically dominant in day zero samples, indicating that they were unable to remain abundant during prolonged oligotrophic summer conditions (**Fig. 7a.1 and 7b.1**; Lindell & Post 1995; Labiosa 2007; Mackey et al. 2007), as would be expected for a bloomer strategist.

By contrast, *Prochlorococcus* was abundant in day zero samples and showed no rapid, substantial growth responses regardless of nutrient additions when light was not limiting in the HL nutrient enrichment experiment (Fig. 7a.3, 7b.3; see also Labiosa 2007). Similar results were observed in the simulated stratification experiment, where the *Prochlorococcus* population declined slightly over a 2 day period when light limitation was reversed but nutrients were still available from deep winter mixing. These data may suggest that *Prochlorococcus* adopts a “survivalist” growth strategy,

enabling them to sustain growth during periods of low nutrient levels, possibly owing to lower growth rates, lower nutrient requirements (Bertilsson et al. 2003; Fuller et al. 2005; Van Mooy et al. 2006) and high affinity nutrient acquisition systems (Scanlan & Wilson 1999) compared to other picophytoplankton. Indeed, Lindell & Post (1995) observed that *Prochlorococcus* became the dominant phytoplankter in the Gulf only after several months of stratification and prolonged nutrient depletion had caused marked decreases in picoeukaryote and *Synechococcus* numbers.

However, while this pattern of succession is typical during most years in the Gulf (Israel National Monitoring Project, Eilat, <http://www.iui-eilat.ac.il/NMP/>, unpublished data), *Prochlorococcus* was a significant contributor to the spring bloom in 1999 (Fuller et al. 2005), suggesting that it may share characteristics of bloom strategists as well. Specifically the hydrographic and chemical conditions (stability and duration of the stratification, amount of nutrients injected, temperature and light intensities etc.) during bloom events and the relevant and variable responses of *Prochlorococcus* should be evaluated in more detail. In the simulated stratification experiment, the lack of *Prochlorococcus* growth could be a function of the antecedent conditions of the sample water, rather than a function of a survivalist growth strategy. In contrast to the *in situ* monitoring at station A (a location in open water away from the coastal shelf), this experiment used water collected closer to shore. The higher concentrations of *Synechococcus* and picoeukaryotes in the time zero samples (Figure 4) compared to the surface water from station A from the same day (March 12, Figure 1) suggests that growth conditions varied slightly between the locations; coastal stratification may have preceded stratification at station A due to faster warming in

shallower water, thereby accelerating the bloom. Therefore, it is possible that the relatively high *Prochlorococcus* concentrations in time zero samples could indicate that the growth response of these cells had already occurred and reached steady state before our sample water was collected, even though *Synechococcus* and picoeukaryotes continued to bloom for the duration of the experiment. Alternately, the size of the seed population of competent high light ecotypes of *Prochlorococcus* (rather than growth strategy) could explain the growth response (Fuller et al. 2005). Therefore, while *Prochlorococcus* has optimized its growth at lower nutrient levels and is abundant in nutrient poor waters (Partensky 1999 and references therein), more work is needed to accurately characterize *Prochlorococcus* growth strategies, particularly with respect to ecotypic diversity.

In addition to identifying multi-nutrient co-limitation in the phytoplankton community and the species specific response to alleviation of this co-limitation, our results also suggested that the Redfield ratio represents an average value of species-specific N:P ratios in the Gulf of Aqaba, as observed in other areas of the ocean (Elser et al. 1996). A model by Klausmeier and coworkers (2004) reports a range of phytoplankton elemental stoichiometries (N:P) of 8.2 to 45 depending on environmental conditions, and notes that variability occurs between and within species due to genetic diversity and physiological flexibility. The range of N:P ratios reported for *Synechococcus* (13.3-33.2) and *Prochlorococcus* (15.9-22.4) (Bertilsson et al. 2003; Heldal et al. 2003) demonstrate the flexibility in phytoplankton elemental stoichiometries in oligotrophic marine environments when faced with low nutrient availability.

Our study demonstrates that the physiological flexibility with which nutrients are assimilated into photosynthetic biomass is important for phytoplankton dynamics during the spring bloom, where phytoplankton regulate and maintain their elemental stoichiometries via preferential uptake of certain nutrients. Phytoplankton with a “bloomer” growth strategy tend toward lower N:P ratios (Elser et al. 1996). Nutrient stoichiometries in the water column were close to Redfieldian prior to stratification (**Fig. 3a**). During the transition from mixing to stratification, the net removal of NO_3 and PO_4 from the water continued at near-Redfield ratios in the surface (likely reflecting a contribution from larger phytoplankton cells not counted in our analysis), whereas bulk uptake ratios were lower (<10) in the middle and lower euphotic zone (**Fig. 3d**) where *Synechococcus* and picoeukaryotes bloomed (**Fig. 1d,e**). Moreover, the ratio reached a minimum value of 1 at 60 m, coinciding with the picoeukaryote maximum identified in **Fig. 1e**. These results showed that as stratification progressed, more P was taken up overall relative to N than would be predicted by the Redfield ratio, possibly indicating luxury P uptake. These trends were consistent with the phytoplankton growth observed during the bloom (**Fig. 1d,e**), which favor resource partitioning toward P-rich cellular assembly machinery, including ribosomes, high energy adenylates, and nucleic acids (Elser et al. 1996; Elser et al. 2000; Geider and La Roche 2002). While this preferential uptake has been suggested based on theory and laboratory experiments, our field results also support it by relating changes in phytoplankton community composition (i.e. bloomers vs. survivalists) to nutrient uptake ratios.

The term “photoacclimation” encompasses the phenotypic changes that occur in an organism in response to changes in environmental factors affecting photosynthesis (MacIntyre et al. 2002). The photochemical yield of PSII is a measure of photoacclimation because it shows how efficiently PSII is able to use light to drive photochemistry. F_v/F_m , which is the maximum photochemical efficiency of PSII in dark adapted cells, is a measure of the number of functional PSII reaction centers, and tends to reach its lowest values at midday due to photoinhibition (Mackey et al. 2008). Φ_{PSII} is a measure of the photochemical efficiency of PSII under a given background (actinic) light intensity. It differs from F_v/F_m in that some of the functional PSII reaction centers are in the reduced state due to exposure to light at the time of measurement. In the HL treatment, an increase in Φ_{PSII} under both 100 and 1000 $\mu\text{mol quanta m}^{-2} \text{s}^{-1}$ shows that after only one and a half days of incubation under relatively high light (incubation irradiance of 1000 $\mu\text{mol quanta m}^{-2} \text{s}^{-1}$), the cells in these samples were more efficient at keeping PSII oxidized during exposure to light compared to initial measurements when cells were acclimated to deep mixing (**Fig. 5a**). In contrast, cells incubated under lower irradiance (i.e. maximum midday intensity of 100 $\mu\text{mol quanta m}^{-2} \text{s}^{-1}$ in the LL treatment) showed a decreased capacity to cope with light and use it to drive photochemistry on the second day of incubation. In these samples a larger number of PSII reaction centers became reduced (i.e. Φ_{PSII} decreased, **Fig. 5b**) following exposure to the actinic light, suggesting that the cells were less efficient at coping with exposure to light (e.g. by drawing electrons away from PSII, possibly due to a lack of light-inducible photoprotective strategies (Cardol et al. 2008)) compared to the first day of incubation.

This response demonstrates that photoacclimation occurs rapidly at the onset of stratification, and likely influences which taxonomic groups become dominant during a bloom. For example, photoacclimation typically leads to an increase in photosynthetic pigment content under decreased irradiance, such that more light is harvested by the photosynthetic apparatus. For both picoeukaryotes and *Synechococcus* populations in the LL nutrient enrichment experiment, similar cellular fluorescence increases were observed in all treatments and the control (relative to initial levels, **Fig. 9**). The incubation of these cells under low light intensities was therefore either associated with a concurrent cellular synthesis of pigments, or a community shift in which cells with higher pigment content became more abundant, replacing their low-pigment counterparts.

When nutrient limitation was reversed but the incubation irradiance was similar to levels that would be experienced at greater depths in the euphotic zone, i.e., in the LL nutrient enrichment experiment, nutrient additions had a smaller effect on photosynthetic biomass than in the HL nutrient enrichment experiment. Specifically, the increase in Chl *a* (**Fig. 6b**) observed under low light conditions did not correspond to increased photosynthetic biomass in the LL nutrient enrichment experiment (**Fig. 8b**) even though shifts in the phytoplankton community were observed relative to initial samples (**Fig. 7b**). For example, picoeukaryote cell concentrations in the LL nutrient enrichment experiment increased over an order of magnitude regardless of nutrient addition treatment (**Fig. 7b.1**). (Picoeukaryote cell numbers in the deep euphotic zone during the spring bloom show similar trends, increasing at 120 m (**Fig. 1e**)). In contrast to the picoeukaryotes, *Synechococcus* and *Prochlorococcus* declined

slightly in abundance for all treatments and the control in the LL nutrient enrichment experiment (**Fig. 7b.2 and Fig. 7b.3**), possibly due to the presence of small (<20 μm) grazers that were able to pass through the mesh at the start of the experiment (Sommer 2000). The results of this LL nutrient enrichment experiment show that when light (rather than nutrients) limits growth, both photoacclimation and considerable shifts in community composition can occur within the phytoplankton community without a net gain or loss of photosynthetic biomass. Therefore, the traditional interpretation of “bloom” dynamics (i.e. as an increase in photosynthetic biomass) may be confined to the upper euphotic zone where light is not limiting, while other acclimation processes are more ecologically relevant at depth.

While *Synechococcus* declined in abundance during the LL nutrient enrichment experiment, samples from the deep euphotic zone during the spring bloom show a slight increase in *Synechococcus* abundance at 100 m (**Fig. 1d**) along with a concurrent increase in cellular fluorescence (**Fig. 2**), suggesting that *Synechococcus* cells are able to grow and acclimate within the light limited regions of the deep euphotic zone. Low-light adapted *Prochlorococcus* ecotypes have also been shown to be dominant and ubiquitous members of deep euphotic zone phytoplankton communities (West & Scanlan 1999; Rocap et al. 2003; Mackey et al. 2008) but did not grow in the LL experiments. One explanation for the difference in *Synechococcus* and *Prochlorococcus* growth responses between cells in the LL nutrient enrichment experiment and cells from the deep euphotic zone during the spring bloom could be the different antecedent conditions to which these populations were acclimated prior to sampling. The LL nutrient enrichment experiment was conducted with water and

phytoplankton collected from stratified surface waters; therefore, it is likely that these cells were acclimated to high light and may have required more than 4 days to adjust to lower incubation irradiances before growing. Moreover, low-light adapted ecotypes were likely less abundant in the sample water used in the nutrient addition experiments than high-light ecotypes (Fuller et al. 2005; Lindell et al. 2005), and would have required more time to become numerically dominant following a light shift. In contrast, cells sampled from the deeply mixed water column (> 300 m) would likely be acclimated to a very different light regime, as before the bloom the water column was mixed from the surface (high light) to below the euphotic depth (very low light). Following stratification of the water column, cells trapped at depth would be primed to acclimate to low irradiances, allowing them to bloom immediately (**Fig. 1d,e**). In addition, larger seed populations of competent low light adapted ecotypes would have been present in the mixed water column than in the surface waters used during the LL nutrient enrichment experiment.

Our data suggest that in the Gulf of Aqaba, physiological acclimation to different nutrient and light regimes help shape the phytoplankton community. However, it is important to note that this physiological flexibility is likely only one factor influencing phytoplankton survival and community succession: multiple taxonomic groups of picoeukaryotes (Moon-van der Staay et al. 2001; Worden 2006), *Synechococcus* (Fuller et al. 2005; Penno et al. 2006), and *Prochlorococcus* (Moore et al. 1998; Rocap et al. 2003) coexist in this and other open ocean regions, and this extra layer of diversity may further enable picophytoplankton communities to adjust rapidly to changes in nutrient and light availability. The dominance of one group of

picoeukaryotes during a bloom may therefore be at least partially attributable to the ability of different ecotypes within that group to thrive under different environmental nutrient and light regimes, rather than entirely through sustained expression of nutrient and light stress-response genes (Lindell et al. 2005).

Clarifying the combined influence of nutrient and light limitation on phytoplankton strategies and bloom dynamics in oligotrophic regions such as the Gulf of Aqaba is important for understanding how oceanic productivity could be affected by global change. Estimates suggest that by the year 2050 climate warming will lead to longer periods of stratification with fewer deep mixing events in seasonally stratified seas, causing expansion of low productivity, permanently stratified subtropical gyre biomes (i.e. ultra-oligotrophic waters) by 4.0% in the Northern Hemisphere and 9.4% in the Southern Hemisphere (Sarmiento et al. 2004). Following oligotrophic ocean expansion, the effect of non-deepwater nutrient sources (atmospheric dry deposition, precipitation, nitrogen fixation, etc) on oceanic net carbon sequestration, export production, and climate could become more significant as the relative contribution of deepwater nutrients decreases. This shift in nutrient availability and source, which would be overlaid upon a more static light environment, could substantially alter phytoplankton community structure and bloom dynamics in these regions. Our results from the oligotrophic Gulf of Aqaba suggest that under present-day conditions the introduction of exogenous nutrients into stratified surface waters supports blooms of picoeukaryotes that, *when present*, increase in number quickly by exploiting the new nutrients (**Fig. 7a.1, Fig. 8**; Labiosa 2007). However, because survivalists like *Prochlorococcus* are more likely to be abundant following

prolonged ultra-oligotrophic periods (Lindell and Post 1996; this work), the effect of exogenous nutrient sources (e.g. dust, nitrogen fixation, precipitation, etc) on carbon sequestration within future permanently stratified oligotrophic seas remains difficult to predict. Specific investigations on the effects of exogenous new nutrients are still needed to fully understand if and how they will influence primary production and shape phytoplankton community structure in the oligotrophic ocean at present and in the future.

ACKNOWLEDGEMENTS

I acknowledge my co-authors Tanya Rivlin, Arthur R Grossman, Anton F Post, and Adina Paytan for help on this manuscript, which was published in 2009 in *Marine Biology*. As a group, we thank our colleagues at the Interuniversity Institute for Marine Science in Eilat, Israel for assisting in data collection and providing laboratory space and equipment during the study. We also thank the anonymous reviewers who provided comments on the manuscript. M. Chernichovsky, Y. Chen, R. Foster, E. Grey, and J. Street assisted with sampling. D. Parks assisted with flow cytometry measurements at Stanford and I. Ayalon provided flow cytometry data analyzed at IUI. R. Labiosa helped develop experimental methods. This research was supported under the National Aeronautics and Space Administration (NASA) New Investigator Program NAG5-12663 to AP, the North Atlantic Treaty Organization (NATO) Science for Peace Grant SfP 982161 to AP and AFP, a grant from the Koret Foundation to AP, National Science Foundation (NSF) Oceanography grant OCE-0450874 to ARG., and Israel Science Foundation grant 135/05 to AFP. KRMM was supported through the National Science Foundation (NSF) Graduate Research Fellowship Program and the Department of Energy (DOE) Global Change Education Program. All experiments comply with the current laws of the countries in which the experiments were performed.

Citation

Mackey, KRM, T Rivlin, A. Grossman, A Post, and A Paytan. 2009. Picophytoplankton responses to changing nutrient and light regimes during a bloom. *Marine Biology* 156 (8): 1531-1546. DOI 10.1007/s00227-009-1185-2

Author contributions

KRM Mackey - planned experimental design; conducted field work; processed samples; analyzed and interpreted data; wrote the manuscript

T Rivlin – helped process nutrient samples for Figure 1 and Table 1

A Grossman - provided funding; provided comments on the manuscript

AF Post - provided funding; provided comments on the manuscript

A Paytan - provided funding; helped plan experimental design; helped conduct field work; provided comments on the manuscript

REFERENCES

- Arrigo K. R. 2005. Marine micro-organisms and global nutrient cycles. *Nature* **437**:349-355
- Bertilsson S., O. Berglund, D. M. Karl, S. W. Chisholm. 2003. Elemental composition of marine *Prochlorococcus* and *Synechococcus*: Implications for the ecological stoichiometry of the sea. *Limnol Oceanogr* **B**:1721-1731
- Cailliau C., H. Claustre, F. Vidussi, D. Marie, D. Vaultot. 1996. Carbon biomass, and gross growth rates as estimated from C-14 pigment labelling, during photoacclimation in *Prochlorococcus* CCMP 1378. *Mar Ecol Prog Ser* **145**:209-221
- Campbell L., H. A. Nolla, D. Vaultot. 1994. The importance of *Prochlorococcus* to community structure in the central north Pacific Ocean. *Limnol Oceanogr* **39**:954-961
- Chase Z., A. Paytan, K. S. Johnson, J. Street, A. Post, A. Genin. 2004. A high iron, low chlorophyll coastal ecosystem: the Gulf of Aqaba, Red Sea. American Geophysical Union, Fall Meeting 2004, abstract #OS44B-05
- Chen Y., S. Mills, J. Street, D. Golan, A. Post, M. Jacobson, A. Paytan. 2007. Estimates of atmospheric dry deposition and associated input of nutrients to Gulf of Aqaba seawater. *J Geophys Res* **112**:D04309
- Davey M., G. A. Tarran, M. M. Mills, C. Ridame, R. J. Geider, J. LaRoche. 2008. Nutrient limitation of picophytoplankton photosynthesis and growth in the tropical North Atlantic. *Limnol Oceanogr* **53**:1722-1733
- Elser J. J., D. R. Dobberfuhl, N. A. MacKay, J. H. Schampel. 1996. Organism size,

- life history, and N:P stoichiometry. *BioScience* **46**:674-684
- Elser J. J., R. W. Sterner, E. Gorokhova, W. F. Fagan, T. A. Markow, J. B. Cotner, J. F. Harrison, S. E. Hobbie, G. M. Odell, L. W. Weider. 2000. Biological stoichiometry from genes to ecosystems. *Ecology Letters* **3**:540–550
- Fuller N. J., D. Marie, M. Yallop, T. Rivlin, N. J. West, A. F. Post, D. J. Scanlan. 2005. Dynamics of community structure and phosphate status of picocyanobacterial populations in the Gulf of Aqaba, Red Sea. *Limnol Oceanogr* **50**:363-375
- Geider R. J., J. La Roche. 2002. Redfield revisited: variability of C:N:P in marine microalgae. *Eur J Phycol* **37**:1-17
- Hansen H. P., F. Koroleff. 1999. Determination of nutrients. In: Grasshoff, K., K. Cremling. and M. Erhardt (eds), *Methods of seawater analysis*, Wiley-Vch Verlag, Weinheim, Germany, pp.159-228.
- Heldal M., D. J. Scanlan, S. Norland, F. Thingstad, N. H. Mann. 2003. Elemental composition of single cells of various strains of marine *Prochlorococcus* and *Synechococcus* using X-ray microanalysis. *Limnol Oceanogr* **48**:1732-1743
- JGOFS Protocols. 1994. Chapter 14. Measurement of chlorophyll *a* and phaeopigments by fluorometric analysis.
- Johnson Z. I., E. R. Zinser, A. Coe, N. P. McNulty, E. M. S. Woodward, S. W. Chisholm. 2006. Niche partitioning among *Prochlorococcus* ecotypes along ocean-scale environmental gradients. *Science* **311**:1737-1740
- Kana T. M., P. M. Glibert. 1987. Effect of irradiances up to 2000 $\mu\text{E m}^{-2} \text{s}^{-1}$ on marine *Synechococcus* WH7803. 1. Growth, pigmentation, and cell composition.

Deep-Sea Research **34**:479-495

- Karl D. M., R. R. Bodigare, R. M. Letelier. 2001. Long-term changes in plankton community structure and productivity in the North Pacific Subtropical Gyre: The domain shift hypothesis. *Deep-sea Res II*. **48**:1449-1470
- Karl D. M., G. Tien. 1992. MAGIC: A sensitive and precise method for measuring dissolved phosphorus in aquatic environments. *Limnol Oceanogr* **37**:105-116
- Klausmeier C. A., E. Litchman, T. Daufresne, S. A. Levin. 2004. Optimal nitrogen-to-phosphorus stoichiometry of phytoplankton. *Nature*. **429**:171-174
- Klinker J., Z. Reiss, C. Kropach, I. Levanon, H. Harpaz, Y. Shapiro. 1977. Nutrients and biomass distribution in the Gulf of Aqaba (Elat), Red Sea. *Mar. Biol.* **45**:53-64
- Labiosa R. G. 2007 Phytoplankton bloom formation in oligotrophic regions : the interplay between ecology and physics in the Gulf of Aqaba Red Sea. Ph.D. Thesis. Stanford University.
- Labiosa R. G., K. R. Arrigo, A. Genin, S. G. Monismith, G. van Dijken. 2003. The interplay between upwelling and deep convective mixing in determining the seasonal phytoplankton dynamics in the Gulf of Aqaba: Evidence from SeaWiFS and MODIS. *Limnol Oceanogr* **48**:2355-2368
- Levanon-Spanier I., E. Padan, Z. Reiss. 1979. Primary production in a desert-enclosed sea: The Gulf of Elat (Aqaba), Red Sea. *Deep-Sea Res I* **26**:673-686
- Li W. K. W., T. Zohary, Y. Z. Yacobi, A. M. Wood. 1993. Ultraphytoplankton in the eastern Mediterranean Sea: towards deriving phytoplankton biomass from flow cytometric measurements of abundance, fluorescence, and light scatter. *Mar.*

Ecol. Prog. Ser. **102**:79-97.

Lindell D., S. Penno, M. Al-Qutob, E. David, T. Rivlin, B. Lazar, A. F. Post. 2005.

Expression of the nitrogen stress response gene *ntcA* reveals nitrogen-sufficient *Synechococcus* populations in the oligotrophic northern Red Sea. Limnol Oceanogr **50**:1932-1944

Lindell D., A. F. Post. 1995.. Ultraphytoplankton succession is triggered by deep winter mixing in the Gulf of Aqaba (Eilat), Red Sea. Limnol Oceanogr **40**:1130-1141

Litchman E., C. A. Klausmeier. 2008. Trait-based community ecology of phytoplankton. Annual Review of Ecology, Evolution and Systematics, **39**: 615-639.

MacIntyre H. L., T. M. Kana, T. Anning, R. J. Geider. 2002. Photoacclimation of photosynthesis irradiance response curves and photosynthetic pigments in microalgae and cyanobacteria. Journal of Phycology **38**: 17-38.

Mackey K. R. M., R. G. Labiosa, M. Calhoun, J. H. Street, A. Paytan. 2007. Phosphorus availability, phytoplankton community dynamics, and taxon-specific phosphorus status in the Gulf of Aqaba, Red Sea. Limnol Oceanogr **52**:875-885

Mackey K. R. M., A. Paytan, A. Grossman, S. Bailey. 2008. A photosynthetic strategy for coping in a high light, low nutrient environment. Limnol Oceanogr. **53**:900-913

Margalef R. 1978. Life-forms of phytoplankton as survival alternatives in an unstable environment. Oceanol. Acta. **1**: 493-509.

- Matear R. J., A. C. Hirst. 1999. Climate change feedback on the future oceanic CO₂ uptake. *Tellus, Ser, B*, **51**:722-733
- Mills M. M., C. Ridame, M. Davey, J. La Roche. 2004. Iron and phosphorus co-limit nitrogen fixation in the eastern tropical North Atlantic. *Nature* **429**:292-294
- Moon-van der Staay S. Y., R. DeWachter, D. Vaultot. 2001. Oceanic 18S rDNA sequences from picoplankton reveal unsuspected eukaryotic diversity. *Nature* **409**:607-610.
- Moore L. R., G. Rocap, S. W. Chisholm. 1998. Physiology and molecular phylogeny of coexisting *Prochlorococcus* ecotypes. *Nature* **393**:464-468
- Partensky F. J., W. R. Hess, D. Vaultot. 1999. *Prochlorococcus*, a marine photosynthetic prokaryote of global significance. *Microbiology and Molecular Biology Reviews* **63**:106-127
- Redfield A., B. H. Ketchum, F. A. Richards. 1963. The influence of organisms on the composition of seawater, pages 26-77 in M. N. Hill [ed.], *The sea*. V. 2. Wiley Interscience.
- Rocap G., et al. 2003. Genome divergence in two *Prochlorococcus* ecotypes reflects oceanic niche differentiation. *Nature*. 424:1042-1046
- Reiss Z., L. Hottinger. 1984. *The Gulf of Aqaba: Ecological Micropaleontology*. Springer-Verlag, Berlin.
- Sarmiento J. L., T. M. C. Hughes, R. J. Stouffer, S. Manabe. 1998. Simulated response of the ocean carbon cycle to anthropogenic climate warming. *Nature* **393**:245-249
- Sarmiento J. L., et al. 2004. Response of ocean ecosystems to climate warming.

Global Biogeochemical Cycles **18**:GB3003, doi:10.1029/2003GB002134

- Seppala J., T. Tamminen, S. Kaitala. 1999. Experimental evaluation of nutrient limitation of phytoplankton communities in the Gulf of Riga. *Journal of Marine Systems*. **23**:107-126
- Smayda T. J., C. S. Reynolds. 2001. Community assembly in marine phytoplankton: application of recent models to harmful dinoflagellate blooms. *J Plankton Res* **23**: 447-461
- Sommer U. 2000 Scarcity of medium-sized phytoplankton in the northern Red Sea explained by strong bottom-up and weak top-down control. *Mar Ecol Prog Ser* **197**: 19-25.
- Sosik H. M., S. W. Chisholm, R. J. Olsen. 1989. Chlorophyll fluorescence from single cells: Interpretation from flow cytometric signals. *Limnol Oceanogr* **34**:1749-1761.
- Stal L. J., M. Staal, M. Villbrandt. 1999. Nutrient control of cyanobacterial blooms in the Baltic Sea. *Aquat Microb Ecol* **18**:165-173
- Van Mooy B. A. S., G. Rocap, H. F. Fredricks, C. T. Evans, A. H. Devol. 2006. Sulfolipids dramatically decrease phosphorus demand by picocyanobacteria in oligotrophic marine environments. *PNAS* **103**:8607-8612
- Verity P. G., C. Y. Robertson, C. R. Tronzo, M. G. Andrews, J. R. Nelson, M. E. Sieracki. 1992. Relationship between cell volume and the carbon and nitrogen content of marine photosynthetic nanoplankton. *Limnol Oceanogr* **37**:1434-1446

- von Liebig J. 1840. Organic Chemistry in Its Application to Agriculture and Physiology. London: Mayfair.
- West N. J., D. J. Scanlan. 1999. Niche-partitioning of *Prochlorococcus* populations in a stratified water column in the eastern North Atlantic Ocean, Appl Environ Microbiol **65**:2585-2591
- Wolf-Vetch A., N. Paldor, S. Brenner. 1992. Hydrographic indications of advection/convection effects in the Gulf of Elat. Deep-Sea Res. I **39**:1393-1401
- Worden A. Z. 2006. Picoeukaryote diversity in coastal waters of the Pacific Ocean. Aquatic Microbial Ecology. **43**:165-175
- Worden A. Z., J. K. Nolan, B. Palenik. 2004. Assessing the dynamics and ecology of marine picophytoplankton: The importance of the eukaryotic component. Limnol Oceanogr **49**:168–179

Table 1: Nutrient data. Initial inorganic N (N_i) and SRP levels following nutrient additions were estimated as the sum of the mean background concentrations of N_i and SRP at day zero plus the calculated amount of N_i or SRP added from the nutrient addition treatments. Standard errors are given following the means. Changes in NO_3 and NO_2 (ΔN) and P (ΔP) concentrations between these initial levels and levels at day 4 of the LL and HL nutrient enrichment experiments are also shown. Negative values indicate consumption and positive values indicate production of nutrients throughout the experiments ($\mu\text{mol L}^{-1}$). Values are averages of triplicate samples.

Treatment	Initial nutrient levels after nutrient addition treatment		Changes in nutrient levels	
	N_i	SRP	ΔN	ΔP
HL experiment				
NH_4PO_4	7.08 ± 0.01	0.43 ± 0.01	0.07	-0.14
NO_3PO_4	7.08 ± 0.12	0.43 ± 0.01	-1.41	-0.08
NO_3	7.08 ± 0.11	0.03 ± 0.00	-0.22	0.01
NH_4	7.08 ± 0.03	0.03 ± 0.00	0.00	0.00
PO_4	0.08 ± 0.00	0.43 ± 0.00	-0.02	-0.01
Control	0.08 ± 0.00	0.03 ± 0.00	0.02	0.00
LL experiment				
NH_4PO_4	7.13 ± 0.03	0.44 ± 0.02	0.07	-0.16
NO_3PO_4	7.13 ± 0.05	0.44 ± 0.01	-1.18	-0.16
NO_3	7.13 ± 0.10	0.04 ± 0.01	0.05	-0.02
NH_4	7.13 ± 0.01	0.04 ± 0.01	0.01	-0.01
PO_4	0.13 ± 0.03	0.44 ± 0.01	-0.05	-0.07
Control	0.13 ± 0.02	0.04 ± 0.01	0.15	-0.02

Table 2: Absolute cell concentrations (cells mL⁻¹) of each picophytoplankton cell type on day 4 of the HL and LL nutrient enrichment experiments as determined by flow cytometry. The total concentration of all picophytoplankton cells is shown in the last column, and concentrations at day zero are also shown. Percentage of cells in each experimental treatment relative to time zero and control are given in parentheses.

Treatment	Picoeukaryotes (cells mL ⁻¹)	<i>Synechococcus</i> (cells mL ⁻¹)	<i>Prochlorococcus</i> (cells mL ⁻¹)	All picophytoplankton (cells mL ⁻¹)
HL experiment				
NH ₄ PO ₄	4,300 (1,433, 2,150%)	33,300 (3,700, 16,650%)	40,400 (205, 878%)	78,000 (373, 1560%)
NO ₃ PO ₄	8,700 (2,900, 4,350%)	29,600 (3,289, 14,800%)	49,800 (253, 1083%)	88,100 (422, 1762%)
PO ₄	600 (200, 300%)	8,500 (944, 4,250%)	14,500 (74, 315%)	23,600 (113, 472%)
NH ₄	700 (233, 350%)	11,800 (1,311, 5,900%)	8,200 (42, 178%)	20,700 (99, 414%)
NO ₃	300 (100, 150%)	20 (2, 10%)	9,200 (47, 200%)	9,500 (45, 190%)
Control	200 (67, 100%)	200 (22, 100%)	4,600 (23, 100%)	5,000 (24, 100%)
Day zero	300 (100, 150%)	900 (100, 450%)	19,700 (100, 428%)	20,900 (100, 418%)
LL experiment				
NH ₄ PO ₄	7,200 (514, 120%)	4,700 (29, 62%)	8,600 (64, 54%)	20,500 (66, 69%)
NO ₃ PO ₄	8,600 (614, 143%)	700 (4, 9%)	3,500 (26, 22%)	12,800 (41, 43%)
PO ₄	3,000 (214, 50%)	8,300 (52, 111%)	10,400 (78, 66%)	21,700 (70, 74%)
NO ₃	4,500 (321, 75%)	5,000 (31, 66%)	8,400 (63, 53%)	17,900 (58, 61%)
NH ₄	2,400 (171, 40%)	5,900 (37, 79%)	5,600 (42, 35%)	13,900 (45, 47%)
Control	6,000 (429, 100%)	7,500 (47, 100%)	15,900 (119, 100%)	29,400 (95, 100%)
Day zero	1,400 (100, 23%)	16,100 (100, 213%)	13,400 (100, 84%)	30,900 (100, 105%)

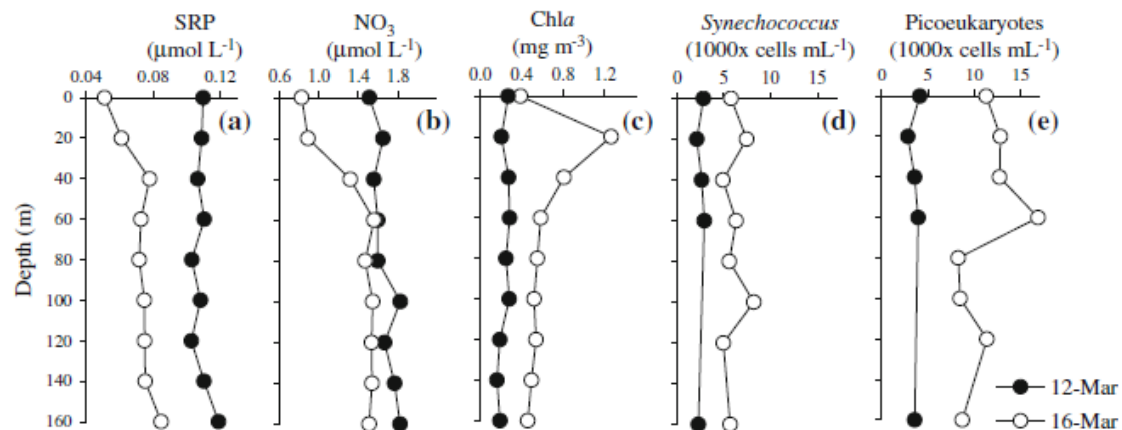


Figure 1: Depth profiles of (a) SRP; (b) NO_3 ; (c) Chl *a*; (d) *Synechococcus* cell concentration; and (e) picoeukaryote cell concentration for the mixed (closed circles) and stratified (open circles) water columns.

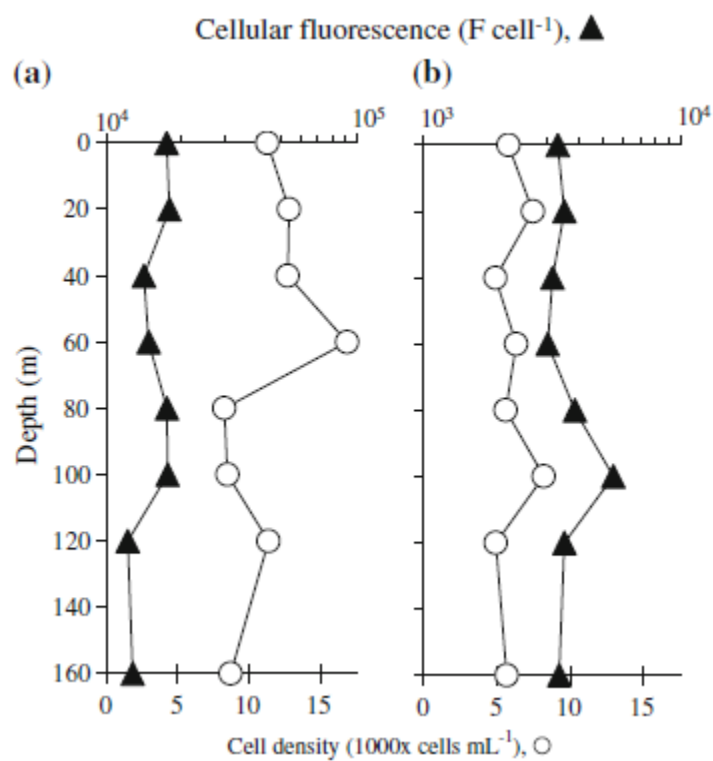


Figure 2: Cellular fluorescence (and corresponding cell densities) for (a) picoeukaryotes, and (b) *Synechococcus* on March 16.

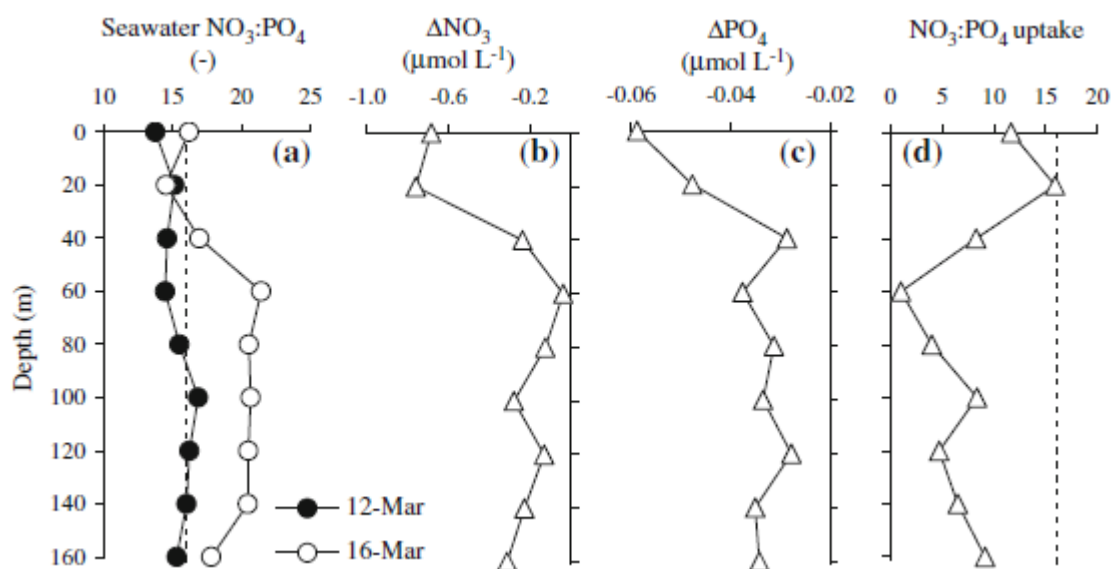


Figure 3: Depth profiles of (a) seawater $\text{NO}_3:\text{PO}_4$ ratios for the mixed (closed circles) and stratified (open circles) water columns; and the changes in (b) NO_3 concentration; (c) PO_4 concentration; and (d) $\text{NO}_3:\text{PO}_4$ uptake ratios during the transition from mixing to stratification.

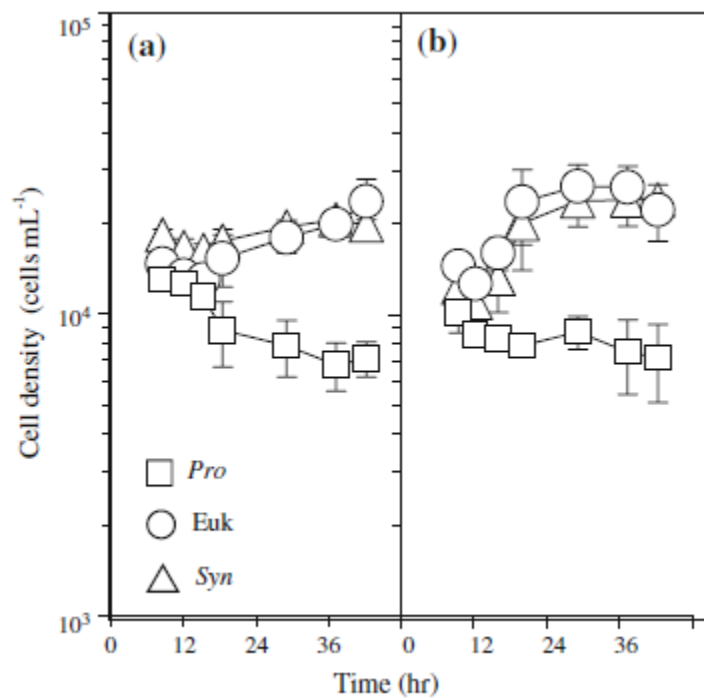


Figure 4: Cell concentration time series for the (a) high light treatment and (b) low light treatment in the simulated stratification experiment. Error bars represent SE of the mean of triplicate measurements and are contained within the symbol when not visible.

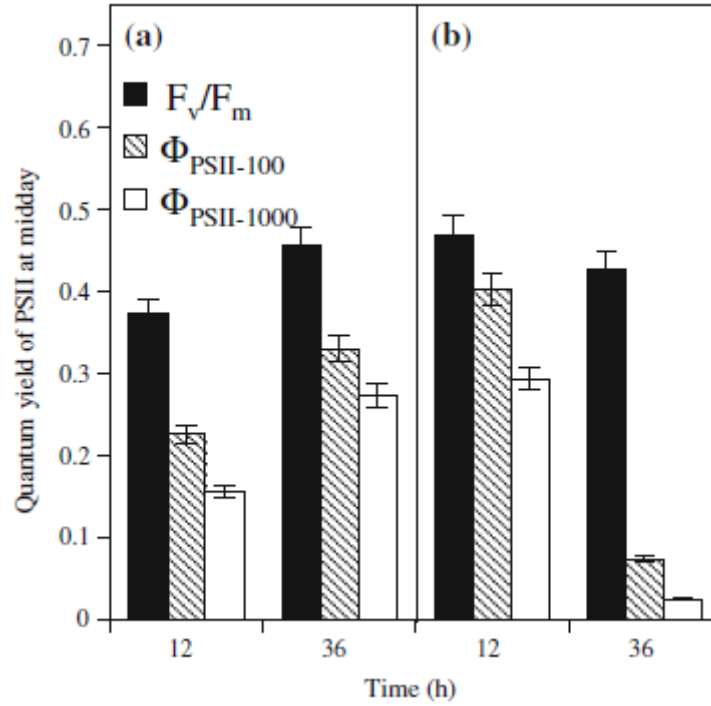


Figure 5: Photochemical efficiency of PSII at midday in the (a) high light treatment and (b) low light treatment in the simulated stratification experiment. Samples were taken at noon on the first and second day of the experiment (hours 12 and 36 respectively). The parameter $\Phi_{PSII-100}$ is the photochemical efficiency of PSII during $100 \mu\text{mol quanta m}^{-2} \text{s}^{-1}$ actinic light, and $\Phi_{PSII-1000}$ is the photochemical efficiency of PSII during $1000 \mu\text{mol quanta m}^{-2} \text{s}^{-1}$ actinic light. Error bars represent SE of the mean of triplicate measurements.

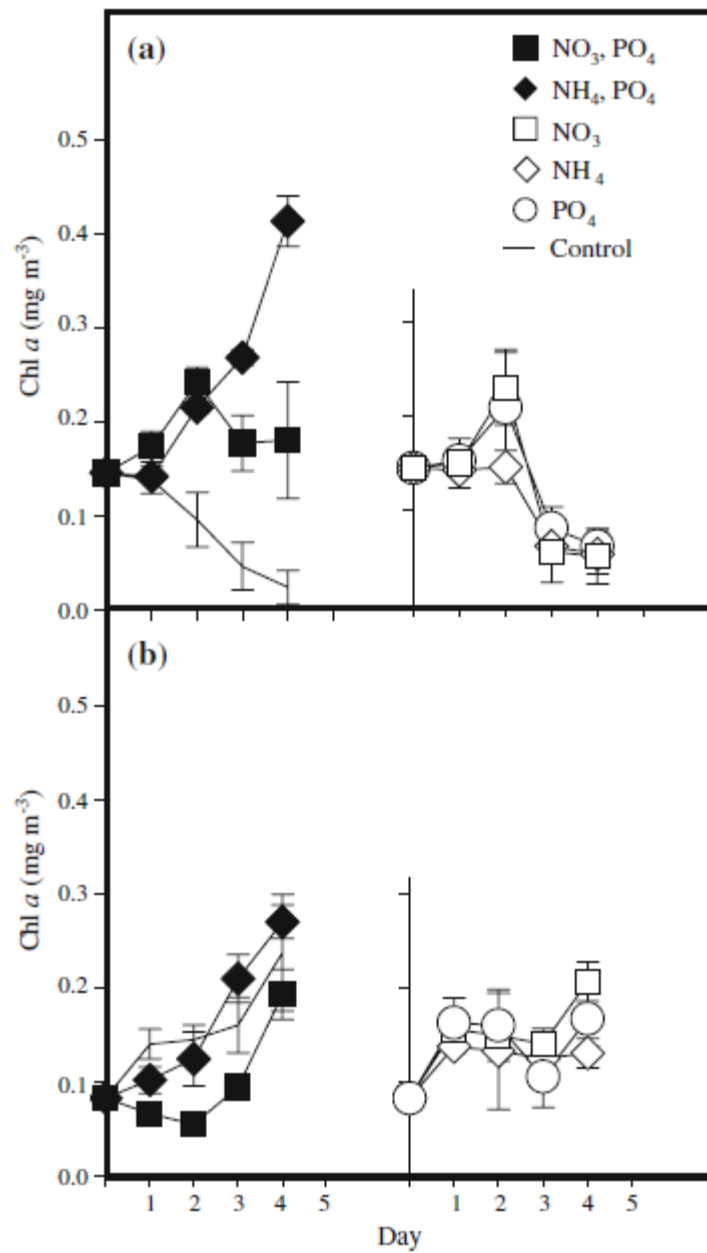


Figure 6: Chlorophyll *a* concentrations for the (a) high light and (b) low light nutrient enrichment experiments. Error bars represent SE of the mean of triplicate measurements.

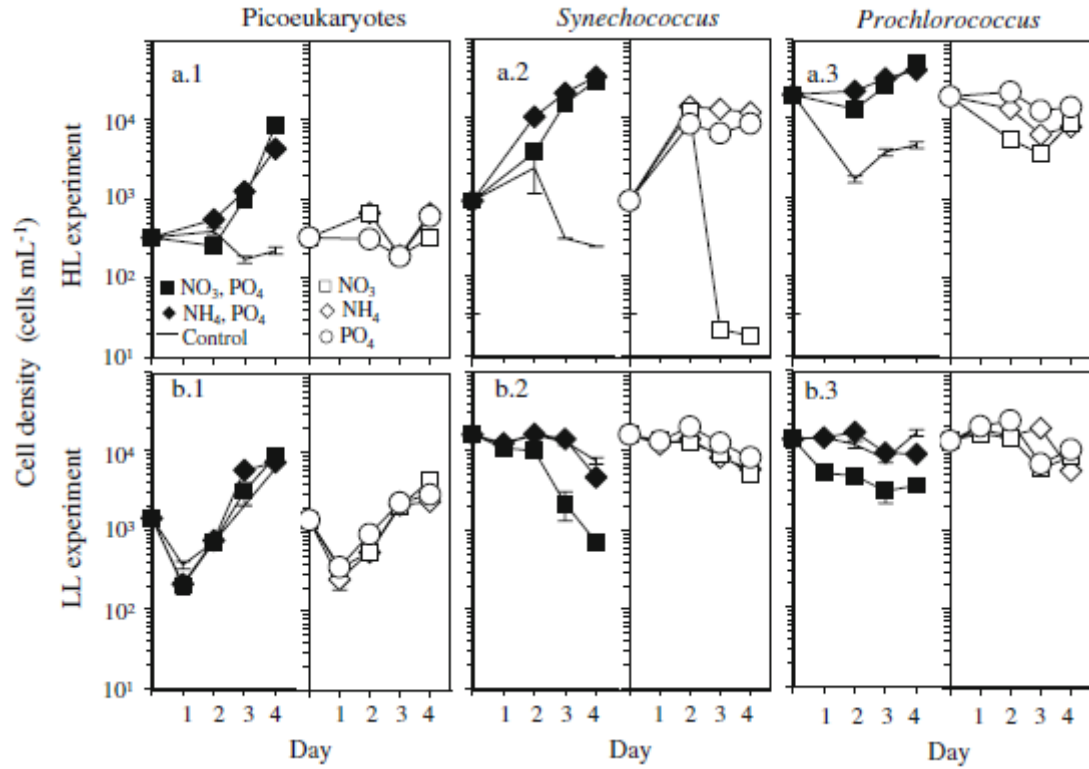


Figure 7: Cell concentration time series for the (a) high light and (b) low light nutrient enrichment experiments for (.1) picoeukaryotes; (.2) *Synechococcus*; and (.3) *Prochlorococcus*. The coefficient of variation for triplicate samples was below 0.15; error bars (SE) are contained within symbols where not visible.

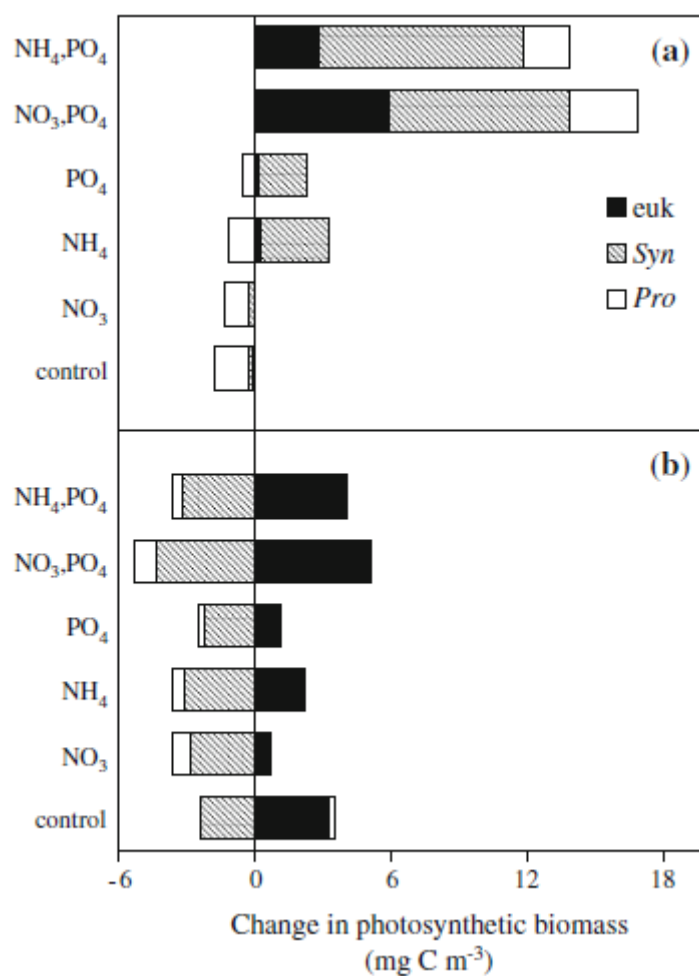


Figure 8: Estimates of picophytoplankton photosynthetic biomass on the final day of the (a) high light and (b) low light nutrient enrichment experiments contributed by picoeukaryotes (black bars), *Synechococcus* (hatched bars), and *Prochlorococcus* (white bars).

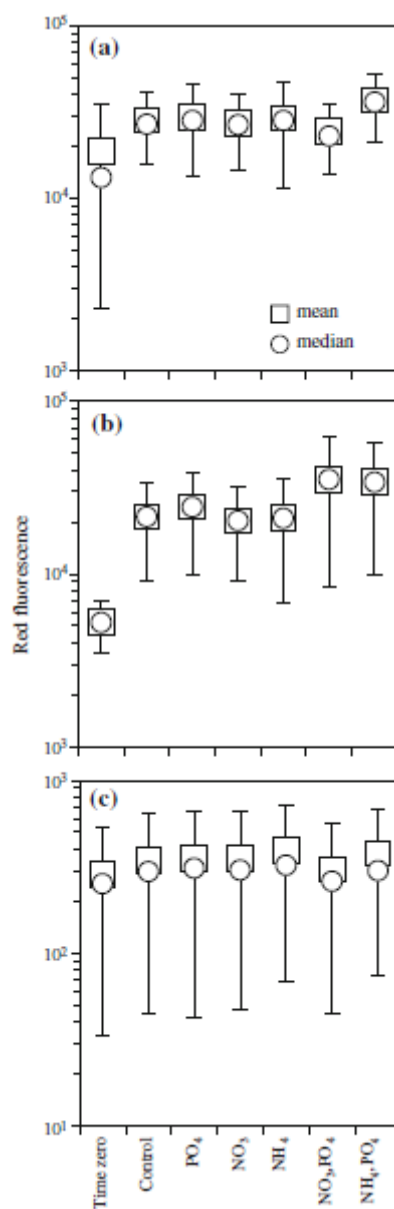


Figure 9: Cellular fluorescence during the LL nutrient enrichment experiment for (a) picoeukaryotes, (b) *Synechococcus*, and (c) *Prochlorococcus*. Plots show fluorescence per cell on day 0 for the initial populations, and on day 4 for each treatment and the control. Error bars show the standard deviations of the cellular fluorescence distributions.

CHAPTER 6

A PHOTOSYNTHETIC STRATEGY FOR COPING IN A HIGH LIGHT, LOW NUTRIENT ENVIRONMENT

ABSTRACT

Phytoplankton in high light, low nutrient ocean environments are challenged with maintaining high photosynthetic efficiency while simultaneously preventing photodamage that results from low levels of electron acceptors downstream of photosystem (PS) II. Here we identify a process in open ocean picophytoplankton that preserves PSII activity by diverting electrons from PSI-mediated carbon assimilation to oxygen via a propyl gallate-sensitive oxidase associated with the photosynthetic electron transport chain. This process stabilizes diel photochemical efficiency of PSII (Φ_{PSII}), despite midday photoinhibition, by maintaining oxidized PSII reaction centers. While measurements of maximum photochemical efficiency of PSII (F_v/F_m) show midday photoinhibition, there is no midday depression in CO_2 -fixation. Moreover, CO_2 -fixation saturates at low irradiances even though PSII electron flow is not saturated at irradiances of $1985 \mu\text{mol photon m}^{-2} \text{ s}^{-1}$. This disparity between PSII fluorescence and CO_2 -fixation is consistent with the activity of an oxidase that serves as a terminal electron acceptor, maintaining oxidized PSII reaction centers even when CO_2 -fixation has saturated and the total number of functional reaction centers decreases due to photoinhibition (reflected in lower midday F_v/F_m values). This phenomenon is less apparent in coastal phytoplankton populations, suggesting that it is a strategy particularly distinctive of phytoplankton in the oligotrophic ocean. Spatial

variability in features of photosynthetic electron flow could explain biogeographical differences in productivity throughout the ocean, and should be represented in models that use empirical photosynthesis and chlorophyll fluorescence measurements from a limited number of ocean sites to estimate the productivity of the entire ocean.

INTRODUCTION

The open ocean presents numerous challenges to photosynthetic organisms. Physiological stresses imposed by a rapidly fluctuating light environment are exacerbated by oligotrophic nutrient conditions that limit the availability of iron, a nutrient required for maintenance and repair of the photosynthetic apparatus, and macronutrients such as nitrogen and phosphorus that are required for cell growth. Despite these challenges, picophytoplankton are remarkably well adapted to life in the open ocean. Recent estimates suggest that the dominant picocyanobacteria genera, *Prochlorococcus* and *Synechococcus*, are responsible for up to two-thirds of primary production in the oceans, or nearly one-third of the total primary production on Earth (Field et al. 1998; Scanlan 2003). Picophytoplankton also comprise eukaryotes such as the Prasinophytes *Ostreococcus* and *Micromonas*. These organisms are primarily located in coastal areas where they can contribute up to 75% of the total CO₂-fixation (Fouilland et al. 2004; Worden, 2004). However, they are also present in the oligotrophic oceans where they have successfully colonized the deep euphotic zone (Campbell and Vaultot, 1993; Díez et al. 2001).

Iron is required for the synthesis of certain components of the photosynthetic apparatus. In eukaryotic phototrophs, the photosystem (PS) II complex incorporates 4 iron atoms, whereas the comparatively iron-rich downstream electron acceptors cytochrome *b₆f* (cyt *b₆f*) and PSI require 6 and 12 iron atoms, respectively (Fig. 1A). The low amount of PSI relative to PSII in open ocean ecotypes of cyanobacteria (Bailey et al. 2007), green algae (P. Cardol, G. Finazzi, and F. A. Wolman personal communication), and diatoms (Strzepek and Harrison 2004) suggests that these

organisms are evolutionarily adapted to coping with the limitations imposed by low iron availability. In the open ocean, photosynthetic CO₂-fixation saturates at relatively low irradiances (100-300 $\mu\text{mol quanta m}^{-2} \text{ s}^{-1}$) compared to the maximum surface irradiance ($\sim 2000 \mu\text{mol quanta m}^{-2} \text{ s}^{-1}$) (Partensky et al. 1993; Li 1994; Partensky et al. 1999 and references therein). This is due in part to limitation of the maximum rate at which carbon can be incorporated into cellular biomass resulting from low nutrient availability and low rates of photosynthesis, possibly as a consequence of low levels of PSI (Strzepek and Harrison 2004; Bailey et al. 2007; P. Cardol, G. Finazzi, and F. A. Wolman personal communication). Low levels of electron acceptors downstream of PSII (e.g., scarcity of iron-rich PSI and cyt *b₆f* complexes) would ultimately restrict the flow of electrons away from PSII during light exposure (Fig. 1A). As a result of this impediment to efficient photochemical dissipation of PSII excitation energy, functional PSII reaction centers (i.e., those able to contribute to photochemistry (Fig. 1B)) are more likely to remain reduced, which can lead to PSII photodamage (Adir et al. 2003). Phytoplankton residing in high light, low iron environments are therefore challenged with maintaining high photosynthetic efficiency while at the same time preventing photodamage stemming from low levels of electron acceptors downstream of PSII.

The development of mechanisms for maintaining oxidized PSII reaction centers and a high ΔpH across the thylakoid membranes would help prevent hyper-reduction of the electron carriers of the photosynthetic apparatus when PSI activity limits PSII electron flow, thereby decreasing the potential for photodamage, and also providing energy for cell maintenance and growth. A strategy that increases PSI light

harvesting efficiency through increased synthesis of the PSI antenna (IsiA) is used by some cyanobacteria (Boekema et al. 2001; Cadoret et al. 2004), although Ivanov and coworkers (2006, 2007) suggest that under Fe-stress IsiA does not increase the absorption cross-section of PSI but may act as a quencher of excitation energy. Analysis of the genome sequence indicates that the marine *Synechococcus* WH8102 surface strain lacks the *isiA* gene, i.e. the PSI antenna polypeptide induced under iron starvation (Palenik et al. 2003; <http://bacteria.kazusa.or.jp/cyano/>). Therefore, other strategies to cope with low levels of PSI under the high light and low nutrient conditions of the open ocean must exist.

In the classical z-scheme for photosynthetic electron flow, electrons passing through PSII are transported to PSI where a second excitation results in the reduction of CO₂ (Fig. 1A). However, reduction of molecular oxygen can also occur at various points downstream of PSII. In the well characterized Mehler reaction, oxygen is reduced at the acceptor side of PSI (Mehler 1951; Mehler and Brown 1952; Asada et al. 1974). Moreover, electrons from the photosynthetic electron transport chain can be diverted to the respiratory pathway leading to cytochrome oxidase (Hart et al. 2005; Fig. 1A). A third pathway that, until recently, has not been explored as extensively involves the plastoquinol terminal oxidase (PTOX) (Peltier and Cournac, 2002; Josse et al. 2003; Hart et al. 2005), which uses electrons from the plastoquinone (PQ) pool to reduce oxygen and regenerate H₂O. The PTOX pseudo-cycle would alleviate PSII excitation pressure by passing electrons to oxygen, while at the same time bypassing the iron-rich cyt *b₆f* and PSI complexes of the photosynthetic apparatus (Fig. 1A). Thus, extracting electrons from the intersystem electron transport chain by specific

oxidases may represent a clear advantage for open ocean organisms that contend with very low levels of iron and nutrients.

Two recent laboratory-based studies provide evidence that a PTOX-like oxidase appears to prevent closure of PSII reaction centers at high light intensities in photosynthetic marine prokaryotes (Bailey et al. 2007) and picoeukaryotes (P. Cardol, G. Finazzi, and F. A. Wolman personal communication). Bailey and co-workers found that *Synechococcus* WH8102 (a photosynthetic picocyanobacterium from oligotrophic surface waters) appeared to have a low PSI to PSII ratio, indicative of constitutive low-iron adaptation. Furthermore, while CO₂-fixation saturated at low irradiance ($\sim 150 \mu\text{mol photon m}^{-2} \text{ s}^{-1}$) in this strain, PSII reaction centers remained open even at very high intensity illumination ($\sim 2000 \mu\text{mol photon m}^{-2} \text{ s}^{-1}$), suggesting a flow of electrons to acceptors other than CO₂. This alternative electron transport out of PSII was abolished under anoxic conditions and in the presence of the oxidase inhibitor propyl gallate (pgal), suggesting that PSII excitation pressure is relieved via the reduction of oxygen by a pgal-sensitive oxidase, possibly PTOX (inhibitors of alternative quinol oxidases (Berry et al. 2002) had no effect). Similarly, the oligotrophic ocean picoeukaryote strain *Ostreococcus* RCC809 has low levels of PSI and cyt *b₆f* relative to PSII, and PSII photochemistry is pgal-sensitive (P. Cardol, G. Finazzi, and F. A. Wolman personal communication). However, the coastal *Ostreococcus* OTH95 isolate did not exhibit pgal-sensitivity and showed unremarkable PSI and cyt *b₆f* levels relative to PSII, suggesting that the photoprotective reduction of oxygen is a strategy distinctive of phytoplankton in the oligotrophic ocean where iron is scarce.

Gene sequences for PTOX are widespread among strains of cyanobacteria closely related to the high-light adapted *Prochlorococcus marinus* MED4, as well as *Synechococcus* in the oligotrophic Sargasso Sea (McDonald and Vanlerberghe 2004). To determine if photoprotective strategies similar to those described above exist in natural assemblages of picophytoplankton in situ, we have explored the redox state of PSII over the diel cycle in environmental samples, its relationship to CO₂-fixation, and factors involved in PSII photochemistry in the oligotrophic waters of the open ocean. Chlorophyll fluorescence measurements were taken from surface waters in the Pacific and Atlantic oceans to assess diel variability in the maximum photochemical efficiency of PSII (F_v/F_m) and in the operating photochemical efficiencies of PSII under actinic irradiance (Φ_{PSII}) throughout the day. The photoprotective role of molecular oxygen reduction was investigated for open ocean phytoplankton from the surface and deep euphotic zone, as well as from coastal locations in the Atlantic and Pacific oceans.

MATERIALS AND METHODS

Site descriptions

Samples from the Pacific Ocean were collected onboard the research vessel R/V Kilo Moana from locations north of Hawaii within the North Pacific Subtropical Gyre (NPSG) at Station ALOHA (22°45'N, 158°W; (Fig. 2A)) from 07-11 November, 2006 on Hawaiian Ocean Time-series (HOT) cruise no. 187 (http://hahana.soest.hawaii.edu/hot/hot_jgofs.html). Hawaiian coast samples were collected from the southeastern coast of Oahu, south of Waikiki Beach, on 05

November, 2006 (Fig. 2A). Samples from the Atlantic Ocean were collected onboard the research vessel R/V Atlantic Explorer south of Bermuda in the Sargasso Sea in and around the Bermuda Atlantic Time-series Study (BATS; Fig. 2B) Station (approximately 32°N, 64°W) from 21-25 November, 2006 on cruise X0619 (<http://www.bios.edu/cintoo/bats/bats.html>). Bermuda coast samples were collected from Ferry Reach (Fig. 2B), the body of water separating St. David's Island and St. George's Island, at the dockside laboratory facility at the Bermuda Institute of Ocean Sciences (BIOS) from November 26-27, 2006.

Flow cytometry

Aliquots of seawater were removed throughout the sampling periods for flow cytometry, and were fixed with glutaraldehyde (Sigma) at a final concentration of 0.1%. All flow cytometry samples were stored and shipped at -80°C, except that the Pacific open ocean samples were stored briefly at -20°C during transport (roughly 6 h). Pacific coastal samples were not collected. Samples were analyzed on a FACSAria flow cytometer, and data analysis was performed using FlowJo software (TreeStar, Inc.) Absolute cell densities for picophytoplankton populations (cells < 2µm in diameter, including *Prochlorococcus*, *Synechococcus*, and picoeukaryotes) were determined by spiking samples with a known volume and concentration of 1 µm fluorescent yellow-green beads (Polysciences). *Prochlorococcus*, *Synechococcus*, and picoeukaryotes were identified based on size (determined by right angle light scatter) and autofluorescence characteristics as described by Mackey et al. (2007). The

coefficient of variation for phytoplankton cell densities determined from triplicate samples was below 0.10 for all samples.

Chlorophyll fluorescence parameters and terminology

Energy absorbed but not used in photochemistry can either undergo non-photochemical quenching (i.e., dissipation as heat; movement of the photosynthetic antennae from PSII to PSI in a state transitions, or PSII photodamage), or fluorescence (re-emission of energy as light). Fluorescence analysis utilizes this energy balance to provide information about the efficiency of photochemistry based on changes in PSII fluorescence under a range of different light treatments. In this study, the values of F_m , F_o , F_m' , F_o' , and F_s were extracted from fluorescence traces (Fig. 3), and all fluorescence parameters were calculated using standard equations (Campbell et al. 1998; Maxwell and Johnson, 2000) (Table 1). F_v/F_m reflects the maximum photochemical efficiency of PSII in the dark adapted state while Φ_{PSII} represents the actual photochemical efficiency of PSII following actinic irradiances of different light intensities. In contrast, the fraction of oxidized PSII reaction centers (qP) at specific light intensities (we used $1985 \mu\text{mol quanta m}^{-2} \text{s}^{-1}$ to simulate natural midday irradiances) reflects the ability of the phytoplankton to cope with changing levels of light throughout the day.

Fig. 1B gives the terminology used to classify PSII reaction centers in this study. In the initial steps of photosynthetic electron transport, energy is used to drive photochemical charge separation in which electrons are generated from the splitting water at the level of PSII. These electrons are transferred from P680, the reaction

center chlorophyll of PSII, to the first stable PSII electron acceptor, Q_A . As long as Q_A is able to contribute to photochemistry, the PSII reaction center is considered functional. The fraction of the functional reaction centers that are in the reduced state at any given time will depend in part on the ambient light intensity (which determines the rate at which electrons are donated to Q_A), and the availability of competent electron acceptors downstream of PSII (which determine the rate at which electrons are accepted from Q_A) (Long et al. 1994). High light intensities and/or a limited availability of downstream electron acceptors will limit how efficiently Q_A is able to become re-oxidized, causing a higher fraction of Q_A to remain in the reduced state, and therefore temporarily unable to accept electrons generated from the splitting of water. PSII reaction centers with reduced Q_A are considered to be “closed” to photochemistry; however, they are still considered functional because they can contribute to photochemistry immediately upon becoming re-oxidized.

If energy from absorbed light is unable to be dissipated efficiently through photochemistry, as could be the case if a large fraction of PSII reaction centers were closed, the excess light energy can contribute to photoinhibition through damage to the D1 polypeptide that binds the P680, Q_A , and other cofactors involved in charge separation (Long et al. 1994). Photodamage renders PSII non-functional (i.e., unable to undergo photochemistry) until D1 repair is accomplished, typically on the order of hours. Photoacclimation via regulation of non-damaged, non-reducing centers also contributes to photoinhibition (Lavergne, 1982; Guenther and Melis, 1990; Oquist et al. 1992b), but these centers do not necessarily require repair in order to regain function. We note that a photoinhibited reaction center does not refer to the oxidation

state of the reaction center but denotes a center unable to perform photochemistry. Photodamage and the presence of non-damaged, non-reducing centers causes a decrease in the overall number of functional reaction centers thereby contributing to a decrease in the maximum photochemical efficiency of PSII (F_v/F_m), which is by definition photoinhibition (Maxwell and Johnson, 2000). Thus, an increase in photoinhibition is evidenced by a decrease in the extent of the F_v/F_m chlorophyll fluorescence parameter, and changes in the latter are commonly used to assess photoinhibition in vivo.

Note that while Φ_{PSII} and qP both pertain to PSII photochemistry, qP incorporates information about steady state chlorophyll fluorescence levels during (F_s) and after (F_o') exposure to actinic light. Throughout the day, the extent to which these steady state fluorescence levels (F_s and F_o') change with respect to each other, and with respect to maximum fluorescence (F_m'), reveals the degree of saturation of PSII photochemistry by light. It is this degree of saturation that reveals the fraction of oxidized PSII reaction centers that the photosynthetic apparatus maintains during exposure to a given actinic irradiance, which is by definition qP. By contrast, Φ_{PSII} does not incorporate steady state fluorescence following exposure to actinic light (F_o'), and as such it reflects the proportion of absorbed light energy that is used in PSII photochemistry. So, while Φ_{PSII} gives information about the efficiency with which PSII is able to use absorbed energy, qP gives information about how the degree of saturation (i.e., the fraction of centers that are oxidized) has altered this efficiency. However, the degree of saturation is only one factor influencing the photochemical efficiency of PSII, and as such qP and Φ_{PSII} will not necessarily co-vary if the effects

of other processes affecting PSII photochemistry, such as changes in the functionality of PSII reaction centers or the regulation of oxidase activity, are significant.

Chlorophyll fluorescence measurements

Chlorophyll fluorescence measurements were taken from natural phytoplankton assemblages in the Pacific and Atlantic oceans. Samples were pre-concentrated in the dark at low pressure onto GF/F filters (Whatman) following in-line size fractionation with 20 μ m mesh. Approximately 2-4 L of seawater were collected onto each filter in the dark over a roughly 30 min interval. At sea, the in-line filtration assembly was connected to the ships' clean underway flow-through systems, which pumped surface water from 2-5 m depth. Samples from the deep chlorophyll maximum (DCM) were collected using a sampling CTD-Rosette (SeaBird) equipped with 12 L Niskin bottles. The depth of the DCM was estimated from real time fluorescence measurements taken during deployment of the rosette. Water was collected from 100 m and 110 m in the Atlantic and Pacific open ocean sites, respectively, and was then transferred to large (20 L), opaque polyethylene cubitainers that had been previously rinsed with sample water. These samples were collected at morning (~08:00 h), midday (~13:00 h), and midnight, and were concentrated onto GF/F filters using a low pressure peristaltic pump. Samples from the Bermuda coast were collected by connecting the in-line filtration assembly to a clean flow-through system at the BIOS dockside laboratory facility that drew surface water from the adjacent inlet. Samples from the Hawaiian coast were collected in the surf zone from 0.5 m depth, and were filtered under low pressure using a Mityvac II hand pump

(Nalgene) following size fractionation as described above. In all locations, samples were kept in the dark during the entire filtration process, including when the filters were placed into the fluorometer chamber.

Chlorophyll fluorescence measurements were made using a WATER-PAM fluorometer and WinControl software (Heinz Walz GmbH). Sample filters were collected into glass cuvettes with approximately 3 mL of concurrently-collected sample seawater and placed directly into the darkened sample chamber. For the diel measurements at the Atlantic open ocean and coastal sites and the Pacific open ocean site, an automated program was run to determine all chlorophyll fluorescence parameters. High frequency diel measurements of chlorophyll fluorescence were not taken at the Pacific coastal site. Actinic irradiance of $1985 \mu\text{mol quanta m}^{-2} \text{ s}^{-1}$ was applied for a 5 min duration for all diel samples. We note that the actinic light intensity used in the fluorescence traces was likely much higher than the light level to which cells from the DCM were acclimated. Oxygen deprivation experiments were performed as above with the following modifications. Each filter was placed in 3 mL seawater within a foil-wrapped cuvette to eliminate exposure to light, and bubbling for 30 min with nitrogen gas was used to purge oxygen from the sample. (Note that because in seawater photoautotrophs obtain CO_2 in the form of aqueous bicarbonate, this process does not deprive cells of CO_2 for photosynthesis.) The cuvette was then placed within the darkened fluorometer chamber for 20 min to allow respiration to draw down any residual oxygen and regenerate some additional CO_2 in solution prior to initiating the automated program. For measurements of relative electron transport in the Pacific open ocean and coastal sites, an automated program was run in which

the actinic irradiances were incrementally increased from 85 to 1985 $\mu\text{mol quanta m}^{-2} \text{ s}^{-1}$ for 5 min at each irradiance, followed by a saturating pulse and 3 min in the dark. The relative electron transport rate was estimated as the product of light intensity and Φ_{PSII} . Note that electron transport rate is considered “relative” because no corrections have been made to account for the partitioning of absorbed light energy between the two photosystems in these calculations. When used, propyl gallate (pgal) was administered at a final concentration of 1 mmol L^{-1} followed by 5 min dark incubation prior to collecting the fluorescence trace.

Photosynthesis-irradiance (PI) relationships

PI relationships were derived from the autotrophic incorporation of radio labeled bicarbonate ($\text{H}^{14}\text{CO}_3^-$) into biomass at morning (~08:00 h) and midday (~13:00 h) for phytoplankton from surface and DCM waters at the Atlantic open ocean site. For each depth and time, twenty-four 20 mL aliquots of seawater were spiked with $\text{H}^{14}\text{CO}_3^-$ solution and incubated for one hour within a temperature-controlled (24°C) photosynthetron (CHPT Manufacturing, Inc.) that provided distinct irradiances of up to $\sim 750 \mu\text{mol quanta m}^{-2} \text{ s}^{-1}$ for each aliquot (Lewis and Smith, 1983). Three randomly selected vials were sub-sampled immediately prior to incubation for total activity measurements. Following incubation, the aliquots were filtered onto glass fiber filters, acidified with hydrochloric acid, and sealed within acid washed vials. Within several days, filters were dried, resuspended in scintillation cocktail, and assessed for ^{14}C incorporation. Photosynthesis rates were normalized to corresponding chlorophyll *a* (Chl *a*) concentrations (data courtesy M. Lomas), and the

PI data was fitted to the following equation of Platt et al. (1980) using curve-fitting software in SigmaPlot (Version 10.0, Jandel Scientific).

$$P = P_s \left[1 - \exp\left(\frac{-\alpha}{P_s} E\right) \right] \exp\left(\frac{-\beta}{P_s} E\right) \quad (1)$$

Equation parameters determined by the program include: α , the initial slope of the best-fit curve; β , the parameter used to express reduction in photosynthetic rates at high irradiances; and P_s , which is an estimate of what the sample's light saturated photosynthetic rate would be if $\beta=0$. The light saturated rate of photosynthesis (P_m) and the saturation irradiance (E_k) were calculated from the following relationships (Platt et al. 1980):

$$P_m = P_s \left(\frac{\alpha}{\alpha + \beta} \right) \left(\frac{\beta}{\alpha + \beta} \right)^{\beta/\alpha} \quad (2)$$

$$E_k = \frac{P_m}{\alpha} \quad (3)$$

RESULTS

Flow cytometry

Prochlorococcus was the dominant organism in Atlantic and Pacific open ocean surface waters at the time of our sampling (Fig. 4A,B). In the Atlantic open ocean, *Prochlorococcus* remained the dominant organism throughout the euphotic zone, whereas a substantial population of picoeukaryotes was encountered near the DCM in the Pacific open ocean. By contrast, *Synechococcus* was the dominant

organism in the coastal Atlantic site, although measurable quantities of *Prochlorococcus* and picoeukaryotes were also present (Fig. 4C).

Diel chlorophyll fluorescence measurements

F_v/F_m , which is dependent upon the total number and configuration of functional PSII reaction centers (Butler 1978), shows distinct diurnal variability with a midday minimum (indicative of the occurrence of photoinhibition) and rapid recovery throughout the afternoon and evening in open ocean samples (Fig. 5A,B). The midday F_v/F_m minimum in the oceanic Atlantic and Pacific suggests a decrease in the total number of functional PSII reaction centers contributing to photochemistry. In contrast, the actual photochemical efficiency in the light (Φ_{PSII}), which indicates the portion of PSII excitation energy going to photochemistry (photosynthetic electrons used for either CO₂-fixation or the reduction of other electron acceptors), does not show a large midday depression. Hence the actual PSII photochemical efficiency remains relatively constant throughout the day despite photoinhibition. Analysis of open ocean photochemical quenching (qP) indicates that a large fraction of PSII reaction centers remain oxidized at midday when photoinhibition is greatest (Fig. 5D,E), showing that when the fewest functional reaction centers are present, the highest fraction of them remain oxidized.

By contrast, in a near shore site along the Bermuda coast, photoinhibition is less pronounced at midday (Fig. 5C), but similar to the oligotrophic open ocean sites, the efficiency of PSII photochemistry in the light, Φ_{PSII} , remains relatively constant over a diel period, with a slight decrease occurring in the evening. The decreased

level of photoinhibition in this near-shore site does not show a concurrent, pronounced midday increase in qP, the fraction of oxidized reaction centers (Fig. 5F).

As observed for the diel patterns of F_v/F_m and qP discussed above, fluorescence analysis of surface populations over a range of increasing actinic light intensities reveals that a higher proportion of PSII reaction centers remain open in the midday than in the midnight samples at any of the light intensities tested (Fig. 6). This midday rise in qP occurs in conjunction with a decrease in maximum photochemical efficiency of PSII ($F_v/F_m = 0.249$ at midday, 0.523 at midnight). A similar midday decrease in F_v/F_m relative to night ($F_v/F_m = 0.448$ at midday, 0.700 at midnight) is also observed for the DCM samples. Thus, occurrence of some photoinhibition throughout the day, as reflected by the F_v/F_m measurements, appears to be the inevitable consequence of light exposure in both populations, despite the extreme differences in ambient light intensity (Barber and Anderson, 1992; Oquist et al. 1992a; Behrenfeld et al. 2006). The fraction of oxidized PSII centers in both surface and DCM samples, at any of the light intensities tested, is higher at midday, i.e. when the number of functional PSII centers is at its lowest. This suggests that natural samples from both the surface and the deep waters of oligotrophic oceans have conserved the capacity to maintain open PSII reaction centers at midday despite photoinhibition. However, the extent of this phenomenon is reduced in populations from the DCM, where the absolute fraction of oxidized reaction centers remains low at midday when compared to surface samples. Midday qP in DCM samples was largely insensitive to the inhibitory effect of oxygen removal (not shown), suggesting that other photoprotective mechanisms may also contribute to PSII reaction center oxidation in these cells.

In addition to the trends described above, diurnal F_o quenching was observed in samples at midday, and F_m' levels following termination of actinic light were generally lower than F_m levels, particularly at midday. Lack of total F_m' recovery could be due to (1) inactivation of PSII during the actinic light treatment, (2) induction of a state transition that did not return to the initial dark adapted state prior to illumination, or (3) inability of the pH gradient across the thylakoid membrane to relax completely during the dark relaxation period we measured (~8 min). While identification of the mechanism for these observations is outside the scope of this text, it is possible that diurnal changes in the state 1: state 2 ratio may occur (Schreiber et al. 1995), and could represent another adaptation to a low Fe environment. Moreover, other processes affecting the redox state of the plastoquinone pool (Mi et al. 1994; Mi et al. 1995) may play an important role in determining the levels of F_o and F_m' throughout the day. More work is needed to clarify the primary source of this trend.

PI curves

Photosynthesis-irradiance parameters were determined for phytoplankton from the Atlantic surface ocean and the DCM at morning and midday (Fig. 7; Table 2). In surface samples, the light saturated photosynthetic rate, P_m , was $8.4 \text{ g C (g Chl } a)^{-1} \text{ h}^{-1}$ in the morning and $7.1 \text{ g C (g Chl } a)^{-1} \text{ h}^{-1}$ at midday. Values of α were similar (0.06336 and $0.05416 \text{ g C (g Chl } a)^{-1} \text{ h}^{-1} (\mu\text{mol quanta m}^{-2} \text{ s}^{-1})^{-1}$); however, values of β (which describes decreases in photosynthetic rates at high irradiances) differed considerably. In the morning, the value of β was $0.000306 \text{ g C (g Chl } a)^{-1} \text{ h}^{-1} (\mu\text{mol quanta m}^{-2} \text{ s}^{-1})^{-1}$, whereas cells that were exposed to approximately 5 hours of natural,

unattenuated sunlight prior to collection at midday when solar irradiance was greatest had a β value equivalent to zero. Despite these differences, morning and midday surface samples had similar E_k values of 131 and 132 $\mu\text{mol quanta m}^{-2} \text{s}^{-1}$ respectively, showing that the irradiance at which the rate of photosynthesis saturated remained similar between morning and midday.

Photosynthetic parameters derived from PI curve data from the DCM differed from surface samples, with lower light saturated photosynthetic rate (P_m) values of 1.3 g C (g Chl *a*)⁻¹ h⁻¹ and 1.6 g C (g Chl *a*)⁻¹ h⁻¹ for morning and midday samples respectively. Values of α from the DCM at morning (0.07496 g C (g Chl *a*)⁻¹ h⁻¹ ($\mu\text{mol quanta m}^{-2} \text{s}^{-1}$)⁻¹) were nearly twice as high as at midday (0.04459 g C (g Chl *a*)⁻¹ h⁻¹ ($\mu\text{mol quanta m}^{-2} \text{s}^{-1}$)⁻¹). In contrast, values of β from the DCM at morning (0.00163 g C (g Chl *a*)⁻¹ h⁻¹ ($\mu\text{mol quanta m}^{-2} \text{s}^{-1}$)⁻¹) were roughly half as great as at midday (0.00384 g C (g Chl *a*)⁻¹ h⁻¹ ($\mu\text{mol quanta m}^{-2} \text{s}^{-1}$)⁻¹). Values of E_k for DCM samples were an order of magnitude lower than in surface samples, and were half as high at morning (18 $\mu\text{mol quanta m}^{-2} \text{s}^{-1}$) than at midday (35 $\mu\text{mol quanta m}^{-2} \text{s}^{-1}$).

Comparison of the relative PSII electron transport rates and photosynthesis-irradiance (PI) curves in surface cells at midday indicate that electron flow through PSII remains high even at irradiances where CO₂-fixation is saturated (Fig. 8). Electron flow to carbon saturates near 131 $\mu\text{mol quanta m}^{-2} \text{s}^{-1}$, while the relative electron transport rate through PSII remains unsaturated up to 1985 $\mu\text{mol quanta m}^{-2} \text{s}^{-1}$ (not shown).

Oxygen deprivation experiments

As shown in Fig. 9, oxygen is necessary in order for open ocean picophytoplankton to maintain PSII reaction centers in an oxidized state. Even under actinic irradiances of $1985 \mu\text{mol quanta m}^{-2} \text{ s}^{-1}$, a large portion of PSII reaction centers remained oxidized in aerobic samples, as indicated by the high value of F_m' relative to F_s (Fig. 9A). By contrast, if oxygen is eliminated from the samples, the PSII reaction centers are completely closed (reduced) at $1985 \mu\text{mol quanta m}^{-2} \text{ s}^{-1}$, and F_m' does not exceed F_s (Fig. 9B). This decrease in the proportion of oxidized PSII reaction centers when the samples are made anoxic is reflected in a significant decreased photochemical efficiency of PSII, Φ_{PSII} ($p < 0.0001$, $n=3$). We note that observation of variable fluorescence under oxic conditions during exposure to $1985 \mu\text{mol quanta m}^{-2} \text{ s}^{-1}$ actinic light, as shown in Fig. 9A, does not indicate a high capacity for carbon incorporation, but rather indicates a high capacity for maintaining PSII reaction centers in an oxidized state. Accordingly, measurements of qP from the anoxic trace (Fig. 9B) do not suggest that oxygen is required in order to initiate CO_2 -fixation because CO_2 -fixation becomes saturated at $131 \mu\text{mol quanta m}^{-2} \text{ s}^{-1}$, and the actinic light intensity we used in these experiments ($1985 \mu\text{mol quanta m}^{-2} \text{ s}^{-1}$) exceeded this level. Moreover, phytoplankton have a range of carbon concentrating mechanisms that compensate for the relatively low affinity of Rubisco for CO_2 , thereby allowing acclimation to a wide range of CO_2 concentrations (Kaplan and Reinhold, 1999). Therefore, the absence of variable fluorescence from the anoxic trace in Fig. 9B does not indicate limitation for CO_2 , but rather limitation for oxygen.

Inhibitor experiments

Using pgal, we tested whether electrons were being used to reduce oxygen through the activity of PTOX or a PTOX-like oxidase in natural populations of open ocean phytoplankton. The proportion of photochemical electron flow inhibited by pgal was estimated by the difference in the relative PSII electron transport rate (ETR) between control and pgal-treated samples. As shown in Fig. 9C, in the Pacific coastal site, inhibition of electron transport by pgal remains below 15% across all actinic irradiances. By contrast, in the oceanic Pacific site a large portion of the photochemical ETR is abolished in the presence of pgal. This effect is particularly remarkable during exposure to high light, where relative ETR is more than twice as high in control samples as in cells treated with pgal.

DISCUSSION

Cells that are adapted to oligotrophic, low iron conditions by maintaining low levels of PSI and cyt *b₆f* relative to PSII are particularly vulnerable to the effects of high light because inefficient dissipation of PSII excitation energy can lead to PSII photodamage (Long et al. 1994; Adir et al. 2003). The development of mechanisms for maintaining oxidized PSII reaction centers would relieve PSII excitation pressure when CO₂-fixation is limited by low nutrient availability and low levels of PSI and cyt *b₆f*, thereby decreasing the potential for PSII photodamage. In surface populations from the open ocean, F_v/F_m and qP showed strong diel periodicity, while Φ_{PSII} remained relatively constant (Fig. 5A,B,D,E). This suggests that at midday when the fewest functional reaction centers are present (low F_v/F_m), a larger fraction of them

remain oxidized (high qP), which allows for the maintenance of high PSII photochemical efficiency (reflected in a stable Φ_{PSII}) and likely prevents cells from incurring lethal levels of photodamage from high midday irradiances. By contrast, in the morning when irradiances are low and the maximum number of functional PSII reaction centers are present (high F_v/F_m), a smaller fraction of the reactions centers remain oxidized during exposure to high light (low qP). This configuration still allows for the maintenance of high PSII photochemical efficiency, resulting in a stable Φ_{PSII} . The maintenance of a higher fraction of oxidized PSII reaction centers at midday is therefore likely to help open ocean picophytoplankton survive despite incurring photoinhibition, a potential consequence of performing photosynthesis in a high light, low nutrient environment.

In contrast to the open ocean, coastal populations showed less variability in F_v/F_m and qP , while still maintaining a relatively stable Φ_{PSII} (Fig. 5C,F). This shows that a greater proportion of the PSII reaction centers remain functional at midday in the coastal relative to the open ocean samples, and that a smaller fraction of the centers need to remain oxidized in order to achieve constant photochemical efficiency throughout the day. In other words, different strategies are used in the open ocean and coastal sites to keep a nearly constant diel photochemical efficiency. In the open ocean, picophytoplankton maintain photochemical efficiency at midday by enhancing oxidation of those reaction centers that are still functional, while simultaneously contending with a decrease in the total number of functional PSII reaction centers from photoinhibition. By contrast, in coastal waters where photosynthesis is less limited by iron and macronutrient availability, more reaction centers remain functional

throughout the day with a smaller fraction of them remaining in the oxidized state. This may reflect a more favorable PSII to PSI ratio in the coastal organisms, allowing balanced electron flow through the two photosystems (Strzepek and Harrison, 2004).

Understanding the mechanism by which open ocean picophytoplankton maintain a large fraction of oxidized PSII reaction centers during the period when there appears to be maximal photoinhibition is critical for understanding how these organisms cope in this high light, oligotrophic environment. In open ocean surface waters, photosynthetic CO₂-fixation saturates at relatively low irradiances (100-300 $\mu\text{mol quanta m}^{-2} \text{ s}^{-1}$) compared to the maximum surface irradiances (2000 $\mu\text{mol quanta m}^{-2} \text{ s}^{-1}$) (Partensky et al. 1993; Li 1994; Partensky et al. 1999 and references therein). Comparison of photosynthesis-irradiance (PI) relationships and the relative PSII electron transport rates (ETR) of natural populations of phytoplankton (Fig. 8) indicate that while CO₂-fixation rates saturate at irradiances of 131 $\mu\text{mol quanta m}^{-2} \text{ s}^{-1}$ (Fig. 7C,D), PSII electron flow saturates at much higher light intensities (Fig. 8). Interestingly, the relative PSII ETR does not saturate in the phytoplankton populations from surface waters of the open ocean even at intensities of 1985 $\mu\text{mol quanta m}^{-2} \text{ s}^{-1}$ (data not shown). Similar results were observed in laboratory cultures of both prokaryotic (Bailey et al. 2007) and eukaryotic (P. Cardol, G. Finazzi, and F. A. Wolman personal communication) picophytoplankton isolated from the oligotrophic open ocean. This data shows that electron flow through PSII at irradiances greater than 131 $\mu\text{mol quanta m}^{-2} \text{ s}^{-1}$ must be used to reduce an electron acceptor other than CO₂.

Because oxygen has been shown to be a major electron acceptor in laboratory strains of open ocean phytoplankton (Bailey et al. 2007; P. Cardol, G. Finazzi, and F.

A. Wolman personal communication), we tested whether electrons were being used to reduce oxygen in natural populations of open ocean phytoplankton. Under oxic conditions, the photochemical efficiency of PSII in cells exposed to high light remains high, and a substantial fraction of PSII reaction centers are oxidized (Fig. 9A). These results show that at irradiances above those that saturate photosynthetic CO₂-fixation, electrons can still exit PSII. However, when oxygen is removed, the photochemical efficiency of PSII drops significantly and none of the PSII reaction centers remain oxidized during exposure to high light (Fig. 9B). This oxygen-dependent transition suggests that excess PSII excitation energy is rerouted to the reduction of molecular oxygen.

The decrease in PSII electron flow during treatment with pgal (Fig. 9C) shows that the activity of a pgal-sensitive oxidase is necessary to keep PSII reaction centers oxidized, and that the activity of such an oxidase appears to be particularly important in high light, low nutrient waters of the open ocean. Our in situ data are further supported by studies performed with laboratory-grown cells using a range of inhibitors specific to various oxidases (Bailey et al. 2007; P. Cardol, G. Finazzi, and F. A. Wolman personal communication). A pgal-sensitive oxidase is critical for maintaining open PSII reaction centers under high light conditions for both *Synechococcus* WH8102 (Bailey et al. 2007) and the open ocean ecotype of *Ostreococcus*, RCC809 (P. Cardol, G. Finazzi, and F. A. Wolman personal communication), both of which have low PSI:PSII and cyt *b₆f*:PSII ratios (Bailey et al. 2007; P. Cardol, G. Finazzi, and F. A. Wolman personal communication). This oxidase activity is negligible in a

coastal ecotype of *Ostreococcus* (OTH95), which does not show features of low iron adaptation (P. Cardol, G. Finazzi, and F. A. Wolman personal communication).

Pgal may have some non-specific physiological effects; in addition to inhibiting PTOX it can also inhibit the alternative oxidase of the mitochondrial electron transport chain in eukaryotes. However, it has negligible effects on other components of the photosynthetic electron transport chain in *Synechococcus* (Bailey et al. 2007). While the photoprotective process identified in this study cannot be definitively attributed to PTOX per se, the sensitivity of the process to pgal together with the high abundance of cyanobacterial PTOX sequences within the environmental metagenomic data set for the oligotrophic Sargasso Sea (McDonald and Vanlerberghe 2004) lend credence to the notion of a photoprotective role for PTOX in open ocean plankton.

Diverting PSII photogenerated electrons from PSI to molecular oxygen may represent an essential and widespread mechanism to alleviate PSII excitation and prevent PSII photodamage in the open ocean. Moreover, the pathway would generate a large ΔpH across the thylakoid membrane via the release of H^+ in the lumen during the splitting of H_2O by PSII, as well as by the consumption of H^+ in the cytoplasm (or stroma in eukaryotes) during the oxidase-mediated reduction of oxygen to H_2O (Fig. 1A). Maintenance of this pH gradient under conditions of limited CO_2 -fixation (i.e., low nutrient and low PSI levels) would provide ATP needed for cell maintenance and nutrient acquisition. Further, it would allow the cell to maintain favorable ATP:NADPH ratios, a photoprotective role filled by PSI in plants (Munekage et al. 2002; Munekage et al. 2004). Therefore, by implementing oxygen reduction in

response to high light, photosynthetic efficiency is optimized, photo-oxidative stress is minimized, and the energetic demands of the cell are satisfied (Kuntz, 2004).

In cyanobacteria, both the PTOX and the cytochrome *c* oxidases are present in the same membrane. Therefore electron diversion to either PTOX or cytochrome *c* oxidase can bypass the iron-rich PSI complex. This is not true for the Mehler reaction, where electrons used to reduce molecular oxygen are generated at the reducing side (i.e. downstream) of PSI (Mehler 1951; Mehler and Brown 1952; Asada et al. 1974). On the other hand, the photosynthetic electron transport chain is physically separated from respiratory electron transport in eukaryotes. Rerouting electrons towards the cytochrome *c* oxidase complex has to be mediated by metabolite exchanges through the cytoplasm and mitochondrial membrane, and requires both the cyt *b₆f* complex and PSI activities (Hart et al. 2005), as does the Mehler reaction. Therefore, under conditions of iron limitation where both cyt *b₆f* and PSI levels may be significantly lower, both of these processes are less advantageous than an oxidase pathway located upstream of PSI and cyt *b₆f*, such as the proposed PTOX pathway (Peltier and Cournac, 2002; Kuntz 2004).

The IMMUTANS (IM) protein is a thylakoid membrane-associated oxidase in vascular plants that accepts electrons from the plastoquinol pool, potentially protecting PSI from photodamage. However, Rosso and coworkers (2006) showed that IM does not act as an electron valve to regulate the redox state of the PQ pool via the reduction of O₂ during stress and acclimation in *Arabidopsis*. By measuring the PSI reaction center redox state, they noted that expression of *IM* did not alter the flux of PSII-generated electrons to the PSI reaction center. In contrast to the results for

Arabidopsis, Bailey and coworkers (2007) used a similar method to show that a pgal-sensitive oxidase, possibly PTOX, appears to compete with PSI reaction centers for electrons generated from the oxidation of water by PSII in *Synechococcus*, supporting the concept that in cyanobacteria the oxidase may have a photoprotective role. While the cause of this difference is not certain, we speculate that the PSI electron flow in *Synechococcus* is sufficiently low that an efficient electron valve upstream of PSI represents a critical photoprotective mechanism in the high light environment of the surface ocean where Fe and nutrient levels are extremely low and can limit CO₂-fixation rates. However, the question of how different photosynthetic organisms have come to regulate photosynthetic excitation energy while minimizing photodamage is clearly complex (Bibby et al. 2003; Asada 2006; Ivanov et al. 2006), and more work is needed to clarify these evolutionary distinctions.

In surface populations from the open ocean, F_v/F_m was not strongly correlated with Φ_{PSII} (Fig. 5A,B), a measure of the efficiency with which energy absorbed by PSII is used to drive photochemistry (i.e. to reduce electron acceptors downstream of PSII). Similarly, our data shows that changes in F_v/F_m do not necessarily correlate with the maximum rate of CO₂-fixation (Fig. 7A,B, Table 2). At first glance, these metrics seem to offer conflicting perspectives about photoinhibition; however, this is due in large part to the fact that the term is used to describe many distinct yet closely related processes (Long et al. 1994; Adir et al. 2003). In linear photosynthetic electron flow, photoinhibition would manifest as a concurrent decrease in F_v/F_m , oxygen evolution, and CO₂-fixation (Long et al. 1994); however, these parameters would not necessarily co-vary if alternative PSII photoacclimation strategies were employed

(Oquist et al. 1992b) or if alternative pathways were used for a substantial portion of the electron flow. Indeed, our findings in the surface of the Atlantic open ocean show midday F_v/F_m depressions consistent with photoinhibition (Fig. 5A), whereas CO_2 -fixation in the same samples is maintained during exposure of the cells to high light (Fig. 7B, Table 2). This indicates that the physiological status of the cells, including the status of all PSII reaction centers and the regulation of oxidase activity, result in a greater fraction of the functional reaction centers remaining oxidized (thereby maintaining non-photoinhibited CO_2 -fixation rates at high light intensities), even while the total number of functional reaction centers decreases suggesting photoinhibition (which is reflected in lower values of F_v/F_m).

In contrast to the high light, low nutrient surface environment, life at greater depths in the open ocean presents a different set of challenges to photosynthetic organisms. Specifically, scattering and absorption attenuate the light intensity with depth and decrease the range of photosynthetically active wavelengths compared to those of surface waters. On the other hand, macronutrient levels tend to increase with depth due to the activity of the heterotrophic bacterial community, which recycles nutrients in sinking organic material (Laws et al. 1984; Azam and Cho, 1987). These inverse gradients of light and nutrients generate a different niche at depth compared to surface waters, and different ecotypes of picoeukaryotes and picocyanobacteria with larger photosynthetic antennae and a higher ratio of chlorophyll *b* (Chl *b*) to Chl *a* are more abundant (Partensky et al. 1997; Urbach et al. 1998; West and Scanlan, 1999).

As many physiological differences have been shown to exist between high and low light picocyanobacterial ecotypes (Moore et al. 1995; Moore et al. 1998; Bibby et

al. 2003), we tested whether natural populations of picocyanobacteria from the DCM are also able to reduce oxygen during exposure to high light as a means of avoiding photodamage. In surface and DCM samples, the fraction of oxidized PSII centers increases at midday, i.e. when the number of functional PSII centers is lowest (Fig. 6). However, unlike the surface samples, the light saturated photosynthetic rate, P_m , is markedly lower in DCM samples, and photoinhibition during exposure to high light is observed in CO_2 -fixation experiments (Fig. 7B,D Table 2). This observation is consistent with other studies involving low light ecotypes of *Prochlorococcus* that measured lower CO_2 -fixation rates at the base of the euphotic zone compared to surface waters (Li, 1994), and show that photoinhibition occurs in low light ecotypes at irradiances that are optimal for the growth of high light ecotypes isolated from the surface ocean (Moore et al. 1995; Moore et al. 1998; Urbach et al. 1998). While we cannot rule out that natural samples from the deep waters of oligotrophic oceans could also have an alternative oxidase pathway, the extent of this phenomenon is reduced in the populations we sampled from the DCM (primarily *Prochlorococcus*, Fig. 4A), where photoinhibition is observed at the level of CO_2 -fixation (Fig. 7C,D, Table 2) and the fraction of oxidized reaction centers does not increase at midday when compared to surface samples (Fig. 5D). More work is needed to identify photoprotective mechanisms in low-light adapted cells from the DCM.

Of the different marine locations (i.e., Pacific, Atlantic, coastal, oceanic, surface, deep) examined in this study, all appear to undergo some degree of photoinhibition at midday. Photodamage, which contributes to photoinhibition (Long et al. 1994; Fig. 1B), can occur at all levels of illumination that generate a PSII charge

separation; even low irradiances can lead to photodamage (Barber and Anderson, 1992; Adir et al. 2003). Note that the number of photoinhibited reaction centers is influenced by both photodamage and other PSII photoacclimation processes (Oquist et al. 1992*b*; *see* Fig. 1B.) Therefore, changes in photoinhibition throughout the day do not necessarily exclusively reflect photodamage of PSII. The extent of photoinhibition is greatest in surface populations from the high light, low nutrient open ocean where oxygen appears to be a major electron acceptor. However, photoinhibition in these populations would likely be even greater if the process of oxygen reduction were absent. Despite the substantial degree of photoinhibition observed from chlorophyll fluorescence measurements at midday in the open ocean, this study indicates that, through oxygen reduction, the cells are still able to maintain stable photochemical efficiencies and CO₂-fixation rates, as well as to recover from photoinhibition rapidly (with complete recovery occurring by evening, as also reported by Behrenfeld and coworkers (2006)). Oxygen reduction is therefore likely to play a photo-protective role that gives certain phytoplankton a competitive edge in the challenging environment of the surface open ocean.

Besides its physiological relevance for photosynthetic life in the open ocean, these observations have other important global oceanographic implications. Marine primary productivity models use direct measurements of primary productivity based on ¹⁴C assimilation experiments from various locations throughout the world's oceans, many of which are coastal (Longhurst et al. 1995; Antoine et al. 1997; Behrenfeld and Falkowski, 1997), to establish algorithms that convert remotely-derived chlorophyll (ocean color) data to productivity estimates (Behrenfeld and Falkowski, 1997).

Discrepancies in the actual and the modeled CO₂-fixation rates in the open ocean have been observed (Behrenfeld et al. 2006), prompting the suggestion of incorporating a scaling factor based on F_v/F_m to account for photosynthetic variability in the open ocean (Behrenfeld et al. 2006). However, our data suggest that F_v/F_m does not necessarily reflect the actual photochemical efficiency of natural phytoplankton populations. In particular, the processes driving variability in F_v/F_m are not necessarily the same processes as those responsible for the observed discrepancy in actual and modeled open ocean CO₂-fixation rates. Comparison of the light saturated photosynthetic CO₂-fixation rates (P_m) during morning and midday indicates a P_m decrease of approximately 15% (Fig. 7A,B; Table 2), which is much smaller than the 57% decrease in the concurrently-measured F_v/F_m values (Fig. 5A, green line). Together, the greater variability in F_v/F_m relative to P_m , along with the observation that photochemical efficiency (Φ_{PSII}) is stable throughout the day (Fig. 5A, orange line), suggest that productivity is not necessarily directly or universally correlated with F_v/F_m .

The reduction of oxygen by phytoplankton in the open ocean could be another source of the discrepancy between actual and predicted productivity rates. Applications of empirical photosynthesis and chlorophyll fluorescence data from locations where oxygen reduction represents a minor fraction of electron flow to those areas in which it is a major process are likely to overestimate oceanic primary productivity. Specifically, empirical data that is weighted toward nutrient-rich coastal waters, where electron flow to oxygen does not appear to be a common adaptation, may not accurately represent the open ocean. More work is needed in order to fully

understand processes underlying carbon sequestration in oligotrophic waters, and to represent them mechanistically in models of marine primary productivity by taking into account the significantly different features of photosynthetic electron flow and CO₂-fixation associated with the different oceanic habitats. A mechanistic understanding of how picophytoplankton in oligotrophic oceans manage the absorption of excess light energy will help clarify their contribution to marine primary productivity, provide a greater understanding of the features of the marine environment that limit growth and CO₂-fixation in situ, and enable us to more accurately predict how they might affect and be affected by future environmental and climatic changes.

ACKNOWLEDGEMENTS

I acknowledge my co-authors Adina Paytan, Arthur R. Grossman, and Shaun Bailey for help on this manuscript, which was published in 2008 in *Limnology and Oceanography*. As a group we thank M. Lomas, D. Lomas, D. Karl, F. Santiago-Mandujano, E. Grabowski, and S. Curless for providing ship time and assistance at sea, and our colleagues K. Arrigo, J. Shrager, G. M. Berg, and G. van Dijken at Stanford University. G. Finazzi, P. Cardol, and two anonymous reviewers provided comments on the manuscript. This research was supported by a National Aeronautics and Space Administration (NASA) New Investigator Program grant NAG5-12663 to AP and a National Science Foundation (NSF) Oceanography grant OCE-0450874 to ARG. KRMM was supported by the NSF Graduate Research Fellowship Program and the Department of Energy (DOE) Global Change Education Program.

Citation

Mackey, KRM, A Paytan, A Grossman, and S Bailey. 2008. A photosynthetic strategy for coping in a high light, low nutrient environment. *Limnol. Oceanogr.* 53:900-913.

Author contributions

KRM Mackey – planned experimental design; conducted field work; processed samples; analyzed and interpreted data; wrote the manuscript

A Paytan - provided funding; helped interpret data; provided comments on the manuscript

A Grossman - provided funding; planned experimental design; helped interpret data;
provided comments on the manuscript

S Bailey - planned experimental design; helped interpret data; provided comments on
the manuscript

REFERENCES

- Adir, N., H. Zer, S. Shochat, and I. Ohad. 2003. Photoinhibition-a historical perspective. *Photosynth. Res.* **76**: 343-370.
- Antoine, D., J. Andre, and A. Morel. 1996. Oceanic primary production. 2. Estimation at global scale from satellite (coastal zone color scanner) chlorophyll. *Global Biogeochem. Cycles* **10**: 57-69.
- Asada, K., K. Kiso, and K. Yoshikawa. 1974. Univalent reduction of molecular oxygen by spinach chloroplasts on illumination. *J. Biol. Chem.* **249**: 2175-2181.
- Asada, K. 1999. The water-water cycle in chloroplasts: Scavenging of active oxygens and dissipation of excess photons. *Annu. Rev. Plant. Physiol. Plant. Mol. Biol.* **50**: 601-639.
- Asada, K. 2006. Production and scavenging of reactive oxygen species in chloroplasts and their functions. *Plant Physiol.* **141**: 391-396.
- Azam, F., and B. C. Cho. 1987. Bacterial utilization of organic matter in the sea. p.261-281. *In*: GM41, Ecology of microbial communities. Cambridge University Press.
- Bailey, S., A. Melis, K. R. M. Mackey, G. Finazzi, P. Cardol, G. van Dijken, G. M. Berg, K. Arrigo, J. Shrager, and A. Grossman. In press. Photosynthesis in marine *Synechococcus* and the critical nature of electron flow to oxygen. *Biochim. Biophys. Acta*.
- Barber, J. and B. Andersson. 1992. Too much of a good thing: light can be bad for photosynthesis. *Trends. Biochem. Sci.* **17**:61-66.

- Behrenfeld, M. J., K. Worthington, R. M. Sherrell, F. P. Chavez, P. Strutton, M. McPhaden, and D. M. Shea. 2006. Controls on tropical Pacific Ocean productivity revealed through nutrient stress diagnostics. *Nature* **442**: 1025-1028.
- Behrenfeld, M. J., and P. G. Falkowski. 1997. Photosynthetic rates derived from satellite-based chlorophyll concentration. *Limnol.Oceanogr.* **42**: 1-20.
- Berry, S., D. Schneider, W. F. Vermaas, and M. Rogner. 2002. Electron transport routes in whole cells of *Synechocystis* sp. Strain PCC 6803: The role of the cytochrome bd-type oxidase. *Biochem.* **41**: 3422-3429.
- Bibby, T. S., I. Mary, J. Nield, F. Partensky, and J. Barber. 2003. Low-light-adapted *Prochlorococcus* species possess specific antennae for each photosystem. *Nature* **424**: 1051-1054.
- Boekema, E. J. A. Hifney, A. E. Yakushevskaya, M. Piotrowski, W. Keegstra, S. Berry, K.-P. Michel, E. K. Pistorius, and J. Kruip. 2001. A giant chlorophyll-protein complex induced by iron deficiency in cyanobacteria. *Nature* **412**: 745-748.
- Butler, W. L. 1978. Energy distribution in the photochemical apparatus of photosynthesis. *Annu. Rev. Plant Physiol.* **29**: 345-378.
- Cadoret, J. C., R. Demouliere, J. Lavaud, H. J. van Gorkom, J. Houmard, and A.L. Etienne. 2004. Dissipation of excess energy triggered by blue light in cyanobacteria with CP43' (isiA). *Biochim. Biophys. Acta.* **1659**: 100-104.
- Campbell, D., V. Hurry, A. K. Clarke, P. Gustafsson, and G. Oquist. 1998. Chlorophyll fluorescence analysis of cyanobacterial photosynthesis and acclimation. *Microbiol. Mol. Biol. Rev.* **62**: 667-683.

- Campbell, L., and D. Vaultot. 1993. Photosynthetic picoplankton community structure in the Subtropical North Pacific Ocean near Hawaii (station ALOHA). *Deep Sea Res. (Part I, Oceanographic Research Papers)* **40**: 2043-2060.
- Díez, B., C. Pedrós-Alió, T. L. Marsh, and Ramon Massana. 2001. Application of denaturing gradient gel electrophoresis (DGGE) to study the diversity of marine picoeukaryotic assemblages and comparison of DGGE with other molecular techniques. *Appl. Environ. Microbiol.* **67**: 2942-2951.
- Field, C. B., M. J. Behrenfeld, J.Y. Randerson, and P. Falkowski. 1998. Primary production of the biosphere: Integrating terrestrial and oceanic components. *Science* **281**: 237-240.
- Fouilland, E., C. Descolas-Gros, C. Courties, Y. Collos, A. Vaquer, and A. Gasc. 2004. Productivity and growth of a natural population of the smallest free-living eukaryote under nitrogen deficiency and sufficiency. *Microb. Ecol.* **48**: 103-110.
- Guenther, J. E., and A. Melis. 1990. The physiological significance of photosystem II heterogeneity in chloroplasts. *Photosynth. Res.* **23**: 105-109.
- Hart, S. E., B.G. Schlarb-Ridley, D. S. Bendall, and C. J. Howe. 2005. Terminal oxidases of cyanobacteria. *Biochem. Soc. Trans.* **33**: 832-835.
- Ivanov, A. G., M. Krol, E. Selstam, P. V. Sane, D. Sveshnikov, Y. Park, G. Öquist, and N. P. A. Huner. 2007. The induction of CP43' by iron-stress in *Synechococcus* sp. PCC 7942 is associated with carotenoid accumulation and enhanced fatty acid unsaturation. *Biochim. Biophys. Acta.* **1767**: 807-813.

- Ivanov, A. G., M. Krol, D. Sveshnikov, E. Selstam, S. Sandström, M. Koochek, Y. Park, S. Vasil'ev, D. Bruce, G. Öquist, and N. P. A. Huner. 2006. Iron deficiency in cyanobacteria causes monomerization of photosystem I trimers and reduces the capacity for state transitions and the effective absorption cross section of photosystem I in vivo. *Plant Physiol.* **141**: 1436-1445.
- Josse, E. M., J. P. Alcaraz, A. M. Laboure, and M. Kuntz. 2003. In vitro characterization of a plastid terminal oxidase (PTOX). *Eur. J. Biochem.* **270**: 3787-3794.
- Kaplan, A., and L. Reinhold. 1999. CO₂ concentrating mechanisms in photosynthetic microorganisms. *Ann. Rev. Plant. Physiol. Plant Biol.* **50**: 539-570.
- Kuntz, M. 2004. Plastid terminal oxidase and its biological significance. *Planta* 218: 896-899.
- Laws, E. A., D. G. Redalje, L. W. Haas, P. K. Bienfang, R. W. Eppley, W. G. Harrison, D. M. Karl, and J. Marra. 1984. High phytoplankton growth rates in oligotrophic Hawaiian coastal waters. *Limnol. Oceanogr.* **29**: 1161-1169.
- Lavergne, J. 1982. Two types of primary acceptors in chloroplasts photosystem II. *Photobiochem. Photobiophys.* **3**: 257-285.
- Lewis, M.R., and J. C. Smith. 1983. A small-volume, short- incubation-time method for measurement of photosynthesis as a function of incident irradiance. *Mar. Ecol. Prog. Ser.* **13**: 99-102.
- Li, W. K. W. 1994. Primary productivity of prochlorophytes, cyanobacteria, and eucaryotic ultraphytoplankton: measurements from flow cytometric sorting. *Limnol. Oceanogr.* **39**: 169-175.

- Long, S. P., S. Humphries, and P. G. Falkowski. 1994. Photoinhibition of photosynthesis in nature. *Annu. Rev. Plant Physiol. Plant Mol. Biol.* **45**: 633-662.
- Longhurst, A., S. Sathyendranath, T. Platt, and C. Caverhill. 1995. An Estimate of Global Primary Production in the Ocean from Satellite Radiometer Data. *J. Plankton Res.* **17**: 1245-1271.
- Mackey, K. R. M., R. G. Labiosa, M. Calhoun, J. H. Street, A. F. Post, and A. Paytan. 2007. Phosphorus availability, phytoplankton community dynamics, and taxon-specific phosphorus status in the Gulf of Aqaba, Red Sea. *Limnol. Oceanogr.* **52**: 875-885.
- McDonald, A. E., and G. C. Vanlerberghe. 2004. Alternative oxidase and plastoquinol terminal oxidase in marine prokaryotes of the Sargasso Sea. *Gene* **349**: 15-24.
- Maxwell, K., and G. N. Johnson. 2000. Chlorophyll fluorescence-a practical guide. *J. Exp. Bot.* **51**: 659-668.
- Mehler, A. H. 1951. Studies on reactions of illuminated chloroplasts. I. Mechanism of the reduction of oxygen and other Hill reagents. *Arch. Biochem. Biophys.* **33**: 65-77.
- Mehler, A. H., and A. H. Brown. 1952. Studies on reactions of illuminated chloroplasts. III. Simultaneous photoproduction and consumption of oxygen studied with oxygen isotopes. *Arch. Biochem. Biophys.* **38**: 365-70.
- Mi, H., T. Endo, U. Schreiber, T. Ogawa, and K. Asada. 1994. NAD(P)H dehydrogenase-dependent cyclic electron flow around photosystem I in the

- cyanobacterium *Synechocystis* PCC 6803: a study of dark-starved cells and spheroplasts. *Plant Cell Physiol.* **35**: 163-173.
- Mi, H., T. Endo, T. Ogawa, and K. Asada. 1995. Thylakoid membrane-bound, NADPH-specific pyridine nucleotide dehydrogenase complex mediates cyclic electron transport in the cyanobacterium *Synechocystis* sp. PCC 6803. *Plant Cell Physiol.* **36**: 661-668.
- Moore, L. R., R. Goericke, and S. W. Chisholm. 1995. Comparative physiology of *Synechococcus* and *Prochlorococcus*: influence of light and temperature on growth, pigments, fluorescence and absorptive properties. *Mar. Ecol. Prog. Ser.* **116**: 259-275.
- Moore, L. R., G. Rocap, and S. W. Chisholm. 1998. Genome divergence in two *Prochlorococcus* ecotypes reflects oceanic niche differentiation. *Nature* **393**: 464-468.
- Munekage, Y., M. Hashimoto, C. Miyake, K. Tomizawa, T. Endo, M. Tasaka, and T. Shikanai. 2004. Cyclic electron flow around photosystem I is essential for photosynthesis. *Nature* **429**: 579–582.
- Munekage Y, M. Hojo, J. Meurer, T. Endo, M. Tasaka, and T. Shikanai. 2002. PGR5 is involved in cyclic electron flow around photosystem I and is essential for photoprotection in Arabidopsis. *Cell* **110**: 361–371.
- Oquist, G., J. M. Anderson, S. McCaffery, and W. S. Chow. 1992a. Mechanistic differences in photoinhibition of sun and shade plants. *Planta* **188**: 422-431.

- Oquist, G., W. S. Chow, and J. M. Anderson. 1992*b*. Photoinhibition of photosynthesis represents a mechanism for the long-term regulation of photosystem II. *Planta* **186**: 450-460.
- Palenik, B., B. Brahamsha, F. W. Larimer, M. Land, L. Hauser, P. Chain, J. Lamerdin, W. Regala, E.E. Allen, J. McCarren, I. Paulsen, A. Dufresne, F. Partensky, E. A. Webb, and J. Waterbury. 2003. The genome of a motile marine *Synechococcus*. *Nature* **424**: 1037-42.
- Partensky, F., W. R. Hess, and D. Vaultot. 1999. *Prochlorococcus*, a marine photosynthetic prokaryote of global significance. *Microbiol. Mol. Biol. Rev.* **63**: 106-127.
- Partensky, F., N. Hoepffner, W. K. W. Li, O. Ulloa, and D. Vaultot. 1993. Photoacclimation of *Prochlorococcus* sp. (Prochlorophyta) strains isolated from the North Atlantic and the Mediterranean Sea. *Plant Physiol.* **101**: 295-296.
- Partensky, F., J. LaRoche, K. Wyman, and P. G. Falkowski. 1997. The divinyl-chlorophyll a/b-protein complexes of two strains of the oxyphototrophic marine prokaryote *Prochlorococcus*- characterization and response to changes in growth irradiance. *Photosynth. Res.* **51**: 209-222.
- Peltier, G., and L. Cournac. 2002. Chlororespiration. *Ann. Rev. Plant. Biol.* **53**: 523-550.
- Platt, T., D. V. Subba Rao, and B. Irwin. 1983. Photosynthesis of picoplankton in the oligotrophic ocean. *Nature* **301**: 702-704.

- Platt, T., C. L. Gallegos, and W. G. Harrison. 1980. Photoinhibition of photosynthesis in natural assemblages of marine-phytoplankton. *J. Mar. Res.* **38**: 687–701.
- Rosso, D., A. G. Ivanov, A. Fu, J. Geisler-Lee, L. Hendrickson, M. Geisler, G. Stewart, M. Krol, V. Hurry, S. R. Rodermel, D. P. Maxwell, and N. P. A. Hüner. 2006. IMMUTANS Does not act as a stress-induced safety valve in the protection of the photosynthetic apparatus of *Arabidopsis* during steady-state photosynthesis. *Plant Physiol.* **142**:574-585.
- Scanlan, D. J. 2003. Physiological diversity and niche adaptation in marine *Synechococcus*. *Adv. Microb. Physiol.* **47**: 1-64.
- Schreiber, U., T. Endo, H. Mi, and K. Asada. 1995. Quenching analysis of chlorophyll fluorescence by the saturation pulse method: Particular aspects relating to the study of eukaryotic algae and cyanobacteria. *Plant Cell Physiol.* **36**: 873-882.
- Strzepek, R. F., and P. J. Harrison. 2004. Photosynthetic architecture differs in coastal and oceanic diatoms. *Nature* **431**: 689-692.
- Urbach, E., D. J. Scanlan, D. L. Distel, J. B. Waterbury, and S. W. Chisholm. 1998. Rapid diversification of marine picophytoplankton with dissimilar light-harvesting structures inferred from sequences of *Prochlorococcus* and *Synechococcus* (cyanobacteria). *J. Mol. Evol.* **46**: 188-201.
- West, N. J., and D. J. Scanlan. 1999. Niche-partitioning of *Prochlorococcus* populations in a stratified water column in the eastern North Atlantic ocean. *Appl. Environ. Microbiol.* **65**: 2585-2591.

Worden , A. Z., J.K. Nolan, and B. Palenik. 2004. Assessing the dynamics and ecology of marine picophytoplankton : The importance of the eukaryotic component. *Limnol. Oceanogr.* **49**: 168-174.

Table 1: Equations used in determining PSII fluorescence parameter values. Variables are defined in Fig. 4. (* I_A is actinic light intensity.)

PSII fluorescence parameter	Calculation
Maximum (dark-adapted) efficiency of PSII photochemistry $\left(\frac{F_v}{F_m}\right)$	$\frac{F_m - F_o}{F_m}$
Actual (light-adapted) efficiency of PSII photochemistry (Φ_{PSII})	$\frac{F'_m - F_s}{F'_m}$
Photochemical quenching; fraction of oxidized PSII reaction centers (qP)	$\frac{F'_m - F_s}{F'_m - F'_o}$
Relative PSII electron transport rate (ETR)	$\Phi_{PSII} \times I_A^*$

* I_A , actinic light intensity.

Table 2: Photosynthesis-irradiance parameters determined for Atlantic open ocean samples from the surface of the euphotic zone and the deep chlorophyll maximum.

	P_s (g C [g Chl a] $^{-1}$ h $^{-1}$)	α (g C {g Chl a } $^{-1}$ h $^{-1}$)/ [μ mol quanta m $^{-2}$ s $^{-1}$])	β (g C {g Chl a } $^{-1}$ h $^{-1}$)/ [μ mol quanta m $^{-2}$ s $^{-1}$])	P_m (g C [g Chl a] $^{-1}$ h $^{-1}$)	E_k (μ mol quanta m $^{-2}$ s $^{-1}$)	R^2
Surface	10.219	0.06336	0.00306	8.4	132	0.85
Surface morning						
Surface midday	7.126	0.05416	0.00000	7.1	131	0.76
DCM morning	1.478	0.07496	0.00163	1.3	18	0.69
DCM midday	2.134	0.04459	0.00384	1.6	35	0.38

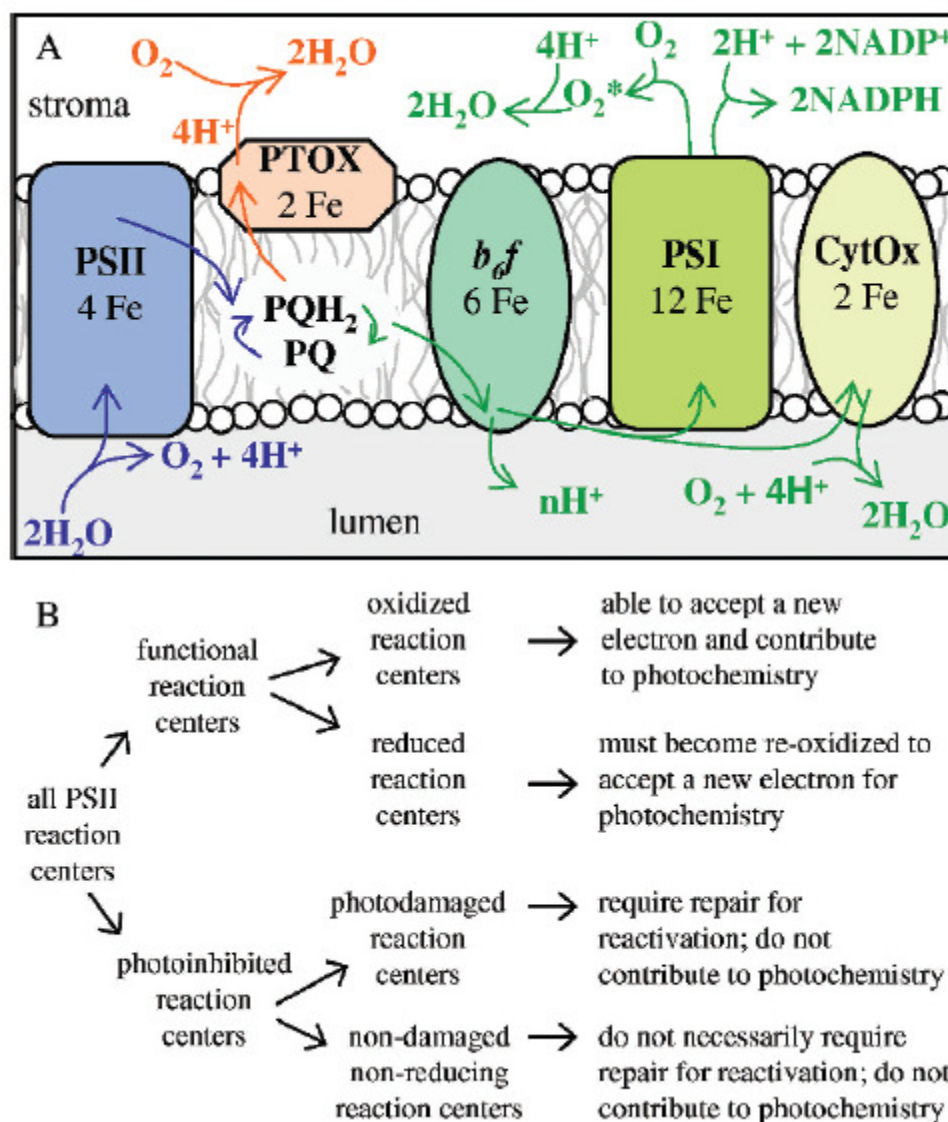


Figure 1: (A) Schematic diagram of principal photosynthetic apparatus components, their electron flow paths, and iron requirements. Blue arrows denote shared pathways, green arrows denote pathways utilizing the iron-rich cyt *b₆f* (designated “*b₆f*” in figure) or PSI complexes, and orange arrows denote the PTOX pathway, which bypasses cyt *b₆f* and PSI. The photosynthetic electron transport sequence is as follows: PSII to the plastoquinone pool (PQ, PQH₂) (blue) to cyt *b₆f* to a mobile carrier (cytochrome of plastocyanin, not shown). (Protons are also transported to the lumen during the reduction of *b₆f*, helping to establish a ΔpH.) From *b₆f*, electrons passed to PSI can be used to reduce NADP⁺ for CO₂-fixation, or to reduce oxygen via the Mehler reaction (green). The Mehler reaction comprises the following steps (not shown): (1) univalent reduction of O₂ to superoxide (designated “O₂^{*}” in figure), (2) disproportionation of superoxide to H₂O₂, and (3) the reduction of H₂O₂ to H₂O

(Asada et al. 1974; Asada 1999; Asada 2006). In prokaryotes, electron transport can also proceed from cyt *b₆f* to the respiratory cytochrome oxidase (green). Electrons can also be donated directly from the plastoquinone pool to a plastid terminal oxidase (PTOX, orange) upstream of cyt *b₆f* and PSI. In this pathway, protons are consumed from the stroma (via PQH₂) during the reduction of O₂ to H₂O, thereby helping to establish a ΔpH .) (B) Flow chart showing the terminology for PSII reaction centre classification used in this study. A “functional” reaction center is one in which Q_A, the first stable PSII electron acceptor, is able to become reduced (upon accepting an electron) and re-oxidized (upon donating the electron) while contributing to photochemistry. A “photoinhibited” reaction center does not refer to the oxidation state of the reaction center but denotes a center unable to perform photochemistry (e.g., following photodamage or down-regulation of PSII reaction centers.)

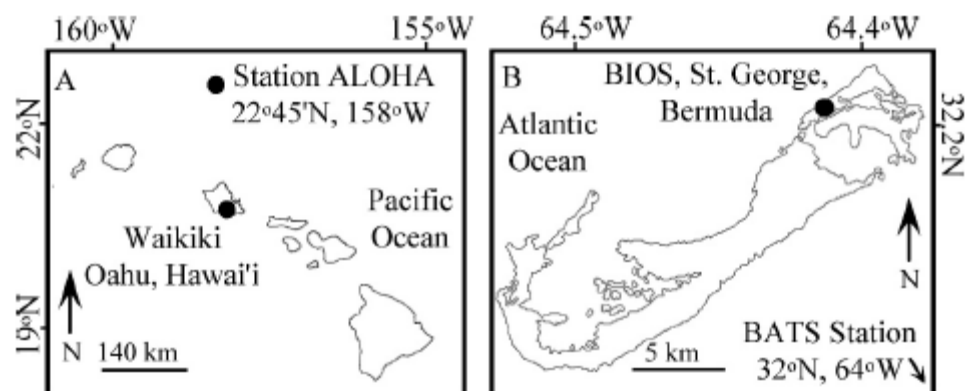


Figure 2: Maps of sampling sites in the (A) Pacific and (B) Atlantic oceans.

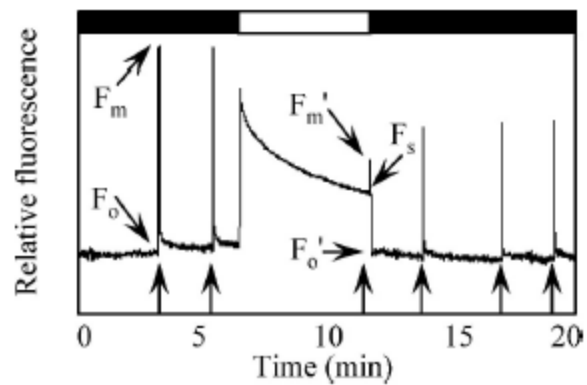


Figure 3: Example chlorophyll fluorescence trace showing the fluorescence levels used for computing the fluorescence parameters in Table 1 from samples collected during diel monitoring. The thick line along the top indicates periods of no actinic light (black) and $1985 \mu\text{mol quanta m}^{-2} \text{s}^{-1}$ actinic light (white). Arrows along the abscissa indicate the timing of the saturating pulses (saturating pulse intensity was $3000 \mu\text{mol quanta m}^{-2} \text{s}^{-1}$ for a duration of 0.8 s). The saturating pulse during periods in which the cells were exposed to actinic light was delivered immediately before the actinic light was turned off.

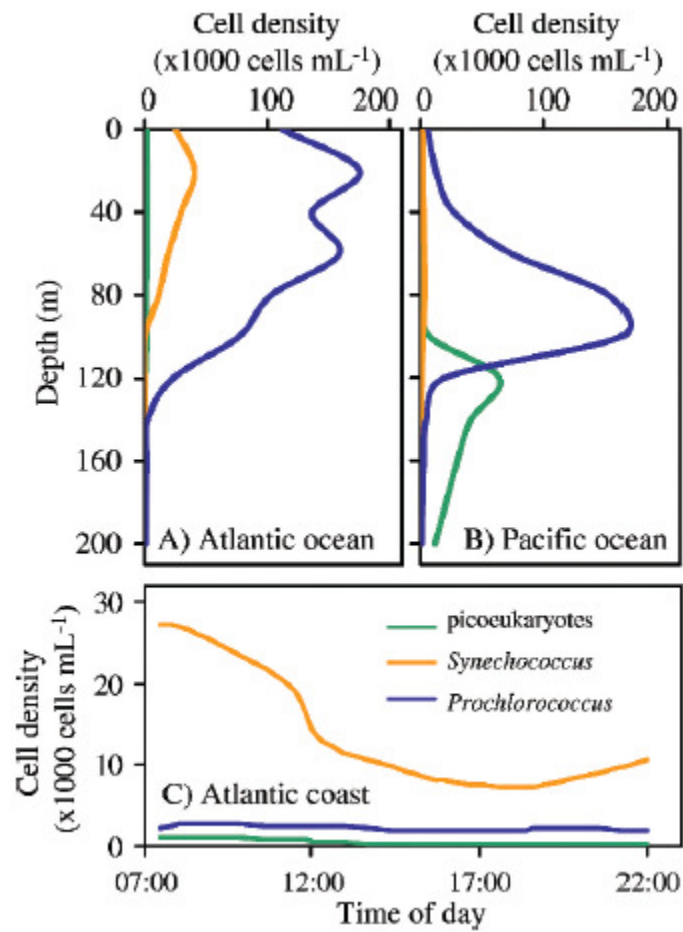


Figure 4: Phytoplankton cell densities of *Prochlorococcus* (blue line), *Synechococcus* (orange line), and picoeukaryotes (green line). Depth profiles of the open ocean sites in the (A) Atlantic Ocean and (B) Pacific Ocean. (C) Cell abundances in surface populations from the Atlantic coastal site throughout the sampling period.

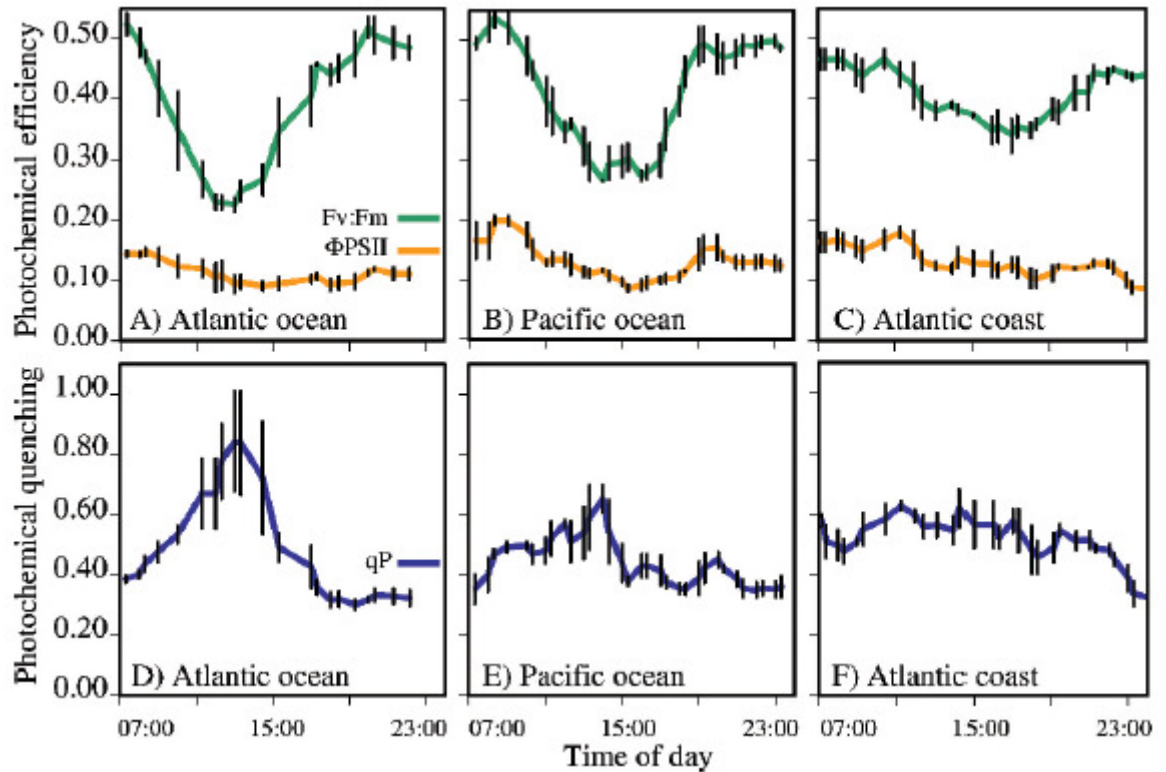


Figure 5: (A,B,C) Diel variation of the maximum (F_v/F_m , green line) and actual (Φ_{PSII} , orange line) PSII photochemical efficiencies in the (A) Atlantic open ocean site, (B) Pacific open ocean site, and (C) Atlantic coastal site. (D,E,F) Diel variation of the proportion of oxidized PSII reaction centers (photochemical quenching, qP , blue line) of phytoplankton from the (D) Atlantic open ocean site, (E) Pacific open ocean site, and (F) Atlantic coastal site. Error bars show ± 1 standard error of the mean.

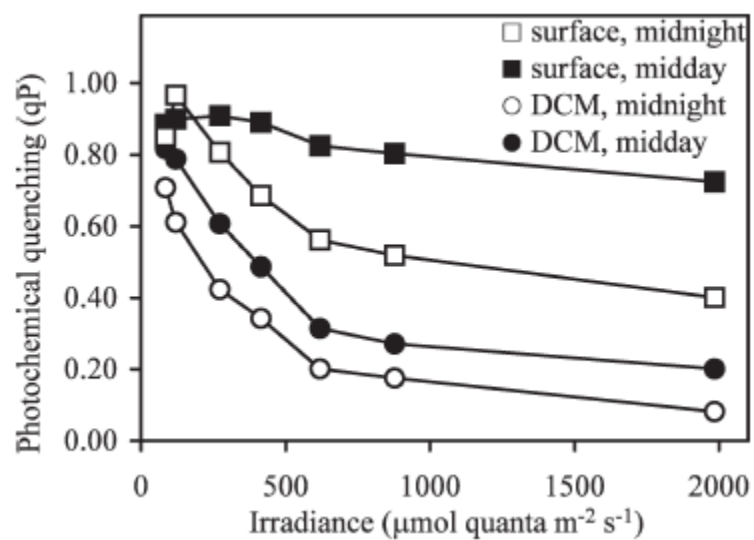


Figure 6: Photochemical quenching at indicated actinic light levels in cells from the Atlantic open ocean surface waters (squares) and the deep chlorophyll maximum (circles) at midday (filled symbols) and midnight (open symbols).

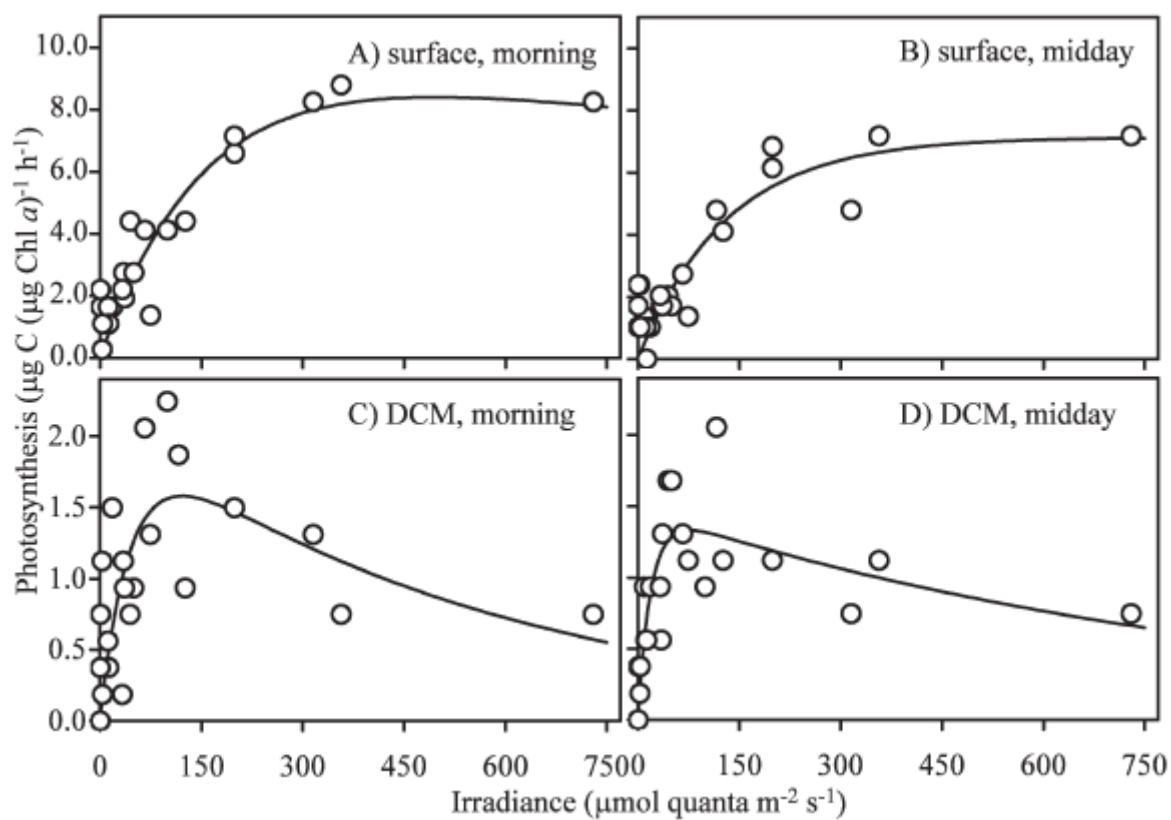


Figure 7: Photosynthesis-irradiance curves from the Atlantic open ocean site for (A) surface samples in the morning, (B) surface samples in midday, (C) DCM samples in the morning, and (D) DCM samples in midday.

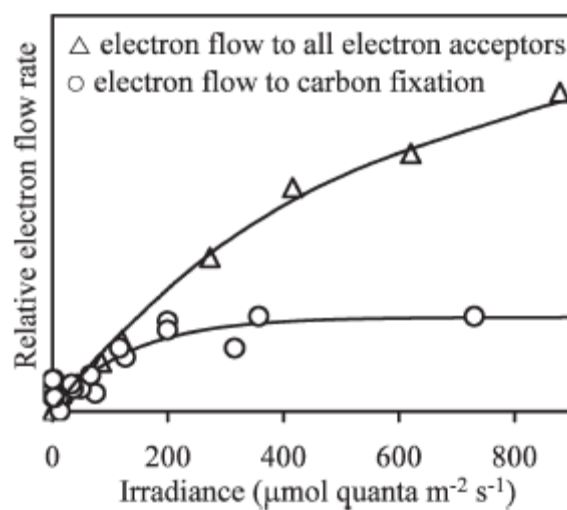


Figure 8: In phytoplankton from the Atlantic open ocean surface waters, the electron flow to carbon (open circles) saturates near $131 \mu\text{mol quanta m}^{-2} \text{s}^{-1}$, while the relative electron transport rate through PSII (open triangles) remains unsaturated. Relative ETR and CO_2 -fixation (photosynthesis) are scaled to facilitate comparison; y-axes use arbitrary units.

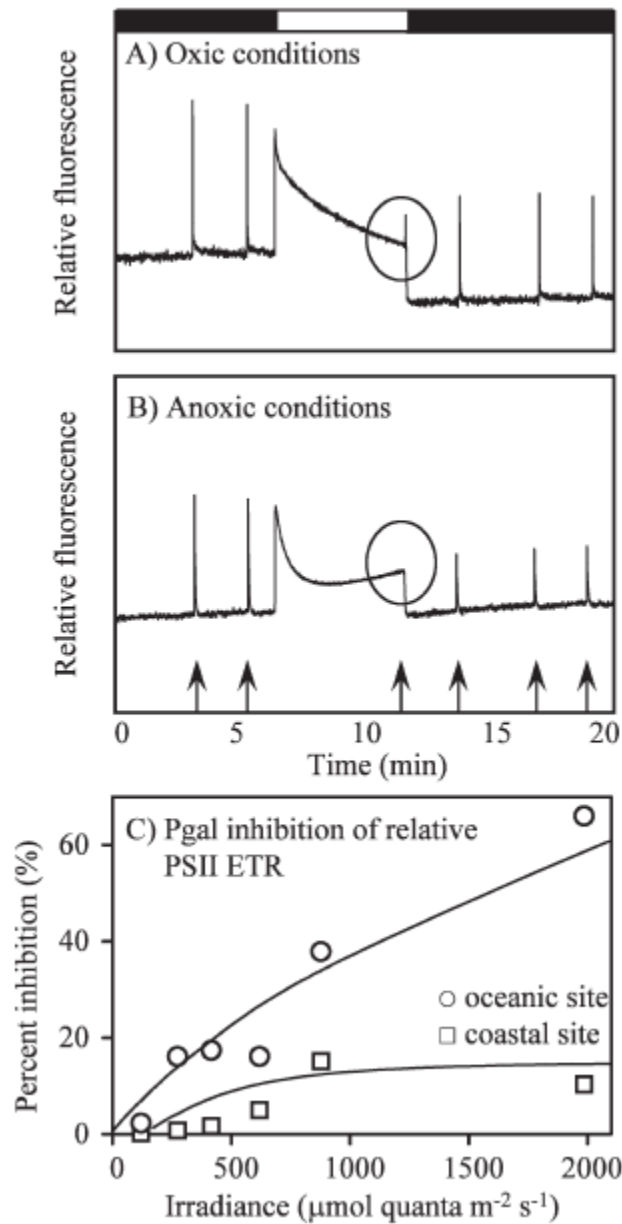


Figure 9: Chlorophyll fluorescence traces of cells from the surface Atlantic open ocean under (A) oxic and (B) anoxic conditions show that the portion of oxidized reaction centers (indicated by circled areas on the traces) are substantially lower in anoxic conditions than in oxic conditions during exposure to high light. The thick line along the top indicates periods of no actinic light (black line segments) and 1985 $\mu\text{mol quanta m}^{-2} \text{s}^{-1}$ actinic light (white line segment) for (A) and (B). Arrows along the abscissa indicate timing of the saturating pulses (saturating pulse intensity was 3000 $\mu\text{mol quanta m}^{-2} \text{s}^{-1}$ for a duration of 0.8 sec). The saturating pulse during actinic light was delivered immediately before the actinic light was turned off. (C) Percent decrease in the relative PSII electron transport rate in the presence of 1 mmol L⁻¹ pgal

for natural populations in the surface Pacific open ocean site (open circles) and the Pacific coastal site (open squares) following 30 minutes dark adaptation.

CHAPTER 7

THE INFLUENCE OF ATMOSPHERIC NUTRIENTS ON PRIMARY PRODUCTIVITY IN A COASTAL UPWELLING REGION

ABSTRACT

Atmospheric deposition is an important source of nutrients to the coastal and open ocean; however, its role in highly productive upwelling regions like coastal California has not been determined. Approximately 0.1-0.2% of new production is attributable to atmospheric deposition of nitrogen (N) annually, but if the estimate is expanded to encompass the effects of iron (Fe), aerosols may support 1-2% of new production on average, and up to 5% on days with high deposition fluxes. Laboratory culture and *in situ* incubation experiments confirm the bioavailability of N from dry deposition in this region. A significant positive relationship between aerosol optical thickness and chlorophyll *a* derived from MODIS is observed for the summer months, and is stronger offshore than near the coast. Moreover, the portion of productivity supported by atmospheric deposition is higher on days without upwelling and during El Niño periods when nutrient input from upwelling is suppressed, a phenomenon that could become more prevalent due to climate warming. Expanding the results from California, we estimate that dry deposition could increase productivity in other major coastal upwelling regions by up to 8%, and suggest that aerosols could stimulate productivity by providing N, Fe and other nutrients that are essential for cell growth but relatively deplete in upwelled water.

INTRODUCTION

Marine productivity is influenced by numerous processes ranging from phytoplankton community succession to global biogeochemical cycles. Among these processes, those contributing to the supply or regeneration of biologically important nutrients are particularly influential in determining productivity rates. Atmospheric deposition, which includes both precipitation (wet deposition) and dry deposition of aerosols and gases, can stimulate productivity by providing macronutrients as well as trace metals in areas of the ocean where productivity is nutrient limited (Paerl 1985; Peierls and Paerl 1997; Jaworski et al. 1997; Seitzinger and Sanders 1999; Paerl et al. 1999). By enhancing ocean productivity and carbon sequestration, atmospheric deposition also influences atmospheric carbon dioxide concentrations and climate. Accordingly, understanding the role of atmospheric deposition in influencing ocean productivity within different marine ecosystems is important.

Atmospheric deposition contributes substantially to the nutrient inventories of oligotrophic ocean environments (Duce et al. 2008). Low nutrient availability in these regions stems from a scarcity of external nutrient sources, including fluvial and groundwater inputs, such that the relative contribution of atmospheric nutrients is significant. In the Atlantic Ocean, dry deposition both provides nitrogen (N) (Duce 1986; Prospero et al. 1996; Jaworski et al. 1997; Paerl et al. 2002) and stimulates N₂ fixation by providing phosphorus (P) and iron (Fe) to diazotrophs (Mills et al. 2004; Chen and Siefert 2004). In the North Pacific, it has been suggested that 40-70% of nitrate is derived from terrestrial aerosol sources (Prospero and Savoie 1989); however, it should also be noted that wet deposition (rainfall) can, at times, contribute

at least as much N and Fe as dry deposition (Herut et al. 1999; Nadim et al. 2001; Paerl et al. 2002). Atmospheric (mostly aerosol) deposition also supports marine productivity in the oligotrophic Red Sea and the Mediterranean Sea, where it supplies bioavailable N and P (Chen et al. 2007; Paytan et al. 2009; Herut et al. 1999), is an important source of new (non-regenerated) N to mesotrophic coastal areas (Paerl and Fogel 1994; Valigura et al. 1996; Jickells 1998; Herut et al. 1999), and has been an important source of Fe in high nutrient low chlorophyll (HNLC) regions over geologic timescales (Martin and Fitzwater 1988).

The extent to which atmospheric deposition contributes to production in highly productive coastal upwelling areas, such as the California coast, has not been elucidated. Coastal areas account for only 15% of the ocean surface area, but are responsible for half of global marine primary production (Wollast 1991) and support up to 90% of global fish catches (Pauley et al. 2002). High productivity in upwelling regions results from introduction of deep-water nutrients, principally N, to the euphotic zone where they are taken up by phytoplankton (Chavez and Messie 2009; Codispotti et al. 1982). However, because they are located along continental margins, many upwelling regions also receive substantial amounts of nutrients via atmospheric deposition. It is therefore important to estimate the contribution of atmospheric deposition to new N in these regions. This contribution could be important during non-upwelling periods when deep water N inputs are small.

Monterey Bay is an open, deep embayment (>1000m) on the central coast of California. Euphotic zone depths typically range from 30 to 60m, while mixed layer depths are generally somewhat shallower (10 to 40m, Oliveri and Chavez 2000).

Three long-term oceanographic observational stations are located in Monterey Bay (**Figure 1A**). Station M0 is closest to shore and is most influenced by coastal and within-bay processes. M1 is situated directly downstream of a major upwelling current, and M2 is the most oceanic of the stations and is less influenced by seasonal upwelling (Pennington and Chavez 2000).

In this study, we assessed the importance of dry and wet deposition in supporting primary productivity in the California upwelling system. We used soluble nutrient measurements from locally-collected aerosol particles (PM₁₀) together with an atmospheric deposition model to (1) estimate the flux of new N and other nutrients from dry deposition, and (2) identify differences in nutrient content for aerosol particles originating from different geographical sources. Phytoplankton growth experiments are used to demonstrate the bioavailability of N from these aerosol samples. We used oceanographic, atmospheric, and satellite data to (1) characterize the relationship between the timing and extent of dry deposition and chlorophyll abundance, and (2) demonstrate spatial and temporal differences in the relationship between dry deposition and phytoplankton growth in coastal and offshore waters.

METHODS

Aerosol Particle Collection

Aerosol particle samples were collected using a Dichotomous Partisol-Plus sequential air sampler (Model 2025, Thermo Scientific) located at the Monterey Bay Aquarium Research Institute from June 2008 through January 2009. Each sample represents aerosol particles collected continuously over two days. The sampler was

placed in a remote area at the site, removed from the direct local impact that could potentially contaminate the samples (e.g. proximity to parking lots and roads). The sampler was located about 10 meters above ground and 30 meters from the shore line and had an airflow rate of 1.67 L min^{-1} for collecting particulate matter 2.5-10 μm in diameter (the “coarse” fraction) and a flow rate of 15.0 L min^{-1} for particulate matter <2.5 μm in diameter (the “fine” fraction). Aerosol particle samples were collected on 47-mm glass fiber filters (Whatman). Prior to sample collection, filters were ashed at 450°C for 5 hours, soaked for 2 days in trace metal grade hydrochloric acid (Sigma), soaked (1 day) and thoroughly rinsed with MilliQ water, dried in a laminar flow hood, and stored individually in acid cleaned polystyrene petri dishes inside new plastic bags. Filters and petri dishes were weighed together before and after sample collection, and the aerosol particle mass on the filter was calculated as the difference. Samples were stored frozen prior to analysis. Our aerosol concentrations (mg m^{-3} of air) are in good agreement with data collected at terrestrial sites in northern California (Wells et al. 2007; John et al. 1973; Herner et al. 2005), lending support to their credibility and lack of local contamination.

Aerosol Particle Chemistry

A total of 14 and 11 sampling dates were randomly selected from the summer and winter filter sets respectively, and the fine and coarse filter samples for each date were extracted separately for a total of 50 extracts. All sample processing was conducted within a laminar flow hood in a clean lab using acid cleaned equipment and storage bottles. The soluble fraction was extracted from the aerosol particle samples

following Buck et al (2006). An aerosol particle sample (e.g. the 47-mm filter) was placed on an acid washed filter tower, and 100 mL MilliQ water was filtered through the sample allowing 10 s of exposure under gentle vacuum pressure. (This method extracts >99% of soluble ions in the first 100 mL of water based on successive filtrations with the same filter (Buck et al. 2006)). Soluble N concentrations are similar in extractions using MilliQ water and seawater (Buck et al. 2006; Chen et al. 2006).

Five operational filter blanks were analyzed along with the sample filters, and their average filtrate concentrations were subtracted from the sample nutrient concentrations as described below. A 10 mL aliquot of each filtrate sample was analyzed for total oxidized nitrogen (NO_x) and ammonium (NH_4) following Hansen and Koroleff (1999) on a flow injection autoanalyzer (FIA, Lachat Instruments Model QuickChem 8000). The FIA was fully automated, and peak areas were calibrated using standards prepared in MilliQ water over a range of 0–60 $\mu\text{mol L}^{-1}$ for NO_x and 0–15 $\mu\text{mol L}^{-1}$ for NH_4 . The detection limits based on three times the standard deviation of 5 blank (pure MilliQ water) measurements were 0.42 $\mu\text{mol L}^{-1}$ for NO_x and 0.24 $\mu\text{mol L}^{-1}$ for NH_4 .

A 10 mL aliquot of the aerosol filtrate was concentrated 10-fold by evaporation to dryness at 55°C in a trace metal clean Teflon tube and re-suspension in 1 mL of 2% trace metal grade nitric acid. These concentrated samples were analyzed for sodium (Na), iron (Fe) and total soluble phosphorus (P). Peaks were calibrated using standards prepared in 2% nitric acid over a range of 1–10 ppm. The detection limits based on three times the standard deviation of eight 2% nitric acid blank

measurements were $11.249 \mu\text{g L}^{-1}$ Na, $0.412 \mu\text{g L}^{-1}$ Fe, and $0.71 \mu\text{g L}^{-1}$ P. Our measurements report soluble Fe concentrations in pure water; however, Fe solubility in seawater might be lower than in pure water (Spokes and Jickells, 1996; Buck et al. 2006; Chen et al 2006; Bonnet and Guieu, 2004). Moreover, Fe arriving on the ocean surface is removed rapidly through precipitation and scavenging in addition to biological uptake by phytoplankton and bacteria. Accordingly, our estimates of soluble Fe deposition and uptake therefore represent an upper limit of bioavailable Fe enrichment by aerosol particles to surface waters.

Air Mass Back Trajectories and Wind Directions

Seven-day air mass back trajectories were generated via a kinematic trajectory analysis using atmospheric data collected at 291 stations worldwide following NCEP (National Centers for Environmental Prediction) analyses <http://croc.gsfc.nasa.gov/aeronet/index.html>. Error in the AMBT simulation increases as the model steps further back in time. The AMBTs are therefore useful as a general guide for air mass provenance, particularly for days immediately preceding the date entered in the model. Sea level AMBTs were determined for the Monterey Bay AERONET (AERosol RObotic NETwork) station (36.59255N, 121.85487W). Daily *in situ* wind velocity data were obtained from the live access server for station M2 (<http://www.mbari.org/oasis/>).

Estimation of Dry Deposition Nutrient Fluxes

The dry deposition speed of an aerosol particle is the sum of its sedimentation speed (V_s) and its dry deposition against aerodynamic and diffusion resistances at the air-water interface. The sedimentation speed for particles less than 20 μm can be calculated by the following equation (Jacobson 2005):

$$V_s = \frac{2r^2(\rho_p - \rho_a)g}{9\eta}G \quad (1)$$

Where r is the particle radius (cm), ρ_p and ρ_a are the densities of the particle and air respectively (g cm^{-3}), η is the dynamic viscosity of air ($\text{g cm}^{-1} \text{s}^{-1}$), g is the acceleration due to gravity (cm s^{-2}), and G is the Cunningham slip-flow correction factor (Cunningham 1910; Davies 1945; Jacobson 2005). (G makes the equation valid for both Stokes and slip flow). An average particle density of 2.5 g cm^{-3} was assumed for all aerosol particles (Lewis and Schwartz 2006; Chen et al. 2007), because particles in our samples were likely dominated by mineral dust and sea-salt based on composition and air mass back trajectory analysis.

For the coarse aerosol fraction comprising particulate aerosols between 2.5 and 10 μm , the effect of gravity supersedes the effect of resistance at the boundary layer, and dry deposition is dominated by the sedimentation speed, V_s . As the exact grain size distribution for each aerosol sample was unknown, we assumed a dry deposition speed of 0.8 cm s^{-1} for the coarse fraction based on equation 1 for particles 10 μm in diameter. This speed is similar to values found for other regions (Chen et al. 2007; Chen et al. 2008). The dry deposition speed for particles 2.5 μm in diameter was approximately 0.05 cm s^{-1} ; therefore, the maximum possible error associated with our

estimate would be 16-fold if all of the particles in the coarse fraction were 2.5 μm in diameter (unlikely). Sea spray also contributes to coastal aerosols. The maximum possible error associated with our density assumption of 2.5 g cm^{-3} would overestimate dry deposition speed by 2-3 fold if all aerosol particles were sea spray, which has the same density as seawater (1.03 g cm^{-3}). Under the same atmospheric conditions assumed in our calculations, a model by Slinn and Slinn (1980) predicts a dry deposition speed of 3.0 cm s^{-1} , and Williams (1982) predicts a speed of $\sim 1.0 \text{ cm s}^{-1}$ for particles 10 μm in diameter. Therefore, while 0.8 cm s^{-1} is a high-end estimate based on particle size using equation 1, it is conservative compared to other values that have been assumed for dry deposition speed of particles on natural waters (e.g. Duce et al. 1991; Buck et al. 2006).

For particles below 1 μm , dry deposition is dominated by diffusion rather than gravitational forces, and is calculated based on the particle's aerodynamic resistance (determined by the friction wind speed, height above the sea surface, the surface roughness length of the particle, and a potential temperature gradient) and the resistance to molecular diffusion in the laminar sublayer (determined by the surface roughness length for momentum, kinematic viscosity, mass diffusivity, thermal diffusivity, and friction wind speed.) Chen et al. (2007) showed that very similar velocities (within 10%) were predicted for small particles of different sizes (e.g. particles $< 2.5 \mu\text{m}$ within the fine fraction) using the model by Jacobson (2005). Accordingly, we assumed a dry deposition speed of 0.05 cm s^{-1} for the fine fraction based on equation 1 for particles 2.5 μm in diameter. The dry deposition speed decreases with particle diameter, reaching a minimum for particles $\sim 1 \mu\text{m}$ in diameter.

Dry deposition speeds increase with decreasing particle diameter for particles $<1\ \mu\text{m}$ because diffusion resistances dominate deposition speeds rather than gravity. The dry deposition speed for particles $1\ \mu\text{m}$ in diameter is $0.01\ \text{cm s}^{-1}$; therefore, the maximum possible error associated with our estimate would be 5-fold if all of the particles in the fine fraction were $1\ \mu\text{m}$ in diameter (unlikely). Similar to the coarse fraction, our estimate is conservative compared to estimates from Slinn and Slinn (1980) and Williams (1982), which predict speeds of approximately $0.2\ \text{cm s}^{-1}$ under the same conditions for particles $\sim 2.5\ \mu\text{m}$ in diameter.

The flux for each nutrient was calculated as the product of the dry deposition speed and the direct determination of the water soluble concentration of the nutrient in each aerosol sample (**Table 1**). By separating calculations for nutrient fluxes from the coarse and fine fraction measurements, errors stemming from uneven distribution of nutrients between these fractions were minimized. For example, NH_4 and some trace metals generally occur in higher concentrations in fine fractions from anthropogenic high temperature combustion emissions (Church et al. 1990; Heubert et al. 1998; Spokes et al. 2001; Jickells et al. 2003), while nutrient species like NO_3 , PO_4 , and other metals are generally associated with the coarse aerosol fraction (Savoie and Prospero 1982; Spokes et al. 2000; Duce et al. 1991; Prospero et al. 1996).

Our flux estimates are for water soluble nutrients in particulate aerosols but may also include input from gaseous nitrate (as HNO_3), which can contribute substantially to the total N input from dry deposition (Kouvarakis et al. 2001). Efficient scavenging of HNO_3 occurs when cellulose or glass fiber filters are used (Appel et al. 1980; Savoie and Prospero 1982; Prospero and Savoie 1989; Schapp et

al. 2004), and can be as high as 100% when aerosol sea salt content is high (Appel et al. 1980; Appel 1981). HNO_3 contributes <10-30% to total NO_3 in the marine boundary layer (Savoie and Prospero 1982; Huebert 1980). Accordingly, soluble NO_x measurements in our samples could represent up to 30% input from HNO_3 , particularly in samples with higher proportions of sea salt.

In contrast to adsorption of NO_3 , volatilization of ammonium nitrate from the filter can underestimate soluble nitrate measurements, particularly in samples with low aerosol masses (Wang and John 1988) and under ambient temperatures greater than 25°C (Schapp et al. 2004). While we cannot quantify the error from volatilization, we expect it to be small compared to the N concentrations in particulate aerosols given the moderate temperatures at the California coast throughout the year. Further, the relatively high particle load recorded for the majority of coarse fraction samples would minimize volatilization in these sample sets (e.g. <10% error; Wang and John 1988). Volatilization may play a larger role (up to 85-95% loss) in the fine aerosol fraction due to lower overall particle loading; accordingly, our estimates should be taken as a lower limit for the dry deposition of new N to coastal California, particularly for the fine aerosol fraction.

In situ data

In situ surface Chl *a* measurements were obtained from the three long term monitoring stations in Monterey Bay (M0, M1, and M2) where they were taken approximately every three weeks, and were measured fluorometrically as described elsewhere (Pennington and Chavez 2000; data courtesy R. Michisaki and F. Chavez).

Daily upwelling index data were obtained from the National Oceanic & Atmospheric Administration (NOAA) Southwest Fisheries Science Center live access server for the Pacific coast at 36°N 120°W (http://las.pfeg.noaa.gov/las6_5/servlets/dataset).

Wet deposition data were obtained from the National Atmospheric Deposition Program database for station CA66, located at Pinnacles National Monument in San Benito County, CA (36.4834°N, 121.157°W, elevation 317 m). Monthly precipitation measurements and annual inorganic N ($\text{NH}_4 + \text{NO}_3$) deposition values were obtained for 2002-2009. N depositions were computed by multiplying the precipitation-weighted mean N concentration (mg/L) for samples meeting the QAQC and data completeness criteria by the total precipitation in centimeters for the summary period. QAQC and data completeness criteria are described on the programs website, <http://nadp.sws.uiuc.edu>.

El Niño Southern Oscillation (ENSO) Indices

Two monthly indices of the El Niño Southern Oscillation (ENSO) were used. The Multivariate ENSO Index (MEI) is calculated from sea-level pressure, zonal and meridional components of the surface wind, sea surface temperature, surface air temperature, and total cloudiness fraction of the sky. MEI data were obtained from the NOAA Earth System Research Laboratory (<http://www.cdc.noaa.gov/people/klaus.wolter/MEI/>). The Southern Oscillation Index (SOI) is based on air pressure differences between Tahiti and Darwin Islands, and SOI data were obtained from the Australian Government Bureau of Meteorology (<http://www.bom.gov.au/climate/current/>). The time series includes data from 2002 -

2009 to overlap with the MODIS record used in our analyses (2002-2008) and to encompass the period during which our particulate aerosol samples were collected (2008-2009).

MODIS Satellite data

Aerosol optical thickness (AOT, 869 nm) and Chl *a* (OC3 algorithm) were determined from satellite images taken by the Moderate Resolution Imaging Spectroradiometer (MODIS) satellite for July 2002-June 2008 at a resolution of 1 km. The MODIS viewing swath width is 2,330 km and scans the entire surface of the Earth every one to two days. A total of 2208 level 2 data files, (each containing AOT and Chl *a* data) were processed to level 3 using SeaWiFS Data Analysis System (SeaDAS) software by applying identical processing scripts to all files as follows. Each data file was projected, generating new individual image files for AOT and Chl *a*. This step yielded a total of 4416 files. Projected files were binned into 8-day groups, images of low quality (e.g. periods with extensive cloud cover) were removed, and each bin was averaged to create a composite image that represented one 8-day 'week'. This step yielded a total of 552 images, i.e. 276 separate 'weekly' images for each of the parameters.

Aerosol optical thickness and Chl *a* were quantified identically in all composite images. Three areas were designated using the blotch analysis function in SeaDAS. Each blotch was a circular region ($\sim 600 \text{ km}^2$) centered on each of the three long-term in situ Monterey Bay monitoring sites M0, M1, and M2 (**Figure 1B**). The histogram function was applied to each blotch and the mean value for each composite

image was recorded. This process was manually repeated for all of the AOT and Chl *a* images. To test if there was a correlation between the timing and magnitude of aerosol optical thickness and Chl *a*, regression analysis of MODIS data was performed. Annual time series, paired correlations, and time-lagged correlations of the composite data were made for each season. "Summer" and "winter" were defined based on annual mean wind stress data from 2002-2008 collected at an offshore mooring in Monterey Bay, which shows the winds are from the northwest March through November (weeks 12-37), with intermittent southerly winds November through early March (weeks 1-11 and 38-48).

A potential caveat in computing satellite-derived Chl *a* data is that thick aerosol layers can cause overestimation of Chl *a* by the satellite algorithms due to enhanced backscatter of the wavelengths used to measure Chl *a*. A study by Volpe and coworkers (2009) explored this issue in the Mediterranean Sea, showing that significant correlations between aerosol optical thickness and satellite-derived Chl *a* levels were not always supported by *in situ* Chl *a* measurements. It was therefore necessary to compare the 8-day averaged Chl *a* levels from MODIS with *in situ* surface measurements of Chl *a* from the long-term monitoring program in Monterey Bay that were collected at roughly 3 week intervals. The agreement between the *in situ* and satellite data was acceptable with R^2 values of 0.52, 0.38, and 0.49 for stations M0, M1, and M2 respectively ($p < 0.05$ for all stations). However, regression statistics indicated that MODIS tended to overestimate Chl *a* slightly, particularly at locations closer to shore. The regression slope (m) approached 1 (i.e. when MODIS perfectly predicts *in situ* Chl *a* levels) with increasing distance from shore, but overestimates

Chl *a* ($m < 1$) closer to shore ($m = 0.58, 0.84$, and 0.97 for stations M0, M1, and M2 respectively).

This discrepancy in predictive power likely stemmed from the MODIS atmospheric correction algorithm, which can yield artificially high Chl *a* values in turbid waters and waters containing high levels of colored dissolved organic matter (CDOM), both of which are more prevalent closer to shore. Another possible reason for the discrepancy included the larger spatial and temporal range of values included in the satellite estimates (due to blotch size and image averaging, respectively), whereas *in situ* measurements were collected at discrete locations and times. Moreover, *in situ* measurements provide surface water Chl *a* levels only, whereas MODIS integrates deeper within the water column (down to 1 optical depth).

Phytoplankton growth experiments

To determine the bioavailability of N from dry deposition to phytoplankton endemic to coastal California, culture experiments were conducted with three cultured strains of phytoplankton isolated from the southern coast of California, and with natural populations of phytoplankton in Monterey Bay. For the culture work, *Synechococcus nigra* CCMP 1284 (collection site: Scripps Institute of Oceanography, 32.8504N 117.2525W) and *Thalassiosira weissflogii* CCMP 1050 (collection site: Del Mar Slough, CA 32.9660N 117.2510W) were obtained from the Provasoli-Guillard National Center for Culture of Marine Phytoplankton (CCMP). *Synechococcus* strain CCMP 2515 (collection site: CalCOFI cruise 93204, 31.9001N 124.1668W) was provided by K. Pennebaker and J. Zehr. Cultures were maintained in F/2 media. Prior

to the experiment, cultures were diluted ten-fold into media without added N (F/2 – NO₃) until stationary growth phase was reached (several days). This step was included to draw down residual N in the inoculum. Cultures were then transferred into fresh media amended with either a full complement of F/2, including NO₃, or F/2-NO₃ plus natural particulate aerosol extract from samples collected at Monterey bay. The final NO_x concentration was ~50mg L⁻¹ in aerosol treatment and ~55mg L⁻¹ in F/2 with NO₃ treatment. The amount of aerosol added was calculated to yield aerosol-NO_x similar to the amount of NO₃ in the F/2 media. Treatments were conducted in triplicate. The optical density of the cultures at 750 nm (OD750) was used to evaluate daily cell growth during the 6 day incubation period.

An incubation experiment was also conducted with natural assemblages of phytoplankton from Monterey Bay beginning October 4, 2009 aboard the Research Vessel John Martin. Surface water (1 m depth) was collected from northeast Monterey Bay (36°48.168N 121°48.268W) at midday near the edge of the “red tide incubator” region (Ryan et al. 2008), where moderately high standing stocks of dinoflagellates generally persist. The following treatments were immediately made: “control” which had no addition, “nitrate” which had 25 µM NaNO₃ added, and “aerosol” which had 1 mg L⁻¹ particulate aerosol added. Treatments were conducted in triplicate in acid washed polycarbonate bottles that were thoroughly rinsed with surface sample water before use. Bottles were kept in an on-deck incubator through which surface water from the Bay was continually pumped to maintain ambient temperature within the Bay. A neutral density shade was used to attenuate sunlight by 50%. After 30 h, Chl *a* was measured according to Mackey et al (2009) with the

following modifications: 100 mL aliquots were removed from each bottle and filtered under gentle pressure onto GF/F filters (Whatman). Filters were frozen at -80°C. Chlorophyll extractions were performed for 24 h at 4°C in the dark using 90% acetone, and fluorescence was measured on a Turner fluorometer (Turner Designs 10-AU-005-CE) before and after acidification with 3.7% HCl. Fluorescence was converted to Chl *a* concentration according to JGOFS Protocols (1994).

Particulate aerosols used in the incubation were collected as described above, and included both fine and coarse fractions. As with the culture experiments, we emphasize that the goal of the experiments was only to determine if the N in dry deposition was bioavailable to phytoplankton in this region. We therefore used relatively large particulate aerosol and NO₃ additions such that we would be able to see a measurable increase in Chl *a* during the experiment. The NO₃ concentration was selected based on typical NO₃ levels following upwelling in the Bay, and the amount of particulate aerosol added was chosen to roughly double the background concentration of NO_x in the seawater from ~0.5 μmol L⁻¹ to ~1 μmol L⁻¹. While this amount of aerosol is higher than would be expected for typical dry deposition events in coastal CA, we emphasize that the goal of the experiment was to determine the bioavailability of N in dry deposition, not to test the effects particulate aerosols using typical deposition rates.

RESULTS

Air mass sources, particulate aerosol loads, and nutrient fluxes

Air mass provenance was determined for summer and winter based on a representative year of wind velocity data collected at station M2 in 2005. Air mass back trajectory (AMBT) analysis of sea level air masses indicated that during the summer, the majority of air masses originated over the North Pacific Ocean and traveled in a southeastern direction parallel to the California coast before arriving at Monterey Bay, consistent with wind speed data recorded at station M2 (**Figure 2A**). Winter AMBTs had diverse origins, reflecting the heterogeneous wind patterns recorded at M2 during winter months (**Figure 2A**). Notably, in the winter about half of the air masses arrived from land (i.e. headed from east to west), while in the summer the vast majority (~93%) arrived from the ocean (i.e. headed from west to east) (**Figure 2A**). **Figure 2B** shows several examples of 7 day AMBTs that occurred during our particulate aerosol collection period.

Particulate aerosol composition showed marked differences between seasons and different size fractions. Total suspended particle (TSP) concentrations ($\mu\text{g m}^{-3}$) determined from all samples collected during the sampling period (i.e. not limited to the 50 extracted filters) were slightly higher in the summer than winter (**Table 1**, **Figure 3**), and higher for the coarse aerosol fraction than the fine fraction (**Figure 3**). NO_x , NH_4 , and soluble P concentrations were higher in the winter than in the summer ($p < 0.05$), though summer particulate aerosols had higher amounts of Na than in winter ($p < 0.05$; **Table 1**). The ratios of NO_x to P were higher in fine aerosol fractions than in coarse fractions (**Figure 4**). Mean NO_x :P values were similar for winter and summer

in the coarse fraction (~140), whereas fine fraction mean values were higher in winter (~500) than summer (~320). The majority of N deposition was attributed to NO_x, although NH₄ also contributed substantial N. The coarse fraction contributed more N deposition than the fine fraction, and N deposition was slightly higher in winter than summer (**Table 2**).

Time series data

As expected over this relatively small area, the AOT levels were similar for all three monitoring sites at all times of the year (**Figure 5**). Aerosol layers generally were thickest in March through June (**Figure 5**), in agreement with *in situ* measurements that showed higher particulate aerosol concentrations in the summer (**Figure 3**). MODIS-derived Chl *a* concentration for the same time interval for the 3 stations are also shown in **Figure 5**, and **Figure 6** shows annual averages of the AOT and Chl *a* data for the three stations. Chl *a* levels were higher closer to shore, and were higher in summer than winter for all sites.

Zonal and meridional components of wind speed (**Figure 5D, E**) were consistent with AMBT model outputs (**Figure 2**), and indicated that the wind trajectory was predominantly in the southeast direction during summer months. No consistent trajectory was observed for winter.

Maximum monthly precipitation (**Figure 5F**) ranged up to ~20 cm per month during the winter, whereas precipitation was negligible during the summer. N input from wet deposition at the closest NADP station averaged 74, 112, 68, 90, 80, 47, and 90 $\mu\text{g N m}^{-2} \text{ d}^{-1}$ for 2002, 2003, 2004, 2005, 2006, 2007, and 2008 respectively, or

$80 \pm 8 \mu\text{g N m}^{-2} \text{ d}^{-1}$ on average based on annually averaged precipitation levels and N contents.

Long-term monthly averages of daily upwelling indices show that upwelling occurred mostly throughout the spring and summer, and was greatest during May through July (**Figure 7**). Upwelling relaxes and occasionally reverses (i.e., downwelling occurs) during the winter months.

Correlations between AOT and Chl *a*

Seasonal differences in the relationship between AOT and Chl *a* might be expected due to different air mass provenances and variable input from other nutrient sources (e.g. upwelling, runoff) in different seasons. No significant relationships were identified for winter at any of the stations based on regression analysis of MODIS data. A statistically significant relationship was identified for stations M1 ($p=0.028$, $n=125$) and M2 ($p=0.004$, $n=122$) during the summer, and indicated that 3.9-6.6% of the variability in Chl *a* at these stations correlated with AOT (**Table 3**). Correlations were not improved for regressions with one week time-lagged data.

However, because regression analysis cannot prove a causal relationship between two data sets that co-vary, it is possible that the co-variance of AOT and Chl *a* was due to their mutual dependence on a third variable. For example, higher wind speeds would be expected to bring more aerosol particles but would also potentially cause more upwelling. To test if the correlation between AOT and Chl *a* existed during periods when the nutricline is suppressed and deepwater nutrients are less abundant, we performed the regression using data only from El Niño periods during

the record (**Figure 8**). Significant relationships were identified for all three stations during El Niño periods (**Table 3**), where AOT accounted for 0.1%, 4.3%, and 11.3 % of the variance in Chl *a* levels at stations M0, M1, and M2 respectively.

Phytoplankton growth experiments

Culture experiments with phytoplankton isolated from coastal California showed similar positive growth with NO₃ and with natural aerosol particles collected near Monterey Bay (**Figure 9**). While growth was not significantly different ($p < 0.05$) between treatments for each strain at all time points during the 6 day experiment, it appears that growth of *Thalassiosira* and *Synechococcus* 2515 cultures receiving particulate aerosols was beginning to decline by day 6. *Synechococcus* 1284 showed a ~3 day lag period in replicates receiving NO₃, whereas the lag period was ~4 days in all replicates receiving particulate aerosols as the sole source of N.

Natural phytoplankton assemblages from Monterey Bay were also able to grow using N from particulate aerosols. The dinoflagellates *Ceratium furca* and *Ceratium divaricatum* var. *balechii* accounted for the vast majority of phytoplankton cells in our sample water, though smaller populations of *Pseudo-nitzschia australis* were also observed. At the start of the incubation the baseline Chl *a* level was 26 mg m⁻³, and after 30 h the control (25 mg m⁻³) was not statistically different ($p < 0.05$) than baseline (**Figure 10**). In contrast, Chl *a* increased significantly relative to control and baseline levels in the other treatments, reaching 40 mg m⁻³ in the nitrate treatment and 34 mg m⁻³ in the particulate aerosol treatment.

DISCUSSION

Atmospheric deposition of N in coastal CA

Seasonally weighted particulate aerosol concentrations (total suspended particle, TSP) at Monterey Bay ranged from 14-160 $\mu\text{g m}^{-3}$ (**Table 1**), and were similar to values reported for other terrestrial sites within northern (Wells et al. 2007; John et al. 1973; Herner et al. 2005) and southern California (Chow et al. 1994), but were 1-2 orders of magnitude more concentrated than over the open Pacific Ocean (Uematsu et al. 1983). The annual dry deposition rates based on our data (24 and 34 $\text{mg m}^{-2} \text{d}^{-1}$ for winter and summer respectively; **Table 1**) were 2-10 fold higher than modeled average deposition rates for the region ($\sim 1.4\text{-}14 \text{ mg m}^{-2} \text{d}^{-1}$; Mahowald et al. 2005), likely because the model also integrates low concentration TSP measurements from the open Pacific Ocean (Uematsu et al. 1983).

In summer, winds generally traveled southeast along the coast before reaching Monterey Bay (**Figure 2, Figure 5D, E**). Summer particulate aerosol samples traversing open water contained less soluble N and P but higher proportions of sea salts (**Table 1**), whereas in winter, when westward winds were more common (**Figure 2A, Figure 5E**), concentrations of soluble N and P were higher, possibly owing to more frequent over-land trajectories that incorporate more nutrient-rich crustal and anthropogenic material. Our particulate aerosol nitrate plus nitrite (NO_x , 0.14-1.2 $\mu\text{g N m}^{-3}$) and NH_4 (0.11-1.2 $\mu\text{g N m}^{-3}$) concentrations were on the low end of published ranges for terrestrial sites in California (Herner et al. 2005), likely because our coastal site is more removed from anthropogenic N sources. As would be expected from particulate aerosols collected closer to land, NO_x and NH_4 concentrations were

approximately an order of magnitude higher in our samples than in those collected over the Pacific Ocean (Parungo et al. 1986; Quinn et al. 1990; Buck et al 2006). Soluble Fe ranged from 1.7-10.7 ng m⁻³ in summer and 4.3-15.3 ng m⁻³ in winter, and was slightly higher than for samples collected from the North Pacific Subtropical Gyre (Buck et al. 2006).

Aerosol particle addition as a sole source of N in laboratory experiments stimulated growth of cyanobacteria and diatoms (**Figure 9**). Moreover, natural populations showed increased Chl *a* following nitrate and particulate aerosol additions (**Figure 10**). The dominant species in our incubation, *C. furca* and *C. divaricatum* var. *balechii*, are both common bloom formers that are observed frequently in Monterey Bay (Ryan et al. 2008). The increased growth and Chl *a* observed in these experiments suggest that N in dry deposition is bioavailable to phytoplankton present in coastal California water.

To determine the contribution of N from atmospheric deposition to overall new production in this region, we calculated the combined input of NO_x and NH₄ from aerosol particles <10 µm using calculated deposition rates and the representative mixed layer depth for each season. For these estimates we define atmospheric deposition here as wet plus dry deposition (excluding deposition of gases), and assume that all of the soluble NO_x and NH₄ are used by phytoplankton and that none is removed by bacteria or other processes) These calculations indicate that dry deposition provides 123 µg N m⁻² d⁻¹ in summer and 164 µg N m⁻² d⁻¹ in winter. A seasonally weighted average gives a dry deposition supported new production estimate of 133 µg N m⁻² d⁻¹, or 10.3 µg N m⁻³ d⁻¹, assuming mixing depths of 10 m and 40 m in the

summer and winter, respectively (Olivieri and Chavez 2000). Wet deposition during the winter months contributes an additional $79 \mu\text{g N m}^{-2} \text{d}^{-1}$ ($2.0 \mu\text{g N m}^{-3} \text{d}^{-1}$), giving a combined deposition (dry plus wet) of $213 \mu\text{g N m}^{-2} \text{d}^{-1}$ ($12.3 \mu\text{g N m}^{-3} \text{d}^{-1}$). Compared to estimates of new production for Monterey Bay under average annual conditions (Kudela and Chavez 2000; **Table 4**), atmospheric deposition of N to offshore waters provides 0.11-0.24% of new N on an annual basis. We note that these are minimal estimates because they are based on NH_4 and NO_x and do not include other forms of bioavailable N present in atmospheric deposition. For example, if gaseous N, which we did not measure directly, is important (Kouvarakis et al. 2001) we may be underestimating the N input. Similarly, organic N may account for ~30% of atmospheric N (Cornell et al. 1995; Peierls and Paerl 1997; Cornell et al. 2003), of which 20-30% is bioavailable to marine phytoplankton (Peierls and Paerl 1997). If atmospheric deposition in coastal California contains similar proportions of bioavailable organic N deposition (e.g. an additional $91 \mu\text{g N m}^{-2} \text{d}^{-1}$, of which $18\text{-}27 \mu\text{g N m}^{-2} \text{d}^{-1}$ is bioavailable), then atmospheric deposition of N to offshore waters would provide up to 0.12-0.27% of new N on an annual basis.

Atmospheric N deposition (including organics) would support productivities of $0.8 \text{ mg C m}^{-2} \text{d}^{-1}$ in the summer and $1.5 \text{ mg C m}^{-2} \text{d}^{-1}$ in the winter, based on average deposition rates and assuming a Redfield C:N ratio of 106:16. We note that natural variability exists in phytoplankton elemental stoichiometries. C:N ratios as low as ~4.5 have been observed in Monterey Bay (Kudela and Dugdale 2000), although most phytoplankton C:N ratios are less than 8.7 during balanced growth (Geider and LaRoche 2002). Our estimates could therefore potentially over- or underestimate the

amount of productivity by ~25%. The Redfield value we use represents a mid-range value for C:N and is also consistent with the assumptions used by Kudela and Chavez (2000) to estimate overall new production in Monterey Bay that we use in **Table 4**.

Although, on an annual average, N in atmospheric deposition contributes a small portion of new production, the role may be more significant during non-upwelling periods. The particulate aerosol NO_x :P ratios in our particulate aerosol samples (**Figure 4**) were approximately an order of magnitude greater than the ratio required for phytoplankton growth (16N:1P). Complete utilization of N from particulate aerosols is likely during non-upwelling periods, when productivity in Monterey Bay is N limited (Kudela and Dugdale 2000). Moreover, N input may increase substantially when large deposition events occur (e.g. the mean depositional flux of PM10 aerosols for summer was $34 \pm 2 \text{ mg m}^{-2} \text{ d}^{-1}$, whereas the maximum flux was $89 \text{ mg m}^{-2} \text{ d}^{-1}$, approximately 2.6 fold higher than the average.) Atmospheric deposition therefore could support 9% of new production during low productivity winter days with average deposition rates, and potentially up to 20% of new production when dry deposition is maximal (**Table 4**). Primary production in Monterey Bay also varies substantially from day to day depending on season (Pennington and Chavez 2000), and is as low as $20\text{-}50 \text{ mg C m}^{-2} \text{ d}^{-1}$ during non-upwelling periods (Bac et al. 2003). Atmospheric deposition could therefore support up to 7.5% of primary production during such low-productivity days, but could be up to 13% of primary production on days with high deposition and no nutrient input from upwelling.

During upwelling events, production rates increase dramatically, reaching over $1000 \text{ mg C m}^{-2} \text{ d}^{-1}$ (Bac et al 2003; Pennington and Chavez 2000). Clearly atmospheric N deposition (mostly dry deposition during the spring and summer) would support only a minor component of total primary production during upwelling periods. However, similar to some high N low chlorophyll (HNLC) regions (Martin and Fitzwater 1988; Coale et al. 1996; Boyd et al. 2000), there is compelling evidence that primary production at such times is limited by Fe rather than N along some sections of the California coast. For example, during the summer and fall upwelling sustains elevated nitrate levels while iron is drawn down along parts of the coast (Johnson et al. 2001; Chase et al. 2005), and Hutchins and Bruland (1998) demonstrate that addition of nanomolar quantities of Fe to near shore waters promotes blooms of chain forming diatoms and results in the complete drawdown of seawater nitrate.

Typical upwelled water brings $20 \text{ } \mu\text{mol L}^{-1} \text{ NO}_3$ to the surface ocean in coastal California (Pennington and Chavez 2000). Assuming a cellular Fe:C ratio of $20 \text{ } \mu\text{mol Fe per mol C}$ (Sunda and Huntsman 1995; Bruland et al. 2001) and a Redfield C:N ratio, phytoplankton would require $\sim 133 \text{ } \mu\text{mol Fe per mol N}$ (Bruland et al. 2001). The average flux of soluble Fe in our samples ($1.5 \text{ } \mu\text{g m}^{-2} \text{ d}^{-1}$) could therefore support an uptake of $2.9 \text{ mg N m}^{-2} \text{ d}^{-1}$ ($0.29 \text{ mg m}^{-3} \text{ d}^{-1}$ assuming a 10 m mixed depth), or the equivalent of $\sim 1.9\%$ of new production at offshore stations M2, during high productivity upwelling periods (**Table 4**). On days with high dry deposition, the Fe supplied could support up to 5% of new production during the upwelling period. A more conservative Fe:C ratio of $40 \text{ } \mu\text{mol Fe per mol C}$ (Martin et al. 1976; Martin and

Knauer 1973, Bruland et al. 2001) would indicate that Fe from dry deposition could support ~0.5-1% of new production at stations M1 and M2, respectively, suggesting that even if luxury uptake of Fe occurs (Sunda and Huntsman 1995), dry deposition may still contribute to new production and possibly impact species abundance and their nutritional requirements in coastal California (Hutchins and Bruland 1998). We note that these are minimal estimates, as wet deposition of Fe has not been accounted for in our study and may contribute significant Fe (Duce and Tindale 1991).

The Aerosol and Chlorophyll Relationship Based on Remote Sensing

The calculations of the contribution of dry deposition to new production in coastal California presented above are based on a relatively small data set of particulate aerosol samples collected from June 2008 through January 2009. To determine how these data fit within the longer-term trends, we used remote sensing data of aerosol optical thickness (AOT) and chlorophyll *a* (Chl *a*) from the past 6 years (the entire MODIS data set; **Figure 5A-C**). Assuming our data of particulate aerosol chemistry is representative we see that despite higher N, P, and Fe concentrations in winter, no significant correlations were found between AOT and Chl *a* for any of the stations during the winter ($p < 0.05$; **Table 3**). This is consistent with our calculated inputs of new N from dry deposition, which were lower in winter than summer on a per volume basis because the nutrients get distributed over a deeper mixed layer in winter. In addition, nutrient inputs from precipitation and fluvial discharge increase dramatically in the winter (**Figure 5F**), contributing a larger proportion of new nutrient inputs along the coast that are likely bioavailable to

phytoplankton (Peierls and Paerl 1997). Specifically, wet deposition during the winter months contributes an additional $79 \mu\text{g N m}^{-2} \text{d}^{-1}$, or ~50% additional N than from dry deposition alone ($164 \mu\text{g N m}^{-2} \text{d}^{-1}$). Aerosol dry deposition therefore contributes a smaller relative portion of new nutrients during the winter, when wet deposition occurs, than in the summer when wet deposition is minimal. Because wet deposition is not reflected in the AOT data, rainfall may contribute to the lack of significant correlation between AOT and Chl *a* during the winter. This effect is most pronounced at the coastal site M0, where nutrient input from perennial river discharge and runoff also serve to obscure any relation between AOT (dry deposition) and Chl *a*.

In contrast, significant correlations between AOT and Chl *a* were observed for stations M1 and M2 in summer ($p < 0.05$; **Table 3**). Coastal upwelling is an episodic, wind-driven event that occurs on the order of days and then relaxes, and in Monterey Bay, is more frequent during May through July than the rest of the summer (Kudela and Chavez 2000; Olivieri and Chavez 2000; **Figure 7**). The significant AOT- Chl *a* correlation during the summer could therefore be due to co-occurrence of high aerosol particle loads and large deep water nutrient input from strong upwelling (e.g. both brought by strong winds), or could indicate a real causal relationship between dry deposition and Chl *a* that is sustained throughout the summer.

During El Niño periods, the nutricline is suppressed along the California coast, restricting intrusion of nutrients from deep water into the euphotic zone (Kudela and Chavez 2000). Indeed, global decreases in primary production have been observed following transitions between La Niña and El Niño periods (Behrenfeld et al. 2006). AOT levels were not statistically different between El Niño and La Niña years during

our period of record ($p < 0.05$). This suggests that in contrast to the Atlantic Ocean, where the North Atlantic Oscillation (NAO) is significantly correlated with AOT over the Mediterranean Sea and African coast (Moulin et al. 1997), aerosol particle concentrations along the coast of California may not be strongly influenced by interannual climate cycles (though other physical processes like upwelling and rainfall are clearly influenced).

Within our data set, significant relationships between AOT and Chl *a* were identified for all stations during El Niño periods ($p < 0.05$; **Table 3**). In addition, the trend indicates that the importance of dry deposition as a nutrient source increased with distance offshore (**Table 3**). Based on new production estimates for Monterey Bay during El Niño periods (Kudela and Chavez 2000; **Table 4**), dry deposition contributes 0.32-0.53% of new N during El Niño periods. While this is still a relatively small amount, it is over twice the amount as when all years are considered. When wet deposition is included, the contribution to new production is approximately 20-40% greater than for dry deposition alone (e.g. wet N deposition during La Niña periods ranged from 47-90 $\mu\text{g N m}^{-2} \text{ d}^{-1}$, whereas it ranged from 69-112 $\mu\text{g N m}^{-2} \text{ d}^{-1}$ during and leading into El Niño periods, (**Table 4**)).

At the coastal station M0, almost no variability in Chl *a* could be attributed to AOT during any season or ENSO condition (**Table 3**), consistent with long term monitoring that indicates near shore sites receive more nutrients from anthropogenic inputs, runoff and fluvial discharge than offshore waters. Therefore, it is possible that carryover of nutrients from near shore processes and efficient nutrient recycling is sufficient to support phytoplankton growth close to shore even during El Niño periods,

whereas phytoplankton in offshore waters, which are still within the coastal zone but further removed from these nutrient sources, may depend more on nutrients from atmospheric deposition.

While suppression of the nutricline during El Niño summers serves to increase the relative contribution of N from dry deposition, increased wet deposition and river discharge during El Niño winters would have the opposite effect. In our overall winter data set, we observed no significant relationship between AOT and Chl *a* during winter months, particularly close to shore where inputs from runoff and river discharge are more concentrated. During El Niño winters this effect is likely to be even larger. For example, during the anomalously strong El Niño conditions in winter and early spring of 1998, a 5-fold increase in Chl *a* was observed that extended from near shore to 300 km offshore (Kudela and Chavez 2004). These observations were attributed to input from the San Francisco Bay outflow, which introduced nitrate levels similar to upwelling conditions (ca 30 μM) close to shore (Friederich et al. 2002; Wilkerson et al. 2002). In such extreme El Niño winters dry deposition would play a negligible role, although the wet deposition role will increase. The greatest impact from atmospheric dry deposition during El Niño periods would be likely to occur offshore in the summer, when fluvial inputs are minimal, precipitation is negligible (**Figure 5F**), and nutrient input from deep water is suppressed. The possible transition to extended or permanent El Niño conditions in response to climate warming-induced ocean stratification (Wara et al. 2005; Sarmiento et al. 2004) may therefore increase the proportion of productivity supported in summer by dry deposition and in winter by wet deposition for coastal California and possibly other upwelling regions.

The role of dry N deposition in coastal upwelling regions

To get an order of magnitude approximation for the amount of productivity that is supported by dry deposition of N in other major upwelling regions, we calculated new production values based on dry N deposition for six other locations. The particulate aerosol concentration and N content values used in the calculations were based on midrange published data and were calculated based on annual average productivity and deposition rates (**Table 5**). Based on these estimates, dry N deposition supports between 0.04-8 % of productivity throughout the world's coastal upwelling regions. The estimate for the California coast, based on published data for central and northern California (0.4%), is within the same range as the values calculated directly from our measured data (~0.1-0.5%, **Table 1**). The estimate of productivity from dry N deposition for the northwest coast of Africa is also within this range (~ 0.1%). Similar to the North America upwelling region, the northwest coast of Africa is highly productive due to substantial upwelling events, though dry deposition is roughly an order of magnitude greater and N content is an order of magnitude lower, likely due to fewer anthropogenic N contributions to the dominant Sahara dust.

The most substantial contribution of dry deposition to productivity occurs in the Indian Ocean along the Arabian Peninsula (8 %) and the west coast of India (6%), where dry deposition is very high. Notably, the effect of total atmospheric deposition could be considerably higher, particularly during the monsoon season. The estimated productivity from dry N deposition for the west coast of Australia (1%) is lower than

for the other Indian Ocean regions, but agrees with satellite observations that aerosol optical thickness is generally lower than would be expected based on Australia's large desert. Perhaps not surprisingly based on their location in the Southern Hemisphere where aeolian particles are scarce, the southwest coast of Africa (0.04%) and the west coast of South America (0.04%) have the lowest estimates of productivity from dry N deposition among the seven major upwelling regions.

As with N deposition in coastal California, the input of N from dry deposition in these regions may be more important during large deposition events and/ or during non-upwelling periods. However, this level of detail is not possible to quantify based on the annually averaged values used in our calculations; higher resolution deposition and primary productivity data would be needed to quantify the role of dry deposition during these shorter periods. Moreover, our calculations may underestimate the actual percentage because they do not account for all bioavailable forms of N present in dry deposition (only NH_4 and NO_3 are considered), and do not consider the potential fertilizing effects of other nutrients (specifically Fe). Increased new production resulting from stimulation of N_2 fixation by nutrients in dry deposition (Mills et al. 2004) is also neglected in these calculations. As noted above, inclusion of wet deposition in these estimates would likely increase the N inputs by 40-100% (Herut et al. 1999; Nadim et al. 2001), roughly doubling our estimates of the percent of productivity supported by N deposition (e.g. up to 16% in some regions).

CONCLUSION

While the estimates made here are sensitive to a number of assumptions, they offer order of magnitude approximations for the contribution of dry N deposition to productivity in coastal upwelling zones; actual values may differ due to variations in particulate aerosol load and N content over interannual cycles. Detailed studies of particulate aerosol load and composition at each of these sites is needed to quantify the role of dry deposition with more accuracy and precision, and to determine the role of dry deposition, if any, in supporting productivity and marine food webs in coastal upwelling regions. Our data indicate that the contribution of dry deposition to highly productive coastal upwelling regions is small but not negligible, and could be important during high deposition, non-upwelling periods (e.g. up to 20% of new production in coastal California). Atmospheric nutrient sources are also more important during El Niño periods when upwelling is suppressed, a phenomenon that may become more common due to climate warming. Dry deposition alone may support up to 8% of production in other coastal upwelling regions by providing N and possibly essential Fe and other metals that are required for cell growth but that are deplete in upwelled water.

ACKNOWLEDGEMENTS

I acknowledge my co-authors Gert L van Dijken, Simran Mazloom, Andrea M Erhardt, Kevin R. Arrigo, and Adina Paytan on this manuscript, which is in review at *Global Biogeochemical Cycles*. As a group we thank M. Jacobson for advice on estimating dry deposition speeds for Monterey Bay, and K. Bruland for advice on cellular iron calculations. Thanks to F. Chavez and R. Michisaki for providing in situ chlorophyll *a* data, E. Gray, C. Buck and R. Franks for assistance in aerosol extract analysis and T.L. Kucsera (GEST) at NASA/Goddard for back-trajectories available at the aeronet.gsfc.nasa.gov website. This research was supported by CA Sea Grant and NSF grant to A.P. S.M. was a participant in the Stanford Earth Science Intern Program for high school students. K.R.M.M. was supported by the Department of Energy (DOE) Global Change Education Program.

Author contributions

KRM Mackey - planned experimental design; conducted field work; helped develop analytical methods and computer code for processing satellite data; processed samples; analyzed and interpreted data; wrote the manuscript

GL van Dijken – helped develop analytical methods and computer code for processing satellite data

S Mazloom – helped process satellite data as part of a high school summer internship

AM Erhardt – helped process aerosol extract samples

KR Arrigo – helped plan experimental design; helped interpret data; provided comments on the manuscript

A Paytan – provided funding; helped plan experimental design; helped conduct field work; helped interpret data; provided comments on the manuscript

REFERENCES

- Appel, B. R., Tokiwa, Y. & Haik, M. Sampling of nitrates in ambient air. *Atmos. Environ.* 15, 549–554 (1981).
- Appel, B. R., Wall, S. M., Tokiwa, Y. & Haik, M. (1980) Simultaneous nitric acid, particulate nitrate and acidity measurements in ambient air. *Atmos. Environ.* 14, 549–554.
- Bac MG, KR. Buck, FP. Chavez and SC. Brassell (2003) Seasonal variation in alkenones, bulk suspended POM, plankton and temperature in Monterey Bay, California: implications for carbon cycling and climate assessment. *Organic Geochemistry* **34**: 837-855
- Baker, A R, French, M, Linge, K L (2006) Trends in aerosol nutrient solubility along a west-east transect of the Saharan dust plume. *Geophysical Research Letters* 33: L07805, doi:10.1029/2005GL024764.
- Boyd, PW et al (2000) A mesoscale phytoplankton bloom in the polar Southern Ocean stimulated by iron fertilization. *Nature* 407: 695-702.
- Behrenfeld MJ, R T. O'Malley, D A. Siegel, C R. McClain, J L. Sarmiento, GC. Feldman, A J. Milligan, P G. Falkowski, R M. Letelier and ES. Boss. (2006) Climate-driven trends in contemporary ocean productivity. *Nature* 444: 752-755
- Bruland KW, J R. Donat and D A. Hutchins (1991) Interactive Influences of Bioactive Trace Metals on Biological Production in Oceanic Waters. *Limnol. Oceanogr.* 36: 1555-1577.

- Bruland KW, EL. Rue and G J. Smith (2001) Iron and Macronutrients in California Coastal Upwelling Regimes: Implications for Diatom Blooms. *Limnology and Oceanography*, 46:1661-1674
- Buck, CS, WM Landing, JA. Resing and G T. Lebon (2006) Aerosol iron and aluminum solubility in the northwest Pacific Ocean: Results from the 2002 IOC cruise. *Geochemistry, Geophysics, Geosystems* An electronic journal of the earth sciences. Vol 7 Q04M07, doi:10.1029/2005GC000977.
- Celis, JE, J R. Morales, C A. Zaror and J C. Inzunz (2004) A study of the particulate matter PM10 composition in the atmosphere of Chillán, Chile. *Chemosphere* **54**: 541-550
- Chavez, FP and M Messie (2009) A Comparison of Eastern Boundary Upwelling Ecosystems. *Limnol Oceanogr*. *Limnol. Oceanogr*. In press
- Chen, Y., S. Mills, J. Street, D. Golan, A. Post, M. Jacobson and A. Paytan. 2007. Estimates of atmospheric dry deposition and associated input of nutrients to Gulf of Aqaba seawater. *Journal of Geophysical Research*, 112, D04309, doi:10.1029/2006JD007858.
- Chen, Y., A. Paytan, Z. Chase, C. Measures, A.J. Beck, S.A. Sañudo-Wilhelmy, and A.F. Post. 2008. Sources and fluxes of atmospheric trace elements to the Gulf of Aqaba, Red Sea. *Journal of Geophysical Research* 113: D05306.
- Chen, Y., and R. L. Siefert (2004), Seasonal and spatial distributions and dry deposition fluxes of atmospheric total and labile iron over the tropical and sub-tropical North Atlantic Ocean, *J. Geophys. Res.*, 109, D09305, doi:10.1029/2003JD003958.

- Chen, Y., J. Street and A. Paytan. 2006. Comparison between pure-water- and seawater-soluble nutrient concentrations of aerosols from the Gulf of Aqaba. *Marine Chemistry* 101: 141-152.
- Chester, R, Elderfield, H, Griffin, JJ, Johnson, LR, Padgham, RC (1972) Eolian dust along the eastern margins of the Atlantic Ocean. *Marine Geology* 13: 91-105
- Chiapello, I., Bergametti, G., Gomes, L., Chatenet, B., Dulac, F., Pimienta, J. and Santos Soares, E., (1995) An additional low layer of Sahelian and Saharan dust over the North-Eastern Tropical Atlantic. *Geophysical Research Letters* 22: 3191–3194
- Chase, Z, K S. Johnson, V A Elrod, J N. Plant, S E Fitzwater, L Pickell, 1 and C M. Sakamoto (2005) Manganese and iron distributions off central California influenced by upwelling and shelf width. *Marine Chemistry* 95, 235-254
- Chow, J C, Watson, J G, Fujita, E M, Lu, Z, Lawson, D R, Ashbaugh, L L (1994) Temporal and spatial variations of PM sub(2.5) and PM sub(10) aerosol in the Southern California Air Quality Study. *Atmospheric Environment*. **28**: 2061-2080
- Church, T.M., Arimoto, R., Barrie, L.A., Dehairs, F., Jickells, T.D., Mart, L., Sturges, W.T., Zoller, W.H., 1988. The long-range atmospheric transport of trace elements: a critical evaluation. In: *The Long-Range Atmospheric Transportation of Natural and Contaminant Substances*. Kluwer Academic Publishers, Dordrecht, pp. 37-58.

- Coale, K. H., et al. (1996), A massive phytoplankton bloom induced by an ecosystem-scale iron fertilization experiment in the equatorial Pacific Ocean, *Nature*, 383, 495– 501.
- Codispoti, LA, Codispoti, Dugdale, and Minas. 1982. A comparison of the nutrient regimes off Northwest Africa, Peru and Baja, California. *Rapp. P. -v. Reun.* 180: 184-201
- Cornell, SE, TD Jickells, JN Cape, AP Rowland, and RA Duce. 2003. Organic nitrogen deposition on land and coastal environments: a review of methods and data. *Atmospheric Environment*. 37, 2173-2191.
- Cornell, S, A. Rendell and T. Jickells. 1995. Atmospheric inputs of dissolved organic nitrogen to the oceans. *Nature* 376, 243–246.
- Cunningham, E., "On the velocity of steady fall of spherical particles through fluid medium," *Proc. Roy. Soc. A* 83(1910)357.
- Davies, CN (1945) Definitive equations for the fluid resistance of spheres. *The Proceedings of the Physical Society* **57**: 259-270.
- Duce, R. A (1986) The impact of atmospheric nitrogen, phosphorus, and iron species on marine biological productivity. in *The Role of Air-Sea Exchange in Geochemical Cycling*, edited by P. Buat-Menard, pp. 497-529, D. Reidel, Norwell, Mass.
- Duce, R. A., et al. (1991), The Atmospheric Input of Trace Species to the World Ocean, *Global Biogeochem. Cycles*, **5**: 193–259.
- Duce, R. A., and NW Tindale (1991) Atmospheric transport of iron and its deposition in the ocean. *Limnol. Oceanogr.* **36**: 1715-1726

- Duce et al. (2008) Impacts of Atmospheric Anthropogenic Nitrogen on the Open Ocean. *Science* 320: 893 - 897
- Ezat, U., and F. Dulac (1995), Size distribution of mineral aerosols at Amsterdam Island and dry deposition rates in the southern Indian Ocean, *C.R. Acad. Sci., Ser. II*, **320**: 9– 14.
- Fiebig-Wittmaack, M, E. Schultz, A.M. Córdova and C. Pizarro (2006) A microscopic and chemical study of airborne coarse particles with particular reference to sea salt in Chile at 30° S. *Atmospheric Environment* 40: 3467-3478
- Friederich, GE, Walz, PM., Burczynski, MG, and Chavez, FP (2002) Inorganic carbon in the central California upwelling system during the 1997–1999 El Niño–La Niña event. *Progress in Oceanography* doi:10.1016/S0079-6611(02)00049-6
- Geider, RJ and J LaRoche. 2002. Redfield revisited: variability of C:N:P in marine microalgae and its biochemical basis. *European Journal of Phycology* 37 : 1-17
- Herner, J D, Aw, J, Gao, O, Chang, D P, Kleeman, M J (2005) Size and Composition Distribution of Airborne Particulate Matter in Northern California: I - Particulate Mass, Carbon, and Water-Soluble Ions. *Journal of the Air & Waste Management Association*. **55**: 30-51
- Herut, B., M. D. Krom, G. Pan, and R. Mortimer (1999) Atmospheric input of nitrogen and phosphorus to the southeast Mediterranean: Sources, fluxes, and possible impact. *Limnol. Oceanogr.*, 44: 1683– 1692.
- Huebert, B. J. (1980) Particle size distribution of nitrate and sulfate in the marine atmosphere. *Geophys. Res. Lett.* 7, 325–328.

- Hutchins, D. A. & Bruland, K. W. 1998. Iron-limited diatom growth and Si:N uptake ratios in a coastal upwelling. *Nature* 393, 561–564
- Jacobson, M.Z. (2005) Sedimentation, dry deposition, and air-sea exchange. In: *Fundamentals of Atmospheric Modeling*. Cambridge University Press, New York, pp.661-680.
- Jaffe, D, S Tamura and J Harris (2005) Seasonal cycle and composition of background fine particles along the west coast of the US. *Atmospheric Environment* **39**: 297-306
- Jaworski, N.A., R.W. Howarth, and L.J. Hetling. 1997. Atmospheric deposition of nitrogen oxides onto the landscape contributes to coastal eutrophication in the northeast United States. *Environ. Sci. Technol.* 31:1995-2004.
- JGOFS Protocols (1994) Measurement of chlorophyll a and phaeopigments by fluorometric analysis, Chap. 14
- Jickells, TD (1998) Nutrient Biogeochemistry of the Coastal Zone. *Science* 281: 217 - 222
- John W, Kaifer R, Rahn K, Wesolowski JJ (1973) Trace element concentrations in aerosols from the San Francisco Bay Area. *Atmos Environ.* **7**: 107-18.
- Johansen, AM, R L. Siefert, and M R. Hoffmann (2000) Chemical composition of aerosols collected over the tropical North Atlantic Ocean. *J. Geophysical Research* 105: 15,277–15,312
- Johnson KS, FP Chavez, VA Elrod, SE Fitzwater, JT Pennington, KR Buck, and PM Walz (2001) The annual cycle of iron and the biological response in central California coastal waters. *Geophysical Research Letters* 28: 1247-1250.

- Kavouras IG, Koutrakis P, Cereceda-Balic F, Oyola P (2001) Source apportionment of PM₁₀ and PM_{2.5} in five Chilean cities using factor analysis. *J Air Waste Manag Assoc.* **51**: 451-64
- Kouvarakis, G., N. Mihalopoulos, A. Tselepidis, and S. Stavrakakis (2001), On the importance of atmospheric inputs of inorganic nitrogen species on the productivity of the eastern Mediterranean Sea, *Global Biogeochem.Cycles*, 15, 805– 817
- Krishnamurti,T. N. , Jha,B. , Prospero,J. M. , Jayaraman,A. & Ramanathan, V. (1998) Aerosol and pollutant transport and their impact on radiative forcing over tropical Indian Ocean during the January–February, 1996 pre-INDOEX cruise. *Tellus B* 50: 521 –542
- Kudela, R. M. and F. P. Chavez (2000) Modeling the impact of the 1992 El Niño on new production in Monterey Bay, California. *Deep Sea Research Part II: Topical Studies in Oceanography* 47, 1055-1076
- Kudela, R. M. and F. P. Chavez (2004) The impact of coastal runoff on ocean color during an El Niño year in Central California. *Deep Sea Research Part II: Topical Studies in Oceanography* 51, 1173-1185
- Kudela, RM and RC Dugdale (2000) Nutrient regulation of phytoplankton productivity in Monterey Bay, California. *Deep Sea Research Part II: Topical Studies in Oceanography* 47: 1023-1053
- Lewis ER and Schwarts, SE (2006) Comment on “size distribution of sea-salt emissions as a function of relative humidity”. *Atmospheric Environment* **40**: 588-590

- Longhurst, A, S Sathyendranath, T Platt and C Caverhill (1995) An estimate of global primary production in the ocean from satellite radiometer data. *J. Plankton Res.* 17: 1245-1271
- Mace, KA, RA Duce, NW Tindale (2003) Organic nitrogen in rain and aerosol at Cape Grim, Tasmania, Australia. *J. Geophys. Res.*, 108(D11), 4338, doi:10.1029/2002JD003051.
- Mackey, K.R.M, T. Rivlin, A.R. Grossman, A.F. Post, A. Paytan. 2009. Picophytoplankton responses to changing nutrient and light regimes during a bloom. *Marine Biology*, DOI 10.1007/s00227-009-1185-2.
- Mahowald, NM, A R. Baker, G Bergametti, N Brooks, R A. Duce, T D. Jickells, N Kubilay, J M. Prospero, I Tegen (2005) The atmospheric global dust cycle and iron inputs to the ocean. *Global Biogeochem. Cycles*, **19**: GB4025, doi:10.1029/2004GB002402.
- Martin JH and SE Fitzwater (1988) Iron deficiency limits phytoplankton growth in the north-east Pacific subarctic. *Nature* 331, 341-343
- Mills, M.M., C. Ridame, M. Davey, J. La Roche (2004) Iron and phosphorus co-limit nitrogen fixation in the eastern tropical North Atlantic. *Nature* 429, 292-294.
- Moulin C, CE Lambert, F Dulac, and U Dayan (1997) Control of atmospheric export of dust from North Africa by the North Atlantic Oscillation. *Nature* 387:691-694
- Nadim, F, MM Trahiotis, S Stapcinskaite, C Perkins, RJ Carley, GE Hoaga and X Yang (2001) Estimation of wet, dry and bulk deposition of atmospheric nitrogen in Connecticut. *J. Environ. Monit.* **3**: 671–680

- Olivieri RA and FP Chavez (2000) A model of plankton dynamics for the coastal upwelling system of Monterey Bay, California. *Deep-Sea Research II* **47**: 1077-1106
- Paerl, H. W. 1985. Enhancement of marine primary production by nitrogen enriched acid rain. *Nature* 316:747 749.
- Paerl, HW (1997) Coastal Eutrophication and Harmful Algal Blooms: Importance of Atmospheric Deposition and Groundwater as “new” nitrogen and other nutrients. *Limnol Oceanogr.* **42**: 1154-1165
- Paerl, H.W, R. L. Dennis and D. R. Whitall. 2002. Atmospheric deposition of nitrogen: Implications for nutrient over-enrichment of coastal waters. *Estuaries* 25:677-693
- Paerl, HW, and ML Fogel (1994) Isotopic characterization of atmospheric nitrogen inputs as sources of enhanced primary production in coastal Atlantic Ocean waters. *Marine Biology* **119**: 635-645
- Paerl, H. W., J. D. Willey, M. Go, B. L. Peierls, J. L. Pinckney and M. L. Fogel. 1999. Rainfall stimulation of primary production in Western Atlantic Ocean waters: Roles of different nitrogen sources and co-limiting nutrients. *Mar. Ecol. Progr. Ser.* 176:205-214.
- Parungo, F. P., C. T. Nagamoto, J. Rosinski and P. L. Haagenson (1986) A study of marine aerosols over the Pacific Ocean. *Journal of Atmospheric Chemistry* **4**: 199-226, DOI 10.1007/BF00052001

- Pauly, D, V Christensen, S Guénette, T J. Pitcher, U. R Sumaila, C J. Walters, R. Watson & D Zeller (2002) Towards sustainability in world fisheries. *Nature* **418**: 689-695
- Paytan, A., K.R.M. Mackey, Y. Chen, I D. Lima, S C. Doney, NM Mahowald, R Labiosa and A.F. Post (2009) Toxicity of atmospheric aerosols on marine phytoplankton. *PNAS* **106**: 4601–4605
- Peierls, B. L. And H. W. Paerl. 1997. The bioavailability of atmospheric organic nitrogen deposition to coastal phytoplankton. *Limnol. Oceanogr.* 42:1819-1823.
- Pennington, J.T. and F. Chavez (2000) Seasonal fluctuations of temperature, salinity, nitrate, chlorophyll, and primary production at station H3/M1 over 1989-1996 in Monterey Bay, CA. *Deep-Sea Research II* 47, 947-973.
- Petit, JR, J. Jouzel, D. Raynaud, N. I. Barkov, J.-M. Barnola, I. Basile, M. Bender, J. Chappellaz, M. Davisk, G. Delaygue, M. Delmotte, V. M. Kotlyakov, M. Legrand, V. Y. Lipenkov, C. Lorius, L. Pepin, C. Ritz, E. Saltzman & M. Stievenard (1999) Climate and atmospheric history of the past 420,000 years from the Vostok ice core, Antarctica. *Nature* 399:429-436
- Phinney, L, W. R Leaitch, U Lohmann, H Boudries, D R. Worsnop, J T. Jayne, D Toom-Sauntry, M Wadleigh, S Sharma, N Shantz (2006) Characterization of the aerosol over the sub-arctic north east Pacific Ocean. *Deep Sea Research Part II: Topical Studies in Oceanography* 53: 2410-2433
- Prospero, J. M., (1981) Arid regions as sources of mineral aerosols in the marine atmosphere, *Spec. Pap. Geo. Soc. Am.*, 186,71-86

- Prospero, J.M., (1996) The Atmospheric transport of particles to the Ocean, in Particle Flux in the Ocean, edited by V. Ittekkot, P. Schäfer, S. Honjo and P.J. Depetris, SCOPE Report 57, John Wiley & Sons, Chichester, 19-52
- Prospero, J. M., K. Barrett, T. Church, F. Dentener, R. A. Duce, J. N. Galloway, H. Levy II, J. Moody, and P. Quinn (1996), Atmospheric deposition of nutrients to the North Atlantic basin, *Biogeochemistry* **35**: 27– 73.
- Prospero, J. M and Savoie, D. L (1989) Effect of continental sources on nitrate concentrations over the Pacific Ocean. *Nature* **339**: 687 - 689
- Quinn, P.K. ; Bates, T.S. ; Johnson, J.E., Covert, D.S., Charlson, R.J. (1990) Interactions between the sulfur and reduced nitrogen cycles over the central Pacific Ocean. *Journal of Geophysical Research* **95**:D10 16,405-16,416
- Rhoads, KP (1998) The influence of continental emissions on the composition of the remote marine boundary layer. Thesis (PhD). University of Maryland, College Park, Source DAI-B 59/06, p. 2630, Dec 1998, 226 pages
- Ryan J, Gower J, King S, Bissett W, Fischer A, et al. (2008) A coastal ocean extreme bloom incubator. *Geophysical Research Letters*. 35:L12602. doi:10.1029/2008GL034081.
- Sadasivan, S. (1978) Trace elements in size separated aerosols over sea. *Atmospheric Environment* **12**: 1677-1683
- Sarmiento JL, Slater R, Barber R, Bopp L, Doney SC, Hirst AC, Kleypas J, Matear R, Mikolajewicz U, Monfray P, Soldatov V, Spall SA, Stouffer R (2004) Response of ocean ecosystems to climate warming. *Global Biogeochemical Cycles* **18**:GB3003. doi:10.1029/2003GB002134

- Saito, MA, TJ Goepfert, and JT Ritt (2008) Some thoughts on the concept of colimitation: Three definitions and the importance of bioavailability. *Limnol. Oceanogr.* **53**: 276-290
- Savoie, D. L., and J. M. Prospero (1977) Aerosol concentration statistics for the northern tropical Atlantic. *Journal of Geophysical Research* **82**: 5945-5964
- Savoie, D. L., and J. M. Prospero (1982) Particle-size distribution of nitrate and sulfate in the marine atmosphere, *Geophys. Res. Lett.*, **9**: 1207– 1210.
- Savoie, DL, JM Prospero, and RT Nees (1987) Nitrate, non-sea-salt sulfate, and mineral aerosol over the northwestern Indian Ocean. *Journal of Geophysical Research*. 92:933-942
- Schaap, M., et al. (2004), Artifacts in the sampling of nitrate studied in the “INTERCOMP” campaigns of EUROTRAC-AEROSOL, *Atmos.Environ.*, **38**: 6487–6496.
- Seitzinger, S.P. and R.W. Sanders. 1999. Atmospheric Inputs of Dissolved Organic Nitrogen Stimulate Estuarine Bacteria and Phytoplankton. *Limnol. Oceanogr.* 44: 721-730.
- Slinn, SA and WGN Slinn (1980) Predictions for particle deposition on natural waters. *Atmospheric Environment* **14**:1013-1016
- Spokes, L. J., T. D. Jickells, and K. Jarvis (2001), Atmospheric inputs of trace metals to the northeast Atlantic Ocean: The importance of southeasterly flow, *Mar. Chem.*, **76**: 319–330.
- Sunda, W. G., and S. A Huntsman. 1995. Iron uptake and growth limitation in oceanic and coastal phytoplankton. *Mar. Chem.* **50**: 189-206.

- Takeda, S. (1998) Influence of iron availability on nutrient consumption ratio of diatoms in oceanic waters. *Nature* 393, 774-777
- Uematsu, M., R. A. Duce, J. M. Prospero, L. Chen, J. T. Merrill, and J. T. McDonald (1983) Transport of mineral aerosol from Asia over the Pacific Ocean, *J. Geophys. Res.*, **88**: 5345– 5352
- VanCuren RA (2003) Asian aerosols in North America: Extracting the chemical composition and mass concentration of the Asian continental aerosol plume from long-term aerosol records in the western United States. *J. Geophys. Res.*, **108**:(D20), 4623, doi:10.1029/2003JD003459.
- Volpe, G., V. F. Banzon, R. H. Evans, R. Santoleri, A. J. Mariano, and R. Sciarra (2009), Satellite observations of the impact of dust in a low-nutrient, low-chlorophyll region: Fertilization or artifact?, *Global Biogeochem. Cycles*, **23**: GB3007, doi:10.1029/2008GB003216.
- Wagener, T, C Guieu, R Losno, S Bonnet, and N Mahowald (2008) Revisiting atmospheric dust export to the Southern Hemisphere ocean: Biogeochemical implications. *Global Biogeochemical Cycles* **22**: doi:10.1029/2007GB002984
- Wang, H. C., and W. John (1988), Characteristic of the Berner Impactor for sampling inorganic ions, *Aerosol Sci. Technol.*, **8**: 157–172.
- Wara, M. W., Ravelo, A. C. & DeLaney, M. L. (2005) Permanent El Nino-like conditions during the Pliocene warm period. *Science* **309**: 758–761.
- Wells, KC , M Witek, P Flatau, S M. Kreidenweis and D . Westphal (2007) An analysis of seasonal surface dust aerosol concentrations in the western US

- (2001–2004): Observations and model predictions. *Atmospheric Environment* **41**: 6585-6597
- Wilkerson, FP, Dugdale, RC, Marchi, A, and Collins, CA (2002) Hydrography, nutrients, and chlorophyll during El Niño and La Niña 1997–99 winters in the Gulf of the Farrallones, California, *Progress in Oceanography* 54, 293–310
- Williams, RM (1982) A model for the dry deposition of particles to natural water surfaces. *Atmospheric Environment* **16**: 1933-1938
- Wollast, R (1991) The coastal organic carbon cycle: fluxes, sources and sinks. *In*: Ocean margin processes in global change. RCF Mantoura et al eds. Wiley. pp:365-382
- Zorn S. R. F. Drewnick, M. Schott, T. Hoffmann, and S. Borrmann (2008) Characterization of the South Atlantic marine boundary layer aerosol using an aerodyne aerosol mass spectrometer. *Atmos. Chem. Phys.*, **8**: 4711–4728

Table 1: Water soluble nutrient and metal concentrations and depositional fluxes for summer and winter aerosol samples.

Summer	Concentration ($\mu\text{g m}^{-3}$)				Flux ($\mu\text{g m}^{-2} \text{d}^{-1}$)			
	minimum	maximum	mean	SE	minimum	maximum	mean	SE
TSP	31	160	69	3.5	12	89	34	2.0
Na	2.5	19	9.1	1.2	108	9737	4771	668
Fe	0.0017	0.011	0.0051	0.00074	0.096	5	1.5	0.37
NO _x	0.14	1.2	0.37	0.073	33	233	87	14
NH ₄	0.11	0.53	0.25	0.032	16	92	36	5.2
P	0.0018	0.0061	0.0039	0.00037	0.095	2.3	1.5	0.18
Winter	Concentration ($\mu\text{g m}^{-3}$)				Flux ($\mu\text{g m}^{-2} \text{d}^{-1}$)			
	minimum	maximum	mean	SE	minimum	maximum	mean	SE
TSP	15	102	50	5.4	7.4	54	24	2.9
Na	1.2	11	5.2	0.92	320	6160	2777	546
Fe	0.0043	0.015	0.0075	0.001	0.7	5.4	2.2	0.41
NO _x	0.22	1.2	0.67	0.095	58	152	103	8.5
NH ₄	0.22	1.3	0.57	0.11	36	79	57	3.6
P	0.0035	0.0092	0.0062	0.00054	1.0	4.1	2.2	0.27

Table 2: Depositional fluxes of N from fine and coarse fractions in summer and winter.

Aerosol season and fraction	NO_x (μg N m⁻² d⁻¹)		NH₄ (μg N m⁻² d⁻¹)	
	Range	Mean ± SE	Range	Mean ± SE
summer coarse	29-220	76±13	10-81	27±5
winter coarse	20-128	80±8	4-72	32±8
summer fine	3-48	11±3	4-22	9±1
winter fine	4-52	24±4	8-52	24±4

Table 3: Regression statistics for MODIS-derived Chl *a* and AOT data for monitoring stations M0, M1, and M2. The correlation is significant ($p < 0.05$, shown in bold typeface) in the summer weeks for stations M1 and M2, and during El Niño periods for all three stations. No significant correlations were found for any of the stations in the winter weeks.

	M0			M1			M2		
	n	R²	p	n	R²	p	n	R²	p
Summer	125	0.2%	0.650	125	3.9%	0.028	122	6.6%	0.004
Winter	97	<0.1%	0.975	99	2.2%	0.145	97	2.2%	0.147
El Nino	148	0.1%	0.006	150	4.3%	0.011	146	11.3%	<0.001

Table 4: Productivity supported by aerosol N. Estimates show the percent of new production attributable to aerosol-derived N on high deposition days, N derived from mean wet and dry deposition combined, and aerosol Fe based on mean nutrient flux data from extracted aerosol samples during annual, upwelling, El Niño, and low productivity periods for Monterey Bay.

*Total new production values for Monterey Bay are from Kudela and Chavez (2000).

**Values for M2 low productivity are not available. We assumed the same proportion between annual and low productivity as for M1.

	New N Production* (mg N m⁻³d⁻¹)	New Production from Atmospheric N during High Deposition Events	New Production from Atmospheric N based on mean annual deposition rates	New Production from Dry Deposition of Fe
M2, annual	5.04	0.5%	0.2%	--
M2, upwelling	15.4	0.2%	0.08%	1.9%
M2, El Nino	1.96	1.3 %	0.6%	--
**M2, low productivity	0.06	50%	13.5%	--
M1, annual	11.06	0.2%	0.1%	--
M1, upwelling	29.12	0.1%	0.04%	1.0%
M1, El Nino	3.22	0.8%	0.4%	--
M1, low productivity	0.14	20%	9%	--

Table 5: Aerosol concentration, N content, deposition rate, and contribution to total primary production in coastal California and six other major upwelling regions throughout the world's oceans: the NW and SW coasts of Africa, the SE coast of the Arabian Peninsula near the Somali coast, the W coast of India, the W coast of Australia, and the W coast of South America. We used mid-range values of aerosol concentration (TSP) and N content, along with modeled aerosol deposition rates (Mahowald et al. 2005) to estimate annual N deposition in each region. We compared the productivity supported by these N additions (assuming a Redfield ratio of 106C:16N) to modeled estimates of annual productivity for each region (Longhurst et al. 1995). These estimates provided an order of magnitude approximation for the fraction of productivity in each region that is supported by aerosol N deposition.

* Geographical provinces and primary productivity values were obtained from Longhurst et al. (1995)

**Dust deposition rates obtained from Mahowald et al. (2005)

+Aerosol-derived productivity was calculated as the product of aerosol concentration ($\mu\text{g aerosol m}^{-3}$ air), aerosol N content ($\mu\text{g aerosol m}^{-3}$ air), and aerosol deposition rate ($\text{g aerosol m}^{-2} \text{y}^{-1}$). A Redfield C:N ratio of 106:16 was assumed to convert from N deposition to C production.

Ocean basin	Location	Longhurst upwelling province*	Aerosol conc - TSP ug aerosol/m ³	NO ₃ aerosol conc ugN/m ³	NH ₄ aerosol conc ugN/m ³	Total Soluble N ugN/m ³	Dust deposition rate** g aerosol/m ² /y	Aerosol-derived productivity+ gC/m ² /y	Annual primary production* gC/m ² /y	Portion of annual productivity from aerosols %	References for aerosol chemistry data
Pacific	W coast of USA, Crater Lake and Mt Lassen	Coastal CA (CCAL)	7.3								VanCuren et al. 2003
Pacific	W coast of USA, Crater Lake, Mt Rainier, Mt Lassen, and Cheeka Peak	Coastal CA (CCAL)	2.04-3.91								Jaffe et al. 2005 PM2.5 only
Pacific	California, Sequoia National Park	Coastal CA (CCAL)	1-30								Wells et al. 2007, PM10 soil
Pacific	W coast of USA, 30-40N 125W	Coastal CA (CCAL)	9.4-17	0.041-0.0565	0.078-0.101						Parungo et al. 1996
Pacific	W coast of USA, 20-29N	Coastal CA (CCAL)	8.9-13	0.020-0.050	0.039-0.058						Parungo et al. 1996

Pacific	W coast of USA, open ocean to coastal	Coastal CA (CCAL)		0.068-0.160							Savoie 1984 in Duce et al 1991
Pacific	Sub-arctic NW Pacific Ocean Station Papa (50N, 145W)	Coastal CA (CCAL)	3.7	0.131	0.07						Phinney et al. 2006 particles diameter >0.8um
Pacific	North Pacific Subtropical Gyre, Midway, Oahu, Enewetak, and Fanning Islands	Coastal CA (CCAL)	0.06-0.84								Uematsu et al. 1983 range of averages
Pacific	Northwest Pacific Ocean and North Pacific Subtropical Gyre near Hawaiian Islands	Coastal CA (CCAL)		0.014-0.280							Buck et al. 2006
Pacific	North Pacific, 30-50N 170W	Coastal CA (CCAL)			0.482-1.400						Quinn et al. 1990
Pacific	North Pacific, 15-29N 170W	Coastal CA (CCAL)			0.187-0.327						Quinn et al. 1990
Pacific	Equatorial Pacific, 11-14N 170W	Coastal CA (CCAL)			0.109-0.389						Quinn et al. 1990
Pacific	San Francisco Bay area, Pittsburg, Richmond, San Rafael, San Francisco, Burlingame, Redwood City, San Jose, Fremont, and Livermore	Coastal CA (CCAL)	43-166								John et al. 1973 values represent measurements made over one day in summer
Pacific	San Joaquin Valley; Davis, Modesto, Sequoia, and Bakersfield	Coastal CA (CCAL)	5-185	0.226-20.323	0.778-31.111						Herner et al. 2005
Pacific	W Coast of CA, Bodega Bay	Coastal CA (CCAL)	20-270	0.226-5.645	0.778-10.111						Herner et al. 2005
Pacific	Los Angeles, CA Summer; Burbank, downtown LA, Hawthorne, Long Beach, Anaheim, Rubidoux, San Nicholas Island, Azusa, and Clarmont	Coastal CA (CCAL)	45.9-120	0.357-6.512	0.661-6.689						Chow et al. 1994; range of averages for all sites
Pacific	Los Angeles, CA Fall; Burbank, downtown LA, Hawthorne, Long Beach, Anaheim, and Rubidoux	Coastal CA (CCAL)	85.1-104	4.785-7.969	4.947-8.042						Chow et al. 1994; range of averages for all sites
Pacific	MBARI	Coastal CA (CCAL)	14-160	0.138-1.219	0.109-1.244						This work, NO3 includes NO2
	"Midrange" values	Coastal CA (CCAL)	20	1			5	1.4	388	0.4	
Atlantic	Izana, Tenerife, Canary Islands	NW Africa (CNRY)	22.28	0.174	0.257						Prospero 1996
Atlantic	Sal Island, Cape Verde Archipelago	NW Africa (CNRY)	5-120								Chiapello et al. 1995

Atlantic	NW African coast 0-20N	NW Africa (CNRY)				0.14-0.91					Baker et al. 2006
Atlantic	Central S Atlantic Ocean	NW Africa (CNRY)				0.21-1.12					Baker et al. 2006
Atlantic	Central N Atlantic Ocean, Transect from Dakar to Azores	NW Africa (CNRY)		0.034-0.309	0.061-0.619						Church et al 1991
Atlantic	Tropical N Atlantic, Transect between Barbados and Cape Verde	NW Africa (CNRY)	0.8-55.6	<0.054-0.298	0.053-0.233						Johansen et al 2000
Atlantic	Near African coast	NW Africa (CNRY)	57								Chester et al. 1972
Atlantic	SE of Cape Verde	NW Africa (CNRY)	133								Chester et al. 1972
Atlantic	Sal Island, Cape Verde Archipelago	NW Africa (CNRY)	29.8								Savoie and Prospero 1977
Atlantic	NW African coast, Canary Islands	NW Africa (CNRY)		0.271							Savoie 1984 in Duce et al 1991
Atlantic	NW African coast, Equatorial Atlantic	NW Africa (CNRY)		0.16							Savoie 1984 in Duce et al 1991
Atlantic	Near the ITCZ	NW Africa (CNRY)	0.25								Chester et al. 1972
	"Midrange" values	NW Africa (CNRY)	30	0.1			50	0.95	732	0.1	
Indian	NW Indian Ocean	Arabian Peninsula/ W India (ARAB/INDW)	1-7.6	0.097-0.228							Savoie et al. 1987
Indian	NW Indian Ocean	Arabian Peninsula/ W India (ARAB/INDW)	0.4-3.9	0.067-0.452	0.156-1.167						Krishnamurti et al. 1998 range of stations 9-31
Indian	NW Indian Ocean	Arabian Peninsula/ W India (ARAB/INDW)	<0.1	0.228	0.187						Rhoads et al. 1998; NHmE region
Indian	Arabian Sea	Arabian Peninsula/ W India (ARAB/INDW)	25								Sadasivan 1978
Indian	Somali Coast	Arabian Peninsula (ARAB)	0.23	0.038							Savoie et al. 1987
Indian	Arabian Sea, Arabian Peninsula and Somali Coast	Arabian Peninsula		0.149							Savoie 1984 in Duce et al 1991

		(ARAB)									
Indian	Arabian Sea along W India Coast	W India (INDW)	4.7-18.4	0.587-1.852	1.011-4.589						Krishnamurti et al. 1998 range of stations 32-35
Indian	Arabian Sea along W India Coast	W India (INDW)		0.075							Savoie 1984 in Duce et al 1991
Indian	Arabian Sea	W India (INDW)	6.2	0.386	0.552						Rhoads et al. 1998; NHcT region
	"Midrange" values	Arabian Peninsula (ARAB)	2	0.6			20	34	454	8	
	"Midrange" values	W India (INDW)	5	1			20	23	369	6	
Indian	Bay of Bengal	W Australia (AUSW)	7.2								Prospero 1979
Indian	Equatorial Indian Ocean 50-100E	W Australia (AUSW)	<0.1	0.05	0.062						Rhoads et al. 1998 SHmE region
Indian	Amsterdam Island	W Australia (AUSW)	0.12								Ezat and Dulac 1995
Indian	Amsterdam Island, KEOPS cruise	W Australia (AUSW)	0.013								Wagener et al. 2008
Indian	Cape Grim, Tasmania, Australia	W Australia (AUSW)		0.034	0.028						Mace et al. 2003
Indian	East Indian Ocean	W Australia (AUSW)		0.020-0.140							Savoie 1984 in Duce et al 1991
	"Midrange" values	W Australia (AUSW)	1	0.09			5	2.6	199	1	
Atlantic	Central South Atlantic	SW Africa (BENG)	0.3	<0.002	0.047						Zorn et al. 2008
Atlantic	SW African coast 30-40S	SW Africa (BENG)	2.18	0.009	0.14						Zorn et al. 2008
Atlantic	SW African coast 0-20S	SW Africa (BENG)				0.14-0.35					Baker et al. 2006
Atlantic	SW African coast, open ocean to coastal	SW Africa (BENG)		0.02							Savoie 1984 in Duce et al 1991
	"Midrange" values	SW Africa (BENG)	1	0.001			20	0.11	323	0.04	

Pacific	Chilean coast, Chillan	W South America (CHIL)	83.4	2.296	4.107						Celis et al. 2004
Pacific	Chilean coast, 30S transect from La Serana to Cerro Tololo	W South America (CHIL)	6.4-55.2								Fiebig-Wittmaack et al. 2006
Pacific	Chilean coast, urban cities Temuco, Rancagua, Valparaiso, Iquique, Vinadel Mar	W South America (CHIL)	55.5-77.6								Kavouras et al. 2001; for PM10
Pacific	W South America, open ocean to coastal	W South America (CHIL)		0.02							Savoie 1984 in Duce et al 1991
	"Midrange" values	W South America (CHIL)	50	0.1		10	0.11	269	0.04		

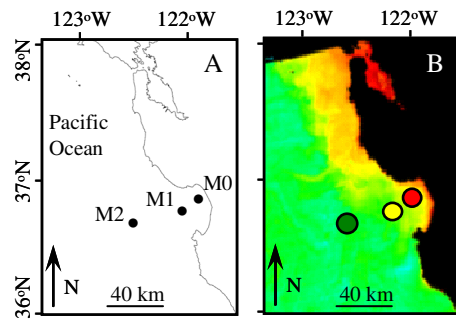


Figure 1: (A) Map showing locations of the long term stations M0, M1, and M2 in Monterey Bay and (B) example composite image of Chl *a* showing locations of the three “blotch” areas applied to obtain spatially averaged MODIS data using SeaDAS.

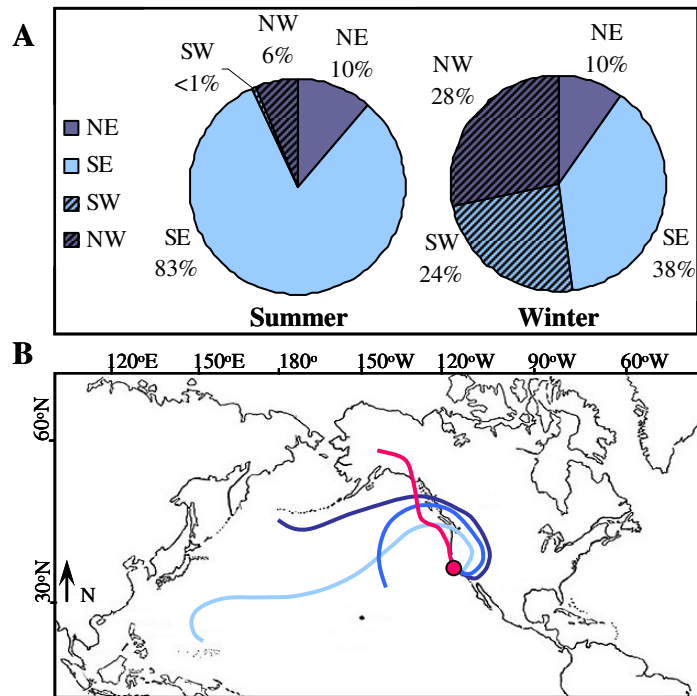


Figure 2: (A) Direction of air mass trajectories arriving at Monterey Bay in the summer and winter based on daily wind velocity measured at station M2. Hatched areas indicate winds blowing to the west, open areas indicate winds blowing to the east, light blue areas indicate winds blowing to the south, and dark blue areas indicate winds blowing to the north. In summer the majority of air masses blow in a southeastern direction parallel to the California coast, while westward winds coming from land are more common in the winter. (B) Example 7 day air mass back trajectories (AMBTs) for Monterey Bay during the summer (red) and winter (blue).

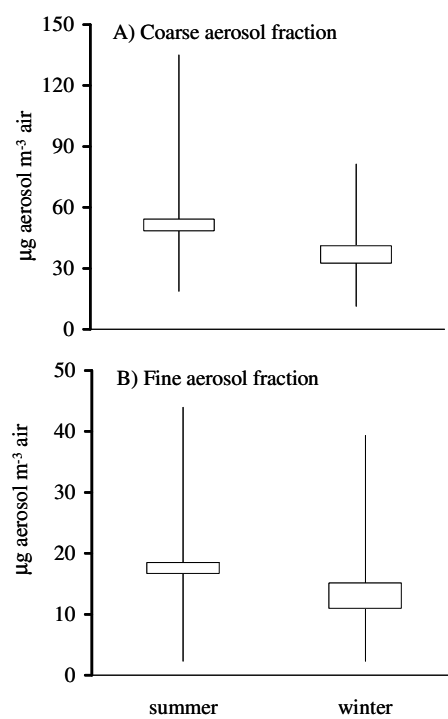


Figure 3: Aerosol concentration for fine and coarse aerosol fractions in summer and winter. Upper and lower box edges depict mean \pm SE. Lines show range.

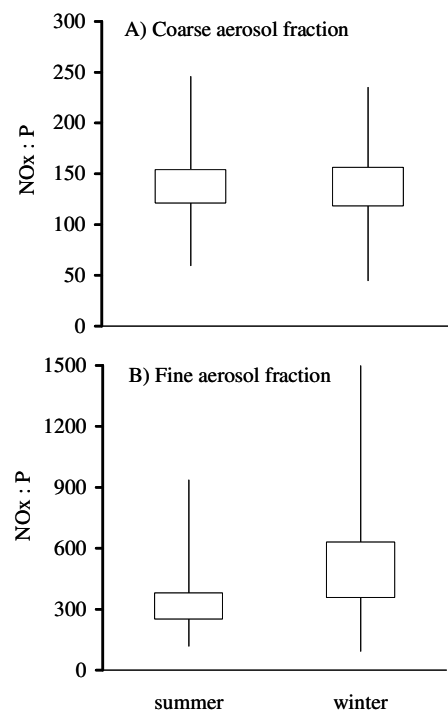


Figure 4: $\text{NO}_x:\text{P}$ ratios for fine and coarse aerosol fractions in summer and winter. Upper and lower box edges depict mean \pm SE. Lines show range.

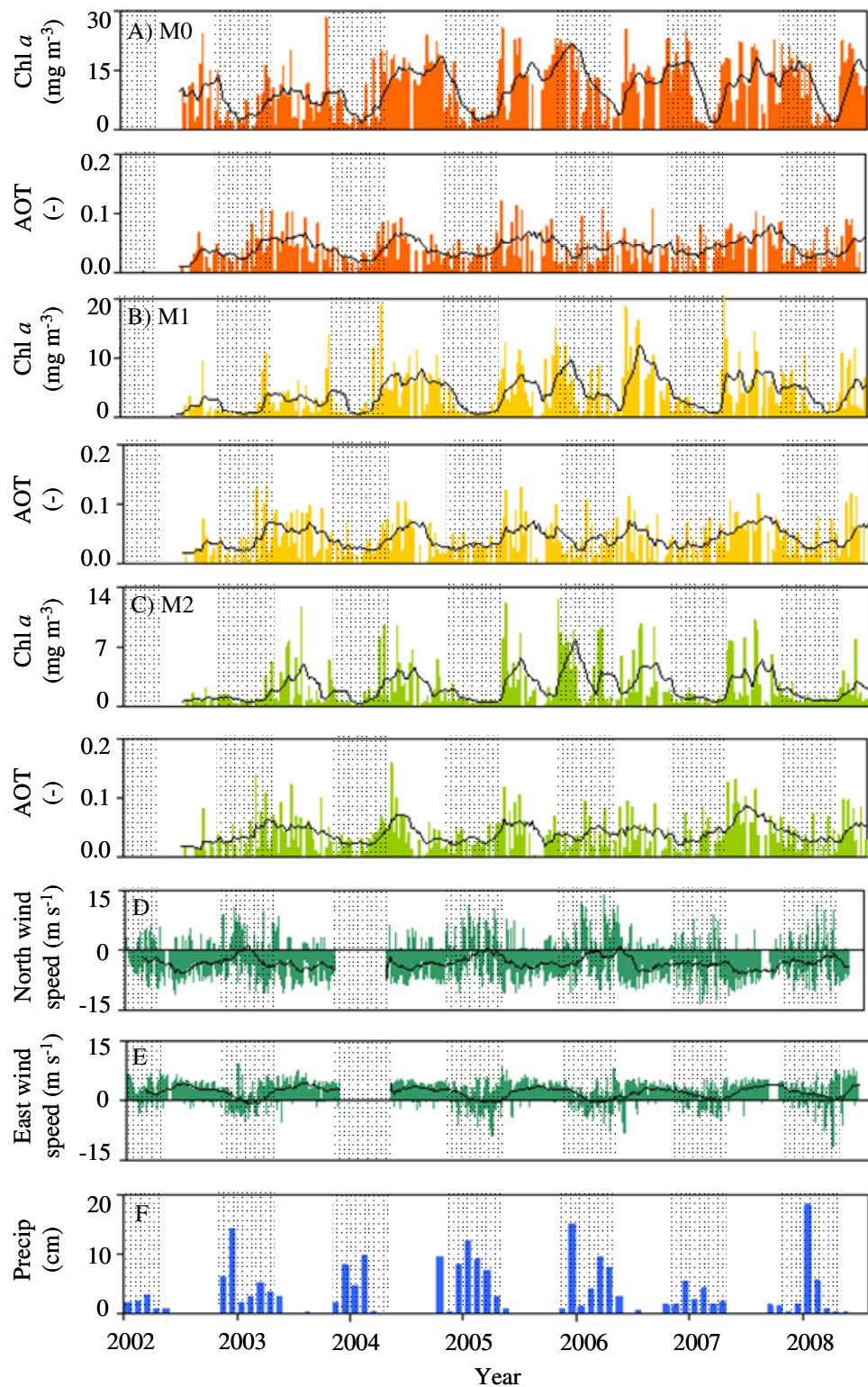


Figure 5: Time series of MODIS-derived weekly averaged AOT and Chl *a* levels for stations M0 (A), M1 (B), and M2 (C) between 2002-2008, along with zonal (D) and meridional (E) components of wind velocity at station M2, and (F) monthly

precipitation at Pinnacles National Monument in San Benito County, CA. Shaded regions denote winter. Trend lines show 2 month moving averages.

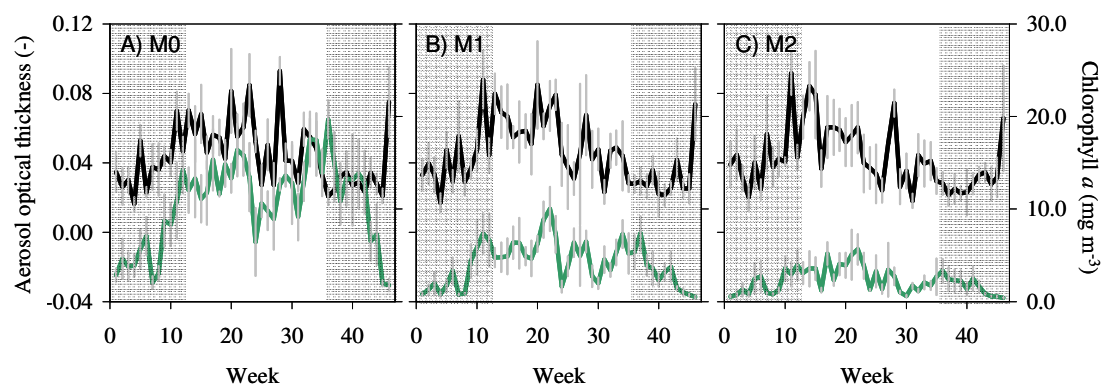


Figure 6: Annual correlations for MODIS-derived aerosol optical thickness and Chl *a* for (A) station M0, (B) station M1, and (C) station M2. Data points are averages for each week from 2002-2008, error bars show standard error of the mean, and shaded regions denote winter weeks.

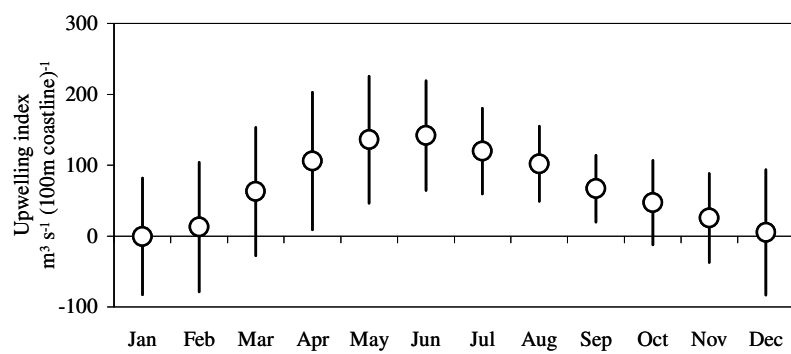


Figure 7: Monthly averaged values of upwelling indices for the period of record 1962-2008. Error bars show standard deviation.

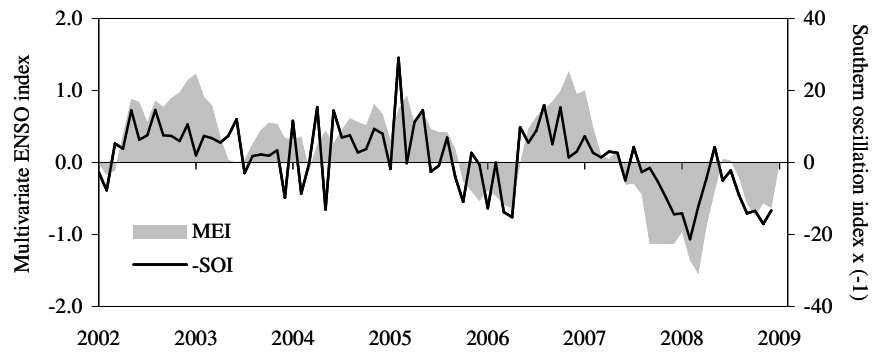


Figure 8: ENSO indices for 2002-2008. Positive MEI values and negative SOI values indicate El Niño periods. In the figure SOI values have been multiplied by -1 to facilitate comparison with MEI values such that positive values on both scales indicate periods of El Niño.

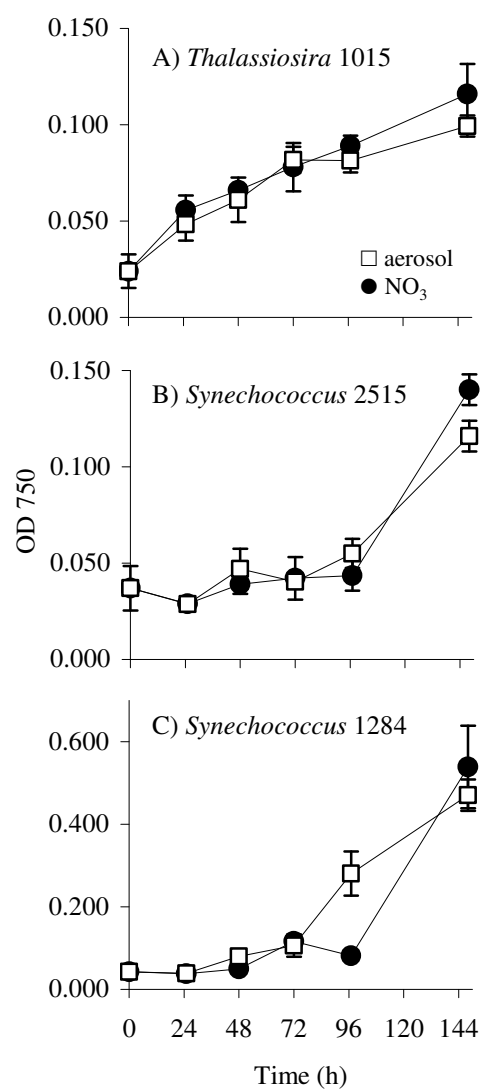


Figure 9: Growth of cultured phytoplankton strains isolated from coastal CA on F/2-NO₃ media with either NO₃ (filled circles) and aerosol derived N (open squares). Error bars show SE and are contained within the symbol when not visible.

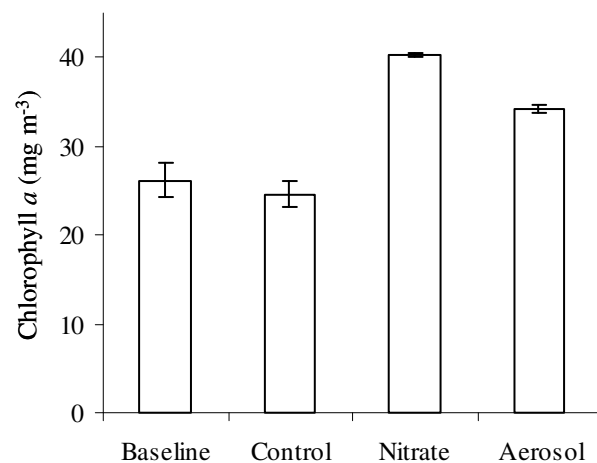


Figure 10: Chlorophyll *a* levels from an incubation experiment with natural phytoplankton assemblages in Monterey Bay. Bars show mean chl *a* concentration at baseline before additions were made, and after 30 h of incubation for the control, nitrate, and aerosol treatments. Error bars show standard error.

CHAPTER 8:

TOXICITY OF METALS ON MARINE *SYNECHOCOCCUS*

ABSTRACT

This chapter presents the results of two studies relating to the impact of metals deposition via atmospheric deposition on phytoplankton. The first study uses aerosols from different back trajectories in incubation experiments with natural phytoplankton communities to show that the growth response to aerosol additions depends on the aerosol chemical composition and differs across phytoplankton species. Aerosol additions enhanced growth by releasing nitrogen and phosphorus. However, toxic effects were observed with some aerosols, where the toxicity affected picoeukaryotes and *Synechococcus*, but not *Prochlorococcus*. The toxicity was likely due to high copper concentrations in these aerosols as support by laboratory copper toxicity tests performed with *Synechococcus* strain WH8102 isolated from the open ocean. However, it is possible that other elements present in the aerosols could have also contributed to the toxic effect. To determine the range of toxicity responses in coastal and oceanic *Synechococcus* strains to various metals, toxicity experiments were performed. Oceanic strains generally had lower toxicity thresholds and had decreased growth rates at sub-toxic metal concentrations, whereas coastal strains were more robust. These strain specific responses have likely arisen from different evolutionary selective forces in the coastal and open ocean, and could play an important role in determining the distribution patterns of *Synechococcus* throughout the world's oceans.

INTRODUCTION

Nutrient availability helps determine the growth rates and global distributions of phytoplankton in the ocean. When identifying factors that limit photosynthetic biomass in the marine environment, generally one or more elements are present in limiting quantities, thereby restricting phytoplankton growth. However, nutrients can also inhibit phytoplankton growth if they are present at toxic levels (Hutchinson 1974; Mann et al. 2002). This chapter examines the responses of coastal and oceanic marine phytoplankton to metal toxicity. Understanding the role of metal toxicity is necessary for understanding succession within phytoplankton communities, which together account for nearly half of Earth's primary productivity (Field et al. 1998).

Marine picocyanobacteria are the most abundant marine phytoplankton, and the two main genera, *Prochlorococcus* and *Synechococcus*, inhabit virtually every area of the surface ocean. In particular, *Synechococcus* is distributed over most latitudes and thrives in the upper euphotic zone (Agusti 2004; Scanlan et al. 2009), though it is also found deeper within the water column. *Synechococcus* is a genetically diverse genus. Based on 16S RNA sequences, marine *Synechococcus* comprises 3 subclusters, and the major group is further divided into at least 10 distinct clades (Scanlan et al. 2009). While all *Synechococcus* strains share certain characteristics in common, such as presence of phycoerythrin-based antenna pigments, different clades exhibit major phenotypic differences and biogeographical distributions. Diverse pigment composition (Palenik 2001), temperature requirements (Moore et al. 1995), substrate bases (Moore et al. 2002), and nutrient requirements (Lindell et al. 2005) have all been identified and help determine the niches of different *Synechococcus*

strains. For example, certain strains of *Synechococcus* coexist with *Prochlorococcus* in the nutrient-poor subtropical gyres of the open ocean (DuRand et al. 2001), while others dominate in nutrient-rich coastal upwelling regions (Palenik et al. 2006) and along highly productive ocean frontal systems (Agusti 2004). Nutrient source and availability in these different regions plays a large role in determining which *Synechococcus* clades become dominant at a given time or location.

Atmospheric deposition contributes significantly to nutrient inventories throughout the world's oceans, and can influence phytoplankton distributions. Atmospheric deposition can have a direct affect on phytoplankton communities by providing limiting nutrients in the coastal and open ocean (Duce 1986; Duce et al. 2008; Prospero and Savoie 1989; Paerl and Fogel 1994; Chen and Siefert 2004; Mills et al. 2004). However, deposition of aerosols is also of particular interest when considering metal toxicity on marine phytoplankton because it can deliver potentially large doses of metals to the surface ocean over short time periods.

This chapter encompasses two principal bodies of work pertaining to metal toxicity in the marine environment. The first data set measures the responses of natural and cultured phytoplankton to toxic levels of copper (Cu) in atmospheric aerosols. The data, along with aerosol chemical analysis and projections from a coupled ocean-atmosphere model, were included in a manuscript entitled "Toxicity of atmospheric aerosols on marine phytoplankton" that was published in 2009 in *The Proceedings of the National Academy of Science* 106: 4601-4605. The second data set includes measurements from laboratory-based metal toxicity experiments with 2 coastal and 2 oceanic strains of *Synechococcus*, and aims to identify differences in

their responses to metal toxicity that might be linked to their biogeographical provenance.

MATERIALS AND METHODS

In situ incubation experiments

Incubation experiments with natural phytoplankton assemblages took place in the Gulf of Aqaba in the northern Red Sea, an oligo- to mesotrophic marine ecosystem with significant aerosol deposition rates (Chen et al. 2007). The nutrient concentrations in these waters during the stratified season when our experiment was conducted were very low – nitrate $\sim 0.2 \mu\text{M}$ and soluble reactive phosphate $\sim 0.02 \mu\text{M}$. Trace metals in the surface layer are high compared with open ocean conditions (Cu, 1.7 nM; Fe, 2.1 nM; Zn, 1.1 nM; Pb, 0.05 nM; Chase et al. 2006).

Incubations were done in clear (acid and sample washed) polyethylene 10-L cubitainers (Fold-A-Carrier, Reliance) filled with 8 L of 100- μm filtered surface seawater collected before dawn from an offshore site (29°28'N, 34°55'E) in the Northern Gulf of Aqaba. Cubitainers were placed in a flow-through pool with circulating Gulf water to maintain surface water temperatures and were incubated for 5 days. Screening material was used to attenuate the sunlight intensity reaching the containers, 50% light attenuation yielded maximum midday irradiance of $\sim 1,000 \mu\text{mol m}^{-2} \text{ s}^{-1}$ and was equivalent to the upper 10 m of the euphotic zone of the Gulf during summer months.

For N and P additions, we used concentrations of 7 μM N (combined nitrate and ammonium) and 0.4 μM P (as phosphate), respectively, which are representative

of the deep-water concentrations in the Gulf. Where no nutrient additions were made, the nutrients were just from the seawater (control) or from the aerosol sources dissolving into the seawater. Aerosol additions were made from aerosol samples collected from two different air mass back trajectories (AMBTs) originating either from Europe or from the Sahara Desert, Africa. For aerosol additions, samples were collected onto 4 replicate filters (acid-washed polycarbonate) over 4-day intervals at the Interuniversity Institute for Marine Science in Eilat, Israel as described by Chen et al. (2007), and ~6 mg of aerosol was added to 8 L of surface seawater for each replicate bottle. This amount was equivalent ($\text{milligrams/Liter}^{-1}$) to ~2 weeks of cumulative deposition during dust storms in this area for a mixed layer depth of 10–20 m. Typical dust storms in this region last several days to weeks, the water column during the summer is stratified, and the residence time of trace metals in surface water is reported to be between 1 and 5 years. Soluble ions, metals, and nutrients (NO_3 , NH_4 , Fe, Al, Zn, V, PO_4 , Cr, Co, Ni, Cu, Cd) were analyzed in each replicate after aerosol addition. All aerosol chemistry data in this study is courtesy Y. Chen. See Chen et al. (2007) for a more detailed description of the methods used for aerosol analyses.

The response of bulk phytoplankton was monitored using chlorophyll *a* concentrations, and the impact on specific phytoplankton taxa was assessed using flow cytometry. All sampling and sample handling was done without opening the incubation vessels to air (e.g., through spigots) and under trace metal clean conditions. Consistency between the trace metal concentrations in our control samples and those in surface seawater support the lack of contamination. Chlorophyll samples were taken as follows: 200-ml culture was filtered over a GF/F (Whatman) filter and

extracted in 90% acetone in the dark at 4 °C for 24 h. The extract was analyzed fluorometrically before and after acidification with 3.7% HCl on a 10-AU field fluorometer (Turner Designs). Flow cytometry samples were prepared and analyzed as described previously (Mackey et al. 2009).

Statistical Analysis. One-way ANOVA tests were used to test for differences among treatments, and Dunnett's post hoc comparisons of the groups were used to determine whether group means ($n = 3$) for each treatment differed significantly ($p < 0.05$) from the control.

Metal toxicity experiments with cultured *Synechococcus* isolates

Metal toxicity bioassays were performed using four strains of *Synechococcus* obtained from the Provasoli-Guillard National Center for Culture of Marine Phytoplankton (CCMP). Two strains were originally isolated from the open ocean, including WH8102 (strain synonym CCMP 2370) from the Sargasso Sea (22.495N, 65.6W) and CCMP 841 from the North Atlantic open ocean (exact coordinates are unavailable). The other two strains were isolated from coastal sites, including CCMP 383 collected off the coast of Woods Hole, MA USA in the North Atlantic Ocean (41.5250N 70.6736W), and CCMP 2606 collected off the coast of Goa, India in the Arabian Sea (15.3100N 72.5900E). Cultures were maintained in EDTA-free SN media (Guillard 1975 under continuous $20 \mu\text{mol quanta m}^{-2} \text{s}^{-1}$ white light.

Threshold toxicity levels were identified for each *Synechococcus* strain for silver (Ag), cadmium (Cd), chromium (Cr), copper (Cu), nickel (Ni), lead (Pb), vanadium (V), and zinc (Zn). Experiments were conducted under trace metal clean

conditions using a laminar flow hood, and all cell culturing materials were acid washed prior to use. Chlorophyll a concentration was measured for each strain at the early log phase at the start of the experiment immediately before metal additions were made. Metals were added in doses ranging from 0.001 – 10 mg metal (mg chl *a*)⁻¹ (which corresponded to roughly 0.2-2000 µg metal L⁻¹ in seawater media) using high-purity atomic absorption standards of each metal dissolved in 2% nitric acid (Sigma Aldrich). Each metal concentration was performed in triplicate test tubes. In addition, 10 control test tubes were included that had no additional metal amendments other than the background amount in the culture media (as described above). Measurements of the culture optical density at 750 nm (OD750) and the maximum photochemical efficiency of PSII (Fv/Fm) were taken before metal additions were made, and approximately 1, 24, 48, 72, and 96 hours after additions were made. OD750 is a measure of scatter and a proxy for cell density that is an indicator of cell growth. Fv/Fm measures the photosynthetic efficiency of photosystem (PS) II based on the ratio of variable to maximum PSII fluorescence, and is a proxy for cell health. These two measurements allowed us to monitor the immediate, short term responses of cell health to the additions, as well as the longer term effect of metal additions on cell growth rate. OD750 measurements were made on an Amersham Biosciences Ultrospec 3100pro spectrophotometer. Fv/Fm was measured using a WATER-PAM fluorometer and WinControl software (Heinz Walz).

RESULTS AND DISCUSSION

Copper toxicity in atmospheric aerosols

In order to assess the short-term response of phytoplankton communities to aerosol deposition, we performed bioassay experiments on northern Red Sea surface seawater (Mackey et al. 2007) using locally collected dry deposition aerosol samples which represent the bulk of the deposition in this arid area. The phytoplankton were under co-limitation of nitrogen (N) and phosphorus (P), as N and P additions on their own did not increase the amount of chlorophyll a (Chl a), whereas there were significant increases in Chl a relative to untreated controls when N and P were added together ($p < 0.001$). Iron (Fe) concentrations are elevated in these surface waters (Chase et al. 2006; Chen et al. 2008), thus the effect of Fe was not considered. Additions of N and P together with 6 mg of locally collected aerosols from the most prevalent (European) air mass source resulted in similar increases as those with combined N and P but without aerosol (**Fig. 1**). Treatments with European aerosols without inorganic N and P or with single nutrient amendment resulted in doubling of Chl a relative to the control (significant increase $p = 0.04$, **Fig. 1**).

The amount of aerosol added in these incubations (6 mg in 8 L) corresponds to the expected dust input (mg L^{-1} of surface seawater) from cumulative deposition (mg m^{-2}) over two weeks and a mixed layer of 10-20 m (typical dust storms in this region last days to weeks). The response of the phytoplankton to aerosol additions indicates that aerosols were able to supply bioavailable N and P (although at concentrations less than those supplied in the nutrient additions we used) and reverse nutrient limitation of the phytoplankton community (**Fig. 1**). The N:P ratio in the aerosols was very high

(on average N:P = 170) compared to the Redfield ratio typically required by marine phytoplankton (N:P = 16), emphasizing the importance and potential impact of atmospheric deposition as a nitrogen source to the ocean (Doney et al. 2007, Moore et al. 2006; Krishnamurthy et al. 2007).

Aerosols of African (Sahara desert) trajectory were also used for comparison to the more common European aerosol (**Fig. 1**). The same amount of aerosol as for the European aerosol additions that stimulated growth was used (6 mg in 8 L). The concentrations of soluble nutrients and trace metals added from these aerosols to the bioassay incubations were determined by measuring the total amount (μg or μmoles) of each component released to seawater from the aerosol filters after adding them to the incubation bottles. **Fig. 2** shows the elements and compounds released from aerosols that were significantly different between the European and African aerosols. Although the African aerosol released more soluble nitrate, ammonium, and phosphate than aerosols from European origin (**Fig. 2**), we nevertheless observed sharp declines in Chl *a* in all treatments (3 replicates) receiving African aerosols (**Fig. 1**). These results indicate that the lack of growth following African aerosol addition may have been a result of toxic effects of one or more of the trace metals added to solution from the aerosol. Because of the high concentrations of copper (Cu) added from the African aerosols compared to the European aerosols (**Fig. 2**) and the well documented negative effects of Cu on phytoplankton Cu is likely to have caused the toxicity (Mann et al. 2002). However, the possibility that other elements present in the aerosols or unknown synergistic effects between these elements could have also contributed to the toxic effect cannot be ruled out.

To determine the threshold Cu toxicity and compare it to that calculated from the *in situ* incubation experiments, serial Cu addition experiments were conducted in the laboratory using the oceanic *Synechococcus* strain WH8102. WH8102 was selected because it is representative of *Synechococcus* from oligotrophic waters, such as the Gulf of Aqaba. Metal toxicity depends on free (non-complexed) Cu concentrations (Sunda and Huntsman 1998); however, in the open ocean, free Cu levels are controlled primarily by Cu-binding organic ligands released by organisms (Sunda and Huntsman 1998, Morel and Price 2003). Accordingly, to account for variable levels of organic ligands in solution (and thus the free non-ligand-bound Cu), we report total Cu concentrations normalized to Chl *a* (a proxy for biomass and proportional to organic ligand levels). Such normalization also allows for global extrapolation of our results using satellite-derived global Chl *a* levels, as was done in the coupled ocean-atmosphere model (Paytan et al. 2009), since data on free Cu concentration in surface seawater is sparse. Toxicity in our lab experiments occurred at levels above 0.2 mg Cu per mg Chl *a* for WH 8102. The toxicity response was rapid, depressing Fv/Fm measurements (a measure of photosynthetic capacity) within 1 h and impairing cell growth within 24 h of Cu addition (**Fig. 4**). These results are consistent with our field observations (toxicity at 0.4 mg Cu per mg Chl *a* apparent within the first day of incubation) and with previously published results from the Sargasso Sea and other culture experiments (Mann et al. 2002, Moffett and Brand 1996).

Flow cytometry measurements (**Fig. 3**) show that photosynthetic picoeukaryotes (**Fig. 3a**), and cyanobacterial populations of *Synechococcus* (**Fig. 3b**),

and *Prochlorococcus* (**Fig. 3c**) did not respond uniformly to aerosol treatments in the Red Sea incubation experiment. Picoeukaryotes showed a large increase in cell numbers when enriched with 6 mg European aerosol, or N and P together. Enrichment with 6 mg African aerosol caused a marked decrease in picoeukaryote cell numbers despite having provided fertilizing levels of N and P (**Fig. 2**). *Synechococcus* abundances were likewise greater than in the control in treatments receiving European aerosol or N and P together. Like the picoeukaryotes, African dust led to a sharp decline in *Synechococcus* cell number. In contrast to strains from the Atlantic (Mann et al. 2002), *Prochlorococcus* in the Gulf of Aqaba showed no large changes in cell number with the different treatments regardless of the aerosol's origin and appear to be less sensitive to Cu toxicity. The results suggest that genetic and physiological properties of individual taxa within the community result in markedly divergent responses to aerosol additions.

To investigate the global implications of atmospheric Cu deposition the data was used in a three-dimensional atmospheric tracer transport model (by I. Lima, S. Doney, and N. Mahowald) to estimate pre-industrial and contemporary aerosol Cu deposition fields (Paytan et al. 2009). Using the toxicity thresholds determined in the incubation and metal toxicity experiments described above, global regions with potential high (toxic) Cu levels were identified by normalizing modeled Cu deposition rates to ocean chlorophyll concentrations from the SeaWiFS (Sea-viewing Wide Field-of-view Sensor) satellite ocean color instrument (McClain et al. 2004). The model shows that under pre-industrial conditions, potential Cu toxicity levels are concentrated in the northern hemisphere downwind of natural dust sources in low-chlorophyll subtropics

in the Atlantic, Mediterranean and Indian Ocean basins. Anthropogenic emissions expand the potential toxicity zones into the Bay of Bengal and small areas in the west Pacific downwind of Asian industrial regions (map shown in Paytan et al. 2009).

Collectively results indicated that: (1) Aerosol addition can contribute substantial amounts of N and P to the ocean and may enhance phytoplankton growth (**Fig. 1**); (2) Aerosols arriving to the northern Red Sea along different trajectories differ in their chemical characteristics (**Fig. 2**); (3) Aerosols from different sources induce considerably different responses of phytoplankton biomass including fertilization as well as adverse toxic effects (**Fig. 1**); and (4) Different phytoplankton taxa respond differently to aerosol additions, thus phytoplankton community structure may be affected by aerosol additions (**Fig.3**). Application of these results in a global atmospheric deposition model suggest that Cu toxicity could affect the global distribution of phytoplankton taxa in areas that receive high amounts of natural aerosol deposition as well as anthropogenic aerosols enriched in Cu.

Metal toxicity in coastal and oceanic *Synechococcus*

The toxic effects of Cu are well documented for marine organisms (Mann et al. 2002; Nayar et al. 2004; Stuart et al. 2009). The Cu toxicity threshold concentration we observed in the field aerosol incubations is consistent with the threshold toxicity levels found in the lab experiments and with previously reported toxic responses (Mann et al. 2002). Together these facts support the conclusion that Cu caused the toxic response in the *Synechococcus* population in our field samples when incubated with African dust. However, a number of other metals were also more abundant in

African aerosols that European aerosols (**Fig. 2**) and their direct or synergistic roles in the toxic response we observed cannot be ruled out. To characterize the sensitivity of *Synechococcus* WH 8102 to other metals that are sometimes abundant in aerosols, metal toxicity bioassays were performed. Metals that were higher on a per mass basis in African aerosols than European aerosols, including Cd, Cr, Cu, Ni, Pb, V, Zn were selected. In addition, Ag was included because it is a known anthropogenic pollutant (Sanudo-Wilhelmy and Flegal 1992) and its toxicity to marine phytoplankton is well established (Hutchinson 1973).

Synechococcus WH 8102 showed sensitivity to all treatments in the experiment, and negative effects on growth were observed for all metals at all concentrations used. Negative effects included decreased growth rate relative to control cultures, as well as complete toxicity in which the cells died (had negligible or negative growth rates). For metal treatments in which complete toxicity occurred, toxicity thresholds were determined as the highest concentration of metal that did not cause cells to die. In addition to Cu, the metals Ag, Cd, Ni, and Zn caused cultures to die at some of the tested concentrations (**Fig. 5**).

To determine if other metals in the African aerosol could have also contributed to the toxicity we observed in the *Synechococcus* population in the incubation experiment, the concentration of metals added from the African aerosol additions were compared to the threshold toxicity levels measured in the metal toxicity experiment (**Table 1**). While both Cu and Ni were present in sufficiently high quantities in the African aerosol to cause toxicity in *Synechococcus*, based on the response over time Cu is still the strongest candidate for causing the toxic response observed among the

metals considered here. The toxic response of *Synechococcus* was rapid following addition of African aerosols, and cell death was apparent after only 2 days of incubation and likely sooner (**Fig. 3**). This rapid response was also observed in the metal toxicity experiment for Cu, where cell death was observed after 1 day for concentrations above the toxicity threshold (**Fig. 4**). The response to Ni toxicity took longer to observe and incubation periods of 4 days were required before cell death was observed (not shown). Therefore, while Ni in the African aerosol was present at a toxic level, the rapid toxicity response observed was likely the result of Cu, which has a more immediate toxic effect.

In general, growth rates relative to control for WH 8102 decreased as metal concentrations increased regardless of whether complete toxicity was reached, and decreased growth rates were observed relative to control cultures for all metals. For example, Cr, Pb, and V all showed impaired growth with increasing metal concentration; however, no toxicity threshold was observed in the range of concentrations we tested (**Fig. 5; Table 2**). Zn was also present at levels close to the toxicity threshold. However, of the three replicate bottles receiving African dust, only one had Zn levels that actually exceeded the toxicity threshold (**Table 1**). Since toxicity was observed in all three bottles, Zn was therefore less likely to have caused the toxic response in the *Synechococcus* population. Nevertheless, while the level of Cu present in the African aerosol addition was sufficient to independently cause toxicity based on the Cu toxicity threshold we measured for *Synechococcus* (**Table 2**), it is possible that other metals in the aerosol could have potentiated the toxic effects

observed even though they were present at concentrations below their respective toxicity threshold levels.

The global model results discussed above (full text in Paytan et al. 2009) were based on the toxicity threshold for Cu for a *Synechococcus* population in the oligotrophic Red Sea and a strain of *Synechococcus* isolated from the oligotrophic Atlantic Ocean (WH 8102). While oligotrophic waters account for over half of the surface area of the world's oceans available for phytoplankton to colonize, nutrient rich coastal waters also provide very important niches for phytoplankton. *Synechococcus* strains inhabit both the oligotrophic open ocean and nutrient rich coastal waters, and considerable physiological diversity exists within the *Synechococcus* genus (Scanlan et al. 2009). Different requirements of oceanic and coastal *Synechococcus* for macronutrients like N are well established (Scanlan et al. 2009). Moreover, genomic comparison of coastal *Synechococcus* CC9311 with oceanic WH 8102 shows that the coastal strain had a greater ability to transport, store, use, and export metals (Palenik et al. 2006). The greater resistance of this strain to Cu toxicity was also directly confirmed in a recent study (Stuart et al. 2009). To gauge the range of toxicity responses in coastal and oceanic *Synechococcus* strains metal toxicity experiments were performed on an additional oceanic strain (CCMP 841) and two coastal strains (CCMP 838 and CCMP 2606).

The strain with the most robust physiological response to metals was CCMP 2606, for which no toxicity threshold was observed for 5 of the 8 metals we tested (Cr, Ni, Pb, V, and Zn; **Table 2**). Toxicity was observed for Cu and Cd, but at concentrations that were an order of magnitude higher than for the other strains (**Table**

2). Interestingly, coastal strain CCMP 838 shared greater similarity in toxicity threshold response with the two oceanic strains than with coastal strain CCMP 2606 (**Table 2**). However, both oceanic strains WH 8102 and CCMP 841 tended to have decreased growth rates at lower metal concentrations than CCMP 838, even though their toxicity thresholds were similar (**Table 2**). For example, all strains shared similar threshold for Ag (0.1-0.4 mg per mg chl *a*); however, the coastal strains showed a sharp threshold toxicity for Ag with no decreased growth rate at lower concentrations (**Fig. 7 and 8**), whereas the growth rates of oceanic strains decreased with increasing Ag concentration until the threshold level was reached (**Fig. 5 and 6**).

The difference in how cells respond to sub-toxic metal concentrations could be due to genetic differences, including the ability to sequester and store metals. For example, coastal *Synechococcus* strain CC9311 has four copies of the *smtA* gene encoding bacterial metallothionein, compared to a single copy in oceanic strain WH 8102 (Palenik et al. 2006), and also has more metal-containing enzymes (Palenik et al. 2006). The ability to safely sequester metals could confer a selective advantage in the coastal ocean where metal concentrations can fluctuate widely due to land-sea interactions. In contrast, the open ocean is in general subject to fewer and less extreme fluctuations in metal concentration. The fact that oceanic strains appear to have scaled back the number of genes involved in metal storage could therefore represent an evolutionary trade off, because those genes would confer less of a selective advantage in the open ocean than along the coast. The competitive advantage of oceanic *Synechococcus* may arise from other adaptations that are more

pertinent in oligotrophic open ocean waters, such as high affinity nutrient uptake genes for macronutrients like N (Palenik et al. 2003).

Whether a certain metal will become toxic in the marine environment depends on a number of factors including the organisms present, the residence time of the water, the surface layer mixing depth, and the input rate of metals from various exogenous sources. The toxicity thresholds measured in our culture studies are most applicable to environmental conditions that introduce sudden pulses of metals, because processes that cause gradual accumulation of metals in the surface ocean give phytoplankton time to acclimate, e.g. through the production of metal binding ligands that reduce the amount of free metal in solution (Moffett and Brand 1996). Stuart and coworkers (2009) note that episodic metal pulses can occur during large rain events, following substantial aerosol deposition, or when deep water is brought to the surface, such as in wind driven mixing or upwelling. During upwelling, metals that accumulate in deep water from the sinking of aerosol particles, phytoplankton, and zooplankton fecal pellets are brought back to the surface, and can raise the concentration of metals in the water significantly over short time periods (Bruland et al. 2001).

Resistance to metal toxicity is an adaptation that would be expected in *Synechococcus* populations that have been exposed regularly to high metal concentrations over evolutionary time scales. Of the four strains examined in this study, strain CCMP 2606 had the most robust response to metal additions. This strain was isolated from the Arabian Sea along the west coast of India, a region with strong potential for very high pulses of metals to occur in the surface ocean. The west coast

of India receives substantial precipitation during monsoons, and is also a major upwelling center. In addition, the region receives substantial amounts of aerosol deposition due to its geographical proximity to deserts within the Arabian Peninsula, Africa, and western Asia. Deposition rates range from 5-50 g m⁻² yr⁻¹ along the west coast of India (Mahowald et al. 2005; Krishnamurti et al. 1998; Rhoads et al. 1998 ; Savoie et al. 1987), which is about an order of magnitude higher than for many other coastal sites worldwide (Mahowald et al. 2005). The high resistance of strain CCMP 2606 to metal toxicity may therefore be the result of selective forces imposed by coastal waters with very high metal concentrations.

The role different metals play in influencing phytoplankton growth is becoming more apparent as the genomes of more marine phytoplankton become sequenced (Palenik et al. 2003; Palenik et al. 2006). As important cofactors and constituents of enzymes, metals play a direct role in determining the competitive fitness of a cell, but may also cause toxic effects when present at elevated levels. This study shows that the growth of oceanic *Synechococcus* strains is more sensitive to sub-toxic metal concentrations than is the growth of their coastal counterparts. Moreover, considerable diversity in toxicity thresholds exists among strains, with coastal strains generally being more robust at higher metal concentrations. The different responses of *Synechococcus* to metal concentrations observed in this study suggest that metals can influence phytoplankton community composition. However, in order for *Synechococcus* distributions to be fully explained and predicted more work is needed to determine the full range of responses and their relevance throughout the world's oceans.

ACKNOWLEDGEMENTS

I acknowledge my co-authors Adina Paytan, Ying Chen, Ivan D Lima, Scott C Doney, Natalie Mahowald, Rochelle Labiosa, and Anton F. Post for their contributions on the first section of this chapter, which was published in 2009 in the *Proceedings of the National Academy of Sciences* (Paytan et al. 2009). I thank my colleagues at the Interuniversity Institute for Marine Science in Eilat, Israel for assisting in data collection and providing laboratory space and equipment during the study. For the second section of this chapter I acknowledge Adina Paytan for help improving the text, and Josh Chan for assistance in taking the laboratory measurements. This research was supported under the NASA New Investigator Program NAG5-1266 to A. Paytan and a NATO Science for Peace Grant SfP 982161 to A. Paytan and A.F. Post. KRMM was supported through the NSF Graduate Research Fellowship Program and the DOE Global Change Education Program.

Citation (in which part of this chapter was published)

Paytan, A, KRM Mackey, Y Chen, ID Lima, SC Doney, N Mahowald, R Labiosa, and AF Post. 2009. Toxicity of atmospheric aerosols on marine phytoplankton. *Proceedings of the National Academy of Science*. 106: 4601 – 4605.

Author Contributions (for the published paper, Paytan et al. 2009)

KRM Mackey – designed research; performed research, specifically, performed field incubation experiments and laboratory Cu addition experiments with *Synechococcus* cultures, and analyzed all chlorophyll and flow cytometry

samples in the study, but did not perform the measurement of aerosol soluble metal concentrations (contributed by Y Chen) or the global deposition models (contributed by ID Lima, SC Doney, and N Mahowald); contributed new reagents/ analytic tools; analyzed data; wrote the paper

A Paytan – designed research; performed research; contributed new reagents/ analytic tools; analyzed data; wrote the paper

Y Chen - performed research; analyzed data

ID Lima - performed research (global deposition model); analyzed data

SC Doney - performed research (global deposition model); contributed new reagents/ analytic tools; analyzed data; wrote the paper

N Mahowald - performed research (global deposition model); contributed new reagents/ analytic tools; analyzed data; wrote the paper

R Labiosa - performed research; analyzed data

AF Post – designed research; performed research; contributed new reagents/ analytic tools; analyzed data; wrote the paper

REFERENCES

- Agusti, S. 2004. Viability and niche segregation of *Prochlorococcus* and *Synechococcus* cells across the Central Atlantic Ocean. *Aquatic Microbial Ecology* 36:53-59
- Brand L. E., Sunda W. G., Guillard R. R. L.(1986) Reduction of marine phytoplankton reproduction rates by copper and cadmium. *J. Exp. Mar. Biol. Ecol.* 96:225–250
- Bruland KW, EL. Rue and G J. Smith (2001) Iron and Macronutrients in California Coastal Upwelling Regimes: Implications for Diatom Blooms. *Limnology and Oceanography*, 46:1661-1674
- Chase Z, Paytan A, Johnson K.S, Street J, Chen Y (2006) Input and cycling of iron in the Gulf of Aqaba, Red Sea. *Global Biogeochemical Cycles* 20:GB3017.
- Chen Y, et al. (2008) Sources and fluxes of atmospheric trace elements to the Gulf of Aqaba, Red Sea. *JGR Atmospheres* 113:D05306.
- Chen, Y., and R. L. Siefert (2004), Seasonal and spatial distributions and dry deposition fluxes of atmospheric total and labile iron over the tropical and subtropical North Atlantic Ocean, *J. Geophys. Res.*, 109, D09305, doi:10.1029/2003JD003958.
- Chen, Y., S. Mills, J. Street, D. Golan, A. Post, M. Jacobson and A. Paytan. 2007. Estimates of atmospheric dry deposition and associated input of nutrients to Gulf of Aqaba seawater. *Journal of Geophysical Research*, 112, D04309,doi:10.1029/2006JD007858.

- Doney S.C, et al. (2007) Impact of anthropogenic atmospheric nitrogen and sulfur deposition on ocean acidification and the inorganic carbon system. *Prod. Nat. Acad. Sci. USA* 104:14580-14585.
- Duce, R. A (1986) The impact of atmospheric nitrogen, phosphorus, and iron species on marine biological productivity. in *The Role of Air-Sea Exchange in Geochemical Cycling*, edited by P. Buat-Menard, pp. 497-529, D. Reidel, Norwell, Mass.
- Duce et al. (2008) Impacts of Atmospheric Anthropogenic Nitrogen on the Open Ocean. *Science* 320: 893 - 897
- Du Rand, MD, RJ Olson, and SW Chisholm. 2001. Phytoplankton population dynamics at the Bermuda Atlantic Time-series station in the Sargasso Sea. *Deep Sea Research Part II: Topical Studies in Oceanography* 48: 1983-2003.
- Field, CB, MJ Behrenfeld, JT Randerson, P Falkowski. 1998. Primary production of the biosphere: Integrating terrestrial and oceanic components. *Science* 281: 237 – 240
- Guillard, R.R.L. 1975. Culture of phytoplankton for feeding marine invertebrates. pp 26-60. In Smith W.L. and Chanley M.H (Eds.) *Culture of Marine Invertebrate Animals*. Plenum Press, New York, USA.
- Hutchinson, T.C. 1973. Comparative studies of the toxicity of heavy metals to phytoplankton and their synergistic interactions. *Water Pollut. Res. J. Can.; (Canada)* 8: 68-90
- Krishnamurti, T. N. , Jha, B. , Prospero, J. M. , Jayaraman, A. & Ramanathan, V. (1998) Aerosol and pollutant transport and their impact on radiative forcing over

tropical Indian Ocean during the January–February, 1996 pre-INDOEX cruise.

Tellus B 50: 521 –542

Krishnamurthy A., Moore J. K, Zender C. S, Luo C. (2007) Effects of atmospheric inorganic nitrogen deposition on ocean biogeochemistry, J. Geophys. Res., 112, G02019, doi:10.1029/2006JG000334.

Lindell, D., S. Penno, M. Al-Qutob, E. David, T. Rivlin, B. Lazar, and A. F. Post. 2005. Expression of the N-stress response gene *ntcA* reveals N-sufficient *Synechococcus* populations in the oligotrophic northern Red Sea. Limnology and Oceanography **50**: 1932-1944.

Mackey K.R.M. et al., (2007) Phosphorus availability, phytoplankton community dynamics, and taxon specific phosphorus status in the Gulf of Aqaba, Red Sea. Limnology and Oceanography 52:873-885.

Mackey, K.R.M, T. Rivlin, A.R. Grossman, A.F. Post, A. Paytan. 2009. Picophytoplankton responses to changing nutrient and light regimes during a bloom. Marine Biology, DOI 10.1007/s00227-009-1185-2.

Mahowald, NM, A R. Baker, G Bergametti, N Brooks, R A. Duce, T D. Jickells, N Kubilay, J M. Prospero, I Tegen (2005) The atmospheric global dust cycle and iron inputs to the ocean. Global Biogeochem. Cycles, **19**: GB4025, doi:10.1029/2004GB002402.

Mann, EL, N Ahlgren, J W Moffett and S W Chisholm. 2002. Copper Toxicity and Cyanobacteria Ecology in the Sargasso Sea. Limnol. Oceanogr. 47: 976-988.

- McClain C.R., Feldman G.C., Hooker S.B. (2004) An overview of the SeaWiFS project and strategies for producing a climate research quality global ocean bio-optical time series. *Deep-Sea Research II* 51:5–42.
- Mills, M.M., C. Ridame, M. Davey, J. La Roche (2004) Iron and phosphorus co-limit nitrogen fixation in the eastern tropical North Atlantic. *Nature* 429, 292-294.
- Moffett J.W, Brand L.E. (1996) Production of strong, extracellular Cu chelators by marine cyanobacteria in response to Cu stress. *Limnology and Oceanography* 41:873-885.
- Moore J.K., Doney S.C., Lindsay K., Mahowald N., Michaels A.F. (2006) Nitrogen fixation amplifies the ocean biogeochemical response to decadal timescale variations in mineral dust deposition. *Tellus* 58B:560-572.
- Moore, LR, R. Goericke, and SW Chisholm. 1995. Comparative physiology of *Synechococcus* and *Prochlorococcus*: influence of light and temperature on growth, pigments, fluorescence and absorptive properties. *Marine Ecology Progress Series* 116: 259-275
- Moore, LR, A F. Post, G Rocap and S W. Chisholm. 2002. Utilization of Different Nitrogen Sources by the Marine Cyanobacteria *Prochlorococcus* and *Synechococcus*. *Limnol. Oceanogr.* 47: 989-996
- Morel M.M.F., Price N.M. (2003) The biogeochemical cycles of trace metals in the ocean. *Science* 300:944-947
- Nayar S, Goh B.P.L., Chou L. M. (2004) Environmental impact of heavy metals from dredged and re-suspended sediments on phytoplankton and bacteria assessed in in-situ mesocosms. *Ecotoxicology and Environmental Safety* 59:349-369.

- Paerl, HW, and ML Fogel (1994) Isotopic characterization of atmospheric nitrogen inputs as sources of enhanced primary production in coastal Atlantic Ocean waters. *Marine Biology* **119**: 635-645
- Palenik, B. 2001. Chromatic Adaptation in Marine *Synechococcus* Strains. *Appl Environ Microbiol.* 67(2): 991–994.
- Palenik B, Brahamsha B, Larimer FW, Land M, Hauser L, Chain P, Lamerdin J, Regala W, Allen EE, McCarren J, et al.: 2003. The genome of a motile marine *Synechococcus*. *Nature* 424:1037-1042
- Palenik, B, et al. (2006) Genome sequence of *Synechococcus* CC9311: Insights into adaptation to a coastal environment. *Proceedings of the National Academy of Sciences* 36: 13555-13559
- Partensky FJ, Hess WR, Vaultot D (1999) *Prochlorococcus*, a marine photosynthetic prokaryote of global significance. *Microbiology and Molecular Biology Reviews* 63:106-127
- Prospero, J. M and Savoie, D. L (1989) Effect of continental sources on nitrate concentrations over the Pacific Ocean. *Nature* **339**: 687 - 689
- Rhoads, KP (1998) The influence of continental emissions on the composition of the remote marine boundary layer. Thesis (PhD). University of Maryland, College Park, Source DAI-B 59/06, p. 2630, Dec 1998, 226 pages
- Sanudo-Wilhelmy, SA, and A. R Flegal. 1992 Anthropogenic silver in the Southern California Bight: a new tracer of sewage in coastal waters. *Environmental Science and Technology* 26 (11): 2147–2151

- Savoie, DL, JM Prospero, and RT Nees (1987) Nitrate, non-sea-salt sulfate, and mineral aerosol over the northwestern Indian Ocean. *Journal of Geophysical Research*. 92: 933-942
- Scanlan, DJ, M. Ostrowski, S. Mazard, A. Dufresne, L. Garczarek, W. R. Hess, A. F. Post, M. Hagemann, I. Paulsen, and F. Partensky. 2009. Ecological genomics of marine picocyanobacteria. *Microbiology and Molecular Biology Reviews* 73: 249-299
- Stuart, R. K., C. L. Dupont, D. A. Johnson, I. T. Paulsen, and B. Palenik. 2009. Coastal Strains of Marine *Synechococcus* Species Exhibit Increased Tolerance to Copper Shock and a Distinctive Transcriptional Response Relative to Those of Open-Ocean Strains. *Appl. Environ. Microbiol.* 75:5047-5057
- Sunda W.G, Huntsman S.A (1998) Processes regulating cellular metal accumulation and physiological effects: Phytoplankton as model systems. *Science of the Total Environment* 219:165–181.
- Waterbury, J.B., Watson, S.W., Valois, F.W. and Franks, D.G. 1986. Biological and ecological characterization of the marine unicellular cyanobacterium *Synechococcus*. In Platt, T. and Li, W.K.I. (eds.) *Photosynthetic Picoplankton*. Can. Bull. Fish. Aquatic Sci. 214: 71

Table 1: Comparison of metal concentrations in the in situ incubation for bottles receiving African aerosols with threshold toxicity concentrations determined from the metal toxicity experiment for WH 8102. The metals Cu and Ni exceeded the toxicity threshold level in the incubation experiment. ND indicates concentrations were not determined. NT indicates no toxicity threshold was observed over the range of concentrations we tested.

Metal	Metal concentration contributed from African aerosol additions mg metal (mg chl <i>a</i>) ⁻¹	Metal toxicity threshold mg metal (mg chl <i>a</i>) ⁻¹
Ag	ND	0.2
Cd	0.02 – 0.03	0.2
Cr	0.03	NT
Cu	0.23 – 0.37	0.2
Ni	0.23 -0.40	0.02
Pb	0.21 – 0.26	NT
V	0.83 – 1.04	NT
Zn	1.25 – 2.08	2

Table 2: Toxicity of various metals on *Synechococcus* strains. Values have units mg metal (mg chl a)⁻¹. The first number gives the toxicity threshold concentration (the highest concentration in which positive growth is observed in Figures 5-8.) Concentrations above the toxicity threshold yield negligible or negative growth rates. Numbers in parentheses indicate the concentration above which cells showed some decrease in growth (but not necessarily toxicity). Control cells were grown without additional metal amendments other than the amount normally in the media. Not determined (ND) indicates that any metal addition greater than the background amount in the media decreased growth, so the exact concentration could not be determined based on the range of concentrations we tested. Where the toxicity threshold concentration and the concentration at which decreased growth was first observed are the same, this indicates a sharp threshold toxicity was observed (such as for Ag in strain 2606, **Fig. 8**). Where the toxicity threshold concentration is greater than the concentration at which decreased growth was first observed, this means that growth decreased gradually with increasing metal concentration until the toxicity threshold was reached (such as for Cd in strain WH8102, **Fig. 5**).

	Oceanic <i>Synechococcus</i> strains		Coastal <i>Synechococcus</i> strains	
Metal	WH 8102	CCMP 841	CCMP 838	CCMP 2606
Ag	0.2 (ND)	0.4 (ND)	0.1 (0.1)	0.1 (0.1)
Cd	0.2 (ND)	0.4 (0.04)	0.1 (0.1)	1 (1)
Cr	NT (ND)	NT (NT)	NT (NT)	NT (NT)
Cu	0.2 (ND)	0.4 (0.4)	0.1 (0.1)	1 (0.1)
Ni	0.02 (ND)	0.4 (0.04)	0.1 (0.1)	NT (0.01)
Pb	NT (ND)	NT (4)	NT (1)	NT (ND)
V	NT (ND)	NT (NT)	NT (NT)	NT (NT)
Zn	2 (0.02)	4 (0.4)	1 (1)	NT (NT)

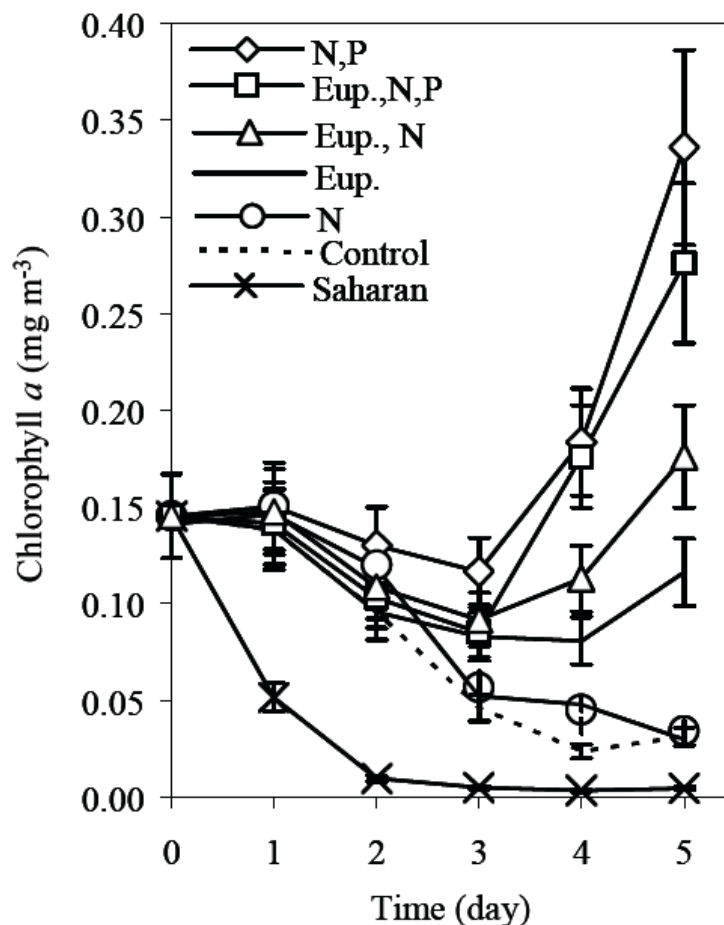


Figure 1: The response of phytoplankton from the Gulf of Aqaba to major-nutrients and aerosol addition monitored over five days in bioassay experiments. A one-way ANOVA indicated that mean Chl *a* levels differed significantly across treatments, $F(6, 17) = 15.4$, $p < .001$. Shown are chlorophyll *a* concentrations relative to control (no additions), combined nitrogen and phosphorus (N, P) addition, European aerosol together with N and P additions (Eup., N, P), European aerosol additions alone (Eup.) or with N addition (Eup.,N), singular amendment with only nitrogen (N), and addition of African aerosol (Sahara). Addition of European aerosol combined with phosphate (Eup, P, not shown) was similar to that of the aerosol with N addition, while addition of P alone (not shown) yielded results similar to the control or addition of N alone. Note that only the addition of African aerosols resulted in lower chlorophyll *a* compared to the control (in all three replicate incubations). Error bars show standard error of the mean of three replicate samples.

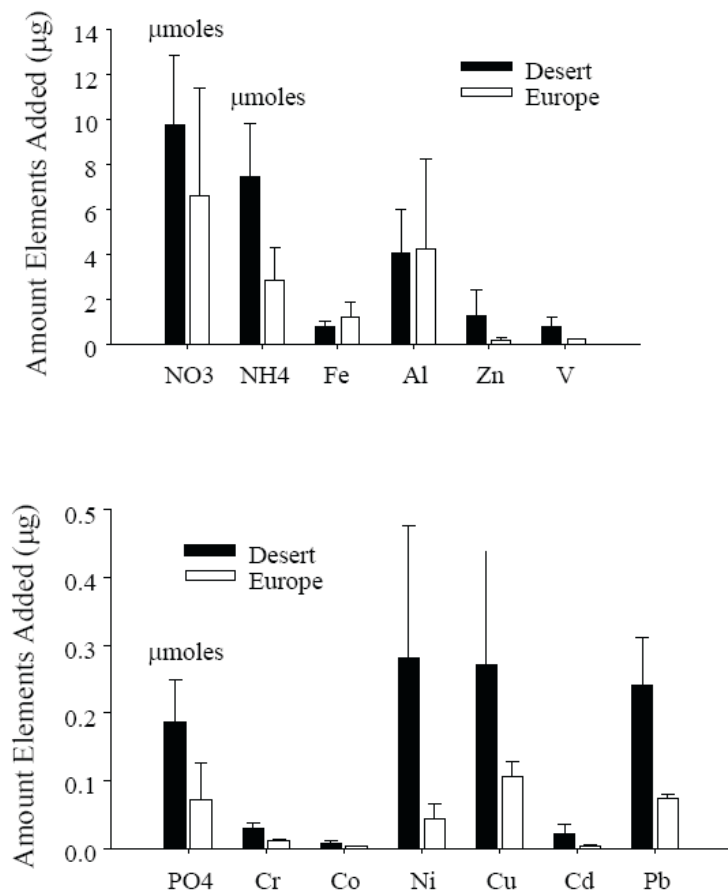


Figure 2: Nutrient and trace metal contribution from aerosols of different origin. Values represent the amounts of each chemical constituent (μg or μmoles) that leached from 6 mg of aerosol. (Six mg aerosol was added per incubation bottle, and each bottle contained 8 L of seawater.) African (Sahara Desert) aerosols (black bars) and European aerosols (white bars) collected locally at the Gulf of Aqaba are shown. Note that each incubation received a distinct aerosol filter collected simultaneously (triplicate treatments were not homogenized) resulting in some variability between triplicates. The top of the wide bar for each component represent the replicate with the lowest measured concentration and the top of the thin line the highest concentration measured (e.g. full range is represented not errors). We use the lower value of Cu in the African dust (top of the broad black bar) for calculating the threshold concentration which corresponds to the chlorophyll levels in the Gulf. The lowest Cu concentration in the African aerosols is about 3 times higher than the highest in the European aerosols. The amount of Cu added from the aerosol resulted in 2 fold increase compared to the ambient Cu concentrations in Gulf of Aqaba surface water (which are similar to Atlantic surface water concentrations). Aerosol chemistry analyses were performed by Y. Chen as described by Chen et al. (2007).

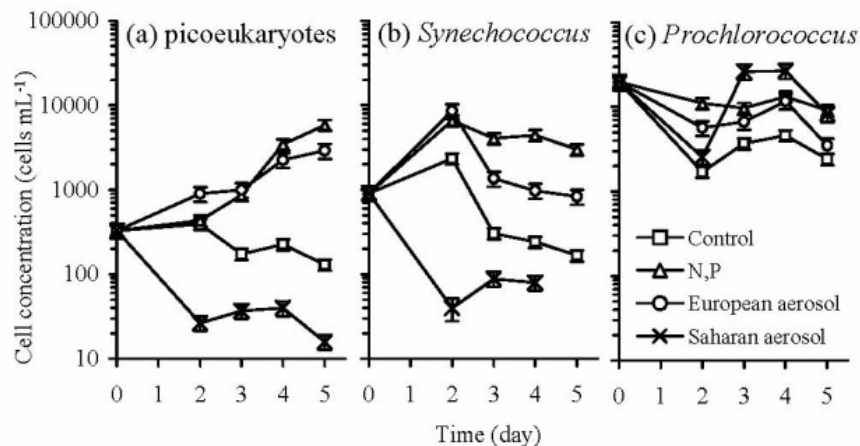


Figure 3: Variable response of local phytoplankton taxa to nutrient and aerosol additions.

The response of (a) *picoeukaryotes* (b) *Synechococcus*, and (c) *Prochlorococcus* from surface seawater in the Gulf to aerosol additions. Note: log scales used in these plots. Error bars denote SE of triplicate measurements. Data for day 5 for *Synechococcus* is not shown in the figure because the levels crashed to zero (i.e. all cells were dead) by day 5, and it is not possible to show a value of zero on the log scale we have used here.

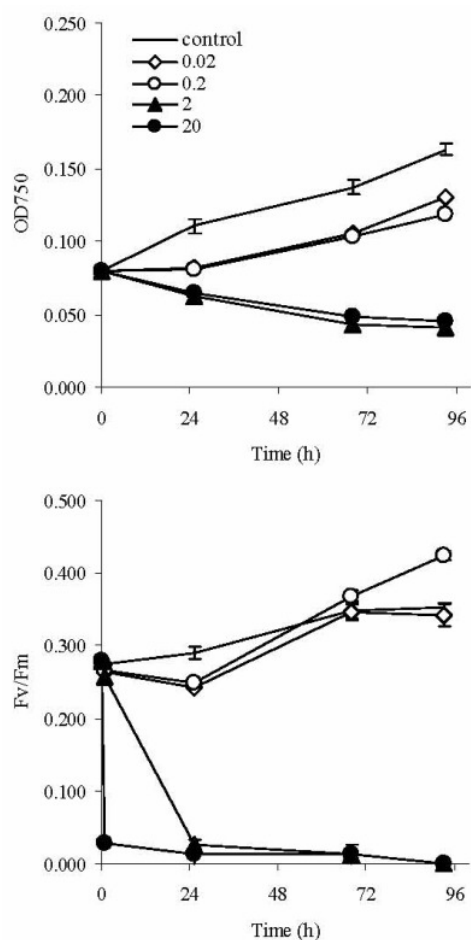


Figure 4: Time series measurements of (A) optical density at 750 nm (OD 750) and (B) Fv/Fm following addition of Cu. Series labels indicate Cu concentrations normalized to chlorophyll a concentration in mg Cu (mg Chl a)⁻¹. A one-way ANOVA was used to test for differences among treatments ($F(4, 10) = 144$, $p < .001$). Treatments receiving Cu at concentrations above the 0.4 mg Cu (mg Chl a)⁻¹ threshold had decreased cell density relative to the control ($p < 0.001$) 25 h following Cu addition that continued throughout the 4-day experiment, suggesting that the toxic Cu levels inhibited growth in these treatments. Cells responded rapidly to addition of Cu above the threshold level, showing a reduction in Fv/Fm in treatments receiving 2 and 20 mg Cu (mg Chl a)⁻¹. These measurements reached values of ~ 0.03 25 h after Cu additions were made and did not recover over the course of the 4-day experiment. Fv/Fm remained comparable in the untreated control and in treatments receiving less than 0.2 mg Cu (mg Chl a)⁻¹. All treatments were conducted in triplicate. Error bars show SE of the mean of three measurements. When not visible, error bars fall within the symbol. In all additions that exceeded the threshold we see a significant reduction of both Fv/Fm and OD 750 after 25 hours compared to control and lower-than-threshold additions.

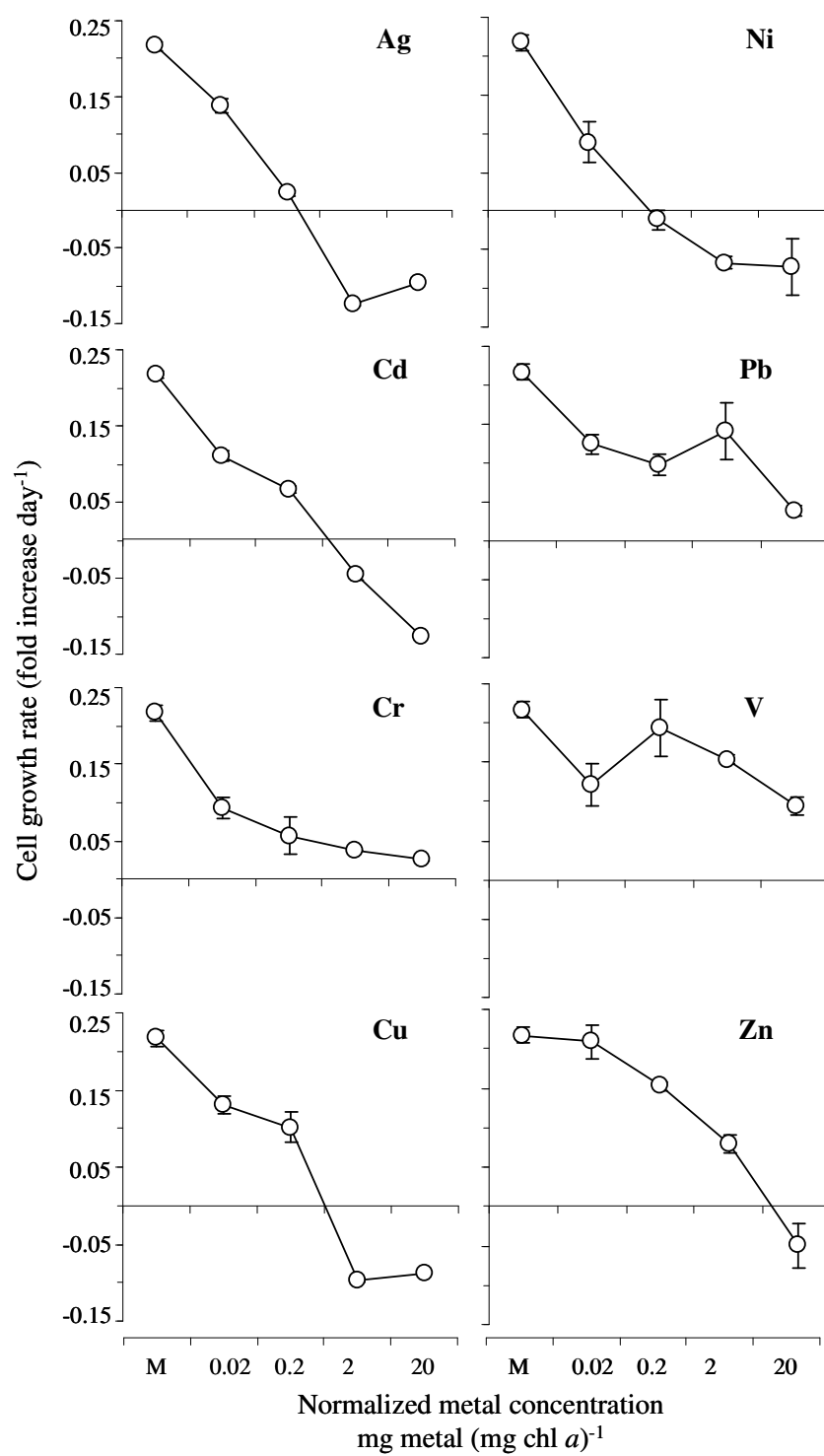


Figure 5: Response of oceanic *Synechococcus* strain WH 8102 to metal additions.

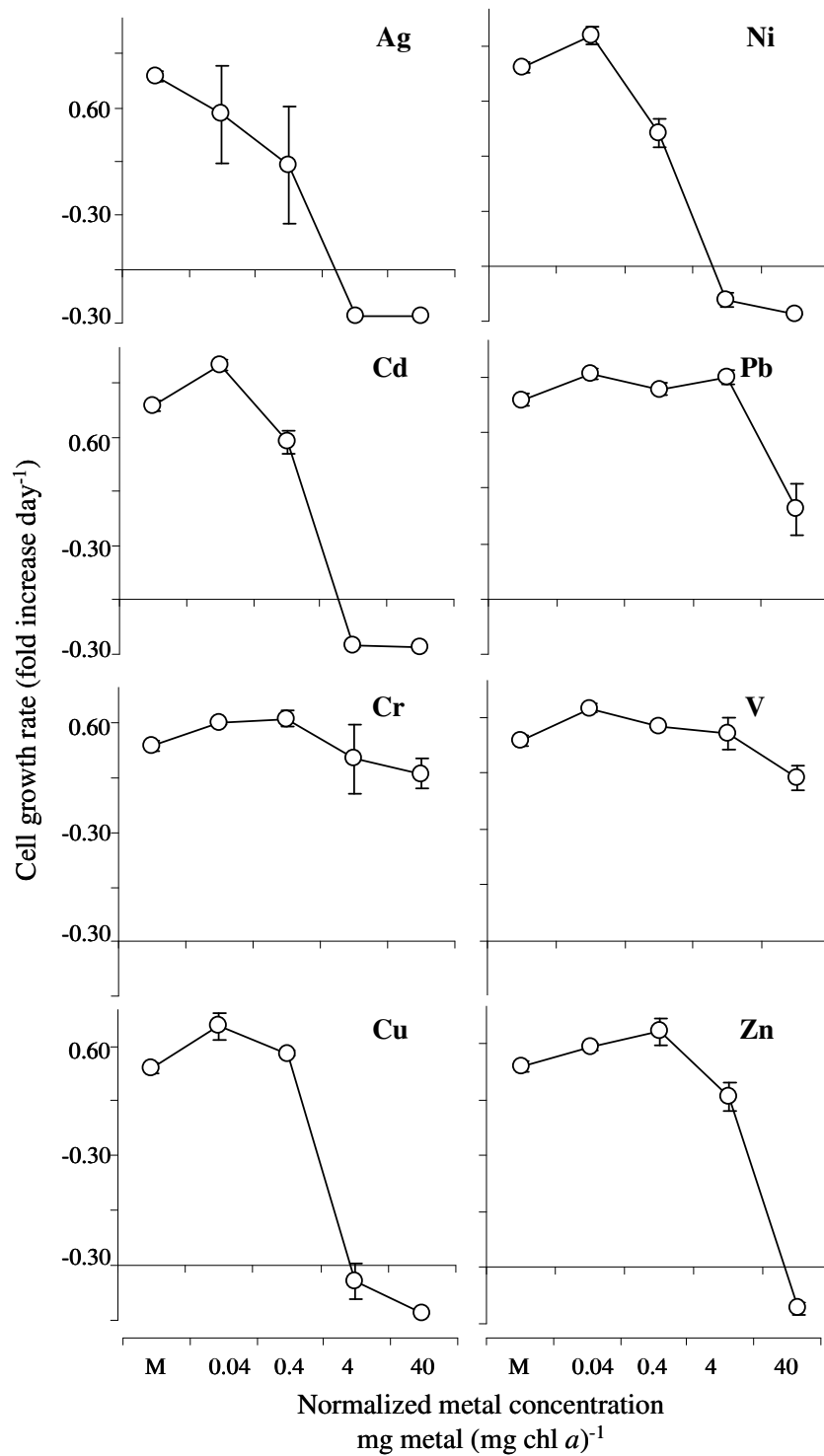


Figure 6: Response of oceanic *Synechococcus* strain CCMP 841 to metal additions.

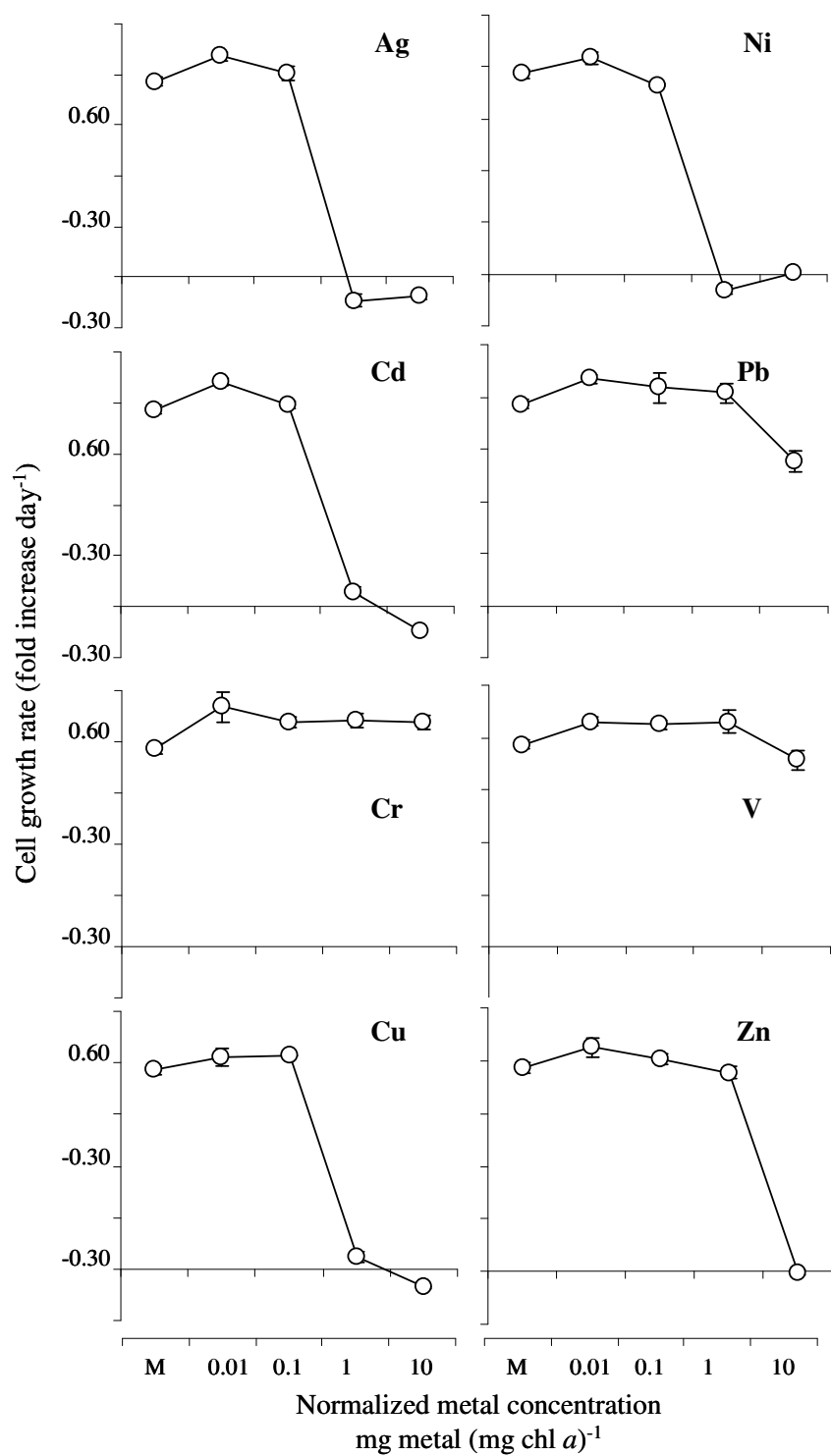


Figure 7: Response of coastal *Synechococcus* strain CCMP 838 to metal additions.

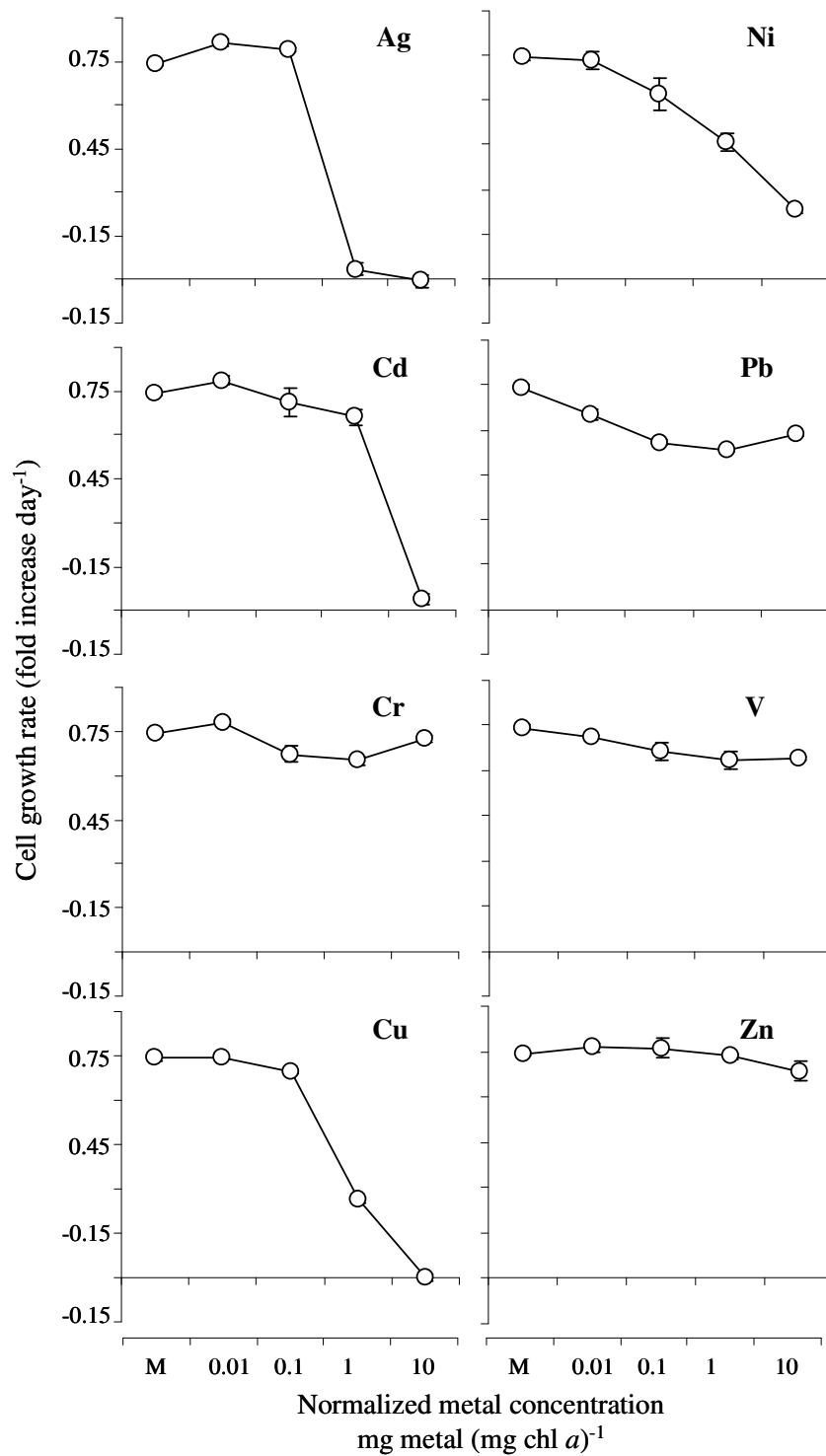


Figure 8: Response of coastal *Synechococcus* strain CCMP 2606 to metal additions.

CHAPTER 9

FUTURE DIRECTIONS

I am currently continuing to work on projects relating to two of the chapters in this dissertation. The first is a project that is already underway and that is an extension of the chapter on alternative electron flow in marine phytoplankton. In the summer of 2009 I spent a month working in David Scanlan's laboratory at the University of Warwick, UK, learning how to apply advanced molecular biology techniques with laboratory strains of *Synechococcus*. We designed primer pairs to amplify a fragment of the *ptox* gene from different *Synechococcus* clades, and have used them to obtain sequence data from a number of cultured and environmental samples. Our goal is to construct a phylogeny based on *ptox* sequences and to tie evolutionary relationships to the biogeographical distributions and photophysiological attributes of these organisms in situ.

I have also developed a single cross over construct to make a *Synechococcus* knockout mutant that lacks the *ptox* gene. We plan to characterize the photosynthetic characteristics of the mutant under different light regimes to compare its fitness relative to the wild type strain. We also plan to use membrane inlet mass spectrometry (MIMS) to directly measure the consumption of O₂ (or lack thereof) in both strains. Together, these experiments should shed light on the global distribution of *ptox* genes in the environment, and help us to understand the role of PTOX in the photophysiology of marine phytoplankton.

The second project is an extension of my chapter on the toxicity of aerosols. As part of my post doctoral appointment with Adina Paytan, we will explore the range of responses of different phytoplankton to aerosols. Specifically, we are interested to see if coastal and open ocean phytoplankton respond differently to aerosol additions in terms of their growth and toxicity responses, much like we observed in the culture experiments described in chapter 8. We have already completed experiments in Bermuda with oceanic phytoplankton collected from the Sargasso Sea and coastal phytoplankton collected from a near shore site, and further experiments are planned for the South China Sea toward the end of 2010.